Dissertation
submitted to the
Combined Faculties for the Natural Sciences and for Mathematics
of the Ruperto-Carola University of Heidelberg, Germany
for the degree of
Doctor of Natural Sciences

presented by

Diplom-Chemiker Ulrich Hoffmanns
born in: Essen

Oral examination: February 15th, 2005

Selective Labelling of Peptides with Organometallic Compounds - Chemical and Biological Characterization

Referees: Prof. Dr. Nils Metzler-Nolte

Prof. Dr. Andres Jäschke

Acknowledgements

I would like to thank all people who supported my work during this Ph. D. period.
I am especially indebted to:

Prof. Dr. Nils Metzler-Nolte, for the opportunity to work in his group and the many things I have learned, not only in the lab. I would also like to thank him for the time he always had and his numerous helpful comments.

Dr. Walter Kramer, for many helpful conversations about synthetic problems and NMR spectroscopy.

Heiko Rudy, who has not only measured numerous mass spectra and elementary analyses but was also a friendly support in whatever technical question.

Tobias Timmermann and Tanja Coelho, for skillfully running the NMR experiments

Angelika Seith, for the measuring of high quality ESI mass spectra

Melanie Ott, for her great assistance and her patience with the cell experiments

Prof. T.J.J. Müller and co-workes for valuable help with the Sonogashira coupling

Michela Doria for carrying out the first logP experiments

Tim Kersebohm and Thomas Happ, for their support and friendship during the last years

Richard Wombacher for his good ideas and some valuable pieces of literature

... and all other colleagues who were interested in my work, for their encouraging conversations.

Meinen Eltern und

Claudia

Zusammenfassung

Hoffmanns, Ulrich Dipl.-Chem. 15. Februar 2005

„Selektive Markierung von Peptiden mit Organometall-Verbindungen - Chemische und biologische Charakterisierung“

Referent: Prof. Dr. N. Metzler-Nolte
Koreferent: Prof. Dr. A. Jäschke

Die Kopplung von Übergangsmetall-Verbindungen an Peptide und Proteine verleiht diesen biologisch aktiven Substanzen einzigartige spektroskopische Eigenschaften, welche sie zu wertvollen Werkzeugen in Diagnose und Therapie machen. In dieser Arbeit wurden neue Methoden zur Einführung von Organometall-Verbindungen in Peptide entwickelt. Diese konnten an einem Pentapeptid, [Leu^5]-Enkephalin, gezeigt werden, während Metallocenderivate als Metall-Marker zum Einsatz kamen.
Die Synthese des Pentapeptids Enkephalin und die nachfolgende Markierung durch Ferrocen- bzw. Cobaltoceniumcarbonsäure wurden mittels Festphasensynthese realisiert. Dabei konnten die Organometall-Gruppen sowohl an den N-Terminus als auch an die Seitenkette eines 4-Amino-modifizierten Phenylalanins gebunden werden. Die unterschiedlichen Eigenschaften der jeweiligen Metallverbindungen erforderten den Einsatz einer Vielzahl verschiedener Harze, Linker und Schutzgruppen.
Im zweiten Teil der Arbeit wurde mit der Sonogashira-Kopplung, einer Palladium-katalysierten Kreuzkopplung, eine weitere Methode zur Verknüpfung eines Biomoleküls mit einer Organometall-Verbindung vorgestellt. Diese Kopplungsreaktion veknüpft ein Iodaren und eine Alkinyl-Funktion und wurde zunächst an einer Reihe von Dipeptiden getestet, welche ein 4-Iodo-Phenylalanin enthielten. Nach erfolgreicher Kopplung einiger Ferrocen-Alkinyl-Verbindungen wurde diese Technik auf das Neuropeptid Enkephalin übertragen, das ebenfalls an der Phenylalanin-Seitenkette markiert werden konnte.
Um den Einfluss des Metall-Markers auf die physiologischen Eigenschaften des Zielmoleküls zu untersuchen, wurde die Lipophilie einer Reihe von Enkephalin-Derivaten mit einer modernen HPLC-Methode gemessen. Zusätzlich konnte die Blut-Hirn-Schranken-Permeabilität in einem *in vitro* Modell bestimmt werden, welches auf porzinen Hirnkapillar-Endothelzellen basiert. Hierbei zeigte sich eine bessere Permeabilität für Substanzen mit höherer Lipophilie, wie es für einen reinen Diffusionsmechanismus erwartet werden kann.

Abstract

Hoffmanns, Ulrich Dipl.-Chem. February 15th, 2005

„Selective Labelling of Peptides with Organometallic Compounds - Chemical and Biological Characterization“

1st Referee: Prof. Dr. N. Metzler-Nolte
2nd Referee: Prof. Dr. A. Jäschke

The modification of peptides and proteins with transition metal compounds is a growing field of interest, since it provides biologically active substances with unique spectroscopic properties, serving as valuable tools in diagnosis and therapy. In this work, new methods for the introduction of organometallic compounds into peptides have been presented, using the pentapeptide [Leu^5]-Enkephalin as a model target molecule, while ferrocene and cobaltocenium compounds served as metal markers.
Preparation of enkephalin and the subsequent labelling with ferrocene- and cobaltocenium carboxylic acids were carried out using solid phase peptide synthesis (SPPS). These synthetic pathways comprised the introduction of the metal marker to the N-terminus, as well as to the side-chain of a 4-amino modified phenylalanine residue, yielding mono- and di-labelled species. The different properties of the metal compounds used demanded the combination of diverse linkers, resins and protecting groups.
In the second synthetic part of this work, the binding of the metal fragment by the use of Sonogashira coupling, a Pd catalyzed cross coupling reaction, was evaluated. As a proof of concept, dipeptides containing a 4-iodo-phenylalanine were synthesized and different alkynylated ferrocene derivatives were successfully coupled. An enkephalin derivative was synthesized next where the natural phenylalanine was substituted by the 4-iodo-phenylalanine residue, to which the ferrocene-alkyne could be successfully coupled.
To study the influence of the metal marker on the physiological properties of the target enkephalin molecule, the lipophilicity was determined for a selection of enkephalin compounds using a modern RP-HPLC method. In addition, the blood-brain-barrier permeation behaviour of selected compounds was tested. These transport experiments were conducted by means of porcine brain capillary endothelial cell (PBCEC) monolayers. It was found that the more lipophilic compounds showed higher permeation, as expected for a passive diffusion mechanism.

Table of contents

Abbreviations

2-ClTrt	2-chloro-trityl
acac	acetylacetonate
Ala	alanine
BBB	blood brain barrier
Boc	*tert*-Butoxycarbonyl
br	broad
Cc	cobaltocenium
cm	centimeter
CV	cyclic voltammetry
d	doublet
DCM	dichloromethane
dd	double doublet
DEPA	diethylpropargylamine
DIPEA	diisopropyl-ethylamine
DMF	dimethylformamide
DMSO	dimethylsulfoxide
DNA	desoxyribonucleic acid
E	potential
EI	electron ionization
Enk	enkephalin
ESI	electro-spray ionization
Et	ethyl
EtOAc	ethylacetate
EtOH	ethanol
FAB	fast atom bombardment
Fc	ferrocene
Fmoc	fluorenylmethoxy carbonyl
g	gram
Gly	glycine
h	hours
HOBt	1-hydroxy-1H-benzotriazole
HPLC	high performance liquid chromatography
Hz	hertz
IR	infrared
J	coupling constant
KRB	Krebs-Ringer buffer
Leu	leucine
log*P*	logarithmized octanol/water partition coefficient
m	multiplet
M	molar
m	meta
m/z	mass per charge
Me	methyl
MeOH	methanol
min	minutes
NMR	Nuclear Magnetic Resonance

o	ortho
p	para
P_{app}	apparent permeability coefficient
PBCEC	porcine brain capillary endothelial cells
Ph	phenyl
Phe	phenylalanine
PIBA	*p*-iodo benzoic acid
ppm	parts per million
q	quartet
RT	room temperature
s	singlet, second, strong
SWV	square wave voltammetry
t	triplet
T	temperature
TBABF	tetrabutylammonium tetrafluoroborate
TBTU	O-(benzotriazole-1-yl)-N,N,N',N' tetramethylurionium tetrfluoroborate
TFA	trifluoroacetic acid
THF	tetrahydrofuran
TIS	tri-isopropysilane
Tyr	tyrosine
UV	ultra violet
VIS	visible
vs.	versus
w	weak
δ	chemical shift
ε	molar extinction coefficient
λ	wavelength

General remarks

In this thesis, ferrocene and cobaltocenium groups are abbreviated by **Fc** and **Cc**, respectively. Both represent the $(C_5H_5)M(C_5H_4)$ moiety, for M = Fe, Co. Within this system ferrocene would be noted as Fc-H and cobaltocenium carboxylic acid as Cc-COOH, like indicated in *Fig. I.*

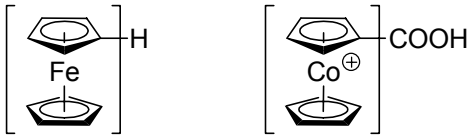

Fc-H Cc-COOH

Fig. I *Ferrocene and cobaltocenium carboxylic acid. Fc and Cc represent $C_5H_5MC_5H_4$ (M = Fe, Co)*

The nomenclature for amino acids and peptides in this thesis is as commonly used in peptide chemistry. It is based on the general amino acid structure shown in *Fig. II*. When bound inside a peptide or protein the amino acid residue only implies the N-terminal NH group and the C-terminal carbonyl function. Glycine, for example, with the formula $H_2N\text{-}CH_2\text{-}COOH$ is referred to as H-Gly-OH.

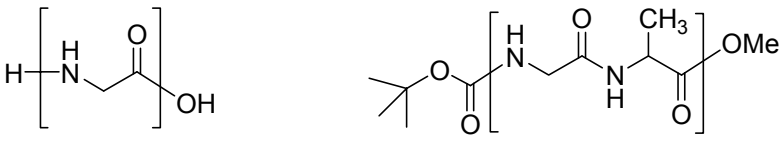

H-Gly-OH Boc-Gly-Ala-OMe

Fig. II *Nomenclature for amino acids and peptides*

1 Introduction

1.1 General introduction

Only a few decades ago the classical areas of chemical research like organic, inorganic and biochemistry were strictly separated. Especially the field of inorganic chemistry, mainly being the study of (transition) metal compounds, and the discipline of biochemistry had been viewed as merely incompatible. This has been changing to an ever increasing extend and techniques of the one field are being used with great success in the other. As a consequence the field of transition metal chemistry for the organic chemist continues to expand and have a significant role in functional group conversion and organic total synthesis.[1-3] On the other hand has Merrifield's invention of solid phase peptide synthesis[4] (SPPS) greatly enriched the field of biochemistry, since it provides a synthetic tool for small to medium sized biopolymers of high purity.[5-7] With the discovery of a growing number of metallo-enzymes[8-10] and other transition metal containing biomolecules,[11, 12] which play an essential role in biology, the two areas of inorganic chemistry and biochemistry become more related, as well.

1.2 Bio-Inorganic Chemistry

Bio-Inorganic chemistry comprises the study of the functions, processing, storage, and applications of metal ions and their complexes in biological systems. It is a rapidly growing field that combines numerous disciplines, including inorganic chemistry, biochemistry, molecular and cell biology, environmental and medicinal chemistry.

Alkaline and earth alkaline metals, especially Na^+, K^+, Ca^{2+} and Mg^{2+} have been known to have vital functions in life[13, 14] for a very long time. These functions include the construction of the skeleton, the building of membrane potentials in nerve cells, the folding of proteins or DNA/RNA and many more. Just lately a Nobel Prize was awarded for the discovery of alkaline ion channels in cell membranes.[15]

Apart from these group 1 and 2 metals we nowadays know that a number of transition metals are also necessary for living organisms. The versatility of these metals may be derived from the high number of stable oxidation states they can accept and we can find them in transport (haemoglobin/transferrin), catalysis (cytochrome P450) and structural motifs (zinc finger).

Hemes, for example, contain iron and have been one of the centers of attention since the earlier days of biological inorganic chemistry.[16-19] Cytochrome P450 is such a heme-containing enzyme from the respiratory system of plants, animals and humans. Its important task is to oxidize, i.e. hydroxylate various substrates. The catalytic center of the enzyme consists of a low-spin Fe^{3+} coordinated by the porphyrine system of the heme and a cystein sulphur atom. After initial reduction to Fe^{2+} one electron is transferred from the iron to the binding O_2 and a high-spin Fe^{3+} with a superoxide ligand is formed. After release of one oxygen atom as a water molecule and the following hydroxylation of the substrate the low-spin Fe^{2+} is restored.[20, 21] Substructures of this catalytic cycle have been presented.[22, 23]

Non-heme iron enzymes catalyze a variety of redox processes, as well.[24, 25] Nitrogenase is such an enzyme which makes environmental dinitrogen available for biochemical processes through reduction to ammonia. The active site contains an iron/sulphur cluster and one molybdenum atom.[26-28] The exact mechanism of the highly energy consuming process is still in the dark.

Angiotensin converting enzyme (ACE), a carboxypeptidase, is responsible for cleaving the two carboxy terminal amino acids His-Leu from angiotensin I to produce angiotensin II, a potent vasopressor octapeptide.[29] The enzyme contains a Zn^{2+} ion as a metal ion cofactor which is at the heart of the active site. The zinc ion is coordinated in a pentahedral geometry first by three amino acid side chains in the active site namely through a nitrogen atom from histidines 69 and 196, and through two oxygen atoms from glutamic acid 72. The fifth bonding position is either a water molecule or an oxygen center from the carbonyl group of Gly 1.[30] The nucleophilic carbonyl oxygen atom of the target peptide binds to the zinc center, therefore destabilizing the C_α-N bond through a betain structure, enabling easy hydrolysis of the peptide.

1.3 Bio-Organometallic chemistry

The metallo-enzymes mentioned above have all in common that the metal ion is coordinated by classical donors like O, N and S atoms. However, enzymes with organometallic moieties are also known in nature, one example thereof being cobalamin, also known as vitamin B12, which contains a cobalt fragment.[31]

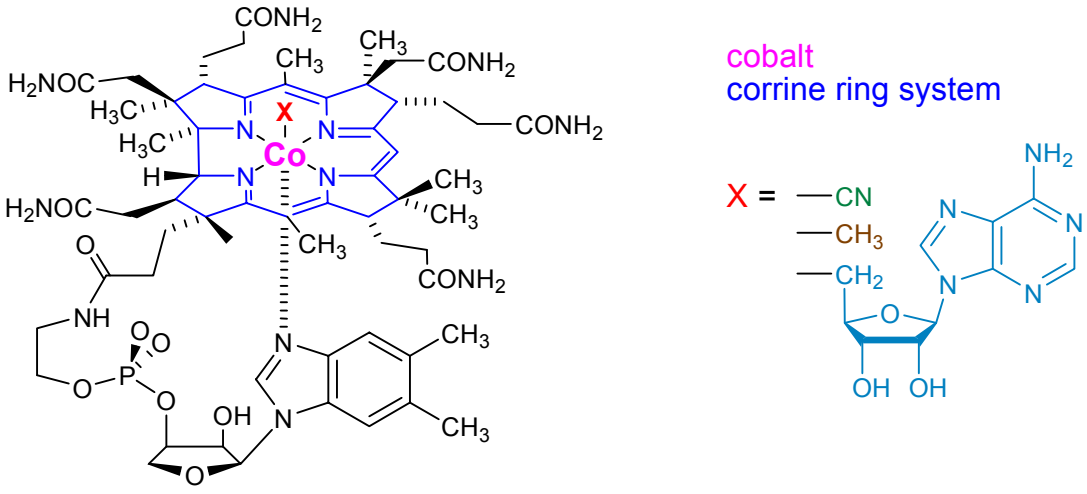

Fig. 1.1 *The structure of cobalamin, vitamin B12*

The Co^{3+} ion is coordinated by a corrine ring which is apart from a higher grade of saturationsaturation and a missing methylene group very similar to the heme's porphyrine ring system. The fifth ligand is a benzimidazol riboside. The synthetically obtained cyano cobalamin is transformed in vivo into the active compounds methyl cobalamin and 5'-desoxyadenosyl cobalamin, respectively.[32] Vitamin B12 serves as a cofactor for biosynthesis of purine- and pyrimidine bases, reduction of ribonuctleotide triphosphates to 2-desoxyribo-nucleotide triphosphates and synthesis of methionine from homocystein.[33] The meta stability of the Co-C bond allows easy methylation and isomerization of the substrate.

A second example is hydrogenase, a bacterial enzyme which catalyzes the reversible transformation of dihydrogen into protons and two electrons. Several forms are known, one of it being [Fe-Ni]-hydrogenase, which contains a heterobimetallic active center, the structure of which has recently been elucidated[8] and is shown in *Fig. 1.2*.

[Fe-Ni]-hydrogenase is truly organometallic, since one carbonyl and two cyanide ligands are bound to the iron atom (*Fig. 1.2*).

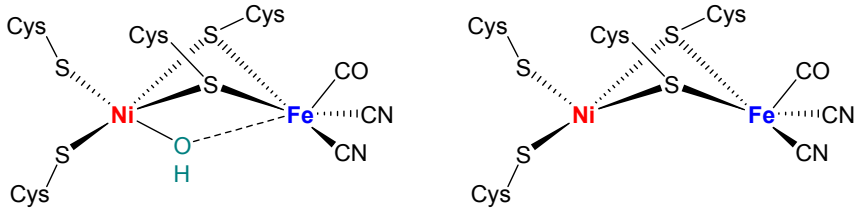

Fig. 1.2 *The catalytic center of [Fe-Ni]-hydrogenase from Desulfovibrio Gigas. The "unready" state (left) can be transformed into the active form (right) by a two electron H_2-reduction.*

The crystal structure of the "unready" state of the enzyme, referred to as Ni-A, discloses a bridging ligand, identified as a hydroxyl group by ENDOR spectrometry.[34] However, the Ni-A state requires prolonged hydrogen exposure to be activated and be transferred into Ni-C, the active form of the enzyme. Other oxidised forms which could be deduced from EPR spectroscopy have been presented, too.[35-38]

1.4 Applications of bio-compatible organometallic compounds

To the uninitiated it may seem that organometallic compounds, generally known for their high reactivity, have no relevance in biological or medicinal applications which usually take place in aqueous media and with dioxygen present. That is clearly not true because quite a range of organometallic substances like ferrocene[39-41] and the cobaltocenium ion[40, 41] show great stability in water at different pH values, making them first row candidates for biological applications (see chapter 2). Showing different properties and reactivity compared to donor coordinated metals, these compounds can add some very powerful spectroscopic probes to the shelf of the analytic scientist.

1.4.1 Immunoassays

Since the early 1960s, the use of immunological tests has revolutionized clinical chemistry and biochemistry. In these so-called immunoassays the selective binding of an antibody to the responding antigen is exploited, with either of both being marked with a

detectable group. In this way the antigen-antibody adduct results in a signal which can be measured easily and with high precision. Possible analytes are proteins and hormones or even small compounds (haptens), which have to be attached to a protein beforehand.[42-44] In the beginning most of these assays were radio immunoassays (RIA), i.e. the label was a radioactive element like ^{125}I or ^{3}H. However, because of the hazards associated with the use of radioactivity, development and commercialization of a number of non-isotopic immunological methods has been driven forth. The most widespread methods now use enzymes[45, 46], fluorescent[47-49], chemi- and bioluminescent[50, 51] and electrochemical[52, 53] probes as labels associated to analytical methods such as colorimetry, fluorescence spectroscopy or electrochemical detection.

A new interesting development in the field has been initiated by Jaouen and co-workers who presented a non-isotopic immunological assay termed CMIA (carbonyl metallo immunoassay) that uses metal carbonyl complexes as tracers and Fourier transform infrared spectroscopy (FT-IR) as the detection method.[54] The assay is based on the very strong absorption bands in the 1800-2200 cm^{-1} spectral range where proteins and biomolecules do normally not absorb.[55]

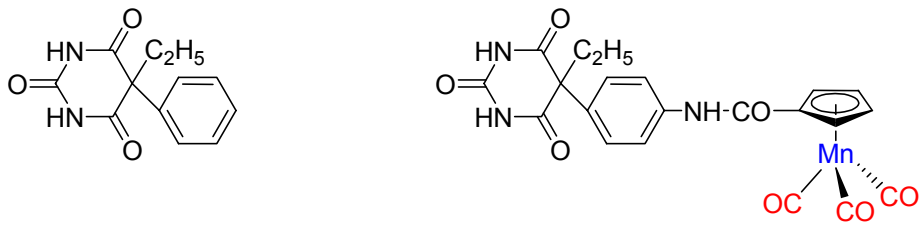

Phenobarbital (analyte) $Mn(CO)_3$-pheno (tracer)

Fig. 1.3 *The antiepileptic drug Phenobarbital (left) is modified with a cymantrene group (right) to enable infrared detection.*

The number of suitable metal carbonyl tracers has increased over the years and work with $Cr(CO_3)$, $Mo_2(\eta^5\text{-}C_5H_5)_2(CO)_4$, $Co_2(CO)_6$ and $Re(CO_3)$ has been published.[56-62] These are examples of the use of an organometallic probe attached to biomolecules, offering new ways of detection.

1.4.2 Radiopharmaceuticals

Another growing and well established sector is the area of metallopharmaceuticals, which are applied both in diagnosis and therapy.[63] Many of these drugs are used in imaging applications some of them being metallo-radiopharmaceuticals.

These drugs contain radioactive material and are administered to the patient either parenterally or orally. After a certain time of distribution in the person's body, an image with high resolution can be recorded using a so-called Anger (gamma) camera.[64]

More than 80% of all radiopharmaceuticals contain technetium (^{99m}Tc), because this nuclide advantageously combines a short half-life of 6 h with a relatively low energy of emitted gamma photons (140 keV) and thus minimizes the radiation hazard for all involved.

The first organometallic ^{99m}Tc compound for use in nuclear medicine has been reported by Davidson *et al.*[65] (*Fig. 1.4*). The monodentate, highly back-bonding, isonitrile ligand allows the complex to form an unstrained octahedral geometry with very strong Tc-C bonds as demonstrated in the crystal structure.[66]

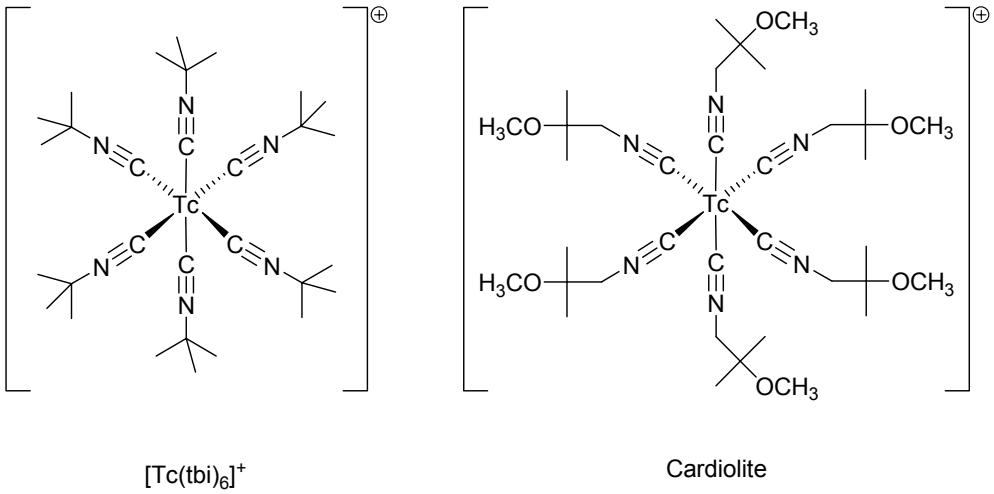

Fig. 1.4 *$[Tc(tbi)_6]^+$ (left), as reported by Davidson et al. Technetium(I) in an octahedral geometry of six isonitrile ligands. Cardiolite (right) is the first clinically applied organometallic compound in nuclear medicine.*

This water and air-stable compound was found to be quite robust and formed readily by simply heating $^{99m}TcO_4^-$ with excess isonitrile and $SnCl_2$ as the reducing agent. Cardiolite and similar organometallic ^{99m}Tc compounds have been successfully used in clinical applications since, but the demand for a more selective enrichment in target tissues is still high. Therefore a system which binds the technetium compound to the targeting (bio)molecule is needed.

Schubiger, Alberto and co-workers presented such a system, reporting the synthesis of the complex *fac*-$[Tc(CO)_3(H_2O)_3]^+$, where Tc is strongly bound to three carbonyl groups and only weakly connected to the water ligands, which easily exchange with a tridentate donor ligand.[67-69] A variety of biomolecules like cobalamin (*Fig. 1.1*), biotin and [Leu^5]-Enkephalin (→ *chapters 4,5*) have been labelled with $^{99m}Tc(CO)_3$ using a modified histidine ligand[70, 71] (*Fig. 1.5*).

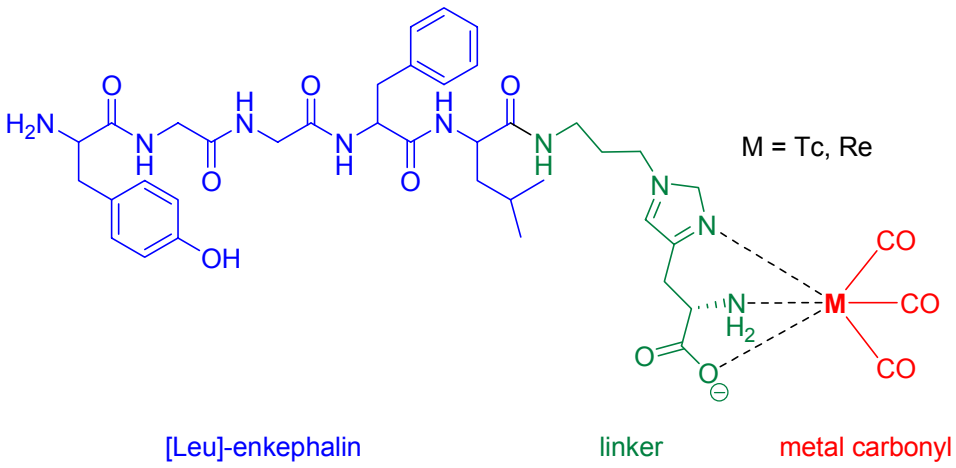

Fig. 1.5 *A modified histidine linker binds the radioactive metal carbonyl moiety to the C-terminal end of the pentapeptide [Leu^5]-Enkephalin. (from Ref. 70)*

The choice of linker depends on a number of aspects, amongst them are the strength of binding to the metal ion, its stability and the complexity of the synthesis.[67] Also the size of the linker is an important issue, since the biomolecule's original properties are influenced by the linker, as well. The choice of the wrong linker might therefore result in loss of activity, bad solubility or aggregation.

1.4.3 Tumor inhibition (cytostatics)

The anti-tumor properties of a series of bent metallocene dihalides and pseudohalides, $[Cp_2MX_2]$ (M = Ti, Mo, Nb, C; X = F, Cl, Br, I, NCS, N_3) have been reported.[72-74] Some of these (*Fig. 1.6*) have very high activities and are being studied in clinical trials.[75-77] The mechanism of the cytostatic effect is still unclear but is supposed to result from the interaction of a hydrolyzed metallocene species with DNA[78]. Several adducts of metallocene dihalides with DNA have been isolated and characterized, but no such adducts have been detected with $[Cp_2VCl_2]$, the most active metallocene *in vitro*. Not only this contradiction concludes that the cytostatic mechanism is very different from that of *cisplatin*, a very active and commercially successful anti cancer drug.[41, 79, 80]

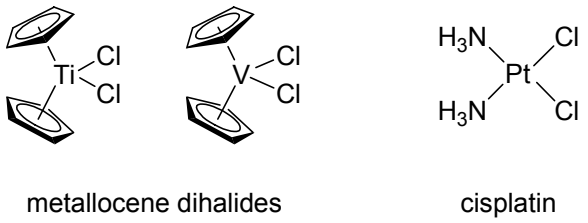

Fig. 1.6 *Titanocene dichloride and vanadocene dichloride (left) the two most active anti-tumor metallocenes. On the right: Cisplatin, a highly active cytostatic, which hinders cell division by crosslinking the two DNA strands.*

Studies on the anti-tumor activity of ferrocene derivatives[81-83] suggest that the oxidation/reduction behaviour of this metallocene plays a key role in the mechanism of proliferation inhibition, shown in many experiments.[84, 85] The water solubility of these compounds is still in important issue, since the ferrocene moiety renders many small molecules insoluble due to high lipophilicity.[85]

These promising properties of metallocenes have led to various attempts to incorporate metallocenes or fragments of them into peptides[86-88] and proteins[89-91]. After Schlögel *et al.* have prepared the first ferrocene amino acid derivatives in 1957,[92] many similar compounds have been used for labelling purposes. Cymantrenylalanine (Cym) and ferrocenylalanin (Fer) are two such derivatives which substitute the natural amino acid phenylalanine.[93, 94] They can be used like a regular amino acid and are tolerant to solid phase synthesis conditions.

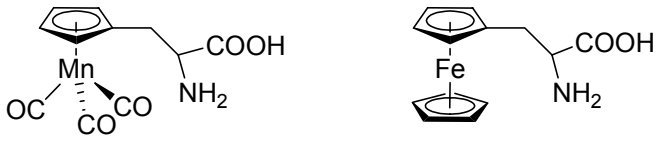

Fig. 1.7 *Molecular structures of cymantrenylalanine (Cym, left) and ferrocenylalanine (Fer, right)*

However, a major drawback is that racemization takes place during their synthesis. Thus, the isolation of the stereochemically pure product can be a very time consuming process.[94, 95] The labelling of enkephalin by replacing the natural amino acid Phe[4] with ferrocenylalanine (Fer) has been reported[96] in 1980. Other biologically relevant peptides have also been marked with Fer by Tartar *et al.* Among these are substance P[86, 97], bradykinin[97] and angiotensin II.[98] All of these Cym and Fer containing bioconjugates have been synthesized under harsh conditions using TFA and HF chemistry, and could only be incompletely characterized by elemental analysis. It has been shown that the activity of Fer-labelled peptides is significantly lower compared to their wild type homologues,[97, 99] which is probably caused by the bulkiness and higher lipophilicity of the ferrocene moiety.[100]

The labelling of biomolecules, which preferably enter specific organs and tissues, with anti-tumor active organometallic groups, is surely one of the most challenging tasks for the bio-organometallic chemist. The knowledge how to precisely deliver the pharmacon to the location of the disease is of great importance for modern drug design.

1.5 Objectives of this thesis

All of the above examples show that the binding of organometallic probes to biomolecules opens new pathways concerning detection of the bioconjugate (diagnosis) and also medicinal treatment (therapy). However, the demand for methods which allow a selective coupling of the metal marker to the biomolecule is high. Since most of all synthetic peptides are realized through solid phase peptide synthesis, it is desirable to have the coupling of the organometallic marker to the target molecule be compatible with the chemical conditions applied during SPPS. This should enable a facile synthesis on the solid support, yielding the readily usable product.

The aim of this thesis is to develop new methods for the selective and biocompatible coupling of organometallic groups to peptides on the solid phase. The use of different linkers, protection groups and coupling strategies should be elaborated in this context. The obtained bioconjugate compounds are to be fully characterized by NMR, mass spectrometry and electrochemical experiments. Furthermore, the impact of the metal label itself on the bioconjugate's physiological properties should be studied by the determination of lipophilicity values and conduction of cell permeation experiments. To fulfil these tasks a pentapeptide, [Leu]-Enkephalin, has been chosen as the model target molecule. Ferrocene and cobaltocenium, two metallocenes containing iron and cobalt, respectively, serve as the organometallic probes. The simplicity of synthesis, isolation and purification of the products is one of the main points of focus.

2 Ferrocene / Cobaltocinium as markers

2.1 Metallocenes

In 1951, the compound dicyclopentadienyl iron (ferrocene) was discovered and the field of organometallic chemistry was thereby transformed. Two independent groups of chemists almost simultaneously arrived at the same conclusions, albeit accidentally. A reaction was carried out on cyclopentadienyl magnesium bromide with anhydrous iron(III) chloride in ether in an attempt to synthesize fulvalene via the oxidation of the cyclopentadienyl Grignard reagent (Kealy and Pauson, 1951).[101] However, via reduction of the iron(III) to (II) by the Grignard species, they instead obtained orange crystals that analysed for $C_{10}H_{10}Fe$.

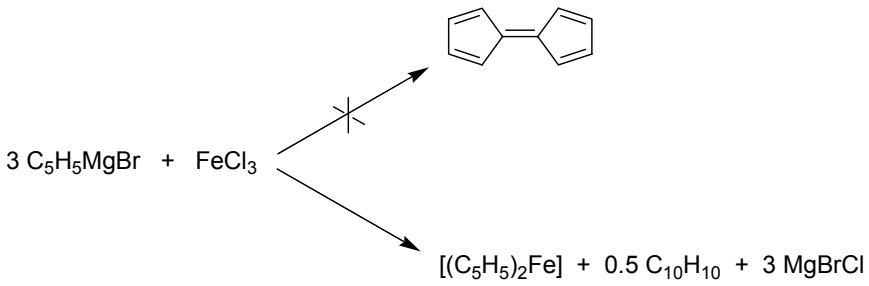

Fig. 2.1 *An attempted formation of fulvalene that lead to the discovery of the first metallocene (from Ref. 41)*

At the same time Miller *et al.*, who where investigating the preparation of amines, reported the formation of an orange compound $C_{10}H_{10}Fe$ by direct reaction of cyclopentadiene with iron in the presence of aluminum, potassium or molybdenum oxides at high temperatures[102].

Both groups noted that the compound was air-stable, sublimable and had a melting point of 173 °C, with excellent solubility in organic solvents but was insoluble in water. It took only short time until the unusual structure of ferrocene was disclosed. In 1952 Wilkinson from Harvard University used chemical, physical and spectroscopic methods to elucidate the correct "sandwich"-like structure,[103] whilst Fischer used x-ray crystal-

lography to structurally characterize the compound.[104] They both shared the Nobel Prize for their achievements in 1973.

After substantial studies had been made on ferrocene, many other transition metal derivatives were synthesized, and the entire class of transition metal dicyclopentadienyl compounds became quickly known as *metallocenes*.

2.2 Synthesis and properties

2.2.1 Group 8 metallocenes

In metallocene chemistry, ferrocene is still among the main areas of interest primarily due to its remarkable stability and ease of preparation. The 18-electron compound, consisting of a Fe^{2+} (d^6) and two $6e^-$ aromatic rings ($C_5H_5^-$), is accessible through a variety of reaction pathways, with the most common being shown in *Tab. 2.1*.

Tab 2.1 *A selection of common synthesis for ferrocene*

1	$[M(C_5H_5)_2]$ (M = Li, Na, K) and anhydrous $FeCl_2$
2	C_5H_6, Et_2NH, anhydrous $FeCl_2$ or $FeCl_3$
3	C_5H_6, KOH, $FeCl_2 \cdot 4H_2O$
4	Fe, $[Et_2NH_2]Cl$, C_5H_6
5	Fe (atoms), C_5H_6 ($+Al_2O_3$ or K_2O in traces, 300° C)

Dicyclopentadienyl ruthenium and osmium (ruthenocene, osmocene) were one of the first metallocenes to be formed following the discovery of ferrocene, but whilst the chemistry of ferrocene has flourished, much less attention has been paid to the more costly and synthetically more challenging group 8 homologues.[105, 106] Ruthenocene can be formed by the reaction of $Ru(acac)_3$ with excess $[(C_5H_5)MgBr]$, from $RuCl_3$ and sodium cyclopentadiene or via the ligand exchange route from ferrocene and anhydrous $RuCl_3$. It is stable in air and has a high melting point of 199 °C. Osmocene is even more difficult to obtain but can be synthesized from $OsCl_4$ and sodium cyclopentadiene in THF in low yields of below 20%. Unlike ferrocene, the higher group 8 analogues prefer an eclipsed conformation for the Cp-rings. This is explained by the longer distance between the two aromatic rings, caused by the increasing size of the metal ion moving

down-group. X-ray diffraction studies of ferrocene had indicated a staggered configuration of the rings with a molecular center of symmetry (D_{5d}), whereas gas-phase electron diffraction observations projected a D_{5h} geometry with C-C distances of 144 pm and a Fe-C distance of 203 pm. The rotational barrier in ferrocene is quite small with 4 kJ/mol, though[107]. All three compounds can be easily oxidised and show E^0 values of +0.11 V, +0.55 V and +0.46 V for iron, ruthenium and osmium, respectively.[108] While ferrocene exclusively undergoes one-electron reversible oxidation, the chemical and electrochemical oxidation of Cp_2Ru and Cp_2Os are still subject to controversy, since also two-electron irreversible processes have been reported for the latter two compounds.[109] Ring substituents strongly influence the energy barrier for a single electron removal by their electron withdrawing or releasing properties.

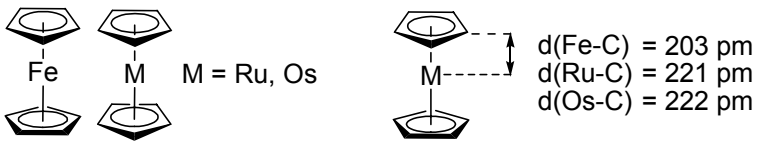

Fig. 2.2 *Ferrocene prefers a staggered conformation, whereas its higher homologues favour the eclipsed geometry (left). The metal-carbon distances of Cp_2Ru and Cp_2Os surpass the Fe-C bond length by 0.2 Å (from Ref. 103)*

Derivatization of the Cp-rings becomes more difficult regarding the heavier metal compounds. While in ruthenocene alkylation and acylation of the cyclopentadienes can still be applied under forcing conditions, osmocene can hardly be Friedel-Crafts monoacylated and no alkylation is possible at all.[41] On the opposite, the exceptional feature of ferrocene is its ability to undergo aromatic-type (electrophilic) substitution reactions in analogy to benzene,[39, 110] but up to 10^6 times faster.

2.2.2 Group 9 metallocenes

Cobaltocene was first synthesized by the reaction of NaCp with $[Co(NCS)_2(NH_3)_4]$ in liquid ammonia. Other routes involve using cobalt bromide or $[Co(NH_3)_6]Cl_2$ giving improved yields.[111] In concurrence with the 18-electron rule cobaltocene ($d^7 + 2 \cdot 6$ electrons from 2 Cp = 19 e^-) is expected to be easily oxidized to reach the inert gas configuration. As a fact, cobaltocene is very rapidly oxidized in air and liberates H_2 from water and dilute acids, producing the extremely stable cobaltocenium ion $[Cp_2Co]^+$.

Although the 18-electron rule does not apply to all metallocene derivatives, it serves as a practical tool of stability prediction.[112, 113] For instance, the 18 VE ions $[Cp_2Rh]^+$ and $[Cp_2Ir]^+$, the heavier group 9 metallocenes, are also very stable[114], as opposed to their neutral monomers Cp_2Rh and Cp_2Ir, which have only been observed so far by mass spectrometry from an electrochemically reduced $[Cp_2M]^+$-solution.[115] The high cost and difficulty of synthesis has left these compounds rather unattended.

From x-ray crystallography, Cp_2Co has been shown to be isostructural with Cp_2Fe. Both cyclopentadienyl rings are parallel and in a staggered configuration. The average C-C distance is 141 pm and the Co-C distance 210 pm.[116] The barrier to rotation for the rings is with 7.5 kJ/mol slightly higher than the one in ferrocene.

Cobaltocenium salts can be easily prepared through a variety of reactions as reported in numerous publications.[117, 118] While these compounds are similar to ferrocene regarding their stability and behaviour in electrophilic substitution reactions, they show a different solubility due to their positive charge and a strong resistance to oxidation.

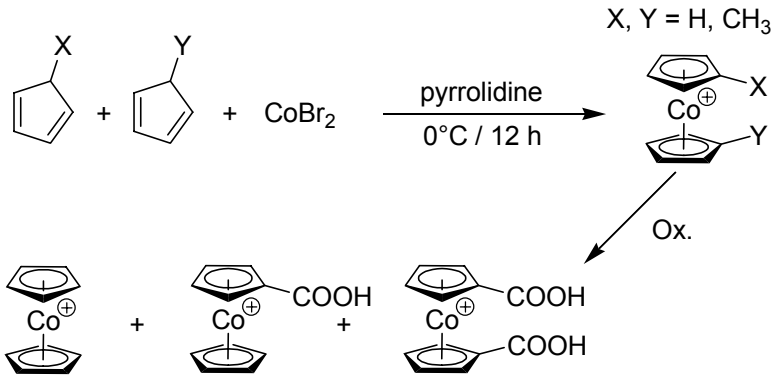

Fig. 2.3 *Synthesis of derivatized cobaltocenium salts according to Sheats et al. (from ref. 118)*

This fact suggests the use of cobaltocenium as a model substance for ferrocene and as a very robust metal marker for all sorts of applications.

Almost every other transition metal forms cyclopentadienyl compounds, the majority of which are useless for the labelling of (bio)molecules, mostly due to instability, their tendency to form binuclear compounds, their expensive and inefficient synthesis and of course the high toxicity these substances often show.

2.2.3 Spectroscopic aspects of ferrocene/cobaltocenium

Among the most important attributes for a marker molecule is the spectroscopic behaviour, which enables exact measurement of the bioconjugate *in vivo* and *in vitro*. As indicated in *chapter 1*, organometallic compounds often show high sensitivity for various types of spectroscopy. As described, Jaouen *et al.* successfully use metal carbonyl compounds, detectable by FT-IR[54] while Alberto and co-workers observe their technetium labels via radioactive detection[67]. Also atomic absorption spectroscopy (AAS) is a common tool for the detection of metals,[119] especially for exobiological species in cells.[120-122] Cais and co-workers, for instance, have introduced metallo immunoassays using metal-labelled antigens and AAS detection.[123]

Ferrocene and cobaltocenium, in particular, show a reversible electrochemical transition and can be detected down to pico-molar concentrations in solution.[124-126] Apart from a quantitative measurement of ferrocene-labelled compounds does the electrochemical method reveal details on the electronical and therefore chemical environment of the metal ion. The high quality and of electrochemical ferrocene signals have lead to an introduction of ferrocene as the standard reference in electrochemistry related literature.

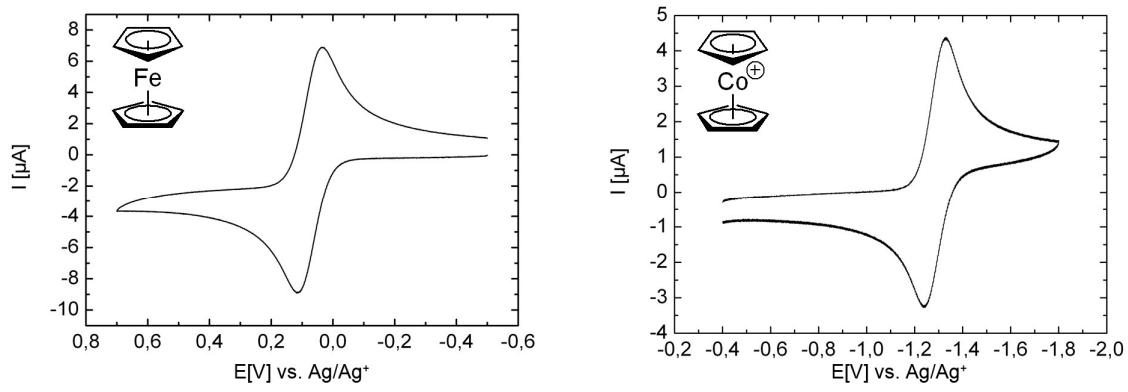

Fig. 2.4 *Ferrocene (left) shows reversible oxidation at about + 80 mV, whereas the oxidation resistant cobaltocenium ion (right) can only be reduced in the far negative*

Cobaltocinium ions are stable towards oxidation but can be converted into cobaltocene at highly reductive potentials (*Fig. 2.4*). Samples containing ferrocene or cobaltocenium labels can be detected by HPLC-ECD (High Performance Liquid Chromatography with ElectroChemical Detection).[127, 128] In view of that, ferrocene and cobaltocenium provide a very sensitive means for the detection of labelled species.

3 Peptides

3.1 General outline

A number of very important physiological and biochemical functions of life are influenced by peptides, amino acid polymers of short length. Peptides are involved as neurotransmitters, neuromodulators, and hormones in receptor-mediated signal transduction. More than 100 peptides with functions in the central and peripheral nervous system, in immunological processes, in the cardiovascular system and in the intestine are known.[129]

Although the formation of a peptide bond is known to be a relatively simple chemical reaction, the biosynthesis of polypeptides is a very complex process. Ribosomal peptide synthesis involves deoxyribonucleic acid (DNA) encoding genetic information, and two different types of ribonucleic acids which convey (mRNA) a blue print of the genetic information out of the nucleus to the ribosome, and carry (tRNA) the attached amino acid to the ribosome for peptide bond formation (*Fig. 3.1*) [130]

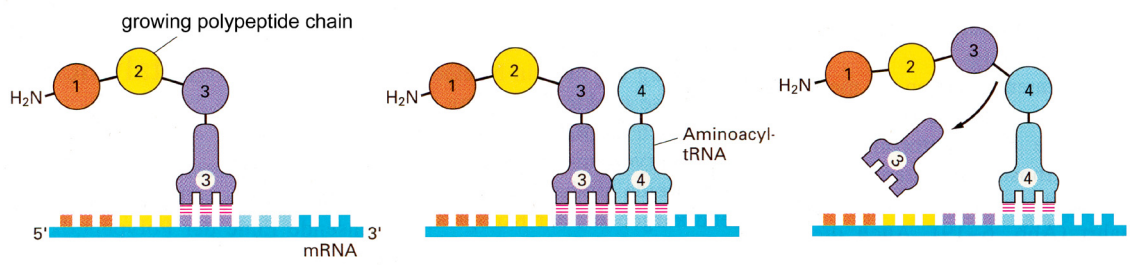

Fig. 3.1 *Peptide synthesis on an mRNA strand. Each amino acid, which is attached to the growing end of the polypeptide chain, is chosen by complementary base pairing between the anticodon of its attached tRNA and the next free codon on the mRNA chain (mod. from ref. 14)*

Each of the 21 natural amino acids is represented by three adjacent nucleotides in the mRNA, a so-called codon, which is recognised by the anticodon of the amino acid delivering tRNA molecule. This highly efficient machinery allows fast polypeptide synthesis with up to 40 couplings per second.[129]

As the biosynthesis even of complicated proteins *in vivo* occurs within seconds or minutes, the relatively tedious classical chemical synthesis of peptides in the laboratory seems to be a rather exhausting enterprise, especially with regard to speed. Nonetheless, is the classical synthesis still a powerful tool compared to recombinant techniques, if the desired amount of substance is in the scale of milligrams or grams. Even more so, since solid phase peptide synthesis has reached a high grade of automation.

3.2 Synthesis in solution

The formation of a peptide bond, resulting in a dipeptide, is seemingly a very simple process. The two component amino acids are connected by a peptide (amide) bond with the elimination of water (*Fig. 3.2)*

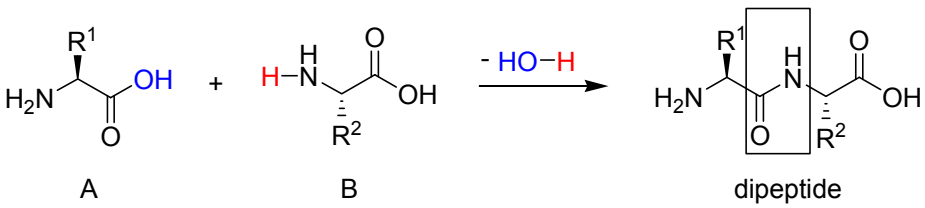

Fig. 3.2 *A simplified scheme of peptide bond formation*

The synthesis of a peptide bond under mild reaction conditions can only be achieved after *activation* of the carboxy function. If the amino function of the carboxy component (A) is unprotected, then formation of peptide bonds occurs in an uncontrolled manner and polymers are formed. Consequently, all functional groups not involved in peptide bond formation must be blocked temporarily. This has led to the development of a high number of specific amino, carboxy and side chain *protecting* groups. Amino acids carrying side chains with reactive behaviour like Tyr, Lys, Cys etc., are usually protected from the beginning and only freed of the blocking groups after the synthesis has been finished. Whether the amino or carboxy group are blocked is determined by the direction of synthesis.

The most common method is the N^{α}-protection of the carboxy activated amino acid, for which two protection groups have become widely accepted, 9-fluorenylmethoxy-

carbonyl (Fmoc) and tert-butoxycarbonyl (Boc). While Fmoc can be cleaved under mildly basic condition, using 20% piperidine or diethylamine in DMF, the Boc removal is performed with strong acids like HCl and TFA. More than 80% of all peptide syntheses follow either of both protection strategies.

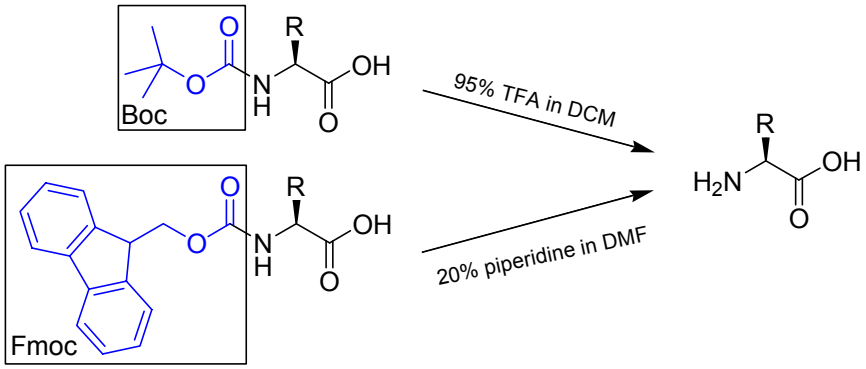

Fig. 3.3 *Boc and Fmoc strategies. Protection groups are removed under indicated conditions after peptide coupling has occurred. This leaves a free amino group for succeeding coupling.*

Solution peptide coupling reactions have employed several types of reagents for the carboxy activation, such as N,N'-dicyclohexylcarbodiimide (DCC), isobutyl chloroformiate (IBCF) and phosphonium salts like BOP. The dipeptides in this thesis have exclusively been prepared with IBCF (*chapter 5*), since the by-products (CO_2 and *i*-butanol) can be easily removed under reduced pressure.

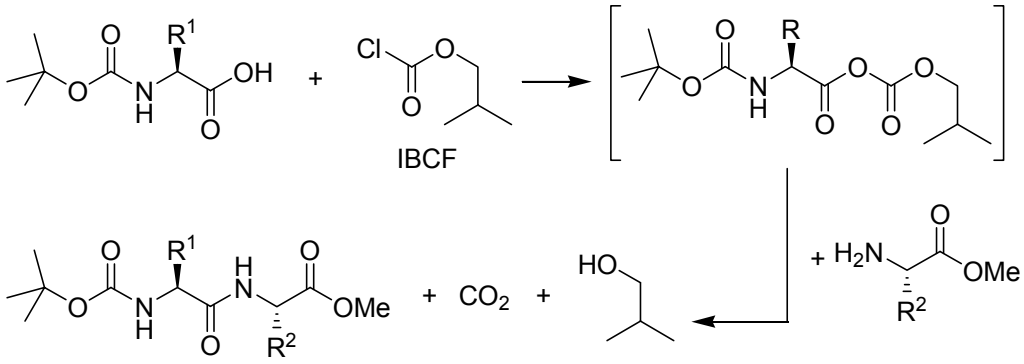

Fig. 3.4 *Activation of the carboxylic group using isobutyl chloroformiate.*

3.3 Synthesis on a solid support

The ingenious concept of peptide synthesis on a solid support, which is now known as SPPS, was developed by Robert Bruce Merrifield in 1963,[4] and provided a major breakthrough in peptide chemistry. In SPPS the peptide chain is assembled in the usual way, starting from the C-terminus. The amazingly simple concept is that the first amino acid of the peptide to be synthesized is connected via its carboxy group to an insoluble polymer that may be easily separated from either solvents or dissolved product by the use of filtration. The general principle is shown in *Fig. 3.5*.

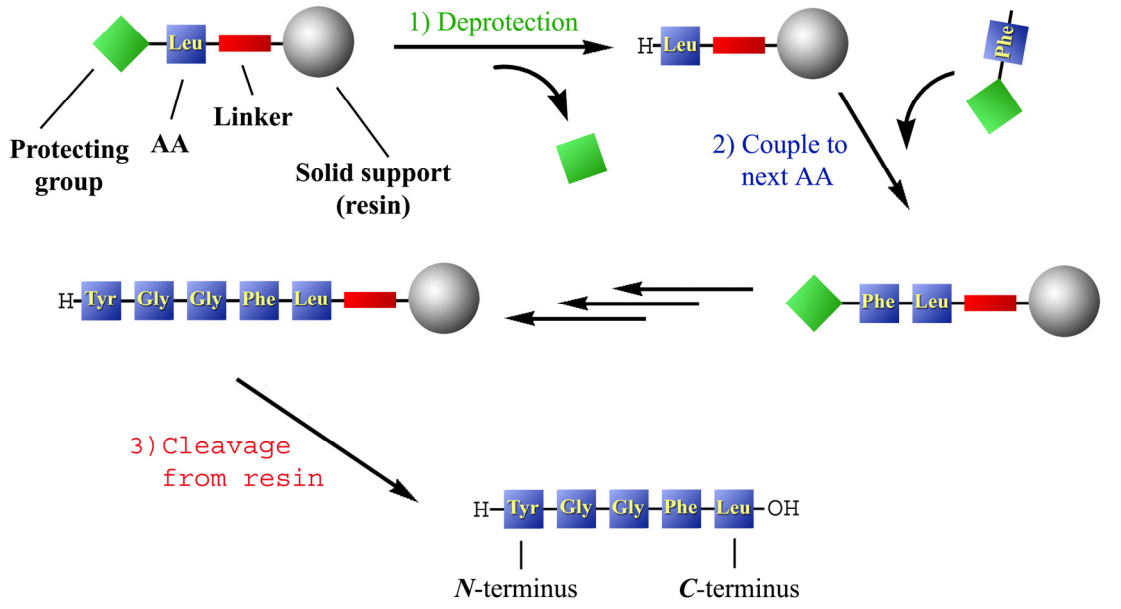

Fig. 3.5 *A scheme of solid phase peptide synthesis as introduced by Merrifield. The protection group (green) is usually Fmoc or Boc. The linker (red) is broken at the end of the synthesis to yield the crude product.*

Resins, generally consisting of cross-linked polystyrene, are offered with a variety of linkers and often with the first N^{α}-protected amino acid already attached.[131] The choice of the linker depends on the desired cleaving conditions which have to be coordinated with the protection strategy. Very common linkers are listed in *Tab. 3.1*, all of which have been used during the syntheses presented in this thesis.

Tab 3.1 *Resins with linkers and the corresponding cleavage conditions*

resin	linker	cleavage	product
4-benzyloxybenzyl alcohol (Wang resin)	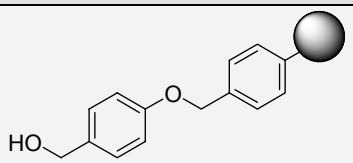	95 % TFA, 2.5 % TIS	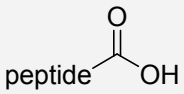 peptide acid
hydroxymethylbenzoic acid (HMBA resin)	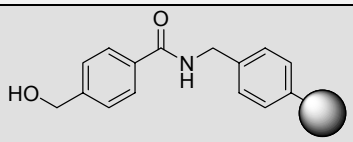	NH_3(sat.) in MeOH	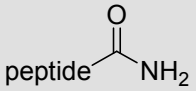 peptide amide
o-chlorotritylchloride resin (Barlos resin)	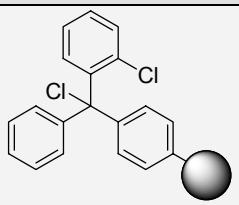	0.5 % TFA, 2.5% TIS	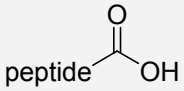 peptide acid

Side chain protection groups should be chosen according to the linker cleavage, to ideally deprotect all side chain functions within the process of cleaving. The addition of scavengers may be necessary to quench meta-stable cations generated from the leaving groups to avoid electrophilic addition to the product. Trisisopropylsilane (TIS) and anisole derivatives are often used as scavengers.

3.4 Neuropeptides – Introduction

Neuro-active peptides are capable of exerting multiple effects in the CNS and elsewhere. The important effects in the CNS have been underlined by increasing numbers of publications that have been reviewed for the years 1980-1985,[132] 1986-1993,[133] and 1994-1999.[134, 135] Among these are regulation of aggression, pain, anxiety, feeding and stress. Some neuropeptides are stored in intracellular vesicles and act as neurohormones upon release in the blood stream. Neuropeptides released into the synaptic cleft are neuromodulators that inhibit the action of excitatory neurotransmitters, or neuromediators which prolong the action of neurotransmitters.

Opioid δ-, μ- and κ-receptors, as well as receptors for bradykinin, tachykinins, angiotensin, neuropeptide Y, vasointestinal peptide and somatostatin have been cloned and characterized. These G-protein-coupled receptors (GPCR) share as a common feature seven transmembrane helices. An extracellular signal is transmitted into the cell and amplified by coupling to G proteins.[136]

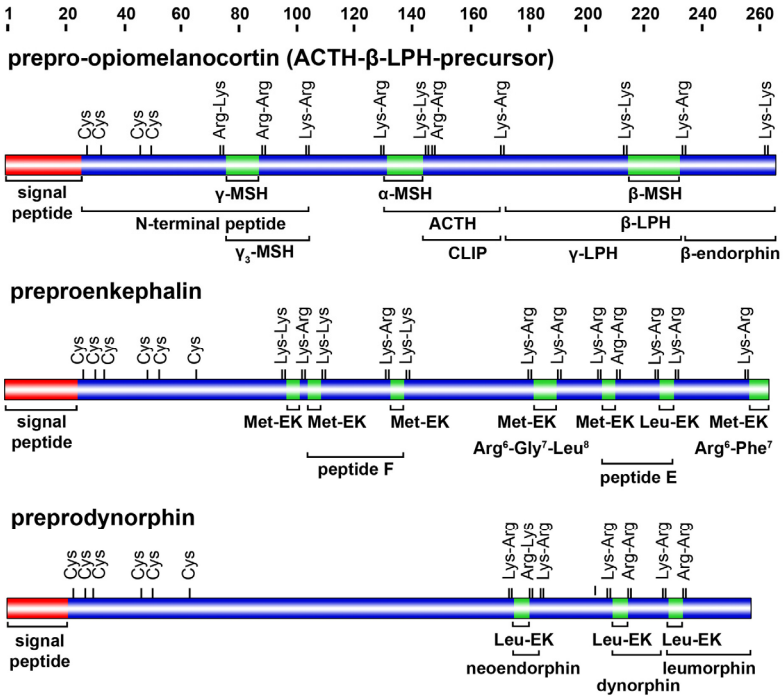

Fig. 3.6 *Schematic representation of the three main sequences of opioid peptide precursors. EK = enkephalin.*

Neuropeptides are synthesized in the form of large protein precursors (*Fig. 3.6*) that undergo protolytic processing to yield the bioactive peptides.

The signal peptide sequence is required for vectorial transport across the membranes of the ER. The conformation of the signal peptide, usually a β-turn, is important for the recognition of the exact cleavage site. The cleavage at pairs of basic amino acids (Lys, Arg) is catalyzed by trypsin-like endopeptidases (prohormone converting enzyme). Post-translational processing can generate a number of active peptides from a single precursor protein[137] which has for example been demonstrated for POMC, this being the common precursor for ACTH, β-endorphin, MSH, corticotropin-like intermediate lobe peptide (CLIP), and related peptides.[138]

3.5 Biological properties of [Leu^5]-Enkephalin

Opiates such as morphine have been widely used by clinicians both for blockade of severe pain and for anesthesia. For more than thousand years has opium been the natural source for morphine, and it was surprising to find that nature provided morphine not only as a plant product (from *papaver somniferum*) but also (as structurally related opiates) in mammals, albeit in very small amounts.[139]

Collier first postulated the existence of "endogenous morphine" in 1972 and the binding of endogenous opioid receptor ligands was independently demonstrated one year later by three groups.[140-142] In 1975 Hughes and co-workers reported the discovery of the first endogenous peptide ligands[143] followed by the characterization of four major types of morphine receptors (μ, δ, κ and σ) a few years later.[144]

The opioid peptides first isolated from porcine brain were named Met-enkephalins and Leu-enkephalins, respectively, according to their C-terminal amino acid (*Fig. 3.7*).

H-Tyr^1-Gly-Gly-Phe-Met^5-OH **Met-Enk**

H-Tyr^1-Gly-Gly-Phe-Leu^5-OH **Leu-Enk**

Fig. 3.7 *Sequences of methionine enkephalin (left) and leucine enkephalin (right). The latter has been exclusively used for the research presented in this thesis.*

These enkephalins (from enkephalos = brain) were found to occur naturally and bind as physiological agonists to the opioid receptors mainly found in the brain, but also being expressed in the spinal region[145] and colon.[146] The structure of [Leu^5]-Enkephalin in solid state could be elucidated by x-ray diffraction, revealing 4 different conformations in the asymmetric unit.[147] These findings indicated the high flexibility of the pentapeptide.

The similarities between enkephalin, morphine and naloxone, which is a morphine antagonist, can be seen in *Fig. 3.8*. The tyrosine- and N-terminal amino-functions are essential for the receptor affinity.[148]

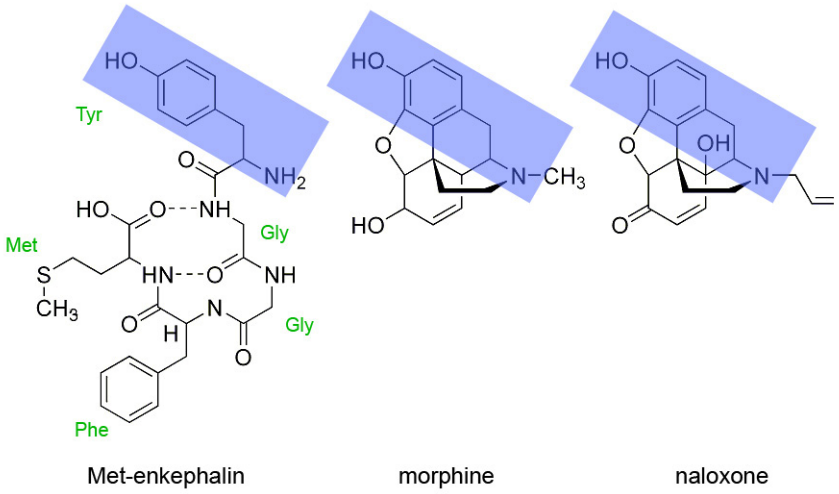

Fig. 3.8 *Comparison of structural motifs between different opioid receptor binding substances.*

Besides the enkephalins, endorphins and dynorphins are the most important of these neuropeptides. They all originate from three large precursor proteins, shown in *Fig. 3.6*. These typical opioid peptides share the N-terminal sequence H-Tyr-Gly-Gly-Phe-, and most of the members bind to more than one type of opioid receptor, though certain selectivity is clear. The so-called “atypical” opioid peptides originate from a variety of precursor proteins, with different N-terminal amino acid sequence and a conserved N-terminal tyrosine residue, which is indispensable for binding to opioid receptors.[149]

4 Selective labelling of [Leu]-Enkephalin with Ferrocene / Cobaltocinium

4.1 Synthesis of metal markers

As shown in the introduction chapters some attempts to label biomolecules with metallocenes, mostly ferrocene,[100] have been made so far. Tartar and co-workers presented an artificial amino acid ferrocenylalanin as a substitute for phenylalanine (*Fig. 1.7*).[94] However, the bioconjugates showed heavily reduced activity and the isolation of enantiomerically pure compounds was tedious. Metzler-Nolte *et al.* reported the stepwise synthesis of ferrocenyl amines in solution,[150, 151] which could be successfully coupled to the C-terminus of amino acids and peptides. Since the synthetic direction in solid phase synthesis is mostly from C-terminus to the N-terminus, a marker containing a carboxy group would be ideal for N-terminal labelling.

The simplest metal markers, which fulfil this demand, seem to be the carboxylic acid derivatives of ferrocene and cobaltocenium. These compounds are known to be stable,[152] can be easily prepared[153] and can be activated using standard amino acid coupling reagents (*chapter 3*).[154]

The synthesis of ferrocenecarboxylic acid **1** is a two step reaction as reported by Reeves.[153] The two synthetic steps comprise a Friedel-Crafts mono acylation followed by hydrolysis (*Fig. 4.1*)

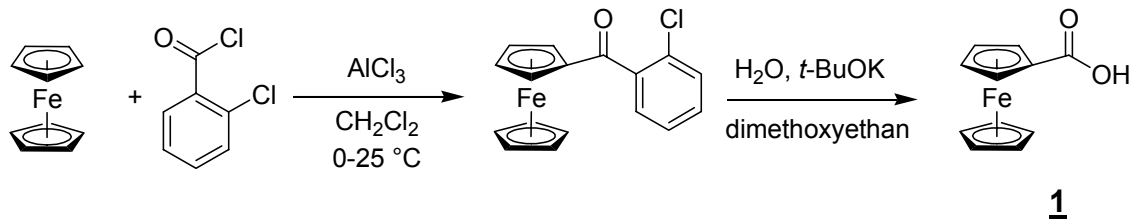

1

Fig. 4.1 *Synthetic pathway for ferrocene carboxylic acid as suggested by Reeves et al.*

This synthesis is very convenient and offers high yields of 80% referred to starting amount of ferrocene. The product is a brown, air-stable solid with a melting point of 220 °C. The crude compound can be recrystallized from toluene to improve purity, which is not necessary for most synthetic tasks, though. The EI mass-spectrum shows a signal at m/z = 230 with the typical isotopic pattern of iron (^{56}Fe, 100%; ^{54}Fe, 6.4%; ^{57}Fe, 2.3%). This pattern should be kept in mind, since it can be used in mass spectra of bioconjugates for fragment identification. ^{1}H NMR signals are clearly resolved and correspond to the literature. Two pseudo-triplets representing each 2 protons of the substituted Cp-ring and one singlet of 5 protons for the unsubstituted Cp-ring can be observed between 4.2 and 4.8 ppm.

Cobaltocenium carboxylic acid was synthesized as the hexafluorophosphate salt **2** according to Sheats and Rausch,[118] who also presented elaborate works on cobaltocenium salts in general.[117]

In the first step methylcyclopentadiene and cyclopentadiene are reacted with anhydrous $CoBr_2$ under argon atmosphere to yield methyl-, dimethyl- and unsubstituted cobaltocenium. The reaction is carried out in dried pyrrolidine and takes 12 h of stirring. After removal of the organic solvent *in vacuo*, dissolution in water and extraction with diethylether, precipitation of the cationic compounds is performed with the addition of sodium hexafluorophosphate in aqueous solution.

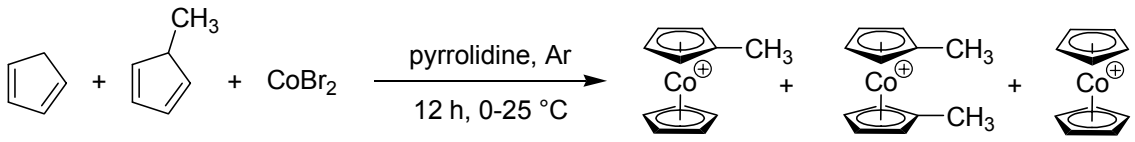

Fig. 4.2 *synthetic scheme of methylcobaltocenium*

To the mixture of methylcobaltocenium (max. 50% of starting material) and the two by-products sodium permanganate and NaOH are added, and the aqueous solution is heated at reflux for a prolonged time of 8 h, which slightly improved the yield compared to literature (2 h). The obtained mono- and dicarboxy compounds can be separated from unsubstituted cobaltocene by the addition of sodium hexafluorophosphate followed by filtration. The two carboxy cobaltocenium salts are then precipitated by the dropwise addition of 6N HCl. Contrary to the mono acid which shows good solubility in acetone,

is cobaltocenium dicarboxylic acid virtually insoluble. The isolation of the desired monocarboxylic acid by soxhlet extraction using acetone seems to be superior to the simple washing process presented in literature.

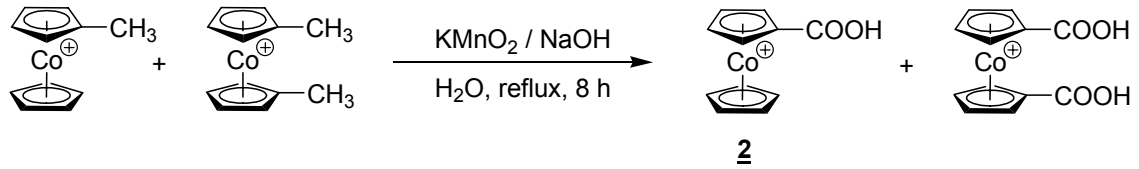

2

Fig. 4.3 *Synthesis of cobaltocenium carboxy compounds from corresponding methyl derivatives by means of oxidation in an aqueous solution*

Cobaltocinium ions can be electrochemically reduced to the corresponding cobaltocenes at negative potentials between -0.8 and -1.5 V, which is strongly influenced by the substituents at the Cp-rings. The electron withdrawing nature of the carboxy group lowers the potential drastically, thus enabling distinction between the desired product and potential by-products, which is useful for purity estimation (*Fig. 4.4*).

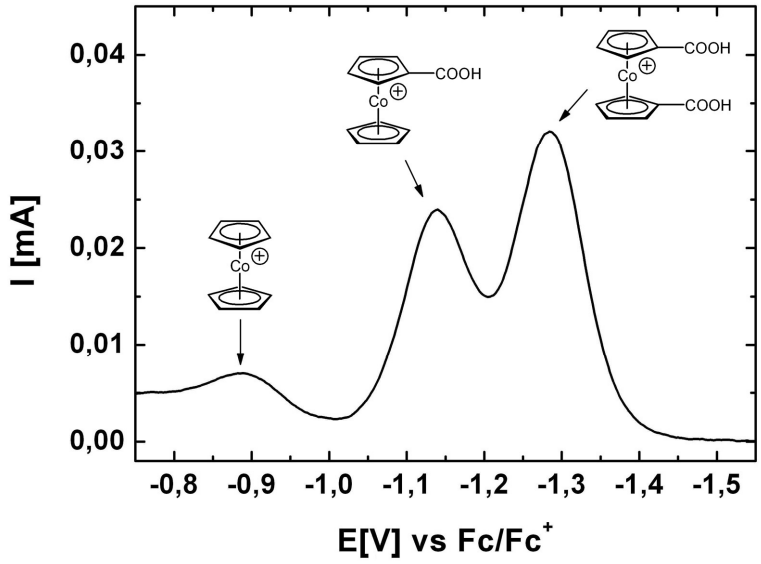

Fig. 4.4 *Square Wave voltammogram of a mixture of cobaltocinium compounds obtained as a crude product, recorded in acetonitrile using TBABF as supporting electrolyte. Detailed conditions for all electrochemical experiments are given in chapter 8.*

The EI mass-spectrum of the purified compound **2** shows a signal of 40 % intensity at m/z = 233, representing the cation. Because cobalt only occurs in its single isotope ^{59}Co,

no metal related isotopic pattern can be observed. Infrared and NMR spectra show the reported signals. The ^{1}H NMR looks similar to that of ferrocenecarboxylic acid but shifted about 1 ppm lower field. Signals appear between 5.2 and 6.0 ppm. Compared to **1**, the four signals in ^{13}C NMR are shifted approximately 20 ppm to the lower field, as well. These shifts originate from the de-shielding effect of the cationic charge.

4.2 Synthesis of [Leu]-Enkephalin

4.2.1 Synthesis of H-Enk-OH 3

[Leu^{5}]-Enkephalin, in the following simply referred to as "Enk", is a neuropeptide consisting of 5 amino acids of the sequence H-Tyr-Gly-Gly-Phe-Leu-OH. The solid phase synthesis of this relatively small molecule was carried out on Wang resin, following Fmoc protection strategy. The Wang or p-hydroxybenzyl alcohol linker can be cleaved by 95% TFA, releasing the product with a carboxylic acid at the C-terminus. The only function to be protected in Enk is the hydroxy group in the tyrosine residue that can be protected by a *t*-butyl group, which is removed within the cleavage procedure.

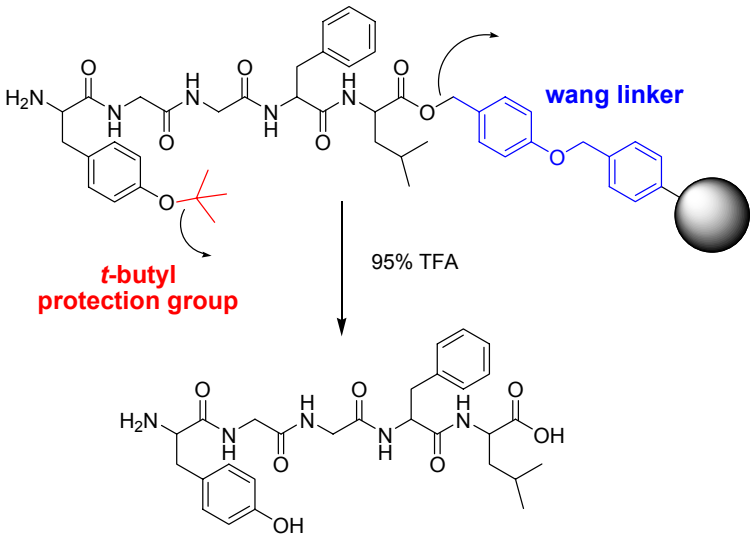

Fig. 4.5 *H-Enk-OH is released from Wang resin by cleavage with 95% of TFA. The Tyr protection group is simultaneously removed under the same conditions.*

N^{α}-protected amino acids have been reacted with TBTU/HOBt prior to coupling to yield the activated OBt-esters, as shown in *Figure 4.6*. To facilitate the deprotonation of the acid and thus the formation of the carboxy activated form, ten equivalents of DIPEA were added.

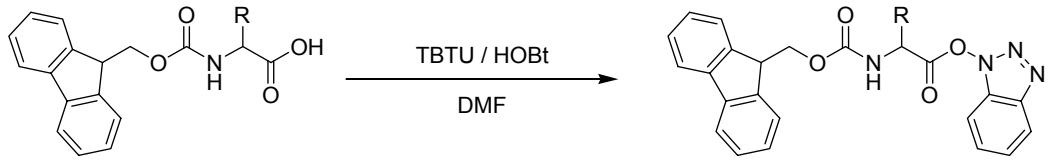

Fig. 4.6 *Conversion of Fmoc-protected amino acids into their activated benzotriazole esters*

After the final step of Fmoc deprotection and excessive washing with DMF and DCM, the resin was dried *in vacuo* and treated with a cleavage mixture of 95% TFA, 2.5% H_2O and 2.5% of TIS, acting as a scavenger, for 3 hours. After removal of the cleavage cocktail under reduced pressure, the crude product was precipitated from cold ether. All following solid phase peptide syntheses correspond to this roughly explained standard procedure if not mentioned explicitly. A more detailed description of SPPS can be found in *chapter 8* (experimental section).

Preparative RP-HPLC purification and subsequent lyophilization of H-Enk-OH **3** resulted in an off-white powder. Negative electron spray ionisation mass spectrometry (ESI-MS, neg.) shows a strong signal at 1109.18 m/z representing the dimeric, negatively single charged 2M-1 Species. The base peak at 554.27 m/z corresponds to M-1.

The ^{1}H NMR spectrum in DMSO-d_6 shows all expected signals except for the N-terminal amine protons (*Fig. 4.7*). The same spectrum measured in MeOH reveals only slight changes in shifts but lacks all five amide and the carboxyl proton signals, caused by proton/deuteron exchange with the solvent. Assignment of signals was supported by HH-COSY 2D NMR.

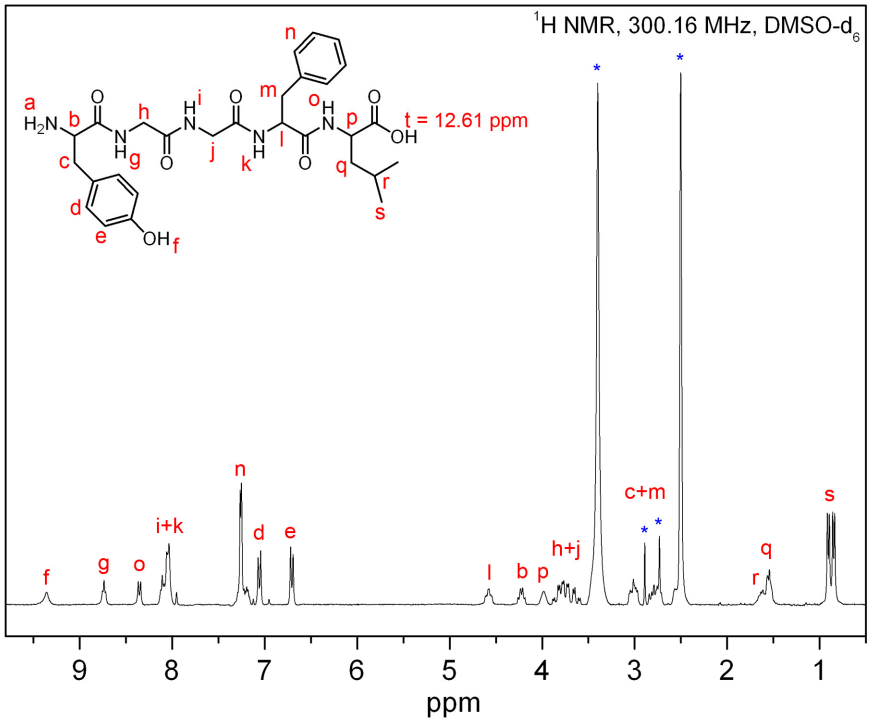

Fig. 4.7 *Proton NMR spectrum of H-Enk-OH **3**, measured in DMSO-D$_6$ at 300.16 MHz.*

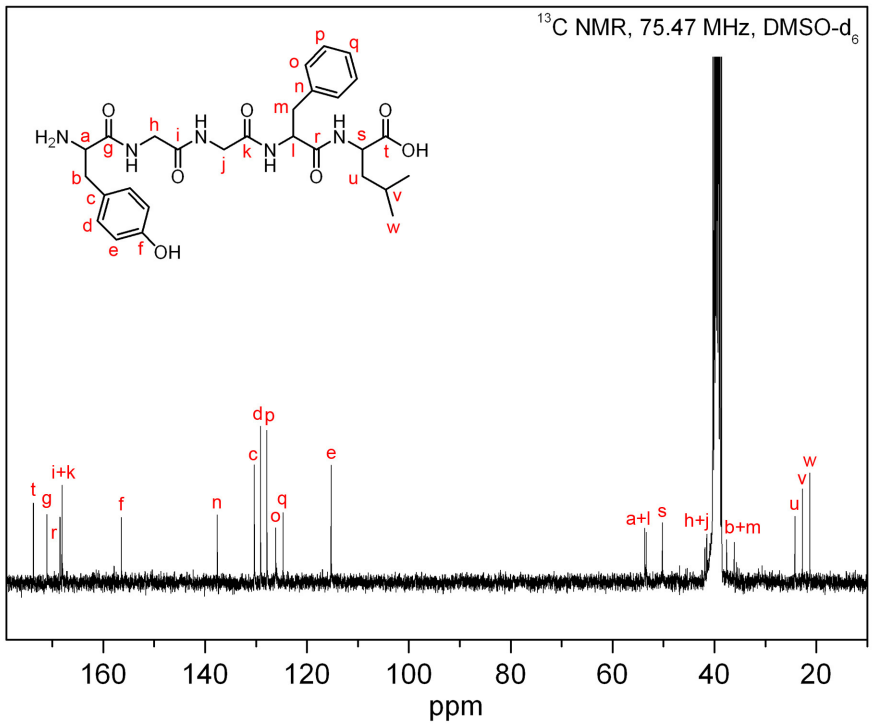

Fig. 4.8 *^{13}C NMR spectrum of H-Enk-OH **3**, measured in DMSO-D$_6$ at 75.47 MHz.*

^{13}C NMR shows all expected signals, although C_α(Gly) and C_β(Phe, Tyr) signals are close to the downfield and upfield sides of the solvent signal (*Fig. 4.8*).

The white substance shows slightly hygroscopic behaviour and is to be stored under argon. Freeze-drying improves the substances stability, because traces of trifluoro acetic acid, dimethylformamide, diethylether and other impurities, originating from synthesis, cleavage or workup procedures, are removed. It was also observed that freeze-dried samples still showed high purity in HPLC even after prolonged storage, whereas crude products seemed to be more sensitive to decomposition. This is even more true for metallocene labelled peptides.

4.2.2 Synthesis of Ac-Enk-OH 4

The preparation of acetyl enkephalin, Ac-Enk-OH **4**, was carried out similar to that of **3**. After the final Fmoc deprotection step, the resin was treated with a mixture of Ac_2O, 2,6-Lutidine, N-methylimidazol and THF (1:1:1:7) for 60 min.[131]

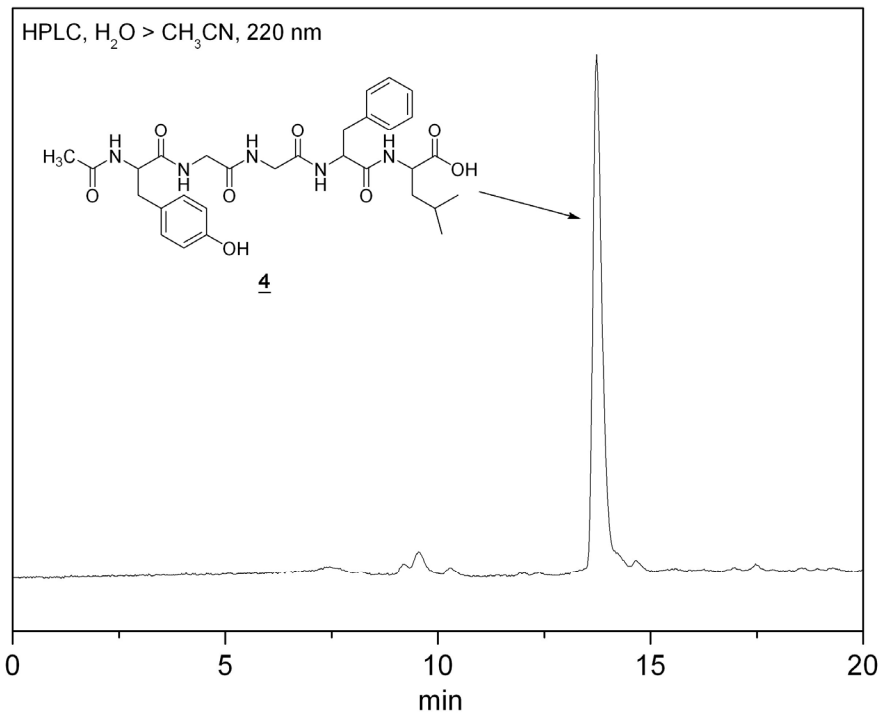

Fig. 4.9 *HPLC chromatogram of crude Ac-Enk-OH **4**, detected at a wavelength of 220 nm.*

After cleavage a slightly yellow powder of 95% purity was obtained, and no further work-up was required, as demonstrated by the HPLC spectrum in *Fig. 4.9*. All analytical HPLC spectra were run using a gradient from 5% CH_3CN in H_2O to 100% CH_3CN in 20 min, with both eluents containing 0.1% of TFA for improved solubility of peptides. Like in the case of **3**, ESI mass spectra indicate that a dimer is formed during mass spectrometry, as well. This could only be observed with the simple peptides **3** and **4**, while metallocene marked peptides only showed monomeric peaks in MS, but tend to be multiply charged (*Fig. 4.10*).

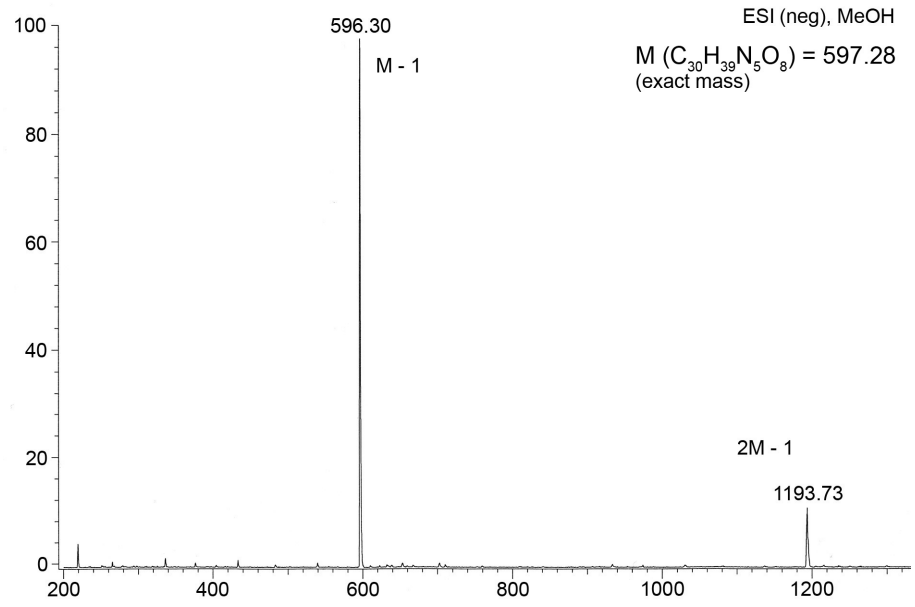

Fig. 4.10 *ESI mass spectrum of Ac-Enk-OH **4***

All signals in ^1H NMR are almost identical to those in H-Enk-OH **3** except for the acetyl peak at 1.75 ppm with a correct integral of 3 protons. One additional ^{13}C signal at 22.4 ppm appears for this acetyl group. UV spectra for both **3** and **4** show strong absorbance at 220 nm related to peptide bond absorption and at 260 nm from the aromatic systems of phenylalanine and tyrosine. As expected, neither compound underwent a redox reaction in electrochemical studies between the potentials of +/- 1000 mV. These experiments were necessary to prove that the peptide itself is stable under the conditions of electrochemical detection of the metallocene markers.

4.3 N-terminal labelling of [Leu]-Enkephalin

4.3.1 Synthesis of Ferrocenoyl-Enkephalin (Fc-CO-Enk-OH) 6

In order to bind ferrocenecarboxylic acid as a sixth amino acid to the N-terminus of enkephalin, it has to be carboxy activated in the same way as a regular amino acid. The most practical approach uses the standard activation protocols for solid phase peptide synthesis, since the aim is to establish a facile method for the labelling of peptides on the resin. However, after activation of ferrocenecarboxylic acid with HOBt and DCC, the activated ester could be isolated and purified by column chromatography, and although the compound is highly reactive towards amino groups it showed prolonged stability under inert atmosphere for weeks.

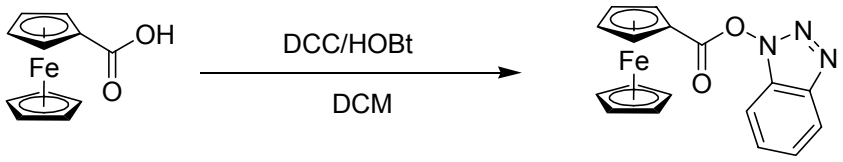

5

Fig. 4.11 *Benzotriazole ester of ferrocenecarboxylic acid **5** as the reactive form for building peptide bonds*

NMR spectra show all desired signals and EI mass spectrometry reveals a peak at 347 m/z which corresponds to the M^+-peak of **5**. All data were similar to that reported by Kraatz *et al.* who have studied and characterized **5** before.[154, 155]

After some successful attempts to couple Fc-OBt to amino acids the system was found to be suitable for the labelling of a peptide on the solid support. As a consequence, enkephalin was synthesized on Wang resin and ferrocene carboxylic acid, this time treated with TBTU/HOBt in DMF to form **5**, was attached as the last amino acid. As an indication of a successful reaction the resin changed color from slightly yellow to dark brown. After the cleavage from the resin had been carried out with standard Wang cleavage solution (95% TFA, 2.5% H_2O and 2.5% TIS) the color changed from red to green

pointing to a possible oxidation of ferrocene. As a fact **6** could only be isolated by HPLC-purification in very low yield of 10%.

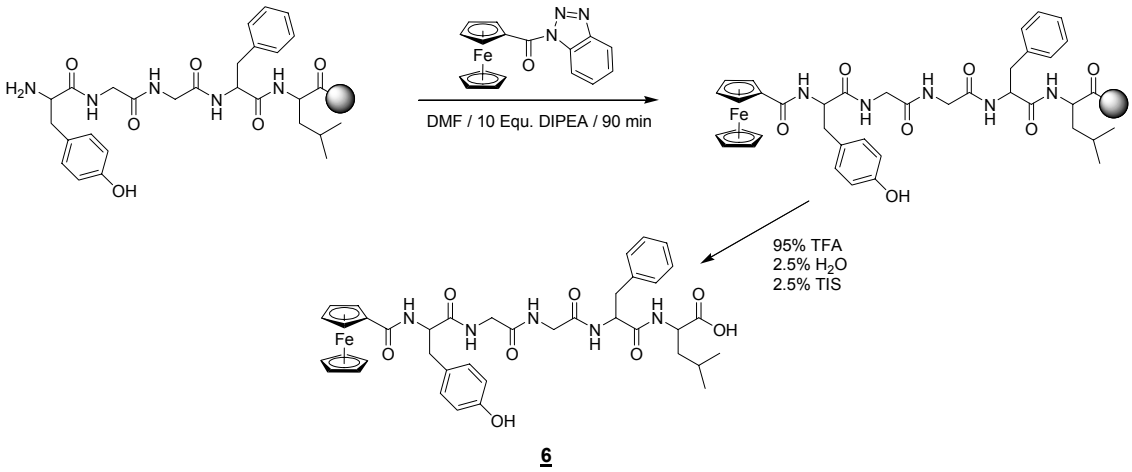

Fig. 4.12 *Synthetic scheme of the reaction between Enk and Fc-OBt to form Fc-CO-Enk-OH **6** on the resin. Cleavage under standard conditions leads to very small yields.*

To prevent the ferrocene from being oxidized during the cleavage procedure an anti oxidizing agent had to be used. First ascorbic acid had been added to the cleavage mixture which resulted in a better yield of approximately 50%, with no good reproducibility, though. The addition of phenol gave yields of 90% and a very smooth workup (*chapter 8*) and was therefore used in all following preparations which contain the ferrocene moiety.

Ferrocenoyl-Enkephalin **6** is a light red solid and stable to air and water. ESI (pos.) mass spectrometry shows clear single charged product peaks at m/z 768.4 $(M+H)^+$, 790.5 $(M+Na)^+$, 806.4 $(M+K)^+$, whereas ESI (neg.) only contains one single peak at m/z 766.4 $(M-H)^-$. No dimers could be observed in any mass spectra. Proton NMR reveals most signals to be identical to those of **4** except for the metallocene Cp-signals between 4 and 5 ppm, which significantly indicate the presence of the ferrocene group in the peptide. The amide proton of the ferrocene peptide bond is the one most up-field at 7.78 ppm, which could be confirmed by HH-COSY NMR.

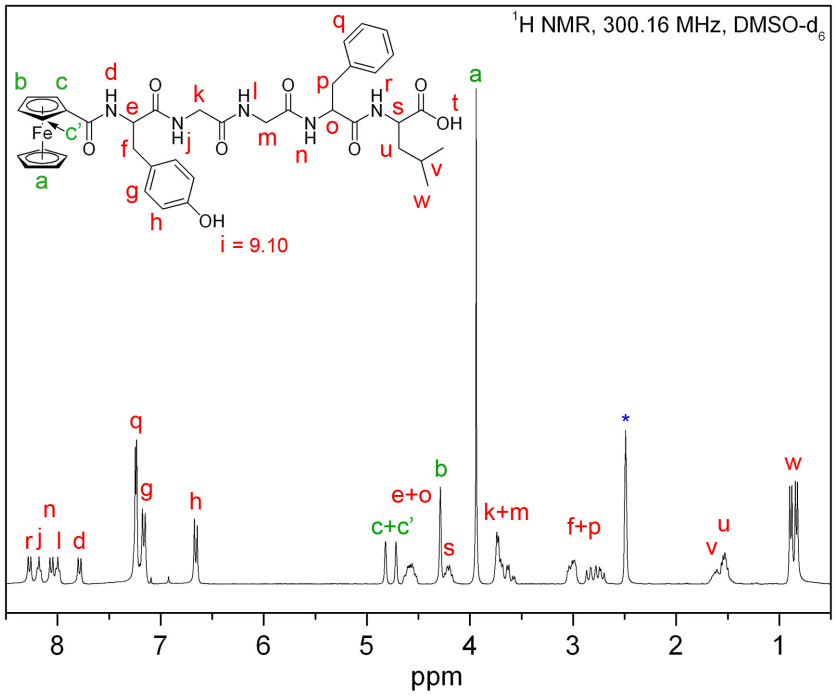

Fig. 4.13 *The ^{1}H NMR of Fc-CO-Enk-OH **6** shows four signals for the ferrocene group (green). C and C' are magnetically different, thus resulting in the formation of two singlet signals*

The cyclopentadiene protons show an interesting pattern, because the nuclei on C_2 and C_5 seem to be different (c and c' in *Fig. 4.13*). This is confirmed by ^{13}C NMR, where C_2 and C_5 result in two signals, as well. The reason for this is the proximity to the closest chirality center, like indicated in *Fig. 4.14*. The distance between the chiral tyrosine C_α and the cyclopentadiene carbons C_2 and C_5 is only 4 carbon bonds, leading to a slightly different chemical environment for both atoms. Carbons C_3 and C_4 are equivalent, because they are too far away from the chiral center to be influenced anymore. The electronic properties of cobaltocenium are much different from ferrocene so that this effect cannot be observed here. When a chiral center is present but too far away from the ferrocene group, equivalency of C_2 and C_5 of the substituted cyclopentadiene results in a singlet for both ^{1}H and ^{13}C NMR spectra, which will be shown by the example of side chain derivatives.

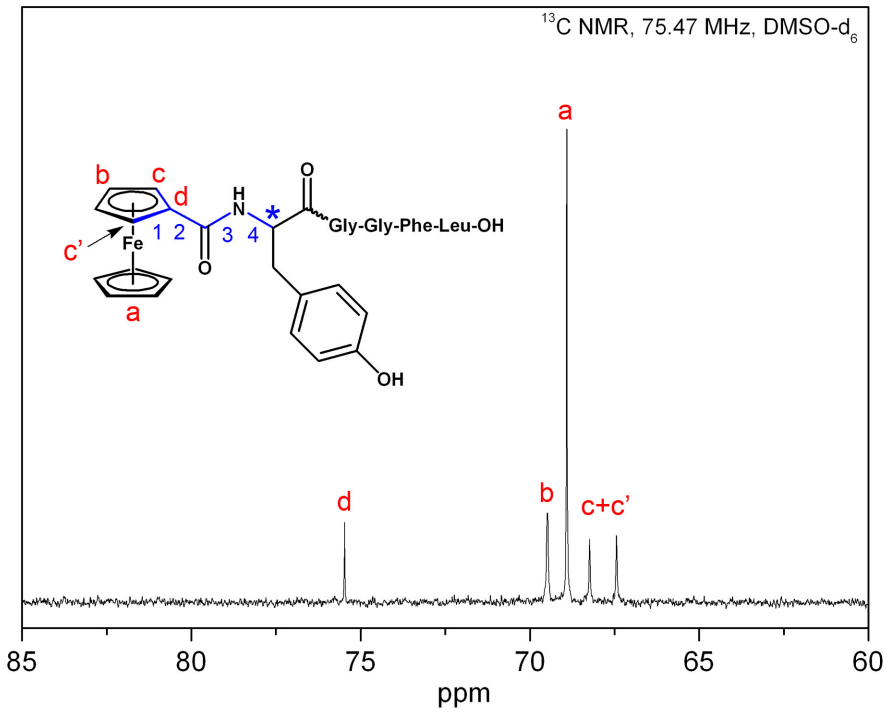

Fig. 4.14 *Chirality of the tyrosine C_α carbon leads to a different chemical environment at the cyclopentadiene ring of ferrocene.*

Electrochemical measurements revealed a one-electron, fully reversible behaviour for the ferrocenyl group with a half-wave potential of E½ = 214 mV and a peak separation of 74 mV.

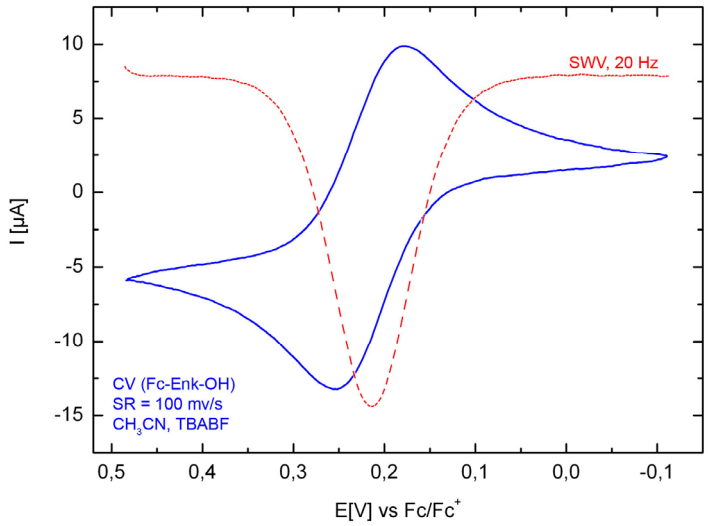

Fig. 4.15 *Overlay of a square wave and cyclovoltammogram of **6**, measured in acetonitrile with TBABF as the supporting electrolyte.*

UV spectra showed a weak absorbance for ferrocene at 444 nm with a molar extinction coefficient of ε = 210 l/mol·cm, and two stronger maxima at 266 and 215 nm with ε_{266} = 5550 and ε_{215} = 27920 l/mol·cm, respectively. The aromatic π-systems of phenylalanine and tyrosine are responsible for the absorbance at 266 while peptide bonds absorb best at 210-220 nm. For this reason all HPLC measurements are recorded at both 220 and 254 nm.

4.3.2 Synthesis of Fc-CO-Enk-NH_2 7 and Fc-CO-Enk-$NHNH_2$ 8

To circumvent the issue of ferrocene oxidation in strong acidic cleavage media, a different resin with a base labile linker was employed. The hydroxymethylbenzoic acid linker (HMBA) releases the product through basic treatment with a variety of functional groups at the C-terminus as shown in *Tab. 4.1*.

Tab 4.1 *Common cleavage conditions for HMBA resin and the corresponding peptide products*

Cleavage reagent	Product
1. NH_3 / MeOH	Peptide carboxamide
2. NH_2NH_2	Peptide hydrazide
3. Aq. NaOH	Peptide acid
4. MeOH / DIPEA	Peptide methylester
5. $NaBH_4$ / EtOH	Peptide alcohol

Before cleaving the peptide from HMBA derivatized resins, it is important that the side-chain protection groups are removed. This is generally achieved by treating the peptidyl resin with 95% TFA, which had to be avoided in this case as the strong acidic media seemed to accelerate ferrocene decomposition. Therefore 2-chlorotrityl as a tyrosine protection group had been chosen, since it can be removed by dilute acid solutions containing 1% TFA.

After synthesis of enkephalin on the resin and the following coupling of ferrocene carboxylic acid, the side-chain protection group was removed by repetitive treatment with a mixture of 1% TFA and 5% TIS in DCM. The peptide cleavage itself was performed using ammonia saturated methanol at 0 °C (*Tab. 4.1*, option 1, product **7**) and 5% hydrazine in DMF (*Tab. 4.1*, option 2, product **8**) for 24 h and 3 h, respectively. Both methods had lower yields of approximately 50%, though, and had to be purified by HPLC, since the crude products contained reasonable amounts of by-products either

originating from the synthesis or more likely from side-chain deprotection and cleavage. Non-labelled [Leu^5]-enkephalin could be identified in major HPLC peaks of both reactions.

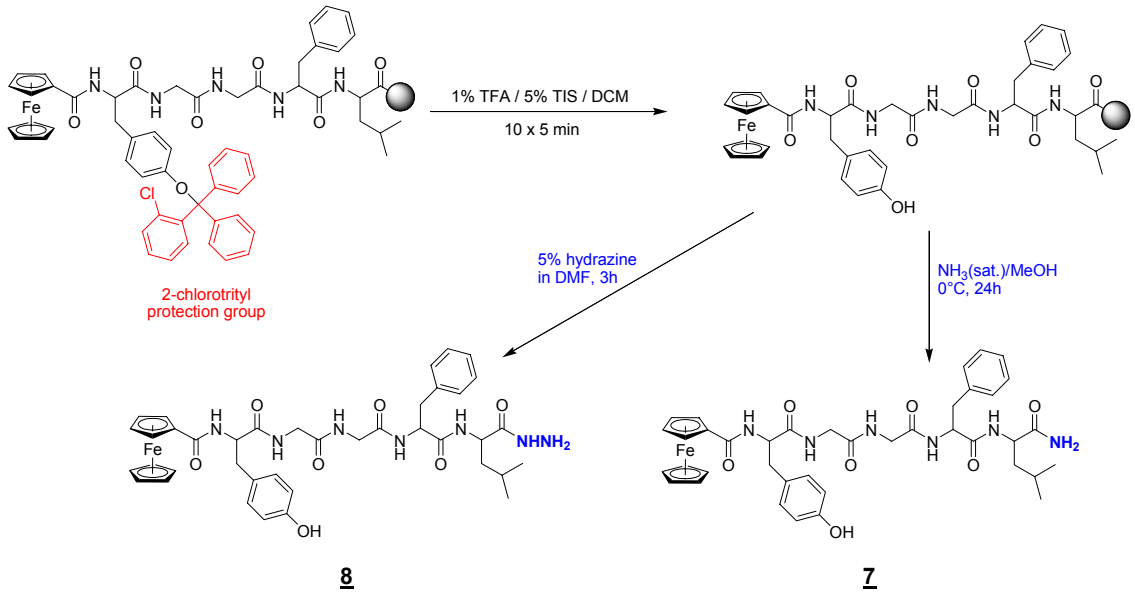

Fig. 4.16 *Reaction scheme of HMBA based Fc-CO-Enk synthesis. Cleavage with different reagents leads to different C-terminal functions.*

Both **7** and **8** show almost the same spectroscopic properties as Fc-CO-Enk-OH **6**, like expected. ESI (neg.) mass spectra show the correct mass with peaks at 765.3 for **7** and 780.3 for **8**, and C-terminal amino and hydrazide amide protons can be observed in ^{1}H NMR at 8.01 ppm and 8.21 ppm. No signal was found for the hydrazine NH_2 group, though. ^{13}C NMR reveal all expected peaks, very similar to **6** and electrochemical behaviour was identical, as well, for both compounds showed reversible oxidation processes at ca. 220 mV. The ferrocene center is obviously unaffected by the C-terminus and the type of functional group attached to it. While these basic cleavage methods evade the problematic decomposition of ferrocene groups they have major drawbacks concerning yield and reproducibility. That is why most of the compounds presented in this thesis were preferably synthesized on Wang resin and cleaved by standard acidic cleavage solutions containing a reducing additive like phenol or ascorbic acid. These additives could be easily removed from the precipitated peptide by repetitive washing with cold ether. Details on selected procedures are given in the experimental section for each compound.

4.3.3 Synthesis of Cobaltocenium-Enkephalin (Cc-CO-Enk-OH) 9

Cobaltocenium carboxylic acid is expected to react in the same way like its isoelectronic congener ferrocene. In addition, no oxidation during synthesis or cleavage is expected, as can be deduced from the electrochemical studies, which only show a reductive event at very high negative potentials between -1200 and -1500 mV (*Fig. 2.4 and 4.4*). The positive charge carried by cobaltocenium ions will change the bioconjugates biological properties drastically, compared to a ferrocene marked species, making this marker an interesting alternative.

The synthetic procedure carried out was similar to that of Fc-CO-Enk-OH **6**. Because cobaltoceniumcarboxylic acid, available as the hexafluorophosphate salt, showed reduced solubility in DMF, an extra addition of DIPEA was necessary, which accelerated the deprotonation of the acid group and thus the formation of the activated benzotriazole ester. Early experiments clearly indicated that the reactivity of activated cobaltocenium carboxylic acid (Cc-CO-OBt) was somewhat lower than that of ferrocene, since HPLC analysis of the freshly cleaved crude product showed major peaks, which could be identified as unlabelled peptide. Therefore prolonged coupling time was granted to the labelling reaction (3 h instead of 60 min), resulting in a total conversion to Cc-CO-Enk-OH. Because the reaction was carried out on Wang resin, again *t*-butyl protection was chosen for the tyrosine residue as it had been cleanly removed during cleavage procedure before. The counter-ion of PF_6^- was completely exchanged by TFA^- from the cleavage mixture.

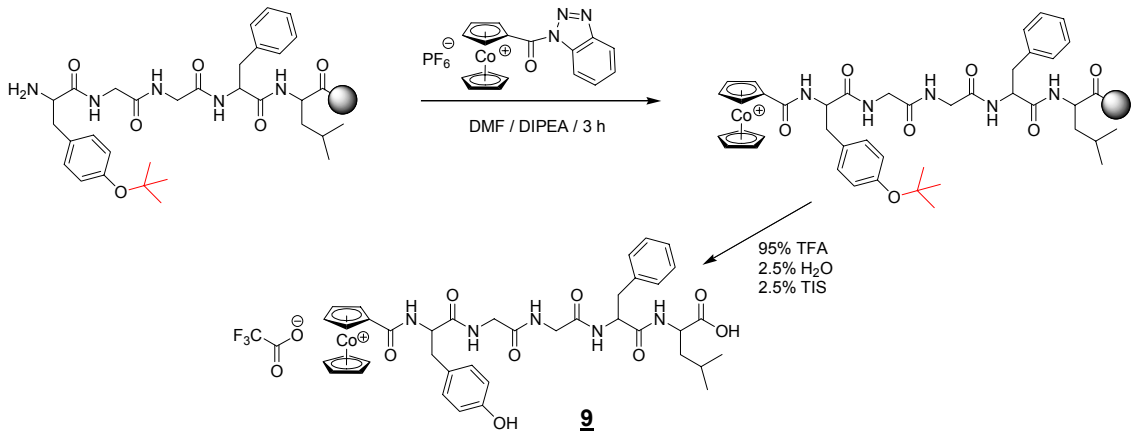

Fig. 4.17 *Reaction scheme of Cc-CO-Enk-OH **9**. Almost full coupling efficiency is reached after 3 h of reaction time. The resulting product is the TFA salt of the cationic bioconjugate.*

ESI (pos.) mass spectrometry of the slightly yellow powder shows a single peak at m/z = 770.5 in accordance with the calculated mass for the cationic species Cc^{+}-Enk-OH of 770.26 g/mol. ^{1}H NMR spectra display all amide protons clearly resolved, as well as the significant Cp-signals of cobaltocenium between 6.5 and 5.5 ppm. Compared to ferrocene, these peaks are shifted down-field due to the positive charge at the metal center and the related de-shielding effect (*Fig. 4.18*). Another noteworthy observation is the fact that the C_2 and C_5 atoms of the unsubstituted Cp-ring show almost the same resonance and do not split clearly into two signals like those of the corresponding ferrocene compound.

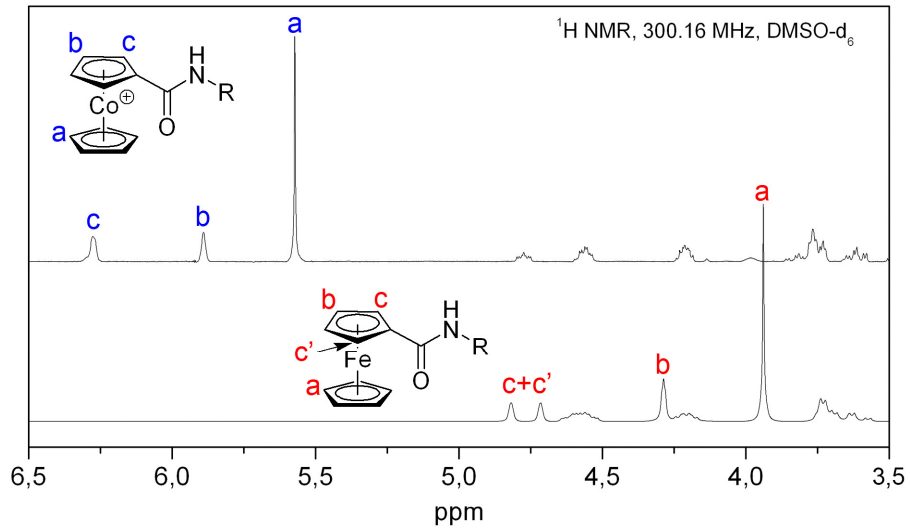

Fig. 4.18 *Positive charge at the cobalt center has a de-shielding effect on the ring current of the Cp-rings, causing a down-field shift. C_2 and C_5 carbon atoms (c+c') seem to be more equivalent than those in ferrocene.*

However, the signal caused by c and c' is always broader than the one of b, indicating that the chiral center of tyrosine does have an effect on the ring atoms, even if it is much smaller, compared to ferrocene. ^{13}Carbon signals for the Cp-system underline this, as only four peaks between 83 and 93 ppm are visible. Here, too, a down-field shift is observed. The electrochemical behaviour of the cobaltocenium labelled enkephalin was expected to be only of partly reversible nature. The reduced cobaltocene species is itself a very good reducing agent and tends to transfer the electron to any nearby intra- or intermolecular electron acceptor, thereby undergoing oxidation again. This non-reversible behaviour can be observed in cyclovoltammetry as shown in *Fig. 4.19*.

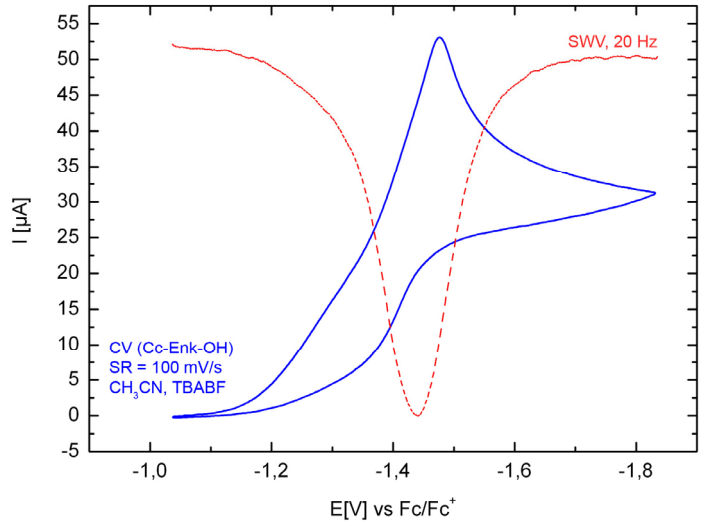

Fig. 4.19 *A cyclovoltammogram of **9**, recorded in acetonitrile, demonstrates an irreversible one-electron reduction of cobaltocenium-enkephalin. The Half-wave potential is E½ = 1439 mV.*

4.4 Side-chain labelling of [Leu]-Enkephalin

While the N-terminal labelling of peptides is an easy way to introduce a metal marker into the desired biomolecule it might be desirable to attach the organometallic probe to a side-chain function and leave the N-terminus untouched. The precise positioning of the metal center inside a possible secondary structure or the decrease in receptor binding activity might be possible reasons. An alkylated or free N-terminal amino group are known to be essential for the receptor binding of enkephalin, for example.[156] This is also true for most of all drugs that bind to opiate receptors (compare *Fig. 3.8*). Enkephalin offers 4 easily accessible labelling sites which are shown in the figure below.

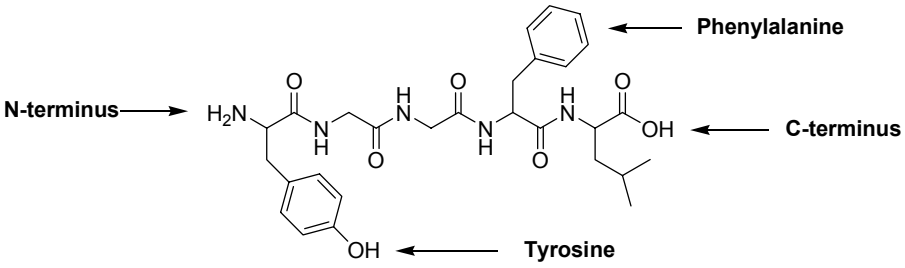

Fig. 4.20 *The four indicated modification sites of Leu-enkephalin are accessible by organic synthesis.*

In the case of enkephalin the N-terminus as well as the tyrosine hydroxy function are essential for the binding properties to the opiate receptor and cannot be labelled if activity is to be retained. Labelling of the C-terminus would mean to reverse the direction of synthesis or to modify the peptide post cleavage, which is both to be avoided. Therefore phenylalanine was chosen as the location of side-chain modification. Another advantage of phenylalanine is the huge number of known substitution reactions, which have already been carried out on the phenyl ring and are thoroughly tested for convenience.

The introduction of a *p*-nitro group would allow an easy handling without the employment of a protection group, because the nitro function is inert under SPPS conditions. In addition, it could be reduced on the resin[157-159] to yield *p*-amino phenylalanine which might be reactive towards carboxy activated metallocene derivatives and undergo a peptide bond formation. Thus, the following reaction pathway had been elaborated to synthesize the modified building block, which is also commercially available but expensive.

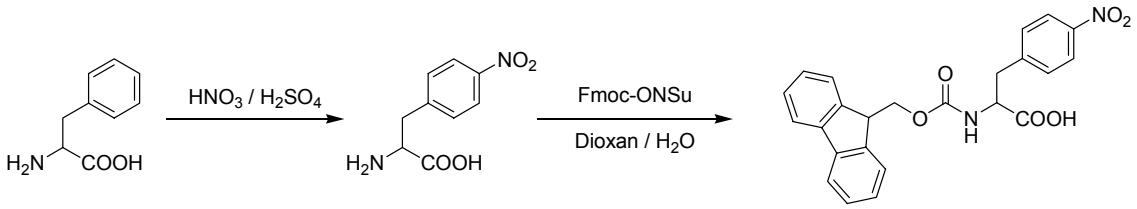

10 **11**

Fig. 4.21 *Reaction pathway to obtain Fmoc-p-nitro-phenylalanine **11** as a building block for SPPS.*

Commercially available and inexpensive L-phenylalanine was nitrated in 4-position according to literature[160] to yield *p*-nitro-phenylalanine **10**, which was then Fmoc protected by standard methods[131] to give **11**, an N^{α}-Fmoc protected amino acid ready for solid phase peptide synthesis.

The preparation of **10** was carried out by addition of L-phenylalanine to a mixture of HNO_3 and H_2SO_4 at 0 °C and the following neutralisation with sodium hydroxide solution until precipitation of the product occurred. The EI mass spectrum shows the M^+ peak at correct 210 m/z and all expected signals in both ^1H and ^{13}C NMR spectroscopy can be observed. Solubility of **10** is poor in most solvents, though.

Fmoc protected *p*-nitro-phenylalanine **11** was synthesized from **10** using standard Fmoc

introduction procedures. Both Fmoc-chloride and N-(9-Fluorenylmethoxycarbonyl)-succinimide (Fmoc-OSu) were successfully used for the conversion. For the Fmoc-chloride procedure a faster reaction could be observed, although at the cost of reduced yield of only 45%. Thin layer chromatography revealed higher purity for this product than for the one obtained through the Fmoc-OSu reaction, which had to be recrystallized from EtOAc. FAB mass spectrometry of **11** confirms the correct molecular mass of 432.12 g/mol with a $[M+H]^+$-peak at m/z = 433.0. The aromatic Fmoc-signals of product **11** can be clearly observed in the ^1H NMR spectrum between 7.8 and 7.3 ppm, while the Fmoc methylene group gives rise to a signal at 4.23 ppm. The single ipso ring proton produces a peak at 4.15 ppm. The ^{13}C NMR spectrum shows all expected resonances, one significant being the methylene carbon of the Fmoc group at 65.6 ppm.

4.4.1 Synthesis of Ac-Enk[Phe^4(4-NH$_2$)]-OH 12

Before the preparation of side-chain labelled bioconjugates could be performed, a verification of the concept was carried out by the synthesis of an N-terminal acetylated Leu-enkephalin containing a *p*-nitro-phenylalanine residue. Before cleavage the efficiency of on-resin reduction using tin(II)chloride in DMF was checked. The obtained product, Ac-Enk[Phe^4(4-NH$_2$)]-OH **12**, was purified by HPLC and fully characterized.

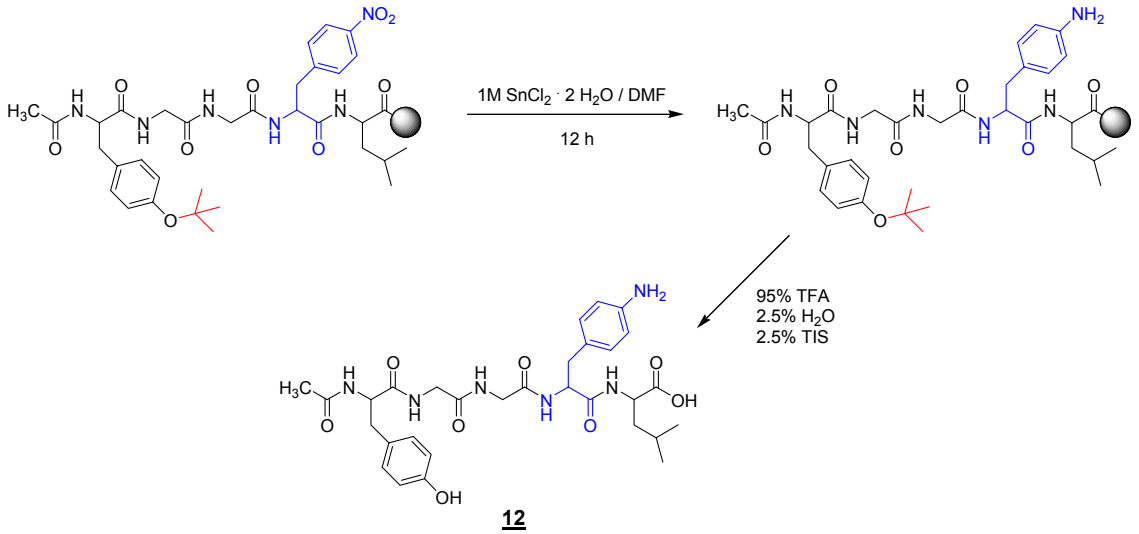

Fig. 4.22 *A p-nitro functionalized phenylalanine was incorporated into enkephalin and reduced to the p-amino derivative using 1 M tin(II)chloride in DMF for 12 hours. Standard cleavage was applied.*

The ESI (pos.) mass spectrum of **12**, confirmed the successful formation of the product, as it showed the calculated molecular mass of 612.29 g/mol with three main peaks at m/z 613.4 ($M+H^+$), 635.4 ($M+Na^+$) and 651.4 ($M+K^+$). Also very weak signals of dimers could be observed at 1225.7 ($2M + H^+$), 1247.6 ($2M+Na^+$) and 1263.8 ($2M + K^+$), like those in the plain peptides H-Enk-OH **3** and Ac-Enk-OH **4**.

^{1}H NMR shows the characteristic AA'BB' pattern of 1,4-disubstituted phenyl-rings for both tyrosine and newly introduced *p*-amino-phenylalanine between 7.3 and 6.6 ppm.

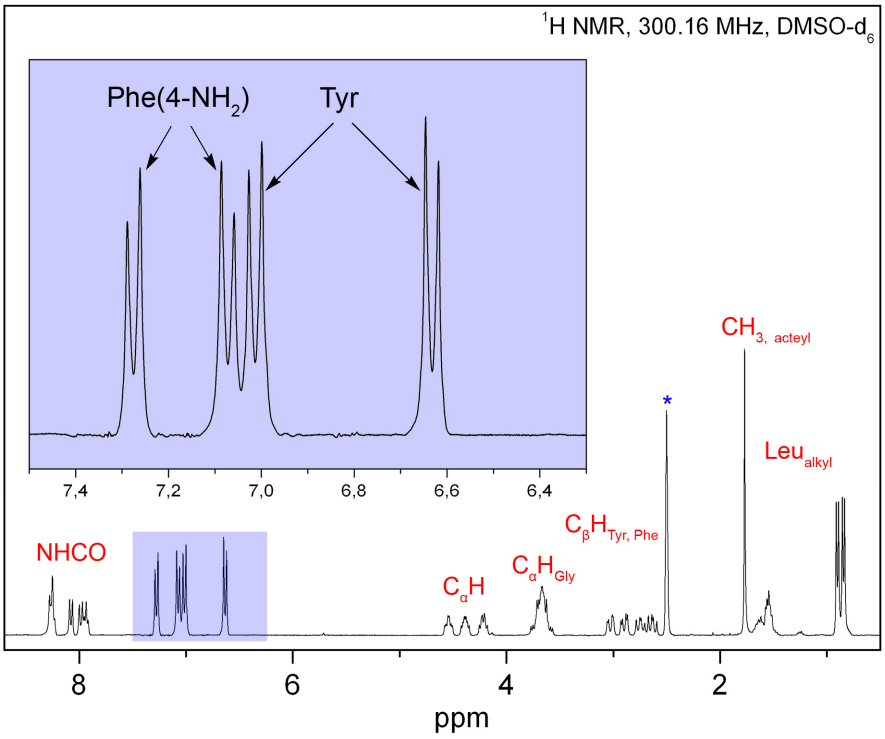

Fig. 4.23 *Proton NMR Ac-Enk[Phe^4(4-NH$_2$)]-OH **12**. Para-substituted phenylalanine shows significant doublets with a distance of 0.2 ppm, while the tyrosine signals a 0.38 ppm apart.*

The *p*-amino modified phenylalanine residue shows two doublets, which are separated 0.2 ppm, while the tyrosine doublets always show a distance of 0.38 ppm (*Fig. 4.23*). The formation of an amide bond at the amino-phenylalanine will drag the two signals apart from each other to a value of 0.38 ppm, which will be shown in the following. This change in spectroscopic properties is useful for monitoring the reaction's progression. All expected carbon signals are visible in ^{13}C NMR, except for the quaternary carbon atoms of the aromatic 4-amino-phenyl system. This is also the case for all deriva-

tives, which contain this function. The relaxation time of these nuclei seems to be too long to gain proper signal strength.

4.4.2 Synthesis of Ac-Enk[Phe^4(NH-CO-Fc)]-OH 13

After the successful integration of the artificial amino acid **10** via SPPS into the peptide's sequence and the succeeding on-resin reduction with tin(II) chloride in DMF have been demonstrated, the labelling with metallocene derivatives **1** and **2** was carried out according to the following scheme.

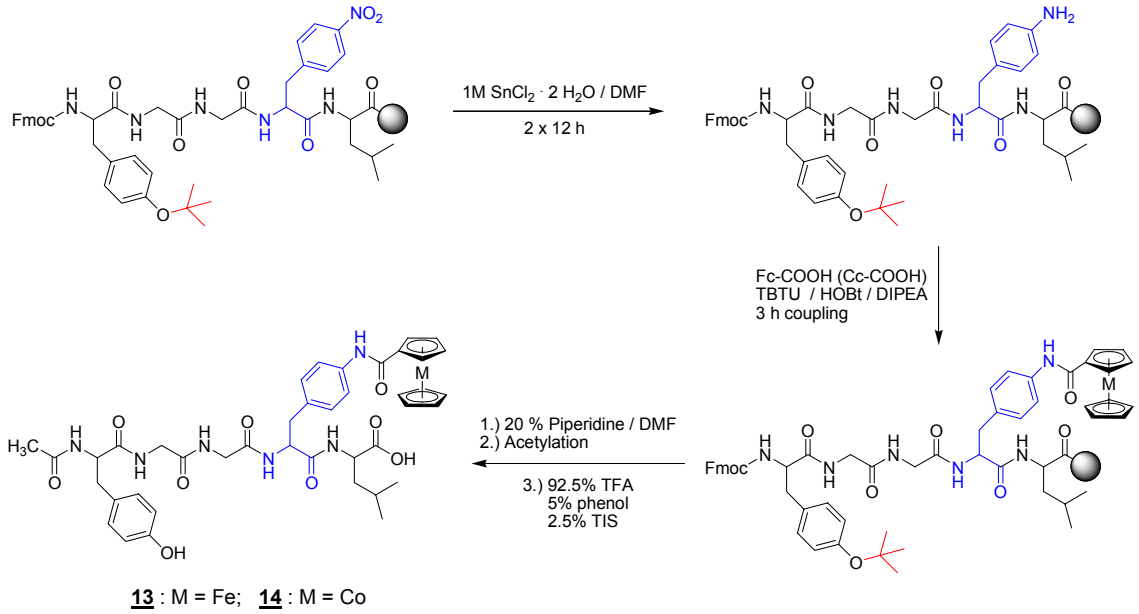

Fig. 4.24 *Reaction strategy for the preparation of side-chain labelled enkephalin. The N-terminal acetylation was chosen to prevent the amino group from undergoing possible side reactions*

The aromatic amino group is expected to show less reactivity towards the formation of a peptide bond due to interaction with the phenyl π-system, so that a prolonged coupling time of 3 h was chosen. Since early HPLC analyses indicated that incomplete coupling had occurred, the excess of the metallocene carboxylic acid was raised from 3-fold to 5-fold. This improved the yield significantly, and no more **12** was observed in HPLC. As well as in N-terminal labelling did the color of the resin change from beige to brown for ferrocene and to intense yellow for cobaltocenium, respectively. Based on the positive

experiences made with the addition of phenol to the cleavage cocktail, the same mixture was used with **13** to avoid oxidative decomposition of ferrocene (see *chapter 4.3.1*).

The ESI (pos.) mass spectrum reports m/z 825.5 $(M+H)^+$, 847.4 $(M+Na)^+$ and 863.4 $(M+K)^+$ for the product **13**, which has a molecular weight of 824.24 g/mol. ESI (neg.) mass spectrometry shows only a single peak at 823.5 for $(M-H)^-$. The proton NMR experiment confirms all expected peaks and shows a shift of the aromatic hydrogen atoms of the substituted phenylalanine ring, caused by the withdrawal of electron density from the ring towards the peptide bond. The doublets also have a distance of 0.38 ppm, which has nearly doubled from the earlier reported 0.2 ppm for the amino-derivative **12**. The Cp-signals can be found between 5.0 and 4.0 ppm, but interestingly do not split into a 1-1-2-5 pattern but show two pseudo-triplets for each 2 protons of the substituted cyclopentadiene and a singlet with an integral of 5 protons. The above discussed influence of nearby chiral centers is too weak, because the nearest location of chirality is too far away.

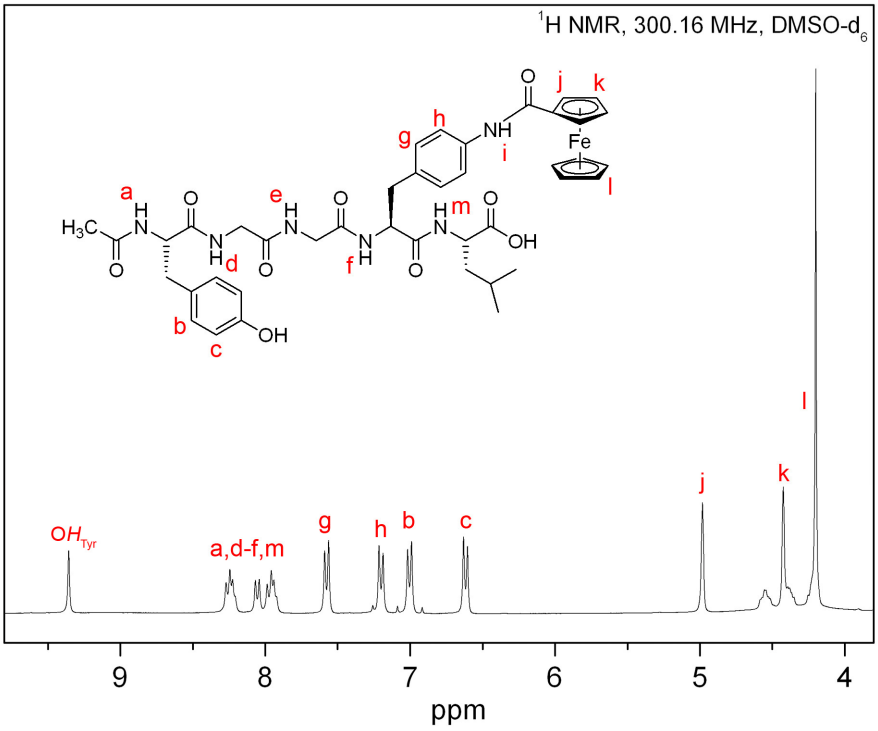

Fig. 4.25 *^{1}H NMR spectrum of Ac-Enk[Phe^4(NH-CO-Fc])-OH **13**. The signal **j** is caused by the protons on C_2 and C_5, which are isochronic in this case.*

The Cp-signals are also slightly shifted down-field in comparison with Fc-CO-Enk-OH **7**, with the unsubstituted ring having moved from 3.95 to 4.20 ppm. The other Cp-signals experience the same shift of 0.25 ppm. This will be shown in the double functionalized compounds presented in the upcoming chapter, where bioconjugates with two simultaneously attached metallocenes will be presented.

The amide proton **i** (*Fig. 4.25*) is observed as a very broad singlet of relative down-field position of 9.03 ppm. HH-COSY NMR spectroscopy was used to identify the amide protons by their coupling with C_α-protons of the related amino acids. It can also be nicely seen, that no coupling event for the OH_{Tyr} at 9.36 ppm occurs, which is correct.

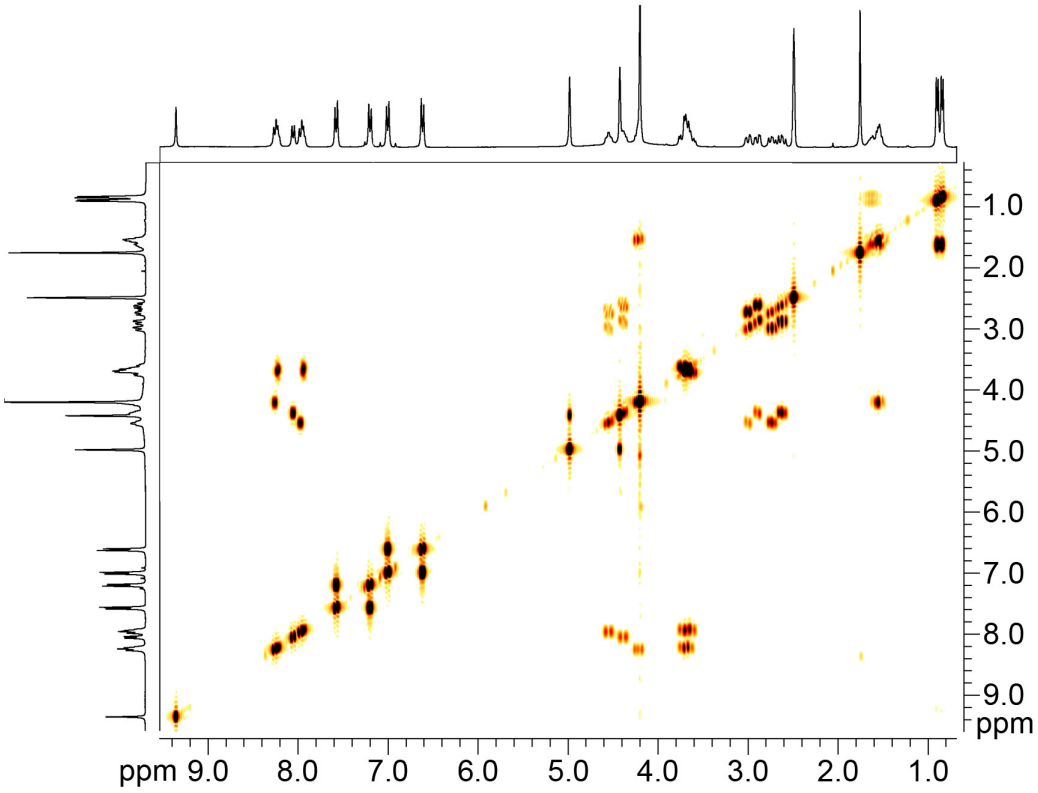

Fig. 4.26 *HH-COSY 2D NMR spectrum of **13**, measured in DMSO-d_6 at 300.16 MHz. The bottom left signal corresponds to the p-amido proton of phenylalanine. No coupling is expected due to the lacking of an adjacent C_α-proton.*

The $C_\alpha H$ of leucine is hidden under the signal of Cp' but can be identified from the above HH correlated spectrum, as well. The ^{13}C NMR spectrum shows all necessary resonances, with the Fc-attached carbonyl carbon giving a signal at 168 ppm which makes it the most up-field shifted carbonyl. The quaternary phenylalanine signals, which were not observable in the *p*-amino derivative **12** are clearly visible at 137.5 and

132.5 ppm. The cyclopentadienyl rings result in only 4 signals, which is in accordance to the observation of proton isochronicity of H_2 and H_5.

Electrochemical measurements reveal a one-electron reversible oxidation, very similar to that of Fc-CO-Enk-OH **7**. The half-wave potential of this redox reaction is E½ = 220 mV vs. Fc/Fc^+ with a peak separation of 75 mV.

4.4.3 Synthesis of Ac-Enk[Phe^4(NH-CO-Cc)]-OH 14

The cobaltocenium compound Ac-Enk[Phe^4(NH-CO-Cc)]-OH **14** was synthesized in analogy to the ferrocene derivative **13**. The only difference being the application of the standard cleavage mixture without any anti-oxidant agent. The crude product in form of a yellow powder contained over 25% impurities according to HPLC UV detection.

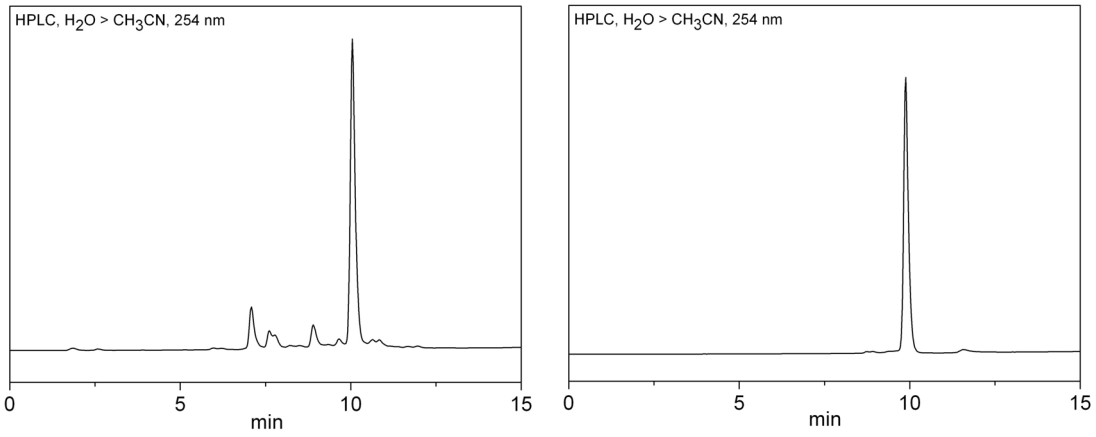

Fig. 4.27 *Analytical HPLC chromatograms of **14** showing the crude product (left) and the purified substance (right). Details on chromatograms and gradients are given in chapter 8.*

After purification by preparative HPLC the pure compound was characterized by ESI (pos.) mass spectrometry, which showed the correct mass of the bioconjugate cation at m/z = 827.3 $(M\text{-}TFA)^+$, 433.3 $(M\text{-}TFA+K)^{2+}$ and 425.3 $(M\text{-}TFA+Na)^{2+}$. The signals observed in proton NMR were identical to those of **13** except for the Cp-signals which are placed between 6.50 and 5.90 ppm. Another interesting change is the position of the CON*H* of the connected cobaltocenium moiety, which can be observed at 10.35 ppm, exactly 1 ppm to the lower field than the corresponding signal in its ferrocene labelled congener. The position of the phenylalanine aromatic signals in ^1H NMR is with 7.61 and 7.28 ppm almost identical to those in **13**, only the distance is somewhat smaller at

only 0.33 ppm compared to 0.38 ppm. All Cp-carbon resonance signals in the ^{13}C NMR spectrum appear at the exact same position as in the N-terminal labelled compound. The position of the cobaltocenium amide carbon signal is with 159.7 ppm remarkably shifted to the higher field.

The electrochemical studies showed indeed something different from the N-terminal labelled cobaltocenium compound **8**. The reduction process seemed to be irreversible at lower scan rates of 100 mV but changed to quasi-reversible behaviour with increasing scan rates up to 600 mV/s. The peak separation changes proportional to the scan rate, identifying the redox reaction as a quasireversible process (*Fig. 4.27*), which means that the reduced cobaltocene decomposes relatively slowly. The half-wave potential is with 1131 mV significantly shifted compared to N-terminal bound Cc ($E_{1/2}$ = 1439 mV).

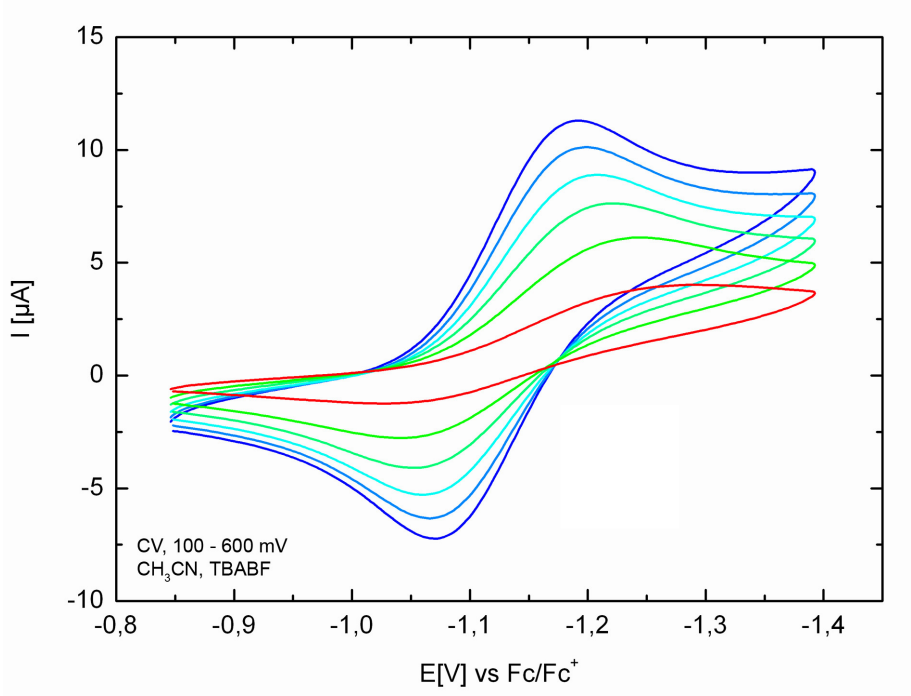

Fig. 4.28 *Cyclovoltammograms from 100 mV (red) to 600 mV (dark blue) show a quasireversible behaviour for* ***14****, indicated by the decreasing peak separation with increasing scan rate.*

The N-terminal cobaltocenium group appears to be of electrochemically irreversible nature, while the side chain labelled species at least shows (quasi)reversible properties. These preliminary results have to be investigated in a more detailed approach, though.

4.5 Multiple labelling of [Leu^5]-Enkephalin

Two different techniques to introduce a metal marker either at the N-terminus or at the side-chain of a modified amino-acid have been presented so far. As a consequence, the possible combination of these techniques was studied, hoping to gain access to bioconjugates which carry multiple organometallic labels. This could either help to increase the peptide/metal ratio in order to improve the detection of low concentrations and also modify the biomolecules chemical properties with regard to solubility, hydrophilicity, transport across membranes, etc. (see *chapter 6*).

4.5.1 Synthesis of Fc-CO-Enk[Phe^4(NH-CO-Fc)]-OH 15

The synthesis was planned as shown in the following reaction scheme (*Fig. 4.29*). The introduction of the metallocene carboxylic acid was performed at both N-terminus and side-chain simultaneously. Post-cleavage analytical HPLC showed an improved reaction progress for double-coupling with each 5 equivalents of metallocene (2.5 equiv. per function) over a single-coupling strategy with double the amount of metallocene.

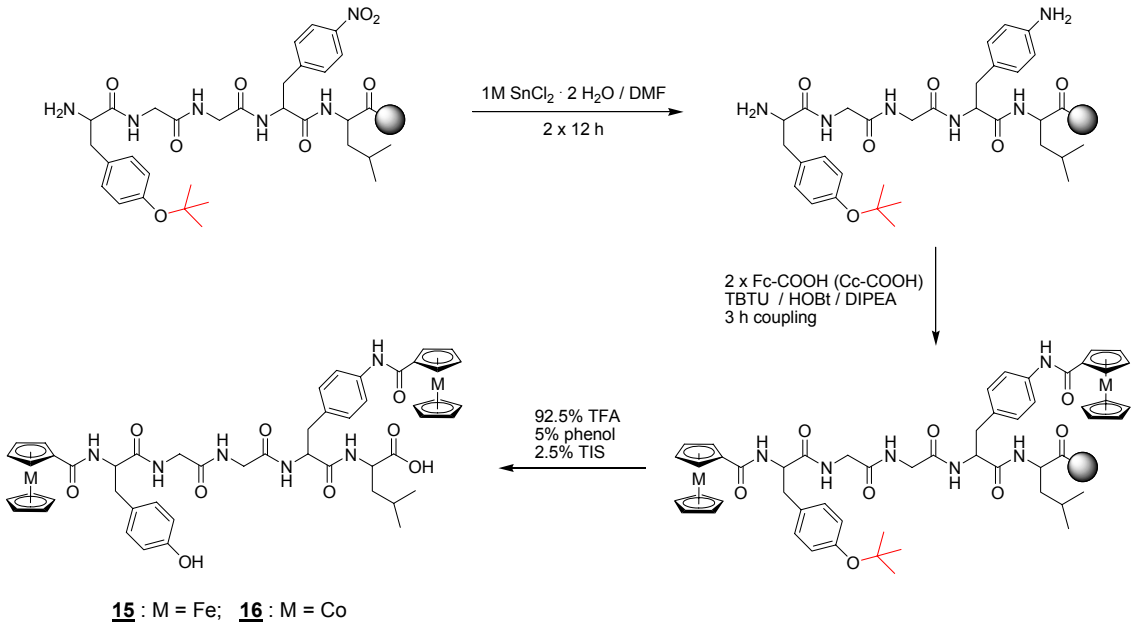

Fig. 4.29 *Synthetic strategy for the preparation of a di-labelled enkephalin derivative.*

That is why the double-coupling strategy has been favoured and used for compounds **15** and **16**. The N-terminal amino group is stable towards treatment with tin(II) chloride and was therefore left unprotected. The color of the resin was significantly darker compared to the single labelled compounds. This more intense color could also be observed after cleavage and purification (*Fig. 4.30*). The absorbance maximum does only slightly shift from 442 (**7**) to 448 nm (**15**), confirming the addition of chromophore absorbance instead of a bathochromic shift.

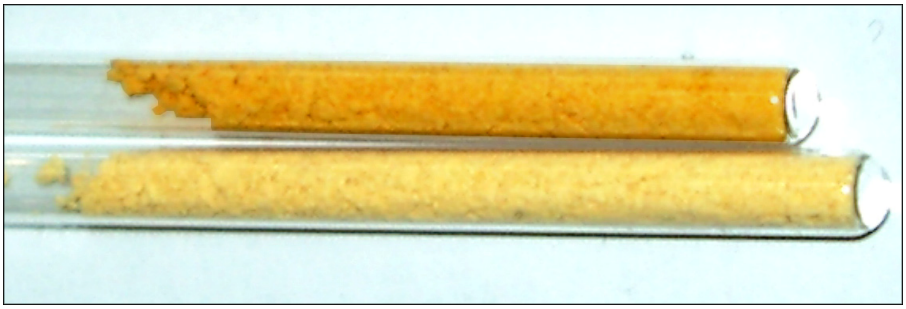

Fig. 4.30 *The color of the ferrocene di-labelled enkephalin **15** (top) is more intense compared to that of the single substituted compound 7 (bottom)*

The HPLC-purified substance **15** (Fc-CO-Enk[Phe^4(NH-CO-Fc)]-OH) was subjected to ESI (neg.) mass spectrometry, yielding the base-peak at m/z = 993.5 for the anion $(M-H^+)^-$. The ^{1}H NMR spectrum showed both sets of Cp-signals from each metallocene (*Fig. 4.31*) between 3.8 and 5.0 ppm. The presence of one signal group with intensities 2-2-5 and of another one with 1-1-2-5 confirms the above postulation that the tyrosine chirality center influences the CH groups 2 and 5 on the substituted Cp-ring, while the side-chain bound ferrocene is not affected in such a way. These corresponding resonances could be identified with the help of 2D NMR spectroscopy. The amide proton signals for the two ferrocenes resonate at 9.05 ppm as a very broad and weak singlet (side-chain Fc) and at 7.78 as a doublet (N-terminal Fc), respectively. The ^{13}C NMR experiment also shows that two sets of Cp-signals can be observed, one from each ferrocene moiety. The peak patterns are simply a superposition of the two ^{13}C NMR spectra of ferrocene side-chain and N-terminal labelled compounds **7** and **13** as is shown in *Fig. 4.32*. The spectrum shows all 8 expected aromatic signals from tyrosine and phenylalanine residues, as well.

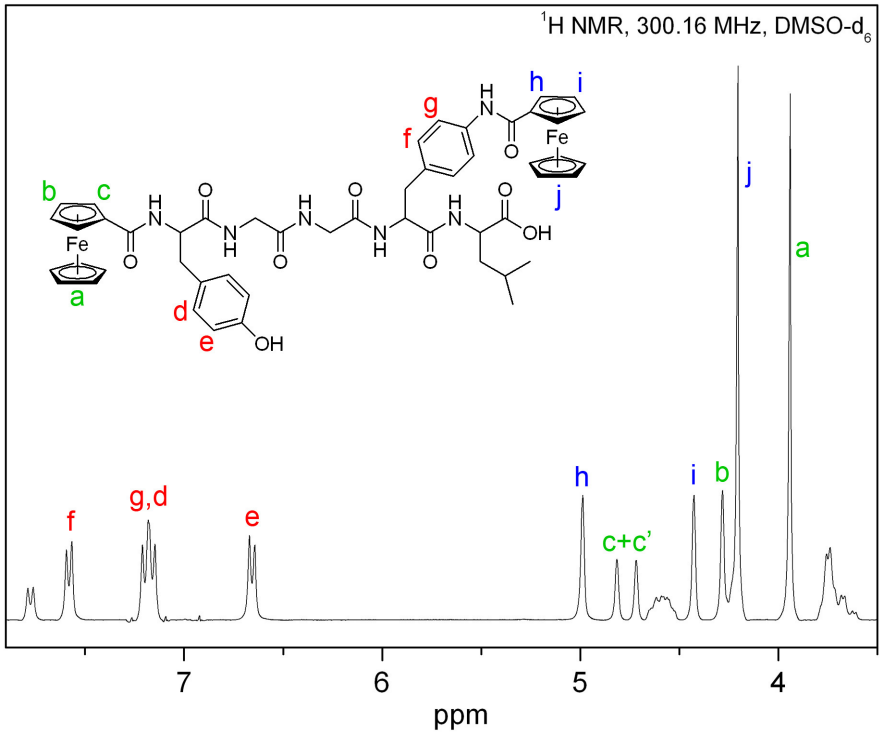

Fig. 4.31 *Selected region from the ^{1}H NMR spectrum of **15** displaying the mixed Cp-signals, related to each of the ferrocene groups.*

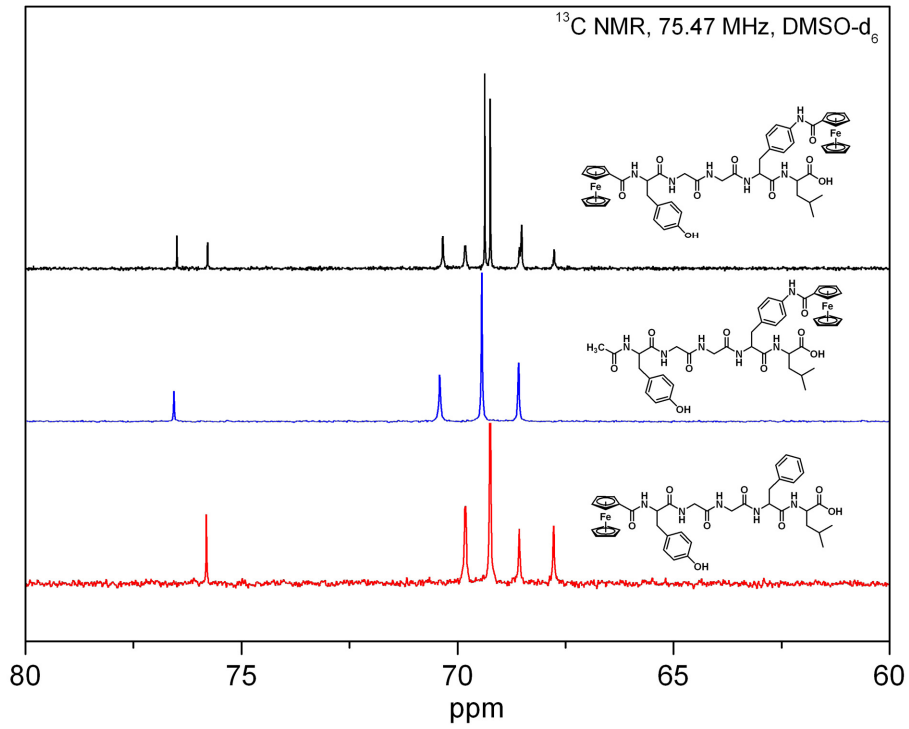

Fig. 4.32 *Cp-carbon resonances from three ferrocene containing enkephalin derivatives.*

The electrochemical experiments show only one reversible event at 199 mV but no second signal for the two metallocene groups. The peak separation is 76 mV, which is close to the 59 mV for the full reversibility of perfect Nernstian system. The difference at the metal centers concerning their oxidation potentials seems therefore to be very small. The half-wave potentials of N-terminal labelled enkephalin **7** and of the phenylalanine side-chain labelled species **13** are very similar with E½ = 214 mV and 220 mV, which explains the presence of only one peak in **15**. The potential seems to be shifted 15-20 mV, though. Coulometric experiments have to be carried out, to confirm the simultaneous oxidation of two ferrocene groups by measuring the amount of electrical charge.

4.5.2 Synthesis of (Cc-CO-Enk[Phe^4(NH-CO-Cc)]-OH) TFA_2 16

The preparation of Bis-cobaltocinium-enkephalin **16** was carried out according to that of the corresponding ferrocene derivative. Again, the only difference was the constitution of the cleavage mixture, which did not contain any anti-oxidizing reagent like ascorbic acid or phenol. The bright yellow color of the resin indicated successful coupling after the SPPS was finished. The crude product was purified by preparative HPLC to remove minor amounts of mono- and unlabelled peptide.

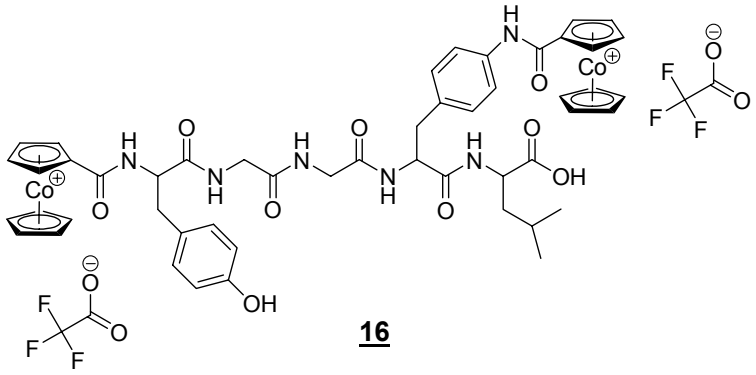

16

Fig. 4.33 *Chemical structure of Cc-CO-Enk[Phe^4(NH-CO-Cc)]-OH + 2TFA*

As each cationic cobaltocenium group is accompanied by a trifluoroacetic acid anion, which originates from the cleavage process, the double marked peptide is expected to be a di-cation. This is confirmed by the ESI (pos.) mass spectrum which shows a di-

cationic peak at m/z = 500.29 for $(M - 2\ TFA^{-})^{2+}$, which is correct since the molecular mass of the di-cation is 1000.5 g/mol. Interestingly a second peak at m/z = 999.31 is observed, which represents the deprotonated mono-cation $(M - 2\ TFA^{-} - H^{+})^{+}$. The recorded ^{1}H NMR spectrum does not reveal any unusual signals and all peptide related resonances known from other enkephalin derivatives can be found. The Cp-signals, however, are similar to that of the ferrocene congener, since one cyclopentadienyl group gives signals of intensities 2-2-5, while the other resonates in a pattern of 1-1-2-5. Anyway, the chiral influence is much weaker on the cobaltocenium than on the ferrocene, as the peak distance is less than 0.02 ppm in **16**, while it is more than 0.1 ppm in the ferrocene case. Both groups of Cc-signals are displaced by 0.35 ppm. This matches exactly the distance in Fc-CO-Enk[Phe^{4}(NH-CO-Fc)]-OH **15** measured between the Cp' resonances in both cases. ^{13}C NMR spectroscopy shows both cobaltocenium-bound carbonyl carbon atoms with 161.3 and 159.8 ppm shifted relatively to high field. All other carbonyl signals appear approximately 10 ppm more downfield. Also the Cp-carbons resonate at roughly 10 ppm downfield of the ferrocene signals, caused by the deshielding effect of the positively charged cobalt ion, as already mentioned above (*chapter 4.3.3*). The electrochemical behaviour of Bis-cobaltocenium-enkephalin was poor and only badly shaped cyclovoltammograms could be recorded. The reduction took place at -1.435 V but was of irreversible character. The electrode had to be polished after each measurement due to a plating effect on the electrode surface and the measurements were often not reproducible. This contributes to the picture of cobaltocenium being a stable and easy to handle metal marker but at the cost of insufficient and inapplicable electrochemical properties.

4.5.3 Synthesis of (Fc-CO-Enk[Phe^4(NH_2)]-OH) 17

While the simultaneous coupling of two identical metal markers is a simple enterprise concerning protection group strategies, the introduction of two different organometallic labels into a biomolecule is a more challenging task. The first attached metallocene has to be stable under the coupling conditions of the second one and has also to survive deprotection steps, which are necessary to avoid double coupling of the first marker. As a first experiment, ferrocene was coupled to the N-terminus of enkephalin, which contained the *p*-nitro-phenylalanine residue. This nitro-function was afterwards reduced to yield the *p*-amino group where a potential second metal marker like cobaltocenium could be attached. This compound **17** was synthesized and isolated to verify the ferrocene's stability under reducing conditions. The preparation was carried out according to the scheme in *Fig. 4.34*.

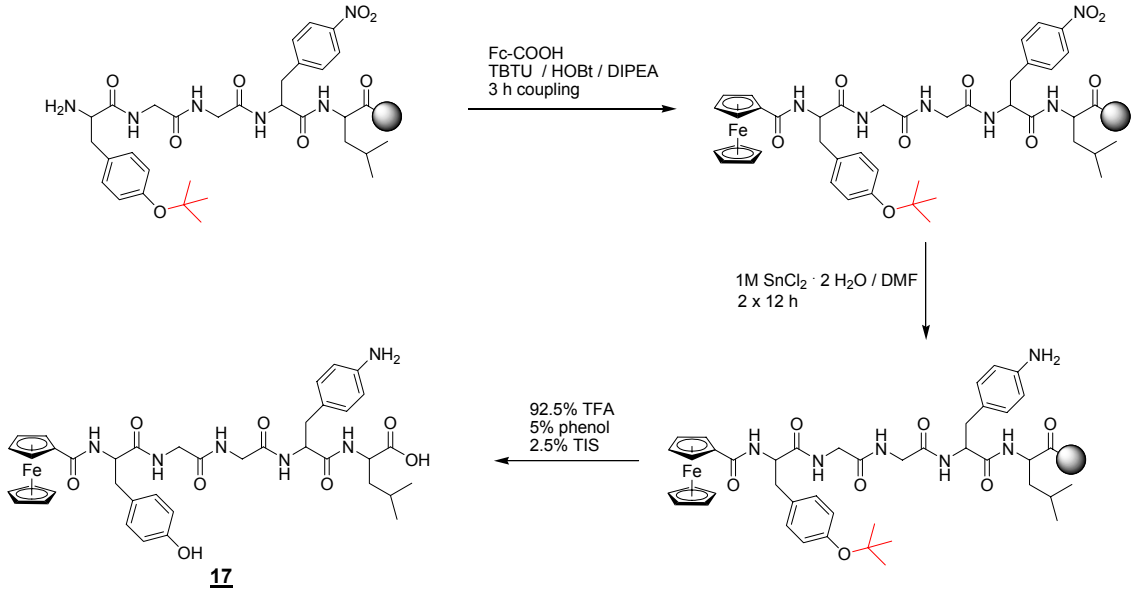

Fig. 4.34 *The Synthesis of **17** was carried out to test for the stability of ferrocene under reducing conditions, enabling a follow-up introduction of a different organometallic marker like Cc.*

The crude compound **17** was obtained in high yields of more than 85%, indicating major stability towards tin(II) chloride reduction. The reduction strength of tin chloride turns out to be high enough to convert the nitro group to an amino function but still low enough not to harm the iron metal center.

The isolated crude product **17** was purified by HPLC to remove any unlabelled or non-reduced fragments and afterwards subjected to ESI (pos.) mass spectrometry. The product shows peaks at m/z = 783.3 $(M+H)^+$, 805.4 $(M+Na)^+$ and 821.3 $(M+K)^+$ for mono-cations and peaks at m/z = 403.3 $(M+H+Na)^{2+}$ and 411.4 $(M+H+K)^{2+}$ representing di-cationic species, confirmed by their isotopic patterns. The ^{1}H NMR spectra show all expected signals and the reduced 1,4-disubstituted phenyl group appears at 7.24 and 7.15 ppm, which is similar to the positions of their related compound **12** , where the doublets resonated at 7.27 and 7.07. The ferrocene signals show in the typical pattern for N-terminal attached ferrocene with intensities of 1-1-2-5. The CH-groups 2 and 5 have shifts of 4.82 and 4.72 ppm, while the other CH-groups resonate at 4.39 (2H) and 3.94 (5H) ppm. Interestingly, again no quaternary carbon atoms can be observed in ^{13}C spectroscopy. The spectrum shows only 6 signals between 155.7 ppm ($C_{Tyr,\ OH}$) and 114.1 ppm (*m*-CH, $_{Tyr}$), confirming the same observation in the compound Ac-Enk[Phe^4(NH_2)]-OH **12**. These signals are only visible after a peptide bond has been established on the amino function.

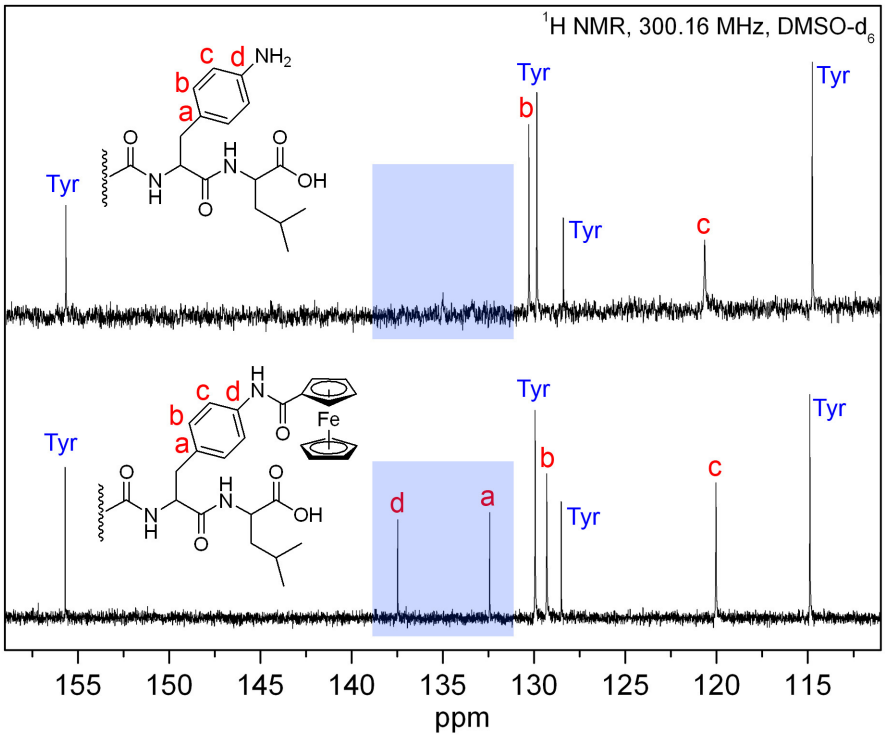

Fig. 4.35 *Comparison between ^{13}C-signals of p-amino phenylalanine before and after a peptide bond has been established. The quaternary signals **a** and **d** are not visible in **17** and **12**.*

The relaxation time for carbons **a** and **d** (see *Fig. 4.35*) is too long in the *p*-amino case to yield a good signal to noise ratio but seems to be faster after a peptide bond has been formed.

4.5.4 Synthesis of Fc-CO-Enk[Phe^4(NH-CO-Cc)]-OH 18

After the successful on-resin reduction of a *p*-nitro-phenylalanine residue in a ferrocene derivatized peptide, the next synthetic step could be carried out, namely the introduction of two different metal markers into one peptide. Besides the reduction with the first metallocene already attached, a second more general Fmoc approach could be used. *Fig. 4.36* shows the two exercised reaction pathways in a schematic way.

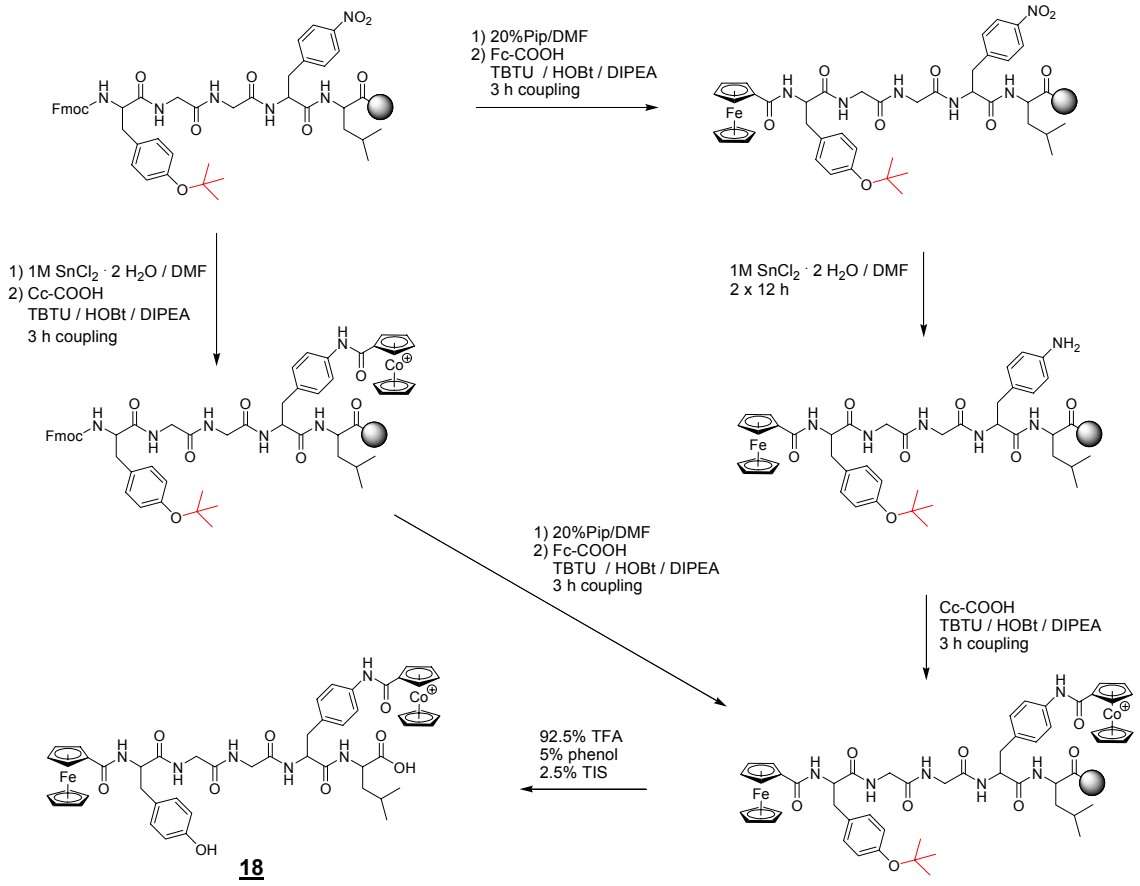

Fig. 4.36 *Two different reaction pathways lead to the bi-functionalized bioconjugate* ***18***

Both strategies lead to the desired product **18** in high yields of over 75%. The purification by means of preparative HPLC is necessary, though, to remove the possible mono functionalized by-products. The purified substance is an orange powder, which is stable in air and aqueous solutions, but decomposes slowly in organic solvents like DMF, MeOH and DMSO. The decomposition can be related to ferrocene oxidation, supported by the observation of broadened NMR signals in DMSO-d6 solution, caused by diamagnetic Fe^{3+}. The positive ESI mass spectrum shows a peak at m/z 997.3 confirming the successful synthesis of the di-labelled enkephalin, which has a molecular weight of 1110.25 g/mol as the TFA salt, while the detected cation has a calculated molecular mass of 997.26 g/mol. All expected resonances are visible in the ^{1}H NMR spectrum and the identification of all signals is supported by the HH-COSY experiment. The amide proton of the side-chain bound cobaltocenium group gives the characteristic singlet at 10.42 ppm, which is identical to the other side-chain functionalized Cc-species **14** and **16**. The Cp signals of both cobaltocenium and ferrocene are clearly visible and show as expected in the typical patterns 2-2-5 (side-chain bound Cobaltocenium) and 1-1-2-5 (N-terminal bound ferrocene) between 6.70 and 5.80 ppm and 4.80 and 3.90 ppm, respectively. The AA'BB' signals of the substituted phenylalanine ring appear at the usual chemical shifts of 7.60 and 7.32 ppm with a slightly reduced distance of 0.28 ppm compared to 0.32 ppm in former compound **16**. All peaks are slightly broadened, most probably due to oxidized Fe^{3+}, why the addition of a non-detectable reducing agent (Tin (II)salts or similar) is advised for future experiments. The ^{13}C NMR spectrum, instead, shows all peaks in a sharp and clear way, as can bee seen in *Fig. 4.37.* The presence of both Cp-signal groups, which are roughly 10 ppm apart, confirms that both different metallocenes are bound. The carbonyl carbon atom of the side-chain connected cobaltocenium resonates at 159.7 ppm, which is again the most up-field shifted carbonyl signal in the ^{13}C NMR spectrum. All eight aromatic signals from the two phenyl rings in tyrosine and phenylalanine can be observed between 155.6 and 114.8 ppm. The quaternary carbon atoms of the phenylalanine residue appear at 136.2 and 134.0 ppm.

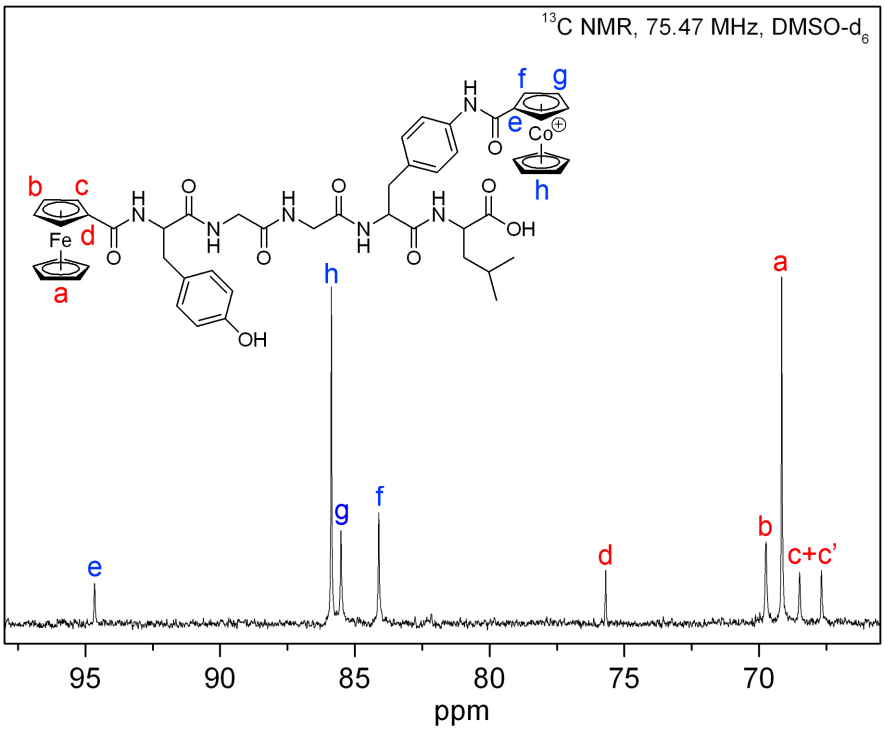

Fig. 4.37 *Selected region from the ^{13}C NMR spectrum of Fc-CO-Enk[Phe^4(NH-CO-Cc)]-OH* ***18****, showing all cyclopentadienyl carbon signals*

Electrochemical studies of a peptide containing both ferrocene and cobaltocenium groups were expected to be more difficult than such experiments with the single substituted peptides, mainly because of the wide scan-range from positive to negative values. However, the cyclovoltammogram shows two single-electron processes, one oxidation event for ferrocene and a reduction of the cobaltocenium (*Fig. 4.38*). Latter was expected to be irreversible, which could be confirmed. The square-wave experiment clearly shows that both electron transfers occur but also reveals an unidentified electrochemical process at -600 mV, which can also bee seen in the CV and is probably related to a side-reaction of the reduced cobaltocene, since it occurs at the back-slope of the cycle. Even the increase in scan-rate did not change the shape of the cyclic voltammogram so that the cobaltocenium reduction has to be regarded as truly irreversible.

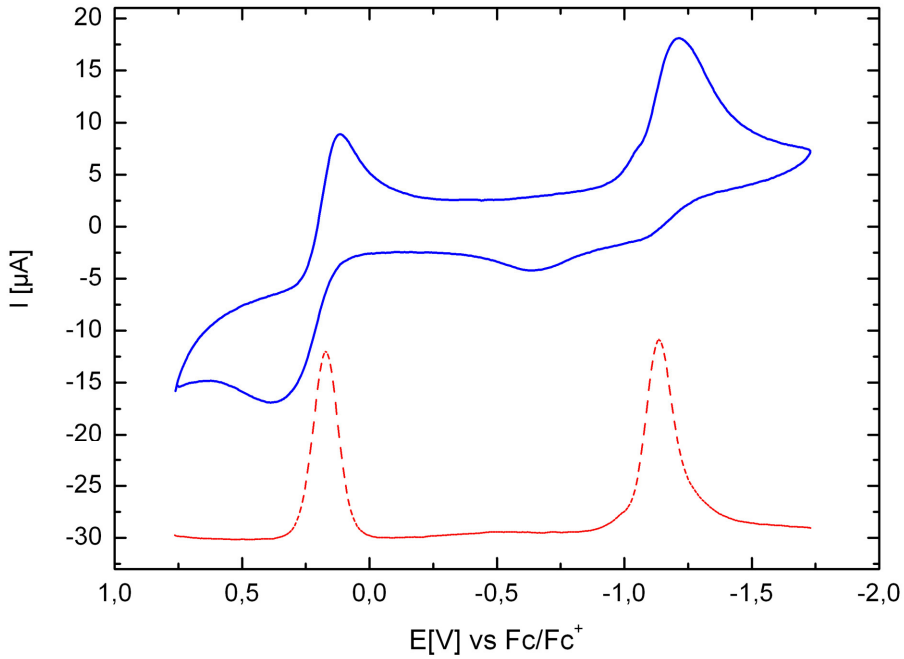

Fig. 4.38 *Cyclovoltammogram (blue) and square-wave voltammogram (red) of **18** (1 mM), measured in pure acetonitrile using Bu_4NBF_4 (0.1 M) as a supporting electrolyte.*

The half-wave potential of the reversible ferrocene oxidation is with 172 mV significantly shifted compared to E½ = 214 mV vs. Fc/Fc^+ in Fc-CO-Enk-OH **6**. The half-wave potential of the cobaltocenium reduction peak is 1133 mV in Fc-CO-Enk[Phe^4(NH-CO-Cc)]-OH **18** and thus identical to that in Cc side-chain bound derivative Ac-Enk[Phe^4(NH-CO-Cc)]-OH **14**, where a value of 1131 mV for E½ could be observed. The remarkable shift of the ferrocene oxidation to lower potentials may be explained by a stabilization of the corresponding oxidized ferrocinium group. Whether the cobaltocenium plays a role in this stabilization process is unclear and has to be eluded by detailed electrochemical experiments.

All results presented in this chapter conclude that a facile introduction of metal markers like ferrocene or cobaltocenium is possible at various positions in the studied peptide. Also the combination of these methods has been practiced, yielding multiple labelled peptides, either as homo- or hetero-metallic compounds. All reactions were performed on solid phase and crude products of high purity were obtained. Since these tools may be still insufficient in certain situations a supplementary approach for the labelling of peptides with metallocenes will be presented in the following *chapter 5*.

5 Selective labelling of peptides using Pd-catalyzed cross-coupling

5.1 Introduction

The direct coupling of a metallocene via its carboxy function to a free amino group through the formation of a peptide bond has been presented in the previous chapter. These methods work flawlessly under the described conditions but can not be applied when there is no amino group available, rendering them less universal than desired. A method which allows the introduction of the organometallic marker at a determined position in the biomolecule has to utilize special chemical reactivity, which has to be orthogonal to the reactivity of all other functional groups in the target molecule. Binding the metal label to the side-chain of a modified amino acid like the above presented *p*-amino-phenylalanine turned out to be a practical method. However, the amino-function had to be generated from the *p*-nitro group by reduction, which is another conversion step to be avoided.

A very promising reaction is the Sonogashira coupling[161], a palladium catalyzed cross-coupling between alkynes and iodoarenes, which was presented by K. Sonogashira in 1975. A variety of functional groups can be submitted to this reaction,[83, 162, 163] which uses mild conditions and can also be run in aqueous solution, the latter being an important demand for many bio-molecular reactions.

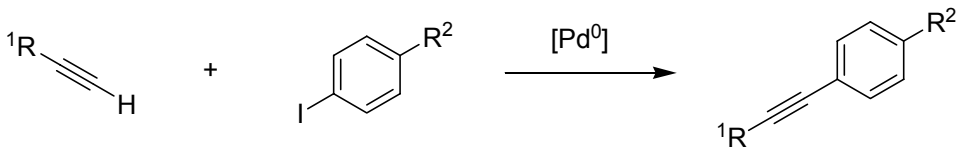

Fig. 5.1 *Simplified reaction scheme of the Sonogashira coupling, first presented in 1975*

Since the Sonogashira coupling demands two different functional groups, an alkyne and a iodo-arene, it is possible to plan the coupling reaction in two ways. The alkyne group

could be attached to the biomolecule and the metal marker therefore modified with a iodo-phenyl group or *vice versa*. Two strong arguments favour the latter strategy, one of it being the easy and well known synthesis of a *p*-iodo-phenylalanine group which offers a useful location for the binding of a metal marker molecule, as already shown in *chapter 4*. Secondly, very recent results from Schultz *et al.* offer innovative recombinant methods for the introduction of artificial amino acids like *p*-iodo-phenylalanine[164] or *p*-azido-phenylalanine[165] into a vast number of biomolecules. Therefore an alkyne modified metallocene marker is a versatile molecule which can bind in aqueous solution to the iodo-phenylalanine residue via Sonogashira coupling and also to the azido group to form a triazole ring. Thus, the development of a practical coupling strategy, where an alkyne modified metallocene is bound to either group in the target molecule, would instantly provide access to the labelling of a huge number of biomolecules.

5.2 Synthesis of dipeptides containing *p*-iodo-phenylalanine

To study the conditions and properties of the Sonogashira coupling, dipeptides were synthesized as model compounds, consisting of a Boc-protected amino acid and the methyl ester protected *p*-iodo-phenylalanine. All reactions were carried out in solution.

5.2.1 Synthesis of *p*-iodo-phenylalanine 19

The preparation of *p*-iodo-phenylalanine **19** was carried out according to the literature,[166] where commercially available and inexpensive phenylalanine was iodized in strongly acidic solution by the addition of iodine.

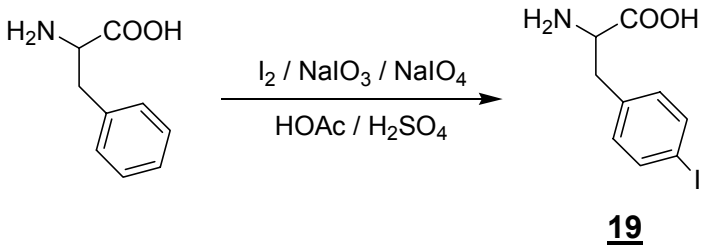

19

Fig. 5.2 *Preparation of p-iodo-phenylalanine **19** as described by Schwabacher et al.*

L-phenylalanine was dissolved in a mixture of HOAc and H_2SO_4 and iodine, sodium iodate and sodium periodate were added. After fading of the dark brown color to a clear orange solution and the following removal of the solvents under reduced pressure, the residual viscous oil was diluted with water and the product **19** was precipitated through neutralization with sodium hydroxide solution. The off-white powder was dried *in vacuo* and submitted to standard characterization procedures including EI mass spectrometry and NMR, which confirmed the correct formation of **19**.

5.2.2 Synthesis of *p*-iodo-phenylalanine methyl ester hydrochloride 20

To enable the formation of dipeptides either the N- or the C-terminus has to be protected to avoid side-reactions, as explained in *chapter 3*. It was chosen to protect the C-terminus with a methyl ester and to couple the free amino-function to the activated carboxy group of a N^{α}-Boc-protected amino acid.

To form this methyl ester, **19** was dissolved in dry methanol and thionylchloride was added dropwise at ice bath temperature. After 60 min. of stirring the solvent was removed on a rotary evaporator and the remaining oil was dissolved in methanol and poured into diethylether to yield the pure product **20** as a white precipitate.

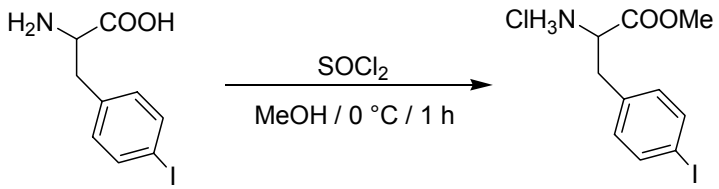

19 **20**

Fig. 5.3 *Treatment of p-iodo-phenylalanine with thionylchloride in methanol leads to p-iodo-phenylalanine methyl ester hydrochloride **20***

EI mass spectrometry, as well as NMR spectroscopy and elemental analysis confirm the expected formation of 4-iodo-phenylalanine methyl ester as the hydrochloride salt **20**, which was straightforwardly prepared through **19** using only standard procedures. The simplicity of modifying the phenylalanine side-chain as shown above with the 4-nitro or the 4-iodo derivatives should be emphasized again, as it makes the whole synthetic strategy practical and affordable.

5.2.3 Synthesis of dipeptides

The dipeptides **21(a-d)** were synthesized from N^{α}-Boc-protected amino acids alanine, leucine, phenylalanine and tyrosine with **20**. The Boc-amino acids were carboxy activated using the mixed anhydride method. The reaction scheme is shown in *Fig. 5.4*.

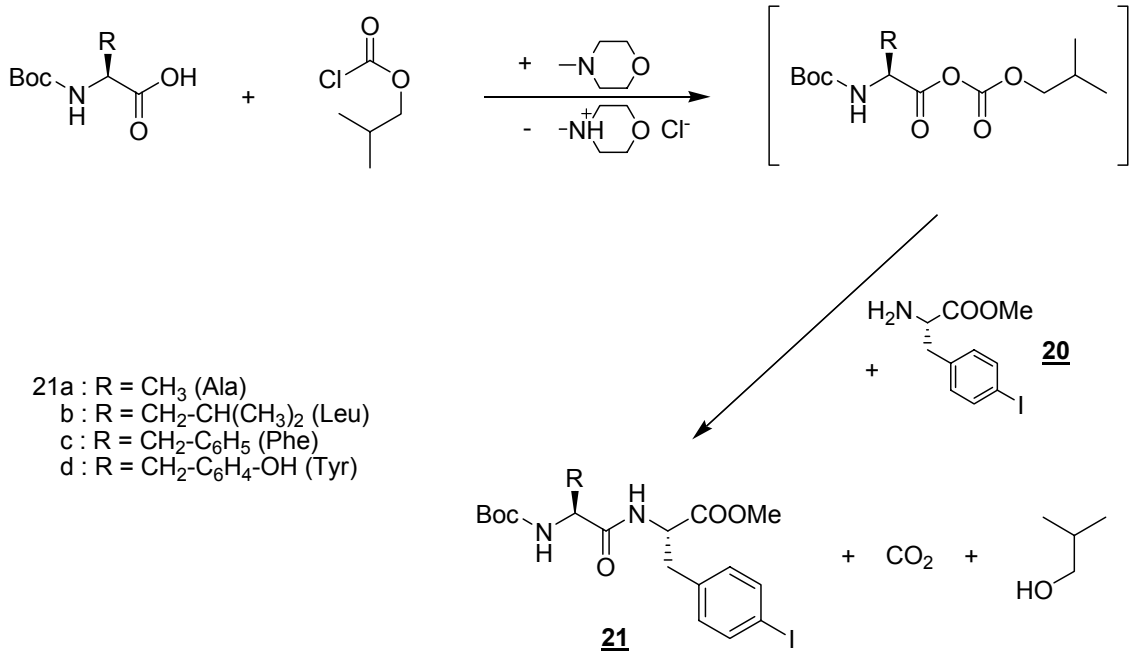

Fig. 5.4 *General reaction scheme for the synthesis of dipeptides using the mixed anhydride method.*

The activation using alkyl chloroformiates like IBCF was preferred to other common techniques such as the carbodiimide activation, which was introduced by Sheehan and Hess in 1955.[167] This was mainly due to the easy removal of by-products like CO_2 and *i*-butanol, whereas the carbodiimide procedure generates derivatives of urea, which are much more difficult to remove. Both methods imply the danger of a possible racemization, which was not observed, though. A number of strategies have been developed to prevent racemization and rearrangement reactions. Among the most widely spread are those that employ 1-hydroxybenzotriazole (HOBt) to yield activated esters, which form the peptide bond under stereochemical retention. These HOBt esters are the basis for modern solid phase peptide chemistry and can be generated by the use of coupling reagents like TBTU, HBTU etc. (see previous *chapter 4*)

The spectroscopic data of the dipeptides **21a-d** did not reveal any unexpected signals and the reactions occurred straightforward. The elemental analyses confirm the correct chemical compositions, as well as the FAB mass spectra always show the calculated $(M+1)^+$ peaks and also molecular fragments of the type $(M-C_4H_9)^+$ and $(M-Boc)^+$. The ^1H NMR spectrum shows the Boc amide proton between 6.76 and 6.87 ppm and the N*H* proton of 4-iodo-phenylalanine between 8.13 and 8.33 ppm. While the position of the Boc amide proton seems to be the same in all 4 compounds, it is obvious that the dipeptides with two aromatic amino acids show a small shift down-field compared to **21a** and **21b**, which contain alanine and leucine as aliphatic residues (*Tab. 5.1*).

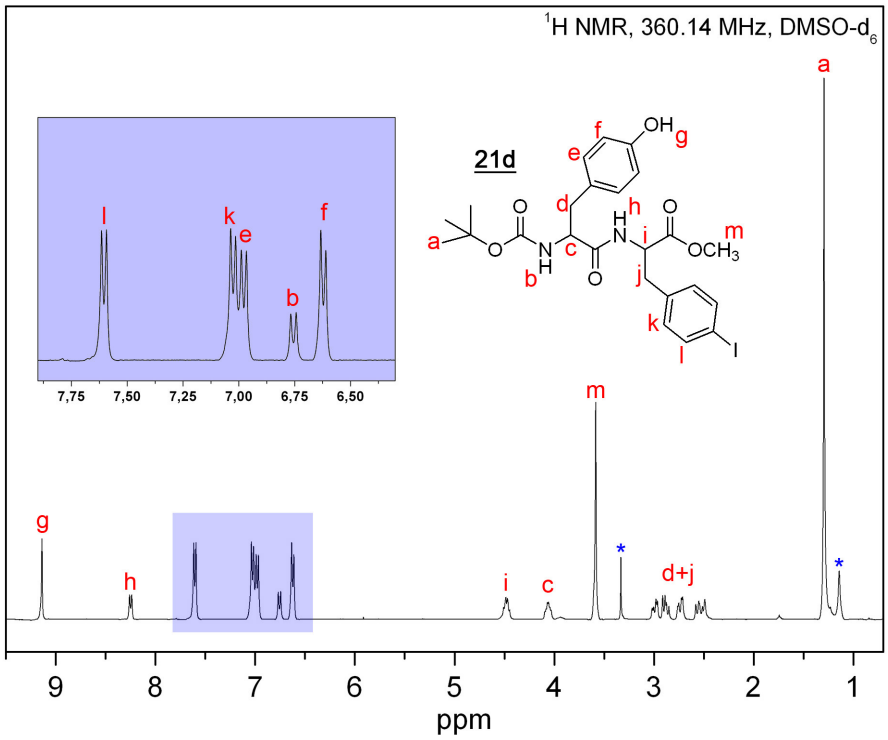

Fig. 5.5 *Proton NMR spectrum of Boc-Tyr-Phe(I)-OMe* ***21d****. The amide resonances* ***b*** *and* ***h*** *show only slight differences between compounds* ***21a-d***

The aromatic protons of the 4-iodo-substituted phenyl ring resonate at 7.60 and 7.00 ppm, leaving a distance of 0.60 ppm between both signal groups. Since the 4-iodo-phenylalanine is the location where the alkyne is being coupled to, the shift and distance of these signals will be of interest for the monitoring of a successful reaction. All dipep-

tides have been recrystallized from ethyl acetate (EA) and as a consequence traces of EA may be observed in some ^{1}H NMR spectra of compounds **a-d**.

Tab 5.1 *Selected shifts of amide protons from ^{1}H NMR. All spectra measured at 360.14 MHz in DMSO-d6.*

Compound	N*H*$_{Boc}$ [ppm]	^{3}J (N*H*$_{Boc}$) [Hz]	N*H*$_{Phe}$ [ppm]	^{3}J (N*H*$_{Phe}$) [Hz]
21a	6.85	7.2	8.13	7.5
21b	6.80	8.4	8.12	7.8
21c	6.87	8.6	8.33	7.6
21d	6.76	8.6	8.26	7.7

The iodine atom has a strong shielding effect on the C_4 carbon of the phenyl ring, which is shifted to 92.3 ppm in the ^{13}C NMR spectrum. This carbon atom will be shifted over 30 ppm down-field after the Sonogashira coupling of the alkyne. This shift is therefore a useful indicator for a successful binding to the target metal complex.

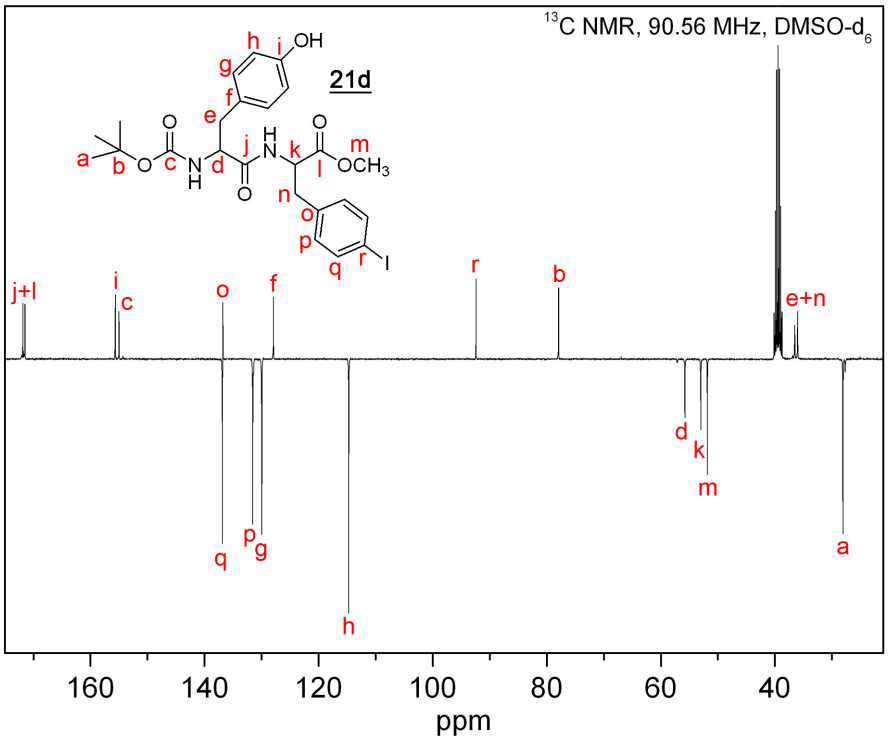

Fig. 5.6 *^{13}C NMR spin-echo spectrum of **21**. Secondary and quaternary signals point upwards.*

The carbonyl carbon atoms of the tyrosine and phenylalanine residues resonate at 172.0 and 171.8 ppm, respectively, whereas the Boc carbonyl carbon atom is shifted up-field to 154.9 ppm due to the positive induction effect of the butoxy group. Infrared spectra (KBr) of all dipeptides show bands of medium intensity below 3400 cm^{-1}, which indicates the existence of hydrogen bonds in the solid state.

5.3 Sonogashira coupling of ferrocene derivatives to dipeptides

5.3.1 Synthesis of ferrocenoyl-diethylpropargylamide **22** (H-DEPA-CO-Fc)

For the introduction of the ferrocene group into a iodo-phenyl derivatized biomolecule through Sonogashira coupling, an alkyne group has to be bound to the ferrocene marker. This can be provided by modification of ferrocenecarboxylic acid **1**. The carboxyl function of **1** readily undergoes peptide bond formation as presented in literature and confirmed in experiments (*chapter 4*). As a consequence, the reaction with an amino alkyne has to result in the formation of the desired ferrocene alkyne derivative. This reaction has already been presented[168, 169] and was well reproducible, according to the following scheme. The structure of **22** has also been reported[168] as obtained from x-ray crystal diffraction.

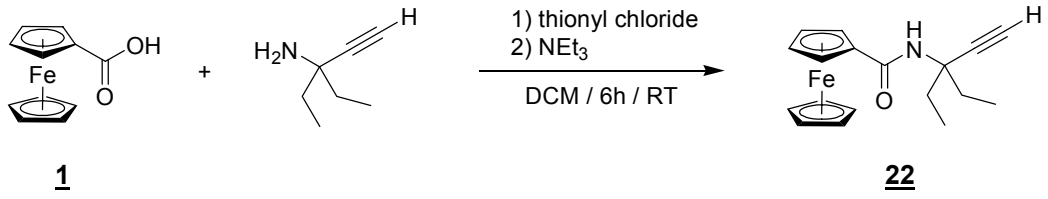

Fig. 5.7 *Simplified reaction scheme for the preparation of an alkyne derivatized ferrocene*

After the treatment of **1** with thionylchloride in dry DCM for 2 hours and the following removal of all volatile reagents on a vacuum pump, diethylpropargylamine and triethylamine was added in DCM and the mixture was stirred for 6 hours. After filtration and extraction with $CHCl_3/H_2O$ an orange solution was obtained, which yielded after evapo-

ration the crude product in a yield of 89%. The orange powder was recrystallized from methanol and analytically pure, as could be confirmed by elemental analysis, HPLC and FAB mass spectrometry. The alkyne hydrogen atom shows at 3.19 ppm in the ^{1}H NMR spectrum, while the alkyne carbon atoms resonate at 85.9 and 72.8 ppm in ^{13}C NMR. Since no chirality center is present the Cp-signals give the expected 2-2-5 pattern in the proton NMR spectrum. The UV spectrum reveals 2 characteristic absorbance maxima at 259 nm (Cp, aromatic) and 444 nm ($FeCp_2$). Especially the 444 nm absorbance peak is observable in all Fc-labelled bioconjugates, as will be shown later. The electrochemical experiments show a perfect reversible one-electron redox event at $E^1/_2$ = 223 mV, which is confirmed by a Randles-Sevcik plot (*Fig. 5.8*).

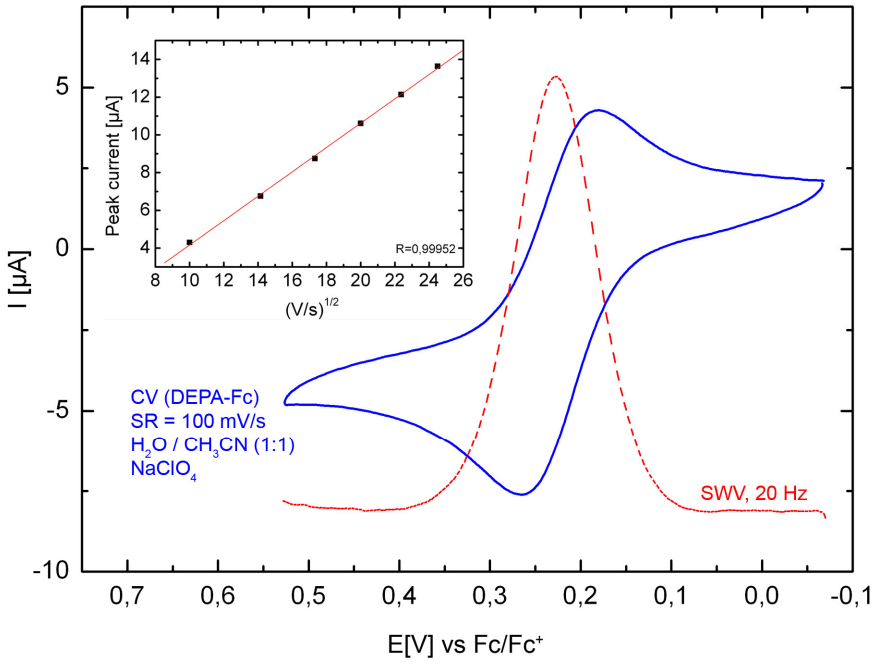

Fig. 5.8 *Cyclic and square wave voltammograms of H-DEPA-CO-Fc **22**. The Randles-Sevcik plot shows good reversibility.*

Randles and Sevcik suggested plotting the square root of the scan rate versus the cathodic peak current of the corresponding voltammogram.[170] A linear behaviour indicates a reversible redox process, while a curve would hint to quasi- or non-reversibility. The outstanding electrochemical properties of this ferrocene compound **22** make it a valuable probe for bio-labelling and redox detection.

5.3.2 Sonogashira coupling

All dipeptides **21a-d** have been labelled with H-DEPA-CO-Fc **22** and also with commercially available ethynylferrocene, to prove the universal character of the reaction. The procedure was the same for both ferrocene derivatives as can be seen in *Fig. 5.9*.

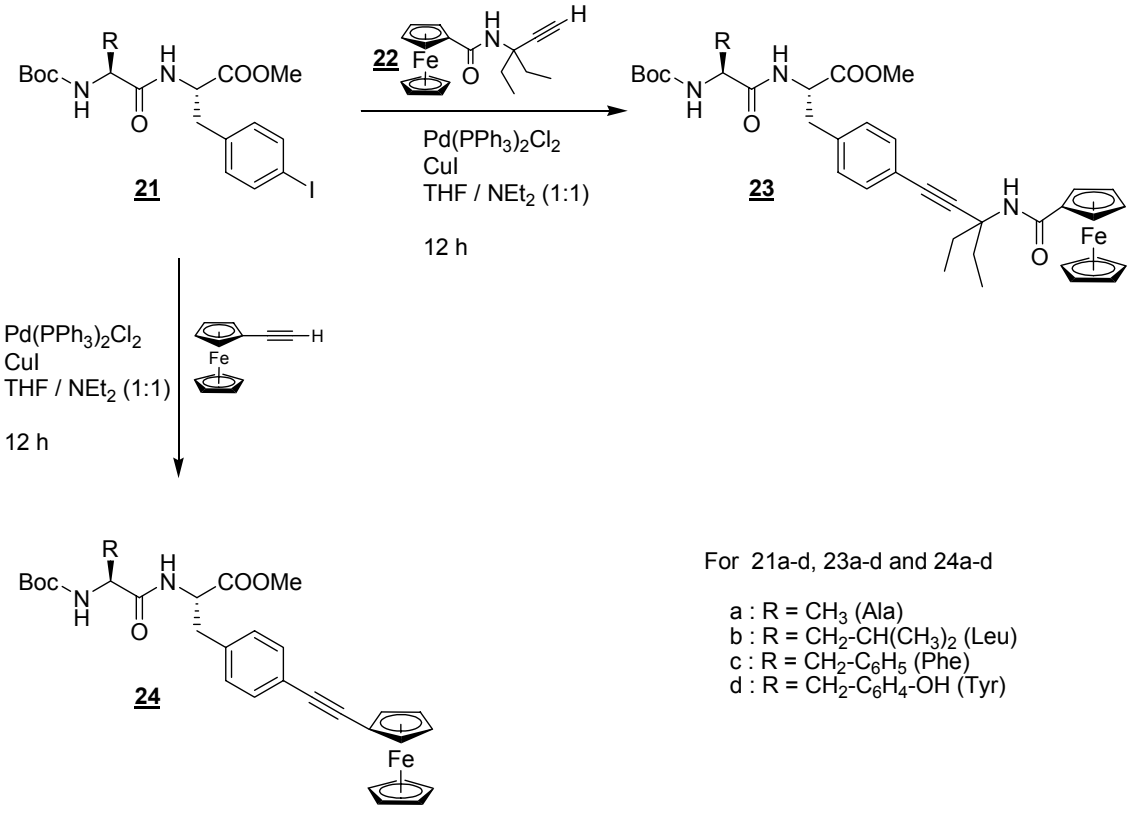

Fig. 5.9 *General reaction Scheme for the labelling of 4-iodo-phenylalanine containing dipeptides with H-DEPA-CO-FC **22** and ethinyl ferrocene*

The reactions were carried out under argon and in degassed and thoroughly dried solvents. After various attempts with different solvents and bases, a mixture of THF and NEt_3 in a ratio of 1:1 turned out to be the most successful. Shortly after all reagents had been added, the clear solutions became cloudy and greenish ammonium salts precipitated, which indicated the proceeding reaction. Directly after filtration the solutions were purified by silica column chromatography, using mixtures of ethyl acetate and hexane. All pure products were orange powders, which readily dissolved in organic sol-

vents like CH_3CN, THF, DMF, DCM, EtOH and MeOH but showed only moderate solubility in water.

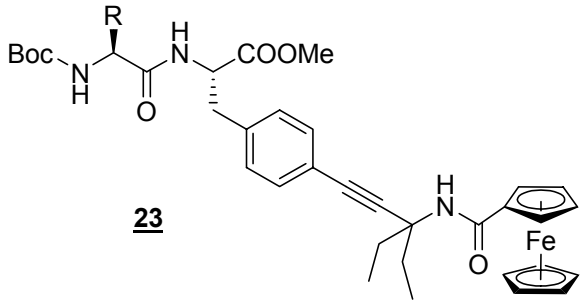

23

23a : R = CH_3 (Ala)
b : R = CH_2-$CH(CH_3)_2$ (Leu)
c : R = CH_2-C_6H_5 (Phe)
d : R = CH_2-C_6H_4-OH (Tyr)

Fig. 5.10 *Constitution of H-DEPA-CO-Fc labelled dipeptides **23a-d**. All substances are orange solids, thus enabling easy purification on a silica column.*

The purified DEPA-CO-Fc labelled dipeptides **23** were submitted to elemental analysis, HPLC and mass spectrometry, confirming the successful reaction. The FAB mass spectra show in addition to the M^+-peaks signals for $[M\text{-}Boc]^+$, $[M\text{-}Boc\text{-}Cp]^+$ and also fragments of m/z = 213 and 185, which can be assigned to $[Fc\text{-}CO]^+$ and $[Fc]^+$, respectively. Proton NMR signals for the Cp rings can be observed at 4.64, 4.30 and 4.21 ppm according to the usual 2-2-5 intensity pattern. The ^1H NMR spectrum also shows a singlet for the DEPA-CO-Fc N*H* amide proton at 5.74 ppm, which is the same for all 4 compounds. The phenyl ring of the former 4-iodo-phenylalanine residue still resonates in form of the two pseudo-doublets of a typical AA'BB' system but the signals have changed positions and distances compared to the dipeptide starting material. Significant changes in these shifts are given in *Table 5.2* (measured in DMSO-d_6).

Tab 5.2 *Comparison of selected ^1H NMR signals before and after labelling with DEPA-CO-Fc.*

Compound	Nr.	δ $Phe_{3,4}$ [ppm]	δ $Phe_{2,5}$ [ppm]	Δ [ppm]	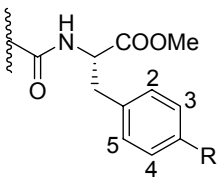
Boc-Ala-Phe(I)-OMe	**21a**	7.61	7.03	0.58	
Boc-Ala-Phe(DEPA-CO-Fc)-OMe	**23a**	7.38	7.20	0.18	
Boc-Leu-Phe(I)-OMe	**21b**	7.61	7.04	0.57	
Boc-Leu-Phe(DEPA-CO-Fc)-OMe	**23b**	7.39	7.21	0.18	
Boc-Phe-Phe(I)-OMe	**21c**	7.62	7.05	0.57	
Boc-Phe-Phe(DEPA-CO-Fc)-OMe	**23c**	7.35	7.16	0.19	
Boc-Tyr-Phe(I)-OMe	**21d**	7.60	7.03	0.57	
Boc-Tyr-Phe(DEPA-CO-Fc)-OMe	**23d**	7.34	7.14	0.20	

R = I, alkyne

The distance between the two pseudo-doublets changes significantly from average 0.57 to 0.19 ppm. This is due to a difference in electron density of the phenyl ring before and after coupling. The methyl protons of both DEPA ethyl groups resonate in form of one triplet signal with the correct intensity of 6 protons at 1.08 ppm (*Fig. 5.11*, signal **f**), while the methylene groups split into two multiplets at 2.38 and 1.91 ppm (signals **m** and **m'**). The singlet signal of the alkyne proton, which was observed in **22** at 3.10 ppm, is not anymore present. As a consequence no free alkyne is left and the coupling has fully taken place.

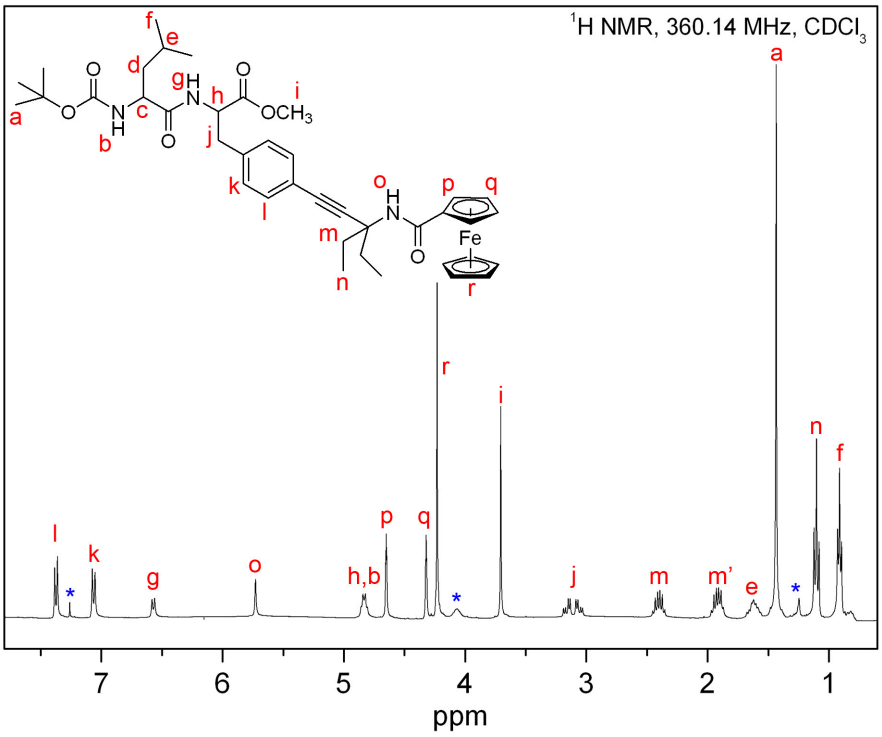

Fig. 5.11 *^{1}H NMR spectrum of Boc-Leu-Phe(DEPA-CO-Fc)-OMe* ***23b***.

The carbon NMR spectrum shows apart from the dipeptide related signals the additional resonances from the added metal marker. An indication for a successful formation of the alkyne-phenyl bond is the down-field shift of the alkyne carbon atoms in the ^{13}C NMR spectrum from 85.9 and 72.8 ppm in H-DEPA-CO-Fc **22** to 91.2 and 83.4 ppm in dipeptide bound DEPA-CO-Fc. Absorbance maxima in the UV-Vis spectrum, measured in chloroform, can be observed at 246 and 255 nm for all compounds **23a-d** (*Fig. 5.12*). These absorbances are $\pi \rightarrow \pi^*$ excitations of aromatic systems with molar extinction

coefficients ε of 25000 and 23000 l/mol·cm, respectively. The significant but weaker ferrocene signal can be observed at 444 nm (ε = 250 l/mol·cm).

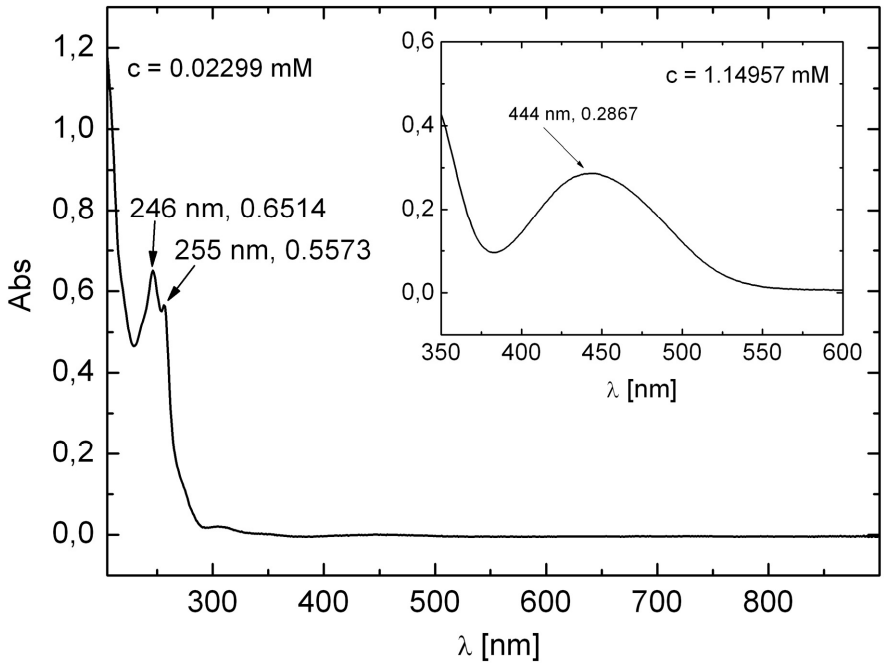

Fig. 5.12 *UV-Vis spectrum of Boc-Leu-Phe(DEPA-CO-Fc)-OMe **23b**. The absorbance peak at 444 nm indicates the presence of a ferrocene group.*

The electrochemical properties of all compounds are very similar, showing that the peptide's influence on the redox behaviour of the marker is small to none. The half-wave potentials are between 209 and 213 mV with peak separations of 80 to 87 mV. *Table 5.3* lists all electrochemical values of compounds **23a-d**.

Tab 5.3 *Electrochemical properties of compounds **23**. All oxidations show full reversibility.*

Compound	E½ [mV]	Peak Sep. [mV]
Boc-Ala-Phe(DEPA-CO-Fc)-OMe **23a**	213.0	82
Boc-Leu-Phe(DEPA-CO-Fc)-OMe **23b**	212.0	80
Boc-Phe-Phe(DEPA-CO-Fc)-OMe **23c**	211.5	87
Boc-Tyr-Phe(DEPA-CO-Fc)-OMe **23d**	209.5	85

The half-wave potential of DEPA-CO-Fc **22** does not change through binding to the target molecule. The pure compound shows the redox event at 223 mV, which is only 10 mV different from the average dipeptide bound DEPA-CO-Fc group.

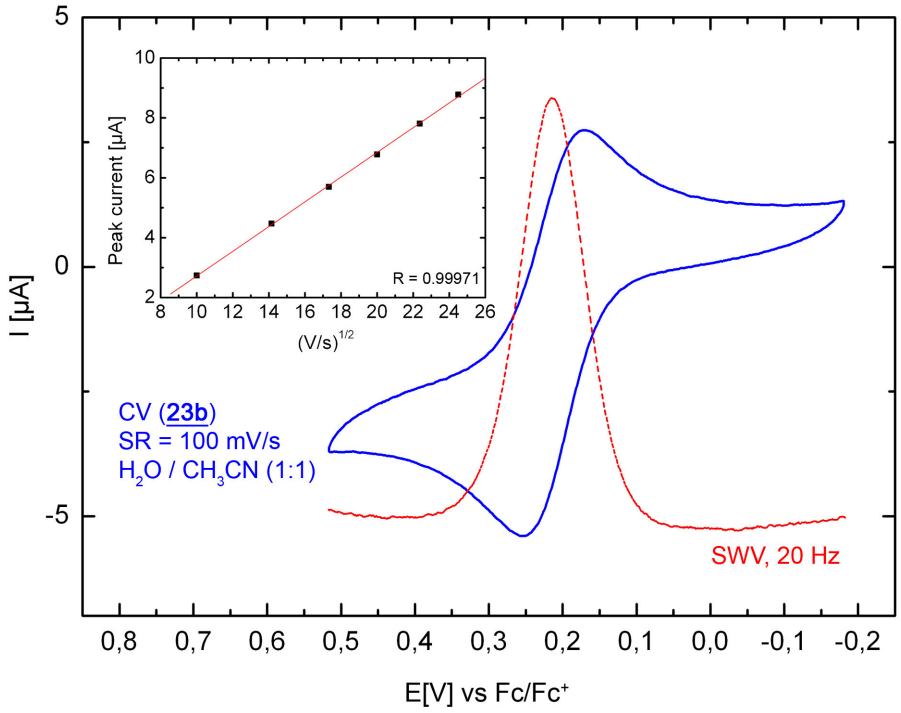

Fig. 5.13 *Voltammograms and Randles-Sevcik plot of **23b** are representative for all compounds **23***

The redox-reaction is still perfectly reversible, confirmed by the strongly linear behaviour of the according Randles-Sevcik plot, which shows a correlation higher than 99.99 %. As a conclusion, the binding of the ferrocene marker to a dipeptide does not worsen the electrochemical properties required for sensitive detection as shown above in *Figure 5.13*. This is promising information for the labelling of bigger molecules like peptides and proteins. Cobaltocenium has not been used as a marker here, since ferrocene better fulfils the electrochemical requirements for detection of bioconjugates even in small amounts.

To verify the universal applicability of the Sonogashira cross coupling method for the introduction of metal markers, all dipeptides have as well been labelled with another ferrocene derivative, the commercially available ethynylferrocene, as already shown in *Figure 5.9*.

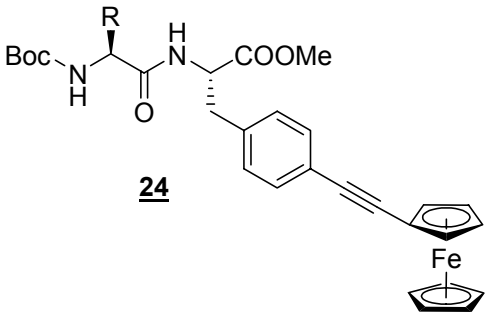

24

24a : R = CH_3 (Ala)
b : R = CH_2-$CH(CH_3)_2$ (Leu)
c : R = CH_2-C_6H_5 (Phe)
d : R = CH_2-C_6H_4-OH (Tyr)

Fig. 5.14 *Ethynylferrocene labelled dipeptides **24a-d**. The synthesis was identical to that of compounds **23a-d**.*

For the synthesis of ethynylferrocene labelled dipeptides the ferrocene marker has been treated under protective atmosphere with the aim to avoid oxidation in air as recommended by the manufacturer. Prolonged contact to air oxygen did not harm the product quality or the yield in any way, though. The Sonogashira reaction went even faster than that of H-DEPA-CO-Fc **22**, as could be observed by TLC. After 3 hours all dipeptide reactant was converted into the labelled product.

All products **24a-d** are orange solids like their DEPA-CO-Fc congeners and also their ability to dissolve in water is very similar, although the additional peptide bond in compounds **23** improves their water dissolution. The purification on silica gel columns is most practical due to the orange color of the compounds. Such purely obtained substances have been characterized by elemental analysis, HPLC and FAB mass spectrometry, with the latter showing $[M]^+$ as the base peak and additional fragments related to $[M\text{-}C_4H_9]^+$ and $[M\text{-Boc}]^+$. All compounds show a strong peak in their mass spectra at m/z = 299, which can be assigned to the cationic species $[Fc\text{-alkynyl-Ph-}CH_2]^+$. ^1H NMR spectra display the expected Cp resonances at 4.53, 4.31 and 4.24 ppm, the methyl ester singlet at 3.59 ppm and the Boc-protons at 1.37 ppm, possessing the highs intensity of 9 protons. *Figure 5.15* shows a selected region of the ^1H NMR spectra of Boc-Leu-Phe(I)-OMe **21b** and Boc-Leu-Phe(ethinyl-Fc)-OMe **24b** to demonstrate the

signal shift of the phenyl protons before and after the coupling process. The values are very similar to those stated in *Table 5.2*, where compounds **21a-d** are compared to the DEPA-CO-Fc derivatized substances **23a-d**.

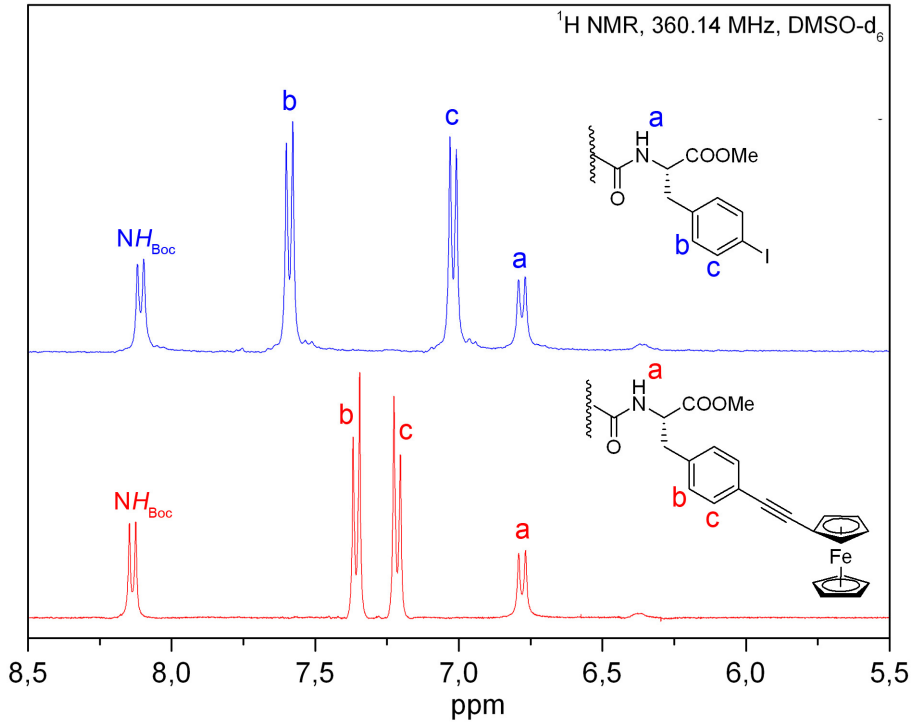

Fig. 5.15 *Aromatic region of the proton NMR spectra of **21b** and **24b**, which shows the shift of the phenyl-ring signals after the iodine has been replaced by an alkyne group.*

The ^{13}C NMR spin-echo spectrum shows both alkyne signals at 88.4 and 85.3 ppm. The binding to the phenyl ring causes a slight down-field shift compared to the free alkyne. The ester and dipeptide carbonyl carbon atoms are the most down-field shifted signals in the spectrum, resonating at 172.2 and 171.1 ppm, respectively. The Boc carbonyl resonance can be found at 155.4 ppm, showing reduced intensity. All four aromatic signals can be observed at 135.4/122.6 ppm (quaternary) and 131.4/129.2 ppm (tertiary). The Cp-signals are slightly different from those observed in the corresponding DEPA-CO-Fc derivative, which is self-explanatory due to electron pushing effect of the alkyne group. This mostly affects the *ipso*-carbon of the substituted Cp ring, shifting it to be the most up-field resonance of all Cp-signals (see *Figure 5.16*). The *ipso*-carbon is hidden under the solvent signal in **23b**.

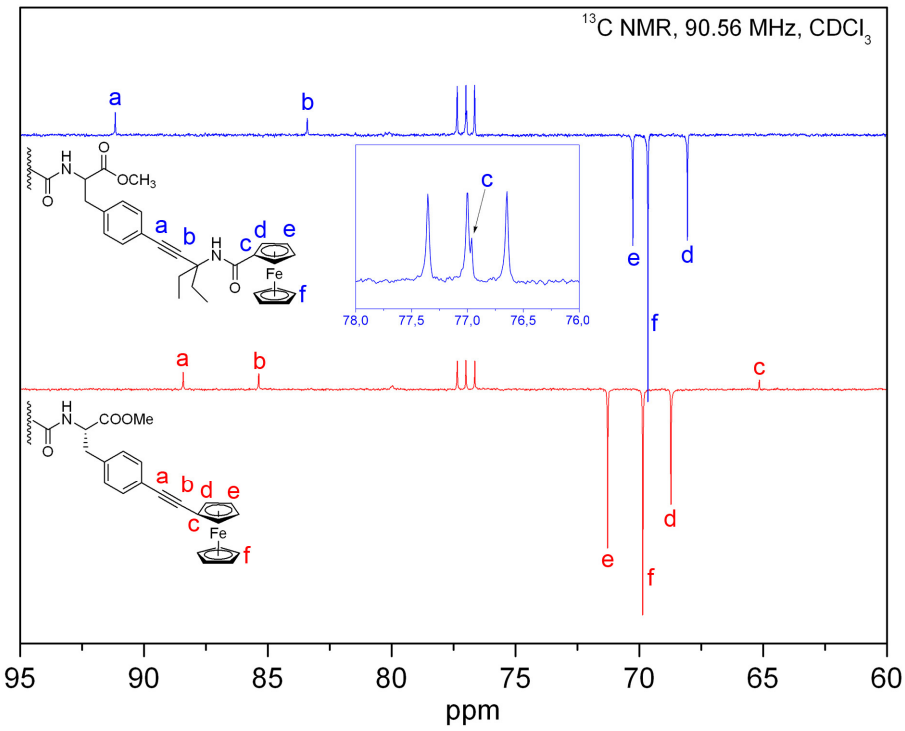

Fig. 5.16 *Selected region from the ^{13}C NMR spectra of Boc-Leu-Phe(DEPA-CO-Fc)-OMe **23b** and Boc-Leu-Phe(alkynyl-Fc)-OMe **24b**. Comparison of alkyne and Cp signals.*

UV-Vis spectroscopy shows an interesting absorbance maximum at 304 nm, which appears next to the already observed maxima at 256 nm (aromatic) and 444 nm (Fc). It can probably be assigned to the conjugated π-system, which extends from the phenyl ring over the alkyne group to the substituted Cp-ring. Another interesting observation is the higher molar extinction coefficient for the ferrocene related absorbance compared to the DEPA derivatives. UV spectroscopic properties of all dipeptides are compared in *Table 5.4*.

Tab 5.4 *Absorbance maxima of all labelled dipeptides from UV-Vis spectra, measured in MeOH.*

Compound	Nr.	$\lambda 1_{max}$	ε (λ1) [l/mol·cm]	$\lambda 2_{max}$	ε (λ2) [l/mol·cm]	$\lambda 3_{max}$	ε (λ3) [l/mol·cm]
Boc-Ala-Phe(DEPA-CO-Fc)-OMe	**23a**	246	24825	256	22150	442	236
Boc-Leu-Phe(DEPA-CO-Fc)-OMe	**23b**	246	28330	255	24240	444	249
Boc-Phe-Phe(DEPA-CO-Fc)-OMe	**23c**	246	27985	256	24510	442	276
Boc-Tyr-Phe(DEPA-CO-Fc)-OMe	**23d**	246	26010	256	22840	442	231
Boc-Ala-Phe(Fc)-OMe	**24a**	256	18335	300	16305	445	563
Boc-Leu-Phe(Fc)-OMe	**24b**	256	17930	301	16030	445	582
Boc-Phe-Phe(Fc)-OMe	**24c**	256	18340	301	16235	446	586
Boc-Tyr-Phe(Fc)-OMe	**24d**	256	18740	301	16360	444	537

Hydrogen bonding in the solid state may be concluded from the IR spectra, where NH-stretch bands appear below 3400 cm^{-1}. The characteristic alkyne stretch band is visible at 2207 cm^{-1}, comparable to that in **23a-d**. The electrochemical experiments deliver the usual one-electron reversible redox reaction from all 4 compounds. The electronic situation for the iron atom is different, though, since the alkyne group is an electron pushing function, opposite to the electron density withdrawing carbonyl group of DEPA-*CO*-Fc **22** and Fc-COOH **1**. Therefore the half-wave potentials of compounds **24a-d** are shifted to lower values between 152.5 to 169.0 mV. Peak separations lie in the range of 73 to 98 mV. Only **24a** shows a higher peak separation of 142 mV. The redox-processes, checked by measurements at increasing scan rates of 100, 200, 300...600 mV and the following constructions of Randles-Sevcik plots, are of highly reversible nature. Correlation values are 99.942 to 99.999 % for a linear behaviour, as calculated from the regression.

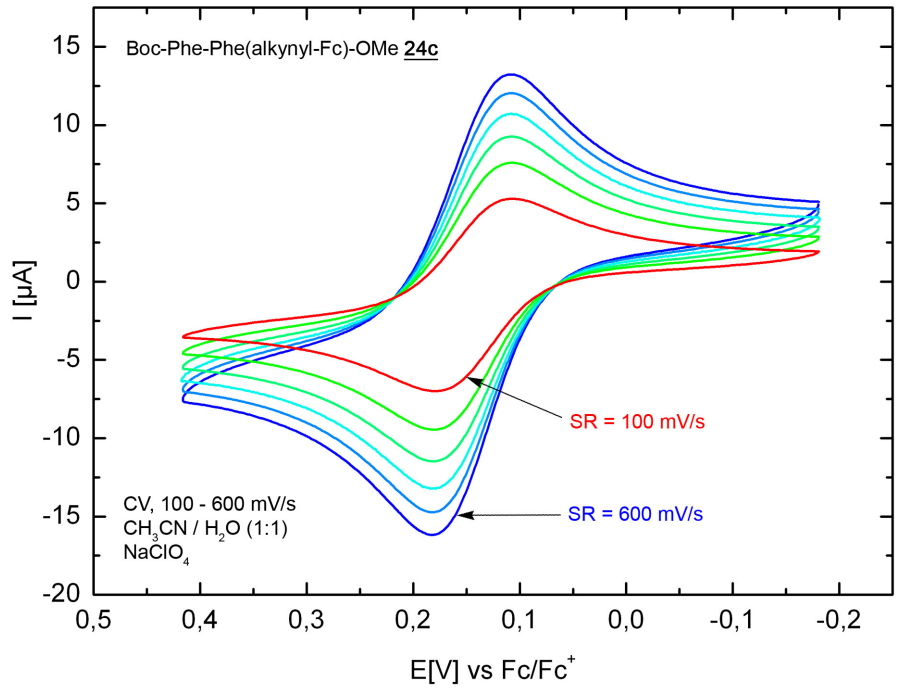

Fig. 5.17 *An Overlay of six cyclovoltammograms of Boc-Phe-Phe(alkynyl-Fc)-OMe **24c** is shown. The scan rate was increased from standard 100 mV/s (red cycle) to 600 mV/s (blue cycle)*

Figure 5.17 shows constant peak positions of all cyclovoltammograms under variation of the scan rate. The electrochemical properties of the ethynylferrocene marker do not rank behind the above presented DEPA-CO-Fc **22** group. Both substances have advantages and while DEPA-CO-Fc is easy to prepare in gram scales from Fc-COOH **1** and less sensitive, the smaller size and even better electrochemical behaviour of ethynylferrocene may recommend the latter. The choice of the marker has to be made according to the proposed synthetic strategy and the demands concerning label size and ease of handling. The fact that two different markers have been tested in this thesis may help to facilitate the planning of a synthetic pathway to a better access of organometallic labelled bioconjugates.

Because the H-DEPA-CO-Fc **22** marker was synthesized in the lab and therefore well characterized, it was chosen to be the candidate for the labelling of a larger peptide like [Leu^5]-Enkephalin via the Sonogashira route, as shown in the following. The results obtained from this dipeptide project suggest that ethynylferrocene would perform according to the DEPA-CO-Fc marker, synthetically and in terms of characterization and detection.

5.4 Synthesis of enkephalin containing *p*-iodo-phenylalanine

5.4.1 Synthesis of Fmoc-Phe(I)-OH 25

The previous *chapter 5.3* has introduced the palladium catalyzed Sonogashira coupling, where an alkyne is bound to a iodo-phenyl group. The dipeptide model approach showed that alkyne derivatized ferrocenes could be coupled to iodo-phenylalanine in a convenient and practical way. Since this method was to be extended, aiming at the labelling of bigger molecules like peptides and proteins, the acquired results were applied to the model peptide [Leu^5]-Enkephalin. As a consequence, the *p*-iodo-phenylalanine moiety had to be inserted into the peptide using solid phase peptide synthesis techniques. Since enkephalin contains a Phe in position 4 it was the ideal location for the introduction of an artificial phenylalanine, without altering the original biomolecule too severely. For the use of *p*-iodo-phenylalanine **19** in SPPS it had to be N$^{\alpha}$-protected,

preferable using Fmoc as protection group, integrating it seamlessly into the whole synthetic workflow. The introduction of Fmoc into H-Phe(I)-OH was carried out following standard procedures, which most often employ Fmoc-OSu or Fmoc-Cl as reagents.

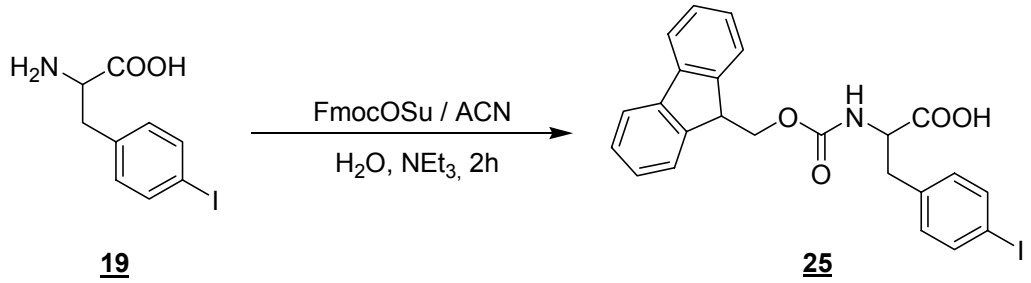

19 **25**

Fig. 5.18 *Simplified reaction scheme for the introduction of the 9-fluorenylmethoxycarbonyl (Fmoc) protection group*

After 2 hours of stirring the reaction mixture was poured into a beaker containing 1.5 M HCl solution whereby a white solid precipitated, which was filtered and repeatedly washed with water. The product **25** was dried overnight *in vacuo* resulting in a yield of 63% of pure substance. Using Fmoc-Cl for the protection process gave better yields (78-85%) but also worse purity. The Fmoc-OSu method was preferred, because the starting material for both methods is not pricey and readily available.

The white powder was characterized by elemental analysis, HPLC and FAB mass spectrometry. The $[M+H]^+$ peak at m/z = 504 and the fragments at m/z = 388 $[M-I+H]^+$, 203 $[M-C_6H_4I+H]^+$ and 165 $[fluorenyl]^+$ found in the mass spectrum confirmed the successful introduction of the Fmoc group. ^1H and ^{13}C NMR spectra showed the typical signals for **19** and additionally all required resonances for the fluorenyl group in the aromatic region and the Fmoc-methylene group at 4.17 and 65.5 ppm, respectively. The solubility in DMF was sufficient as 500 mg clearly dissolved in 2 ml solvent.

5.4.2 Synthesis of Ac-Enk[Phe^4(I)]-OH 26

With the N$^{\alpha}$-Fmoc-protected *p*-iodo-phenylalanine **25** in hand, Ac-Enk[Phe^4(I)]-OH **26** was synthesized by standard solid phase peptide synthesis, where Fmoc-Phe-OH was simply replaced by the modified amino acid. The synthesis was carried out on Wang resin and the cleavage conditions comprised a mixture of 95% TFA, 2.5% H_2O and 2.5% of TIS and a duration of 3h.

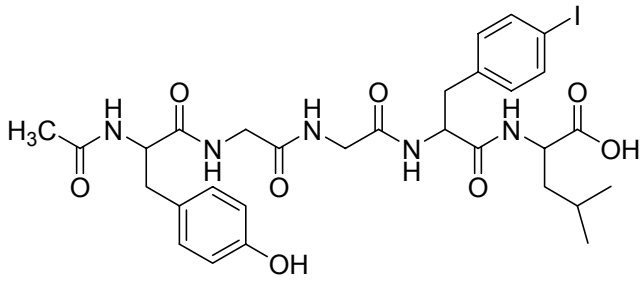

26

Fig. 5.19 *Chemical constitution of the p-iodo-phenylalanine modified and N-acetylated enkephalin*

The crude product (yield: 79%) was purified by preparative HPLC to give a white powder, which shows good solubility in both organic solvents and water. The FAB mass spectrum displays two product peaks for m/z = 746 $[M+Na]^+$ and m/z = 724 $[M+H]^+$ and a number of fragment signals which could be assigned to $[M-(Leu\text{-}OH)]^+$, $[M-(Phe(I)\text{-}Leu\text{-}OH]^+$ and $[M-(Gly\text{-}Phe(I)\text{-}Leu\text{-}OH]^+$, observable at m/z =593, 320 and 263, respectively. The typical signals for [Leu^5]-enkephalin can be found in the proton NMR spectrum but also the unambiguous resonances for the *p*-iodo-phenylalanine residue, forming pseudo-doublets at 7.99 and 7.60 ppm, are visible. The distance is with 0.39 ppm smaller than the value of 0.57 ppm that was observed in the dipeptides. The C*H*$_3$ acetyl group resonates in form of a singlet at 1.77 ppm, as shown in *Fig. 5.20*. The assignment of all signals was supported by HH-COSY 2D NMR spectroscopy.

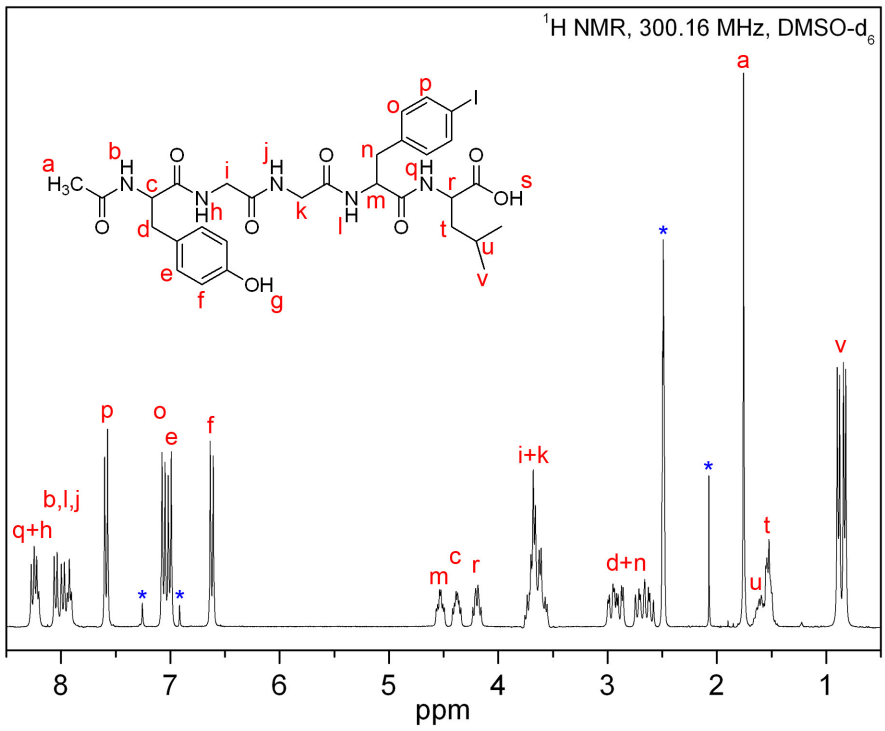

Fig. 5.20 *^{1}H NMR spectrum of Ac-Enk[Phe^{4}(I)]-OH **26** in DMSO-d_6. Signals **p** and **o** correspond to the 1,4-disubstituted phenyl-ring of the modified amino acid **25**.*

All expected carbon signals are observable in the ^{13}C NMR spectrum. Most interesting is the chemical shift of the ipso-carbon atom, which is directly connected to the iodine atom. This quaternary carbon signal resonates at 92.1 ppm but is expected to move approximately 30 ppm to the lower field after the iodine has been substituted by the alkyne group of the ferrocene marker. UV-Vis spectroscopy reveals two major absorbance maxima at 225 nm and 259 nm which can be assigned to peptide bond and aromatic $\pi \rightarrow \pi^*$ excitations.

5.4.3 Synthesis of I-Ph-Enk-OH 27

Among the main demands for a versatile labelling methodology is a high grade of variability which allows not only to choose between different types of marking agents and reaction conditions but also to select a certain coupling site inside the biomolecule. Metal markers have been successfully attached to the N-terminus and the side-chain of enkephalin as presented in *chapter 4*. To provide the same flexibility for the Sonogashira coupling strategy, the introduction of a *p*-iodo-phenyl function at the N-terminus was carried out using *p*-iodo-benzoic acid (PIBA) as a 'sixth' amino acid in SPPS.

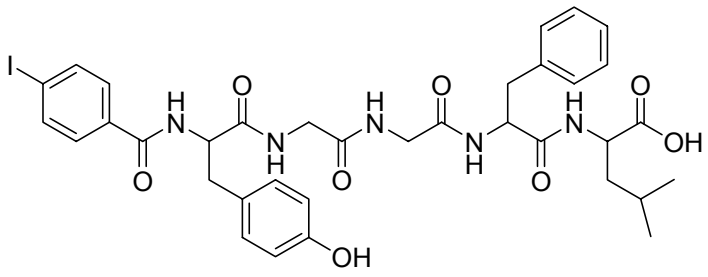

27

Fig. 5.21 *[Leu]-enkephalin was derivatized at the N-terminus using p-iodo-benzoic acid, thus introducing a Sonogashira compatible function.*

The reaction was carried out according to the synthesis of **26**. The cleavage of the Wang-attached product was performed under standard conditions and after removal of 90% of the solvents and the subsequent precipitation in diethylether, nearly pure compound **27** was obtained in a yield of 86%. The white powder was submitted to FAB mass spectrometry showing the correct peaks at m/z = 808 $[M+Na]^+$ and 786 $[M+H]^+$. Additional fragments are observable in analogy to **26**. The successful introduction of the *p*-iodo-phenyl residue at the N-terminal side of the peptide is confirmed by the corresponding aromatic signals at 7.82 and 7.57 ppm, which each possess coupling constants of 8.4 Hz. These values are similar to those found in all previously presented 1,4-disubstituted phenyl groups, which range from 7.8 to 8.6 Hz. A selected part of the aromatic region of the measured ^{1}H NMR spectrum is shown in *Figure 5.22*.

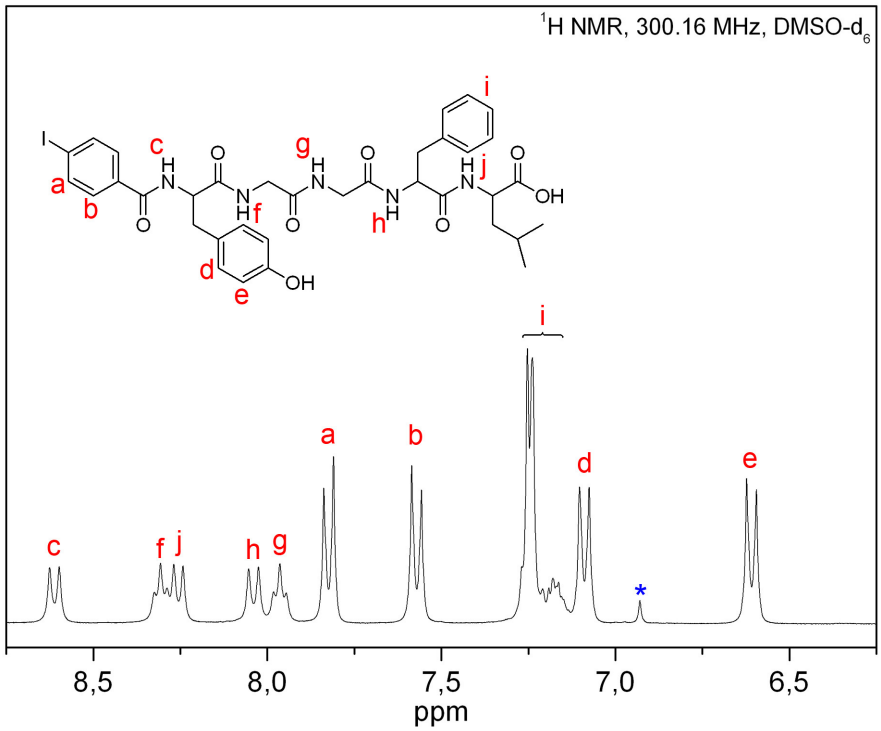

Fig. 5.22 *Aromatic region of the ^{1}H NMR spectrum of I-Ph-Enk-OH **27**. Glycine amide protons can be identified by their triplet shape (**f** and **g**).*

The ^{13}C NMR spectrum shows 6 carbonyl carbon resonances between 173.7 (*C*OOH) and 165.6 ppm (PIBA). In addition, all 12 aromatic carbon signals can be observed, being positioned between the highly down-field shifted signal of tyrosine (155.6 ppm) and the iodine bound carbon atom resonance at 98.7 ppm. As well as in the case of compound **26**, the shielding effect of the iodine atom is responsible for the shift to higher field and the cross coupling reaction is expected to make the signal move down-field by more than 30 ppm. Therefore the signal can be consulted as an indicator for the monitoring of a successful Sonogashira coupling.

5.5 Sonogashira coupling of H-DEPA-CO-Fc to [Leu^5]-Enkephalin

5.5.1 Synthesis of Ac-Enk[Phe^4(DEPA-CO-Fc)]-OH 28

Differently from the synthesis of the ferrocene coupled dipeptides **23a-d** and **24a-d**, the side-chain modified enkephalin derivative **26** was reacted in a mixture of DMF/NEt_3 (1:1) out of solubility reasons. Apart from the change of solvents the synthesis of **28** was carried out in analogy to the dipeptide Sonogashira reactions, as given in *Fig. 5.23*.

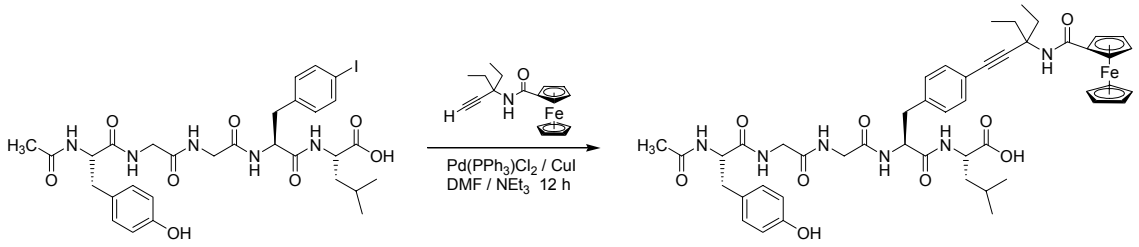

26 **28**

Fig. 5.23 *An alkyne derivatized ferrocene is bound to the p-iodo-phenylalanine side-chain of modified enkephalin **26** to yield the labelled biomolecule **28***

The reaction progress was monitored by HPLC and the synthesis was finished after 12 hours, when no more peptide starting material was detected. The solvents were removed on the vacuum pump and the residual oil was re-dissolved in acetonitrile and purified by preparative HPLC. The light yellow powder was characterized by ESI (neg.) mass spectrometry where the spectrum shows a peak for $[M-H]^-$ at m/z = 917.4, while the ESI (pos.) spectrum confirms this observation showing three molecular peaks at m/z 919.4 $[M+H]^+$, 941.4 $[M+Na]^+$ and 957.5 $[M+K]^+$. The successful introduction of the ferrocene label had occurred as can be deduced from the typical 2-2-5 Cp signal pattern in the ^{1}H NMR spectrum. The Cp-protons resonate at 4.92, 4.33 and 4.19 ppm. *Table 5.5* shows the comparison between the Cp signal positions of all DEPA-CO-Fc **22** labelled compounds. The influence of the biomolecule on the chemical shifts of the Cp-protons seems to be small, which is explainable by the long distance of the peptide to the ferrocene moiety.

Tab 5.5 *Overview of the chemical shifts in DEPA-CO-Fc compounds as observed in ^1H NMR spectroscopy (all spectra measured in DMSO-d_6).*

Compound	Nr.	δ $Cp_{2,5}$ [ppm]	δ $Cp_{3,4}$ [ppm]	δ Cp' [ppm]	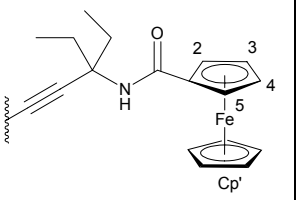
H-DEPA-CO-Fc	**22**	4.89	4.33	4.18	
Boc-Ala-Phe(DEPA-CO-Fc)-OMe	**23a**	4.89	4.31	4.17	
Boc-Leu-Phe(DEPA-CO-Fc)-OMe	**23b**	4.90	4.32	4.19	
Boc-Phe-Phe(DEPA-CO-Fc)-OMe	**23c**	4.90	4.33	4.20	
Boc-Tyr-Phe(DEPA-CO-Fc)-OMe	**23d**	4.95	4.35	4.27	
Ac-Enk[Phe^4(DEPA-CO-Fc)]-OH	**28**	4.92	4.33	4.19	
Fc-DEPA-Ph-Enk-OH	**29**	4.95	4.37	4.21	

Except for the phenylalanine ring protons all other peptide related proton NMR signals stay unchanged before and after the coupling reaction. The amide protons produce signals above 7.5 ppm, because hydrogen bonds are formed with the solvent DMSO. The dipeptide compounds **21**, **23** and **24** have additionally been measured in chloroform, where the amide signals occur below 7.5 ppm, suggesting that no intermolecular hydrogen bonds are present, whereas infrared spectroscopy (KBr) shows the formation of hydrogen bonds both in dipeptides and enkephalin in the solid state. Beyond these observations no other conclusions concerning molecular conformations can be drawn. The carbon atom to which the iodine atom was connected has shifted from 92.1 ppm in **26** to 120.5 ppm in **28**. The Cp-carbon signals of the tethered ferrocene compound resonate between 76.5 and 68.2 ppm and underlining the successful reaction. The DEPA ethyl groups show signals at 8.4 for CH_3 and at 29.9 ppm for CH_2, while the alkyne carbon atoms resonate at 91.7 and 82.0 ppm. A comparison of the carbon NMR spectra before and after the coupling process is shown in *Fig 5.24*.

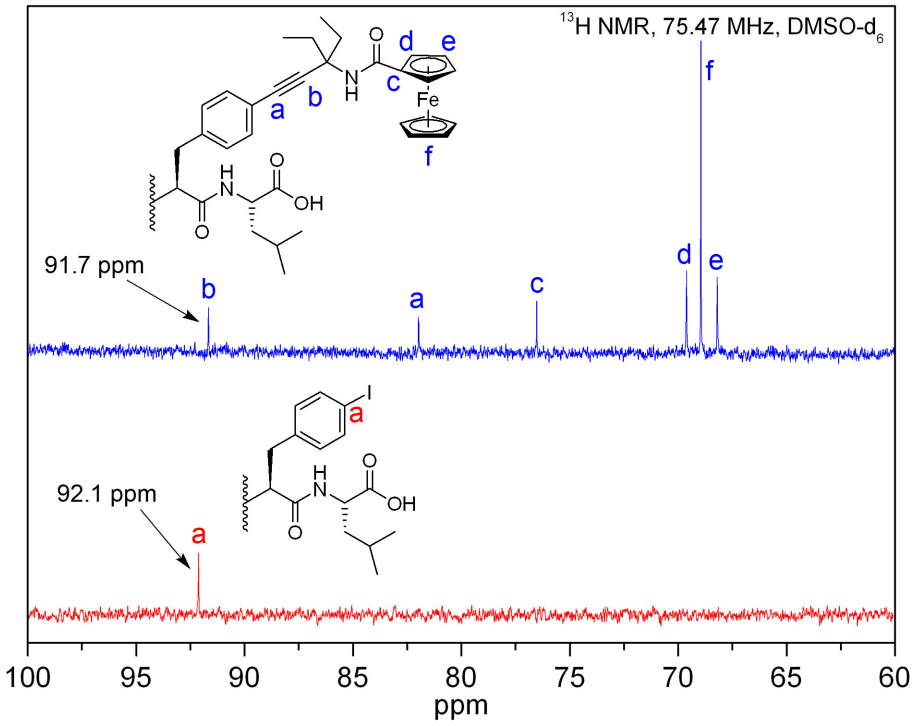

Fig. 5.24 *Selected regions from ^{13}C NMR spectra of Ac-Enk[Phe^4(I)]-OH **26** (red) and Ac-Enk[Phe^4(DEPA-CO-Fc)]-OH **28** (blue). Signals **b** (blue) and **a** (red) are coincidentally almost isochronic.*

The ferrocene characteristic absorbance maximum at 444 nm is visible in the UV-Vis spectrum, which was measured in methanol. The experimentally determined extinction coefficient ε is 272 l/mol·cm and therefore congruent with all other DEPA-CO-Fc derivatives. Only the ethynylferrocene dipeptides **24a-d** have higher extinction coefficients between 535 and 585 l/mol·cm, albeit with the same absorbance maximum at 445 nm (see *Table 5.4*). By the tethering of a ferrocene group new electrochemical properties are introduced. Those have been studied by the recording of cyclovoltammograms and square wave voltammograms, which are shown in *Fig. 5.25*. The half-wave potential value E½ was determined to be 210 mV, which is comparable to other DEPA-CO-Fc compounds. The one-electron redox process is reversible as can be read from the Randles-Sevcik calculations and a peak separation of 80 mV.

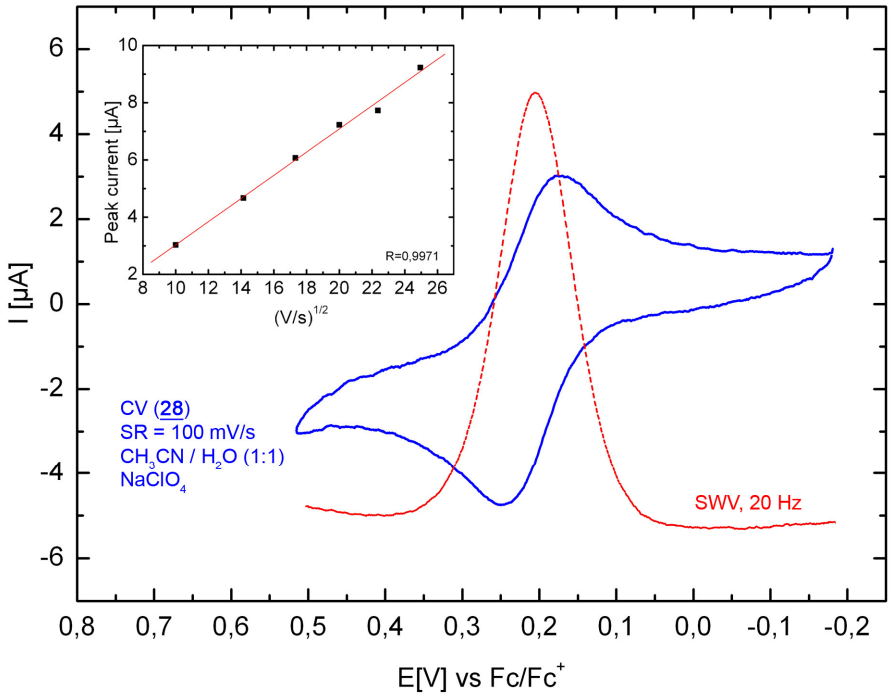

Fig. 5.25 *Electrochemical measurements prove the presence of a ferrocene group in the biomolecule revealing the typical one-electron reversible redox process.*

5.5.2 Synthesis of Fc-CO-DEPA-Ph-Enk-OH 29

DEPA-CO-Fc **22** was coupled to the N-terminal PIBA-derivatized enkephalin **27** under the same reaction conditions like those employed for the synthesis of **28.** Again, the reaction progress was followed by analytical HPLC and the conversion was finished after 10 hours. The solvents were removed and the crude product was purified by preparative HPLC. However, the yield was significantly lower in comparison to **28**, and only a few mg of pure substance were obtained. A reaction scheme for the formation of Fc-CO-DEPA-Ph-Enk-OH **29** can be regarded in *Fig. 5.26*.

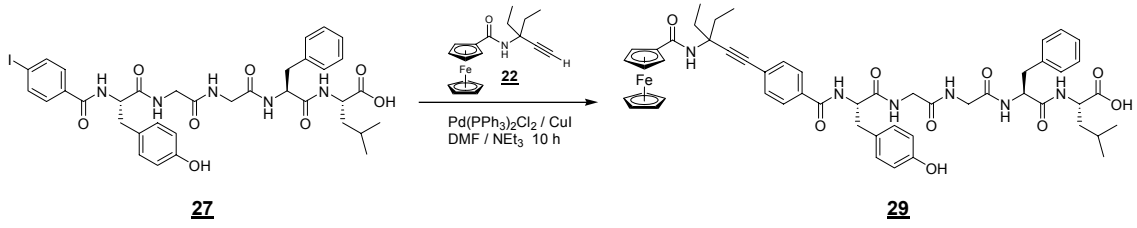

Fig. 5.26 *Synthesis of Fc-CO-DEPA-Ph-Enk-OH **29** by Sonogashira coupling in solution*

The mass peak at m/z = 979.5 (ESI, neg.) can be assigned to the single deprotonated molecular mass $[M-H]^-$ anion. The signals found in the proton NMR spectrum tell that the bond formation has occurred indicated by the disappearance of the alkyne resonance of **22**. In addition, the Cp-signals are visible at 4.92, 4.34 and 4.19 ppm. These chemical shifts are identical to those of all other measured DEPA-CO-Fc compounds (see *Tab. 5.5*).

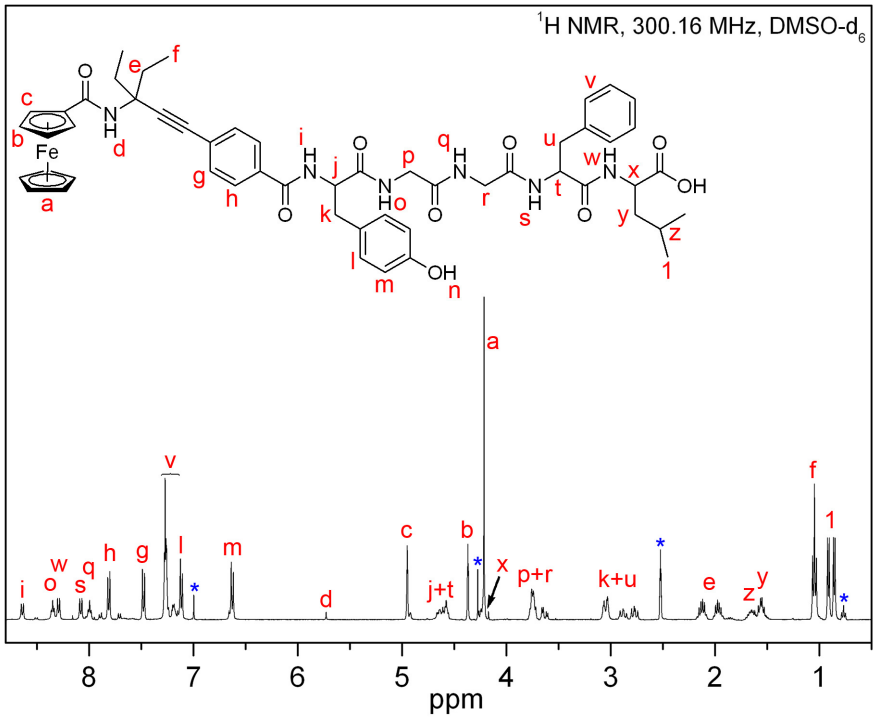

Fig. 5.27 *^{1}H NMR spectrum of Fc-CO-DEPA-Ph-Enk-OH **29** recorded at 300.16 MHz in DMSO-d_6*

Not enough substance was obtained to measure a qualitative satisfying ^{13}C NMR spectrum but still the required signals in the carbonyl area between 175 and 160 ppm and all four Cp-carbon resonances around 75 ppm can be identified. The signal to noise ratio is not good enough to identify the alkyne carbon atom, which have small intensities by nature, anyway. The UV-Vis experiment shows one huge absorbance peak at 269 nm and the demanded Fc-absorbance maximum at 442 nm, which is responsible for the yellow-orange color of all ferrocene containing bioconjugates presented so far.

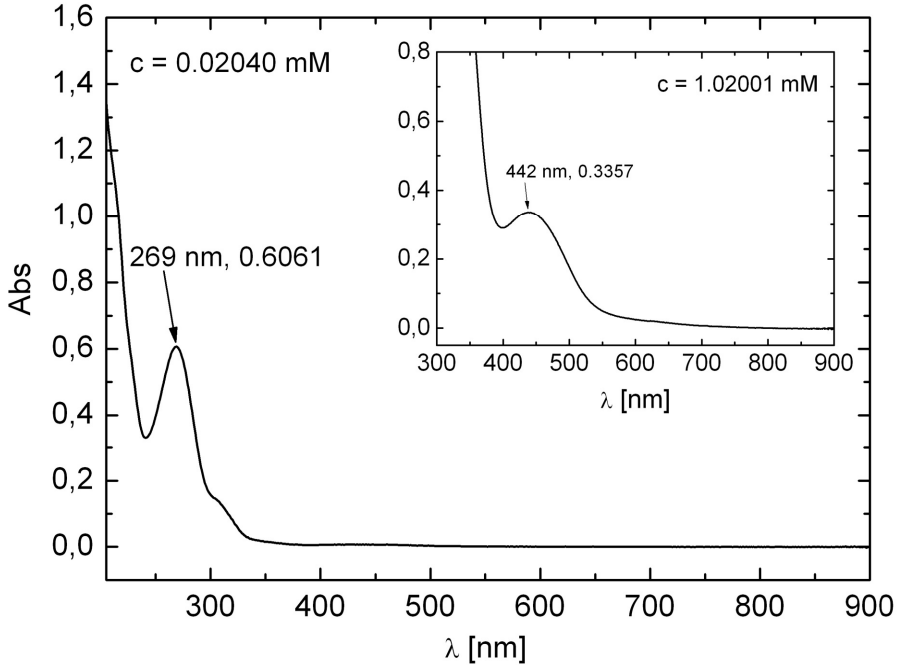

Fig. 5.28 *UV-Vis absorbance spectrum for Fc-CO-DEPA-Ph-Enk-OH **29**. Spectrum recorded in MeOH*

The concluding electrochemical studies show the same reversible behaviour as all other ferrocene derivatives. Similar to the side-chain derivative **28** the working electrode had to be polished after each run, because the recorded cyclovoltammograms became mis-shaped after repetitive use. The same effect was observed with the peptide bound Fc/Cc derivatives (*chapter 4*) and can be interpreted as a passivation of the electrode surface by a plating process of oxidized peptide material. Table 5.7 contains comparison of electrochemical data of all Sonogashira labelled compounds.

Tab 5.6 *Half-wave potentials and peak separation values of Fc-labelled biomolecules*

Compound	Nr.	mol. mass [g/mol]	E½ [mV]	Peak Sep. [mV]
H-DEPA-CO-Fc	**22**	323.10	223.0	86
Boc-Ala-Phe(DEPA-CO-Fc)-OMe	**23a**	671.27	213.0	82
Boc-Leu-Phe(DEPA-CO-Fc)-OMe	**23b**	713.31	212.0	80
Boc-Phe-Phe(DEPA-CO-Fc)-OMe	**23c**	747.30	211.5	87
Boc-Tyr-Phe(DEPA-CO-Fc)-OMe	**23d**	763.29	209.5	85
Boc-Ala-Phe(CC-Fc)-OMe	**24a**	558.18	163.0	142
Boc-Leu-Phe(CC-Fc)-OMe	**24b**	600.23	169.0	98
Boc-Phe-Phe(CC-Fc)-OMe	**24c**	634.21	152.0	73
Boc-Tyr-Phe(CC-Fc)-OMe	**24d**	650.21	161.0	82
Ac-Enk[Phe^4(DEPA-CO-Fc)]-OH	**28**	918.36	210.0	80
Fc-CO-DEPA-Ph-Enk-OH	**29**	980.38	216.0	80

The successful introduction of alkynylated Fc derivatives into dipeptides and different positions of a pentapeptide has been presented in *chapter 5*. These results prove the Sonogashira coupling method to be of high value for the easy tethering of metal compounds to modified biomolecules. Together with the experimental results of *chapter 4* two strategies for the selective labelling of biomolecules are provided to the chemist who is interested in structural elucidation of large biomolecules, electronic modifications or the wide area of diagnostic agents. Especially for the latter it is important not only to chemically bind the metal marker to the desired biomolecule but also to monitor the change in biological properties like hydrophilicity, bio-availability and pharmacokinetics/dynamics. To gain insight into the metal marker's impact on such key attributes, biological studies have been carried out with selected substances from *chapters 4 and 5*. These interesting results will be explained in the following chapter.

6 Biological properties of metallocene labelled Leu-Enkephalins

6.1 Introduction

The detection of biomolecules like hormones, enzymes, nucleic acids and peptides inside a biological system is among the main interests in modern diagnostic medicine. This requires in most cases the introduction of a chemical probe, which provides unique spectroscopic properties. However, this may lead to altered biological characteristics, which can affect uptake, activity, metabolism and toxicity of the original target molecule. It is therefore essential to gather information about the marker's influence on these biological and pharmacological attributes.

An important factor for cell uptake is the lipophilicity of a substance, which has to be high enough to enable passage through the phospholipid cell membrane. The n-octanol/water partition coefficient $P_{o/w}$ is commonly used to describe the lipophilicity of a compound and is usually given in the logarithmized form, log*P*. The labelling of enkephalin with metallocene derivatives is expected to have a huge influence on the log*P* values of the peptide, because lipophilic metallocenes are bound to the rather hydrophilic biomolecule. Partition coefficients are either determined by the shake-flask method[171] or more conveniently by RP-HPLC methods.[172, 173]

Lipophilicity is also a reliable physicochemical parameter for the prediction of blood-brain-barrier (BBB) permeation,[174-176] which is given in form of apparent permeability coefficients (P_{app}). These P_{app} values are measured in transport experiments, where the time dependent permeation of a substance through a cell monolayer is studied. These *in vitro* blood-brain-barrier models make use of bovine, rat or porcine brain endothelial cells, which are extracted, purified and cultured.

In this thesis, log*P* values have been determined for various enkephalin derivatives, which were presented in *chapter 4*. In addition, blood-brain-barrier permeation experiments through pig brain endothelial cells have been conducted with selected enkephalin compounds. These results will be compared and presented in the following chapter.

6.2 Log*P* measurements of Enkephalin derivatives

6.2.1 Theoretical background

Since the introduction of the Hansch approach[177] to drug design, the lipophilicity of drug molecules, agrochemicals and general chemicals gained great importance. Fujita *et al.* first proposed the octanol water coefficient ($P_{o/w}$) as a good model for biological partition.[178] Since then, the logarithm of the octanol-water partition coefficient (log*P*) has become the most widely used lipophilicity parameter. The log*P* property value is taken from the ratio of the respective concentrations of a compound in the octanol and water partitions of a two-phase system at equilibrium. The concentration measurements are made at a constant temperature, normally 25° C.

$$\log P = \log\left(\frac{[X]_{oct}}{[X]_{aq}}\right) \qquad (1)$$

The calculation of logP values: [X]= concentrations, oct = octanol, aq = water

The shake flask method[171] is the oldest and most tedious way of measuring log*P* values. The UV absorbance (fluorescence, radioactive decay, etc.) of an aqueous solution is measured before and after being shaken with a known volume of octanol. The method is messy and smelly but is still the best procedure that can be used in cases of very low log*P* values. One advantage is that the appearance of compound in the octanol phase may be checked against the disappearance from the aqueous phase to see if any surface effects have occurred. Some molecules may form effective surfactants and by that falsify the observed results.

High performance liquid chromatography (HPLC) provides an easy, reliable and accurate way to measure the concentrations of dissolved compounds, thus it can be used as a method to obtain octanol-water partition coefficients. However, the technique has greater potential to determine the partition properties of compounds based on their chromatographic retention times.[179]

Considering retention in a chromatographic partition system as a dynamic equilibrium process with an equilibrium constant K_R, the retention process can be described by

$$\ln K_R = \frac{-\Delta G_R}{RT} \tag{2}$$

where ΔG_R, R and T are the Gibbs free energy change of retention, gas constant and absolute temperature, respectively. The chromatographic retention time directly relates to the compound's distribution between the mobile and the stationary phase. The capacity factor k', determined from the retention time (t_R) and dead time (t_0), is equal to the ratio of the average number of analyte molecules in the stationary phase to the average number of molecules in the mobile phase (Eqn. 3) during the elution process.

$$k' = \frac{N_s}{N_m} = \frac{t_R - t_0}{t_0} \tag{3}$$

N_s, N_m = number of molecules in the stationary/mobile phase, t_R = retention time, t_0 = dead time

The calculation of the capacity factor requires knowledge of the system's dead time, t_0. In theory, t_0 is equal to the retention time of a solute "identical" to the mobile phase,[180] a value which is experimentally impossible to determine. In practice, several approaches have been applied to solve this problem. The most frequently applied procedures include (a) the use of labelled mobile phase components, (b) the use of non-retained polar solutes and (c) the use of organic or inorganic salts.[180-183]

The capacity factor is related to the thermodynamic equilibrium constant K_R via

$$k' = K_R \Phi \tag{4}$$

where Φ is the phase ratio of the stationary to the mobile phase. Combination of equations (2) and (4) yields

$$\ln k' = -\frac{\Delta G_R}{RT} + \ln \Phi \quad \text{or} \quad \log k' = -\frac{\Delta G_R}{2.3\,RT} + \log \Phi \tag{5a,b}$$

Equations 3 and 5 show that the capacity factor *k'* (3) is directly connected to retention times via the system's free energy.

The addition of an organic solvent like MeOH to the water phase reduces the surface tension and enables the analytes to dissolve easier in the mobile phase, thereby decreasing the energy demand of the system and with that the retention time. As a result, a different capacity factor is obtained for each water-organic solvent ratio. This behaviour is found to be linear under certain conditions[184] and follows the expression

$$\log k' = \log k_W + S\varphi \qquad (6)$$

where φ is the volume fraction of the organic solvent (MeOH) in the water-organic solvent mixture, k_W represents the capacity factor of the analyte at 100% water as mobile phase (obtained by extrapolation to the intercept of the ordinate) and *S* the slope of the regression curve.

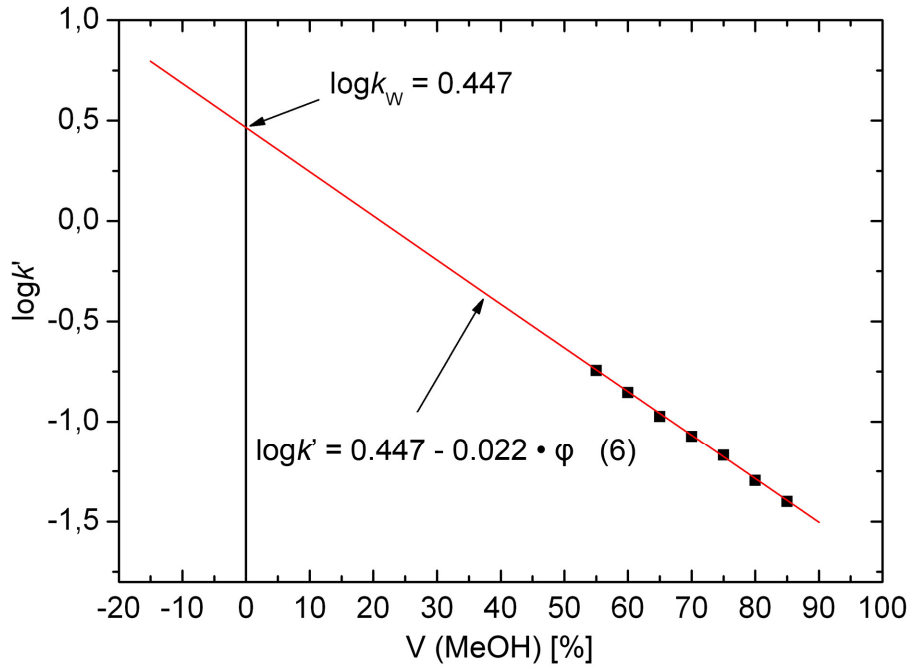

Fig. 6.1 *Retention times of a substance have been measured at different MeOH/H_2O mixtures (55-85% MeOH) and the resulting capacity factors, calculated according to (3), have been plotted versus the MeOH fraction. Extrapolation to 0% MeOH gives $\log k_W$.*

Such obtained logk_W values have been much more successfully correlated to log*P* than the simple capacity factors.[185, 186] The best results were obtained for neutral and lipophilic compounds, whereas ionic substances show a more complex behaviour than that of simple partitioning. No universal system has been found so far and it can be observed that experimentally determined log*P* values of more complex molecules show high deviations when measured by different methods.[179] On the other hand, HPLC methods are besides computational approaches still the most feasible tools to determine log*P* values.

6.2.2 Quantitative structure-activity relation (QSAR)

Lipophilicity expressed in form of log*P* appears in almost every analysis of physicochemical properties related to absorption and permeation.[187] In modern drug design it is one of four key properties that are taken in account to predict the drug's solubility and permeation behaviour. These four properties are (a) molecular weight, (b) log*P*, (c) the number of H-bond donors and (d) the number of H-bond acceptors. After analysis of more than 6000 potent drugs Lipinski[188] found that poor absorption and permeation are more likely when:

(a) The molecular weight is over 500
(b) The log*P* is over 5
(c) There are more than 5 H-bond donors (the sum of OH and NH groups)
(d) There are more than 10 H-bond acceptors (the sum of O and N atoms)

Because the cut-off values for these four parameters are all close to 5 or multiples of 5, the system was named the 'rule of 5'.[189] The predictive power of this rule lead to the development of a great number of techniques to measure or calculate the log*P* of a desired lead structure. A major drawback of computational methods is their weakness concerning metal complexes or organometallic groups. These are either not supported[190] or only added in form of an incremental approach[191], both leading to unsatisfying results. Therefore, lipophilicity of the metallocene labelled enkephalin derivatives could only be determined experimentally (*chapter 6.2.3*).

Typical log*P* values range from -3 to +6 with the higher numbers representing higher lipophilicity. Functional groups that can establish hydrogen bonds with water decrease the lipophilicity drastically. The same is valid for functional groups which can yield ions through dissociation. Alkyl and aryl groups, on the other hand, increase the log*P* of a substance. *Table 6.1* gives a few examples of log*P* values of some small peptides, drugs and general chemicals.[188, 192-197]

Tab 6.1 *A selection of various types of substances and their corresponding logP values*

Compound	log*P*	Ref	Compound	log*P*	Ref
phenol	1.46	185	Aspirin	1.70	181
3-hydroxyphenol	0.80	185	Captopril	0.64	181
anisole	2.11	185	Diclofenac	3.99	181
4-methoxyanilin	0.95	185	Ibuprofen	3.23	181
thymol	3.30	185	Naloxone	1.53	181
$AcTyrNH_2$	-0.79	186	Omeprazol	-4.34	181
$AcGlyNH_2$	-1.76	186	Diazepam	3.36	181
$AcPheNH_2$	0.04	186	Erythromycin	-0.14	181
$AcLeuNH_2$	-0.04	186	Mannitol	-2.50	181
$AcTyrLeuNH_2$	0.32	187	Glycine	-3.44	181
$AcGlyPheNH_2$	-0.56	187	Met-Enkephalin	-1.15	188
$AcPheValNH_2$	0.43	187	Morphine	-0.55	189
$AcLeuIleNH_2$	0.68	187	Leu-Enkephalin	-1.55	190

From a survey of the literature, it is possible to obtain some general guidelines about the optimum log*P* values for certain classes of drugs.[198] The meaning of log*P* for passive absorption and dosing is given in *Table 6.2*.

Tab 6.2 *Ideal ranges of lipophilicity (logP) for passive absorption and dosing forms*

Type of absorption	ideal log*P*	Type of formulation	ideal log*P*
oral	1.80	injectable	below 0
intestinal	1.35	oral	0-3
colonic	1.32	transdermal	3-4
sublingual	5.50	toxic build-up in fatty tissues	5-7
percutaneous	2.60		

A rough guideline as shown above enables better estimation of how the target molecule is going to behave in a biological environment. However, it should be kept in mind that log*P* values cannot easily be compared when measured by different systems. Albeit, for an internal comparison or correlation to results from biological experiments these methods are of great value and may help to better describe the substance's properties *in vivo*.

6.2.3 log*P* values of selected Enkephalin derivatives

Minick *et al.* have presented a simple procedure for the calculation of log*P* by determination of logk_W values.[192] Since this method has been experimentally confirmed by other groups,[199] it was chosen to be suitable for investigating partition coefficients of the synthesized metallocene-enkephalin derivatives.

The eluents were prepared according to literature. The water phase was saturated with 1-octanol using a separatory funnel and was subsequently filtered before use. Then the buffering agent (MOPS, 0.02 M) and the amino modifier (*n*-decylamine, 0.15% v/v) were added. Because not all silanol groups of the stationary phase are substituted by C18 chains, RP-columns show partly hydrophilic behaviour, which hinders a correct emulation of a water/octanol system. Therefore an amino modifier is used to mask the majority of free silanol groups. The pH of the water phase was afterwards adjusted to 7.4. The methanol phase was simply mixed with *n*-octanol (0.25%, v/v).

Four different standards with known log*P*s (4-methoxyanilin, 4-bromoanilin, naphthalene and *tert*-butylbenzene) were chosen for calibrating the system and to establish a correlation between logk_W and log*P*. These substances were dissolved in methanol (0.1 mM) and uracil was added (0.01 mM) to indicate the system's dead time. In first experiments, dead time was also measured by urea but the results compared to uracil were found to be nearly identical. For the final log*P* experiments uracil was preferred due to its additional 254 nm chromophore, while urea only absorbed at 220 nm in UV. The standard mixture was run with 7 isocratic gradients containing between 55 and 85% of MeOH. The retention times, together with the dead times obtained from uracil, were used to calculate the corresponding capacity factors *k*' according to eqn (3) for every water/methanol ratio. *Table 6.3* shows the results for 4-methoxyanilin as an example.

Tab 6.3 *The retention times of 4-methoxyanilin measured in different isocratic mixtures of water/methanol were used together with the dead times to calculate the capacity factors k'.*

MeOH	t (uracil) dead time	t (4-Methoxyanilin)	*k'* (4-Methoxyanilin)	log*k'* (4-Methoxyanilin)
55	3,439	4,057	0,180	-0,745
60	3,446	3,927	0,140	-0,855
65	3,457	3,824	0,106	-0,974
70	3,395	3,681	0,084	-1,074
75	3,377	3,606	0,068	-1,169
80	3,303	3,470	0,051	-1,296
85	3,313	3,445	0,040	-1,400

In the same way, capacity factors *k*' were obtained for all four standards, logarithmized and plotted against the related methanol fraction, resulting in linear functions by regression (*Fig. 6.2*). The extrapolation to 100% water (0% MeOH) gave the desired logk_W value for each standard.

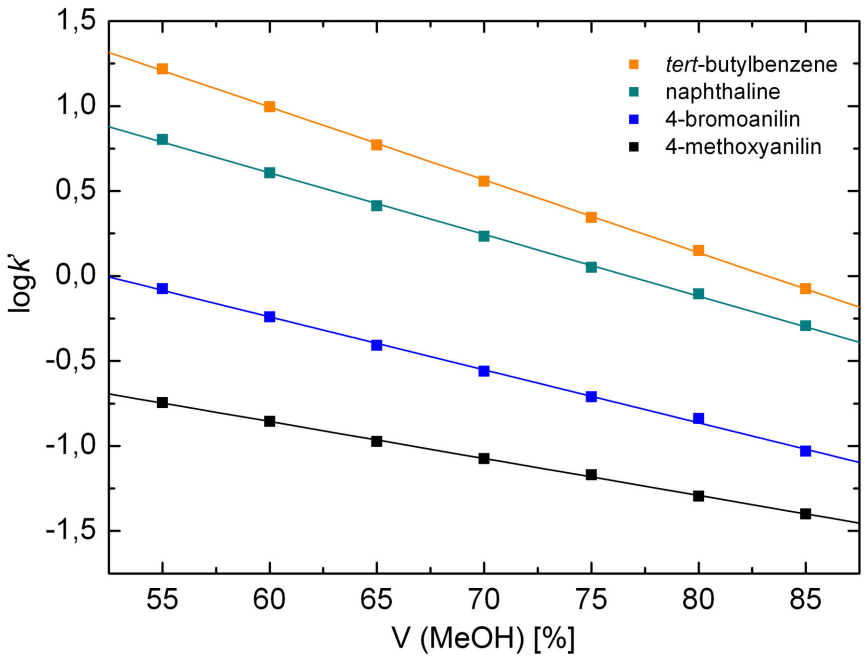

Fig. 6.2 *Plot of calculated logk' versus the methanol fraction of all 4 standards. The extrapolation to 0% of methanol gives logk_W*

The calibration showed high confidence levels of > 99.9%. The linear equations and the resulting capacity factors for a 100% water phase (logk_W) of each standard substance are shown in *Table 6.4*.

Tab 6.4 *The linear equations obtained for the calibration system and the determined logk_W values*

Compound	log*P* (from ref. 185)	linear equation	correlation (R^2)	logk_W
tert-butylbenzene	4.11	y = -0.0428x + 3.5652	0.9996	3.5652
naphthalene	3.30	y = -0.0363x + 2.7824	0.9991	2.7824
4-bromoanilin	2.26	y = -0.0312x + 1.6330	0.9985	1.6330
4-methoxyanilin	0.95	y = -0.0217x + 0.4463	0.9991	0.4463

Calibration was concluded in a last step, where all 4 logk_W values were plotted against the literature log*P* values of the standard compounds to obtain a linear function which correlates both parameters (*Fig. 6.3*). This function was then used to determine all other log*P*s from their logk_W values, measured in the same way like those of the standard substances.

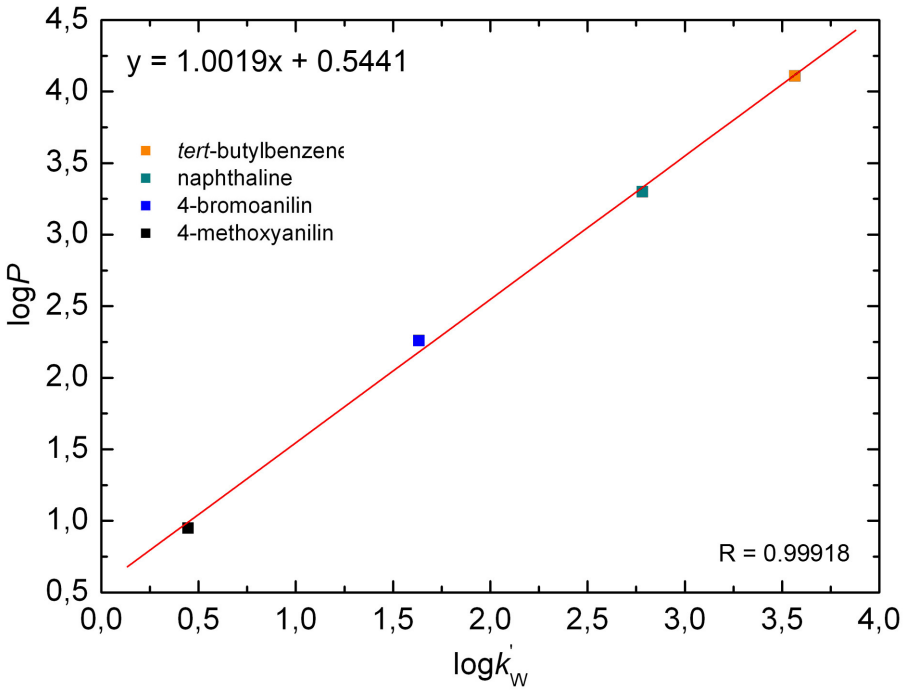

Fig. 6.3 *The correlation of logk_W of the four standards with their logP values shows a linear function, which can be used to calculate logP out of any logk_W value measured on that system*

The linear function, derived from the plot shown in *Fig. 6.3* was repeatedly determined and was found to vary only marginally. Thus it can be noted that equation (7) is temporally valid for the system but must be re-checked every time to compensate for column degradation and other effects.

$$\log P = 1.0019 \times \log k_W + 0.5441 \qquad (7)$$

Every sample was measure at 55, 60, 65, 70, 75, 80 and 85% of methanol but the log*k*'/V(MeOH) plot was not linear over the whole range in all cases (*Fig. 6.4*). If nonlinearity occurred, only those values were taken in account that showed a linear behaviour. The same method has been suggested by literature.[192]

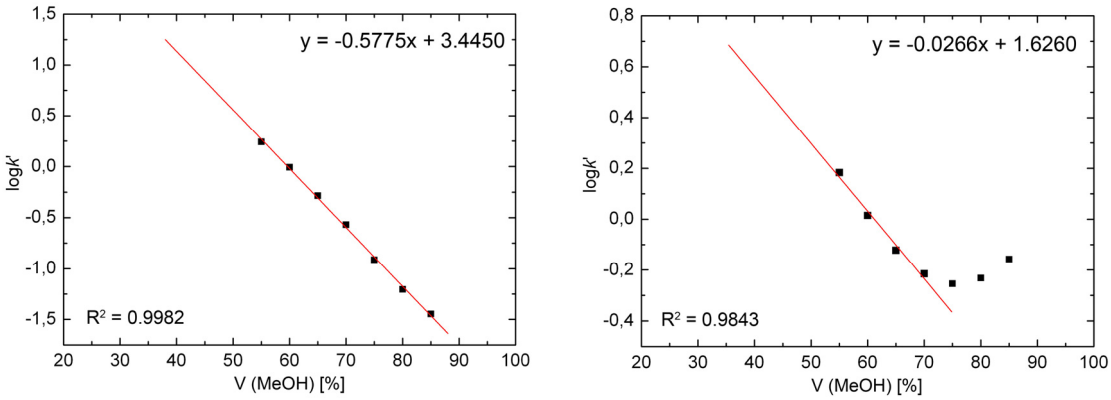

Fig. 6.4 *The majority of all measured samples showed linear relation between logk' and V(MeOH), following eqn. (6), (left, Fc-CO-Enk-NH$_2$ **7**). Especially the cobaltocenium compounds diverged from linearity (right, Cc-CO-Enk-OH **9**).*

When non-linearity was found, only those points were used for linear regression, which gave a correlation of $R^2 > 0.98$. For a more exact analysis, a quadric function has to be applied.[200] This was abandoned, because the linear approach seemed to be exact enough. The following table shows an overview of all measured samples.

Tab 6.5 *Summary of all measured samples. Regression range gives the range of points (% MeOH) used for each regression. LogP is calculated from logk_W by the use of eqn. (7)*

Compound	Nr.	regression range	logk_W	log*P*
H-Enk-OH	**3**	60-80	-1.741	-1.20
Ac-Enk-OH	**4**	50-70	4.348	4.90
Fc-CO-Enk-OH	**6**	50-70	5.231	5.79
Fc-CO-Enk-NH$_2$	**7**	55-85	3.444	4.00
Fc-CO-Enk-NHNH$_2$	**8**	55-85	3.443	3.99
Cc-CO-Enk-OH	**9**	55-70	1.626	2.18
H-Enk[Phe^4(NH-CO-Cc)]-OH	--	65-85	-1.265	-0.72
Ac-Enk[Phe^4(NH-CO-Cc)]-OH	**14**	55-70	1.004	1.55
Fc-CO-Enk[Phe^4(NH-CO-Fc)]-OH	**15**	55-75	5.936	6.49
Cc-CO-Enk[Phe^4(NH-CO-Cc)]-OH	**16**	non-linear	--	--
Fc-CO-Enk[Phe^4(NH$_2$)]-OH	**17**	55-75	4.498	5.05
Fc-CO-Enk[Phe^4(NH-CO-Cc)]-OH	**18**	55-75	1.993	2.54
Ac-Enk[Phe^4(I)]-OH	**26**	55-80	5.876	6.43
I-Ph-Enk-OH	**27**	55-80	6.548	7.11
Cc-CO-Enk[Phe^4(I)]-OH	--	55-85	3.884	4.44

6.3 Blood-brain-barrier permeation experiments

6.3.1 Theoretical background

The concept of a barrier between the blood and the brain arose in the late 19th century when bacteriologist Paul Ehrlich observed that certain dyes, which had been administered intravenously to small animals, stained most tissues except for the brain.[201] One of Ehrlich's students, Edwin Goldmann, reported later[202] that subarachnoidally injected dyes had exclusively stained the brain but no other organ had been effected, and by that confirmed the existence of a barrier between the brain and the circulating blood. More than half a century later the hypothesis that brain capillaries provide the anatomical basis of the blood-brain barrier (BBB) was confirmed by Reese and Karnovsky[203] using electron microscopy. Today it is known that the endothelial cells which form these cerebral capillaries possess several unique features that serve the purpose to protect the brain from xenobiotic substances. Most importantly they have been shown to be joined by *tight junctions*, leaving no intercellular clefts like those found in most other systemic microvessels (*Fig. 6.5*).

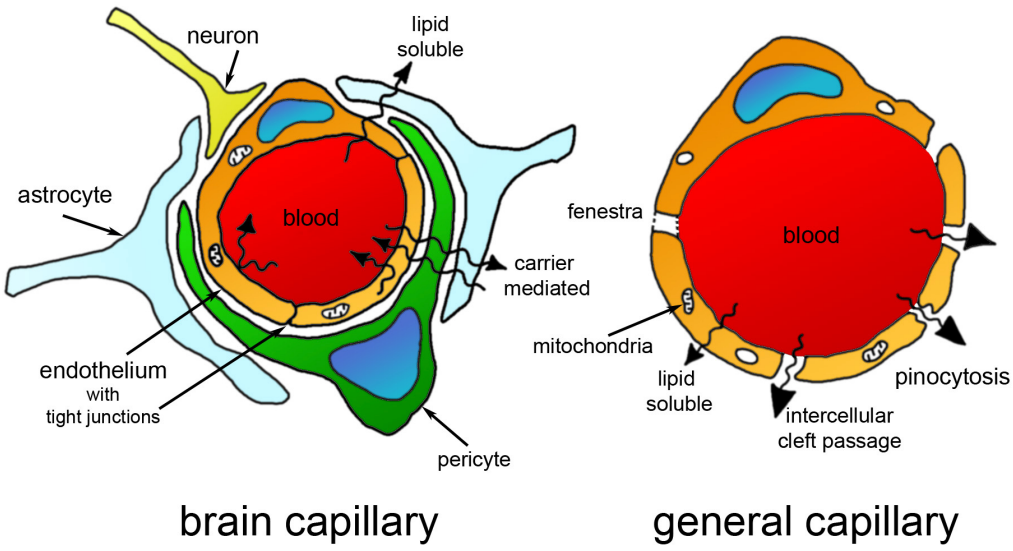

Fig. 6.5 *Brain capillaries consist of endothelial cells connected by tight junctions, which hinder solute flow into the brain, whereas general capillaries show intercellular clefts and pores.*

Apart from such physical barrier functions also carrier mediated mechanisms have been identified (*Fig. 6.6*). There are specific transporters on the endothelial cells of the brain for small and large hydrophilic molecules and essential nutrients. Transmembrane proteins also exist on brain capillaries for transporting a number of lipophilic molecules that enter the endothelial cells back to the capillary lumen. P-glycoprotein (P-gp) is one such transporter present in high concentration on brain capillaries,[204, 205] and is an important component of the BBB.[206] The barrier also has an additional enzymatic aspect: solutes crossing the cell membrane are subsequently exposed to a variety of degrading enzymes that are present inside the endothelial cells, which contain large densities of mitochondria, metabolically highly active organelles.

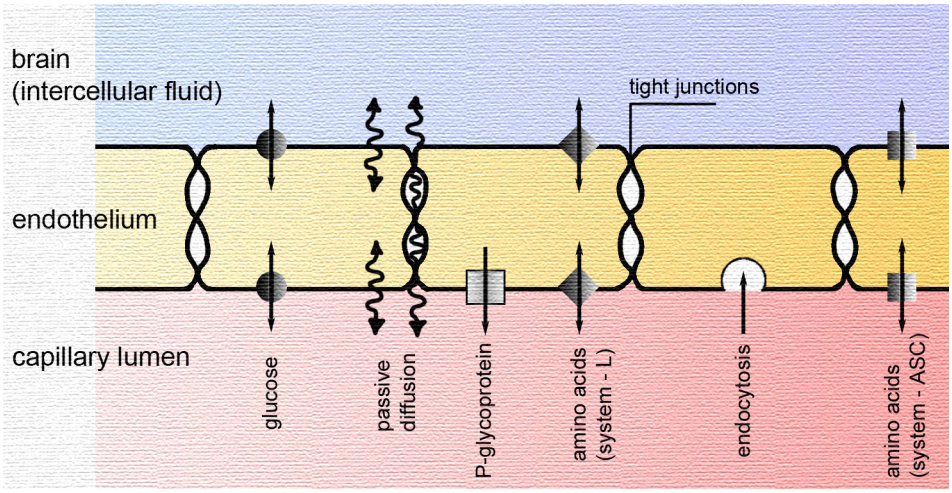

Fig. 6.6 *A Schematic of transport mechanisms through brain capillary endothelial cells. Only lipophilic substances may passively diffuse through the membrane, while hydrophilic substances are either actively transported by specific carriers or blocked*

Despite the total length of 650 km and the estimated surface area of 12 m^2 of capillaries in human brain, this barrier is highly efficient and makes the brain practically inaccessible for lipid-insoluble compounds, such as polar molecules and small ions. As a consequence, not only undesired substances are withheld from the brain but also most therapeutic drugs are hindered from reaching their target, which is why cerebral diseases generally prove to be most refractory to therapeutic interventions. For a better understanding of transport mechanisms and the development of manipulative tools, *in vitro* models of the blood-brain-barrier have been developed, which find a wide area of appli-

cation in basic research and pharmaceutical drug development.[207-209] Microvessel endothelial cells have mainly been isolated from human, bovine, rat and porcine brains[210] and although there is de-differentiation of the brain capillary endothelial cells when grown in culture, primary and established cultures of the cerebral microvessel endothelium have maintained several functional characteristics of the BBB. The access to human brains is due to ethical and technical constraints strongly limited and the use of cattle brain has become problematic because of the spread of bovine spongiform encephalopathy. Because rat brains only yield small amounts of endothelial cells (1-2 million cells per brain)[209], porcine brain has become a favourable source for the construction of *in vitro* BBB models. The use of primary cultures of porcine brain capillary endothelial cells (PBCEC) has been pioneered by Galla and co-workers[211] with detailed description of the technique published.[212] The isolation process essentially involves enzymatic digestion of brain tissue homogenate by dispase followed by isolation of capillary microvessels through density centrifugation within a dextran solution. Capillary endothelial cells are then obtained following collagenase/dispase incubation and harvested by density centrifugation upon a Percoll gradient. From each porcine brain (4 to 6 month old pig), approximately 50 million endothelial cells can be isolated. Primary or low passage cell cultures represent the most frequently used cell population type for *in vitro* models. These are cultures of endothelial cells, directly taken from the brain tissue, which retain many blood-brain-barrier characteristics.

Two principal types of cultures are known, monocultures and co-cultures, which are used to conduct either cell uptake or cell permeation experiments. Monocultures build the most common basis of BBB *in vitro* experiments.

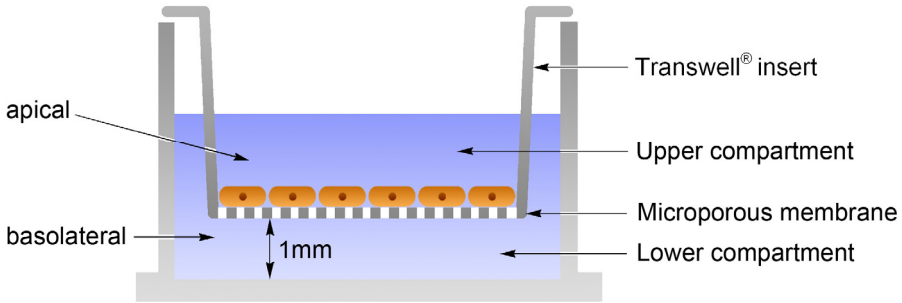

Fig. 6.7 *Monoculture of cerebral capillary endothelial cells grown on a Transwell© filter*

The cells grow on the culture surface to form a confluent monolayer and are, as *in vivo*, functionally polarized. Cell surfaces are being described as apical (luminal) and basolateral (abluminal) sides (*Fig. 6.7*). In addition to monocultures, also co-cultures are used for BBB *in vitro* models. For a better retention of brain capillary endothelial specific properties, monocultures can be treated with an astrocyte conditioned medium. Astrocytes, which belong to the family of glial cells that provide physical and nutritional support for neurons, are attached to the brain capillaries' abluminal side *in vivo*. By adding them to the monoculture, a better simulation of the capillary cell neighbourhood is achieved. Astrocytes are either grown on the bottom of the filter insert or on the floor of the receiving vessel. These setups are known as direct-co-culture or transfilter-co-culture, respectively.

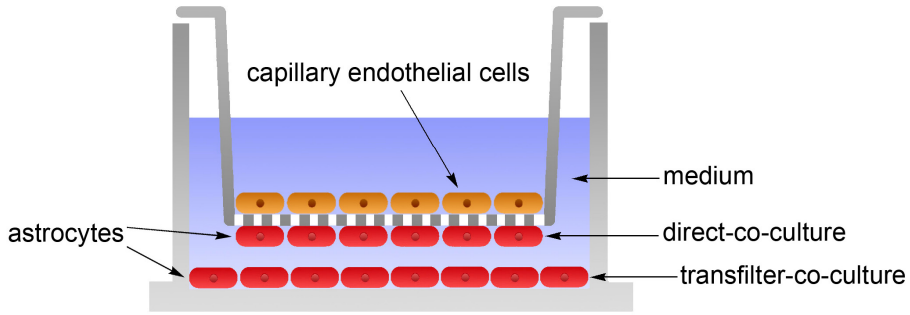

Fig. 6.8 *Astrocytes are co-cultured with brain capillary endothelial cells.*

For the analysis of test substances two types of experiments have been described, cell-uptake and permeation experiments.[213, 214] To determine the uptake of a substance into the cells, sowing and cultivation was carried out on the bottom of the culture plate. Afterwards the confluent cell monolayer was incubated with the test substance. In analogy to nature, the uptake happens on the apical (luminal) membrane side (*Fig. 6.9, left*). To determine the permeation of a substance through the blood-brain-barrier *in vitro*, brain capillary endothelial cells are grown on a permeable membrane filter. This variable setup allows for the measuring of permeation in two directions, namely apical to basolateral (blood to brain) and from basolateral to apical (brain to blood). The comparison of permeation in both directions is especially important for the elucidation of carrier mediated transport mechanisms, since passive diffusion is independent from the direc-

tion. Carriers like P-glycoprotein (P-gp) transport their substrates back to the lumen of the microvessel, meaning they catalyze the transport from brain to blood.

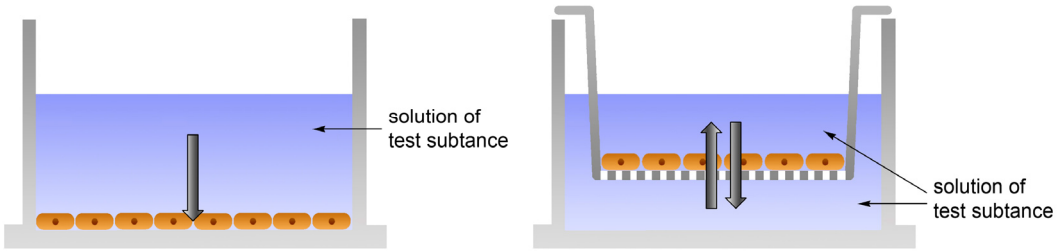

Fig. 6.9 *Setups of cell-uptake (left) and cell permeation (right) experiments.*

While the results of uptake experiments are generally given as amount of substance per time and per 10^6 cells, the permeation of a substance through the cell monolayer is described by the apparent permeation coefficient P_{app} in cm/s. This P_{app} value is connected to a number of parameters as shown in *eqn 8*.

$$P_{app} = \frac{dA}{dt} \times \frac{V_{acceptor}}{A} \times \frac{1}{C_0} \times \frac{1}{x} \tag{8}$$

P_{app}	apparent permeation coefficient [cm/s]
$\frac{dA}{dt}$	permeation rate [%/s]
$V_{acceptor}$	acceptor volume [ml]
A	area of the filter insert [cm^2]
C_o	initial concentration of donor [100%]
x	volume correction factor (ratio acceptor volume : donor volume)

The detailed description of the calculation can be found in the experimental section in *chapter 8.1*.

6.3.2 Blood-brain-barrier permeation of selected [Leu^5]-Enkephalins

Enkephalin, as a neuropeptide, can be transported through the blood-brain-barrier as shown in various experiments.[215-218] However, the transport from the capillary blood into the brain is limited due to active efflux by P-gp[219] and to degradation caused by membrane attached peptidases.[220] Whether chemical modification of the natural occurring pentapeptide [Leu^5]-Enkephalin (H-Tyr-Gly-Gly-Phe-Leu-OH) by organometallic markers can improve BBB permeation was studied in transport experiments using porcine brain capillary endothelial cell monolayers.[196]

PBCECs were cultured on 12-mm polyester filter inserts of a 12-well Transwell Clear© plate (0.4 µm pore size), previously treated with rat tail collagen (5µg/cm^2). Each well was seeded with 250000 cells and cultivated for 7 days before the experiments were carried out. Cell monolayer growth and confluence were monitored by light microscopy. In addition, the integrity of cell monolayers was confirmed by carboxyfluorescein as a paracellular marker. Cells were grown in 'medium 199' containing PenStrep, HEPES and glutamine, as well as 9 % of defined equine serum (see *chapter 8*). The medium was replaced on days 1, 2 and 4. At the 6th day it was exchanged by DMEM/Ham's F12 (1:1) medium, which was free of serum. After one week of cell cultivation the medium was removed and the filters containing the cell monolayers were washed twice with Krebs-Ringer buffer (KRB) and subsequently inserted into a freshly prepared 12-well plate, containing 1500 µl of KRB in the acceptor wells. Each of the 4 selected Enk derivatives, H-Enk-OH **3**, Ac-Enk-OH **4**, Fc-CO-Enk-OH **6** and Cc-CO-Enk-OH **9**, was prepared as a 50 µM solution in KRB of which 500 µl were used for incubation of the PBCEC layer in the donor vial. Samples of 200 µl were taken from the acceptor vial after 30, 60 and 90 minutes and immediately replaced by the same volume of Krebs-Ringer buffer.

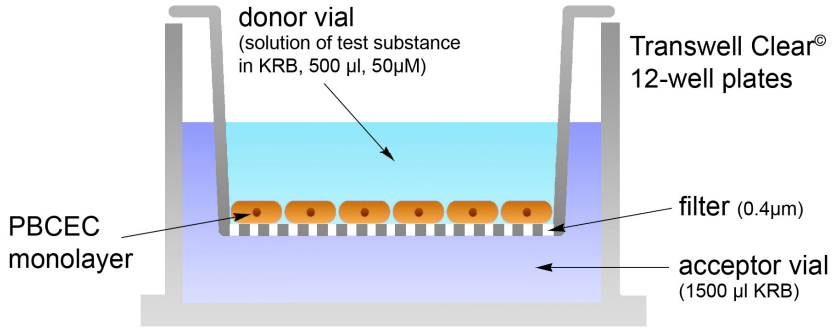

Fig. 6.10 *Setup of BBB transport experiments for apical to basolateral direction (blood→brain)*

All samples, taken in triplicate, were directly frozen at -70° C to avoid decomposition or enzymatic degradation and only defrosted prior to HPLC injection. The test substance stock solutions (50µM) were used to generate calibration curves by injection of 1, 2, 5, 10, 25, 50, 75 and 100 µl of each solution into HPLC. These calibration curves were of high significance, as shown by the example of H-Enk-OH **3** in *Fig. 6.11*.

injected volume [µl]	amount of substance [nmol]	peak area
1	0,05	13,56
2	0,10	27,72
5	0,25	63,76
10	0,50	128,53
25	1,25	333,64
50	2,50	662,96
75	3,75	999,16
100	5,00	1322,90
H-Enk-OH **3**		

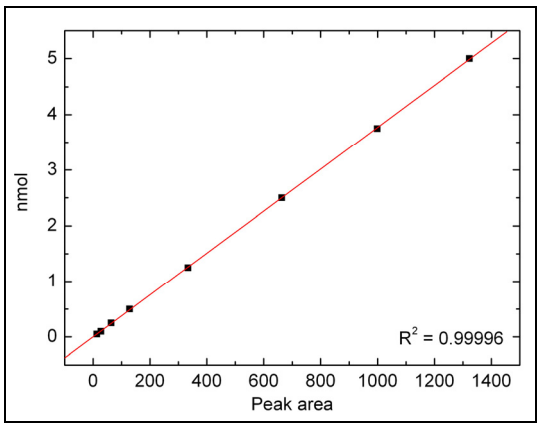

Fig. 6.11 *For the generation of calibration curves, the peak area, obtained by integration, was plotted against amount of substance in nmol.*

100 µl of each 200 µl sample was injected into HPLC running a gradient from 5% CH_3CN in H_20 (t = 0 min.) to 100% CH_3CN (t = 20 min.), which then returned to initial conditions at 25 min. and equilibrated for another 5 min. Both eluents contained 0.1 % of TFA for improved solubility. The signals, recorded at 220 nm, were manually integrated and the amount of substance was calculated from the linear regression function

of the corresponding calibration curve. Despite the very small amount of substance which was in the range of 60 to 200 pmol per injection, all peaks could be identified clearly by means of retention time, which was taken from the calibration experiments. *Figure 6.12* shows the HPLC spectrum of H-Enk-OH **3** after 90 minutes of incubation.

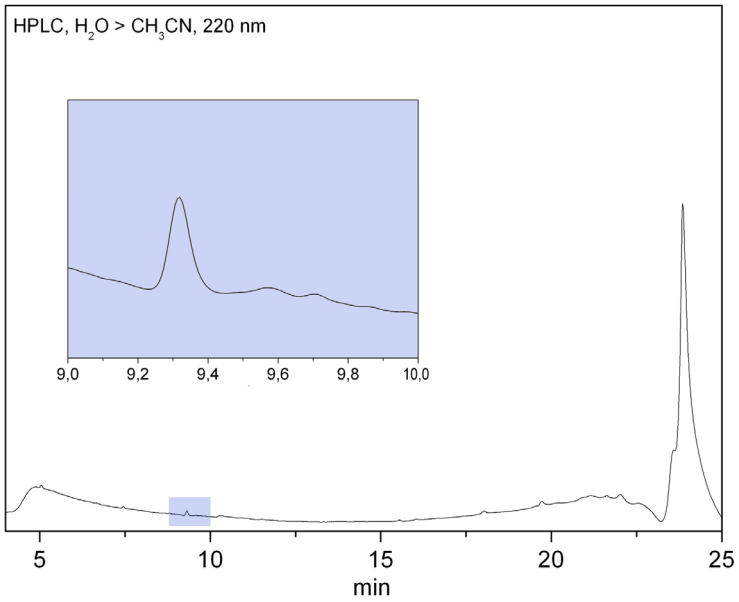

Fig. 6.12 *HPLC of H-Enk-OH **3** after 90 minutes of incubation. 100 µl of a 200 µl sample taken from the acceptor vial have been injected onto a C-18 RP-HPLC column. Peaks were manually integrated.*

For the calculation of transported amounts of substance all three measurements have been used to create mean values. No mavericks were omitted. Although 3 measurements are in principle insufficient to perform correct error estimation, the consistency of most values leads to the assumption that the results are quite significant. The amount of transported material for each compound is shown in *table 6.6*.

Tab 6.6 *The mean values of transported material during the three half-hour periods of incubation and the final amount of substance, which was permeated through the PBCEC monolayer.*

substance	Nr.	ret. time [min]	mean amount of substance [nmol]			final amount [nmol]
			30’	60’	90’	
H-Enk-OH	**3**	9.317	0.5151	0.2879	0.3942	1.1972
Ac-Enk-OH	**4**	10.490	0.6776	0.5299	0.5398	1.7473
Fc-CO-Enk-OH	**6**	13.264	0.8800	0.6584	0.6859	2.0699
Cc-CO-Enk-OH	**9**	9.591	0.7207	0.3789	0.5423	1.6239

All 4 substances showed slight saturation behaviour when incubation time was plotted versus permeated amount of substance (*Fig. 6.13*).

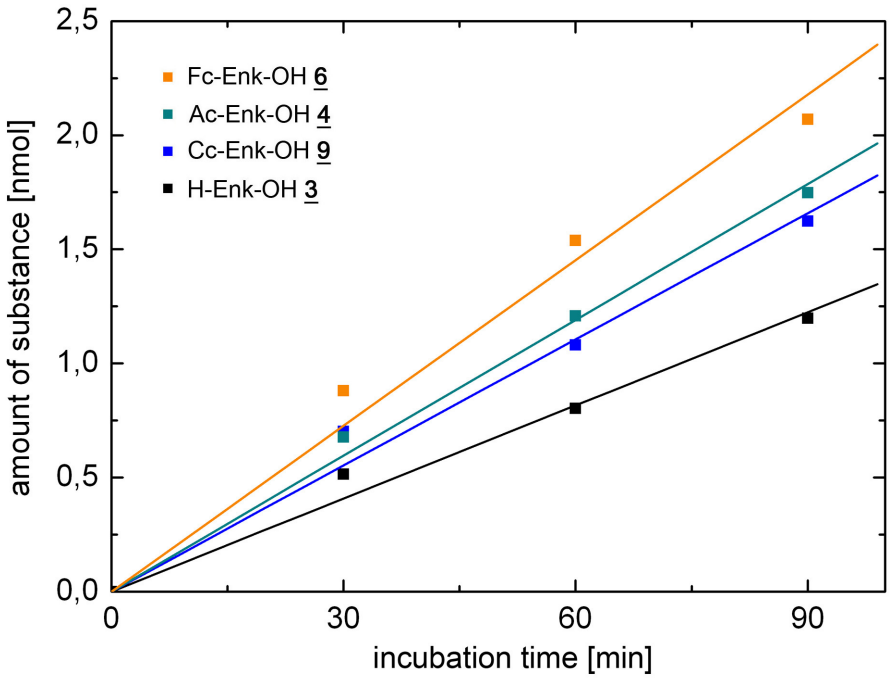

Fig. 6.13 *Plot of incubation time against the permeated amount of substance*

It can be noted that all three N-terminal modified [Leu^5]-Enkephalin derivatives show increased permeation through the PBCEC monolayer. The apparent permeation coeffi-

cients of all 4 compounds have been calculated according to equation (8) and are presented together with selected results from literature[221-224] in *table 6.7*.

Tab 6.7 *Apparent permeation coefficients P_{app} of selected enkephalin derivatives, determined by an in vitro blood-brain-barrier model based on porcine capillary endothelial cells.*

substance	Nr.	type	mean P_{app} [10^{-5} cm/s]	error P_{app} [10^{-5} cm/s]	Ref.
H-Enk-OH	**3**	porcine	0.38	± 0.04	this work
Ac-Enk-OH	**4**	porcine	0.57	± 0.17	this work
Fc-CO-Enk-OH	**6**	porcine	0.68	± 0.13	this work
Cc-CO-Enk-OH	**9**	porcine	0.52	± 0.12	this work
Met-Enkephalin	--	bovine	7.74[a]	± 0.71	214
Cisplatin	--	bovine	3.80	--	215
Morphine	--	porcine	3.33	± 0.25	216
Dopamine	--	bovine	0.93[a]	--	217
Nicotine	--	bovine	1.94[a]	--	217

[a] these values were determined in a slightly different way and cannot be directly compared

6.4 Discussion

6.4.1 Lipophilicity by partition coefficient log*P*

The different enkephalin derivatives show log*P* values between -1.20 for H-Enk-OH **3** and 7.11 for I-Ph-Enk-OH **27**. The lipophilicity determined for H-Enk-OH is consistent with experimental data reported for [Leu^5]-Enk in literature[197] (-0.88 to -1.55) and even more with calculated results presented by Fujita and co-workers[225] (-1.20 to -1.22). It is also close to the log*P* of -1.15, which was determined for [Met^5]-Enk-OH by Lang *et al.*[195] The log*P* values of 7.11 for I-Ph-Enk-OH **27** and 6.43 for Ac-Enk[Phe^4(I)]-OH **26**, respectively, seem to be extraordinarily high for molecules belonging to the class of peptides. The iodine atom has obviously a huge impact on the lipophilic properties, even more so, in a small molecule like a pentapeptide. The relatively high values of all Enk compounds appear to be reasonable, when the lipophilic side chains of H-Tyr-Gly-Gly-Phe-Leu-OH are taken into consideration. A variety of hydrophobicity scales for the natural amino acids have been presented,[226, 227] in which Phe and Leu are generally among the top four hydrophobic amino acids, whereas Tyr and Gly are to be found in the medium area.

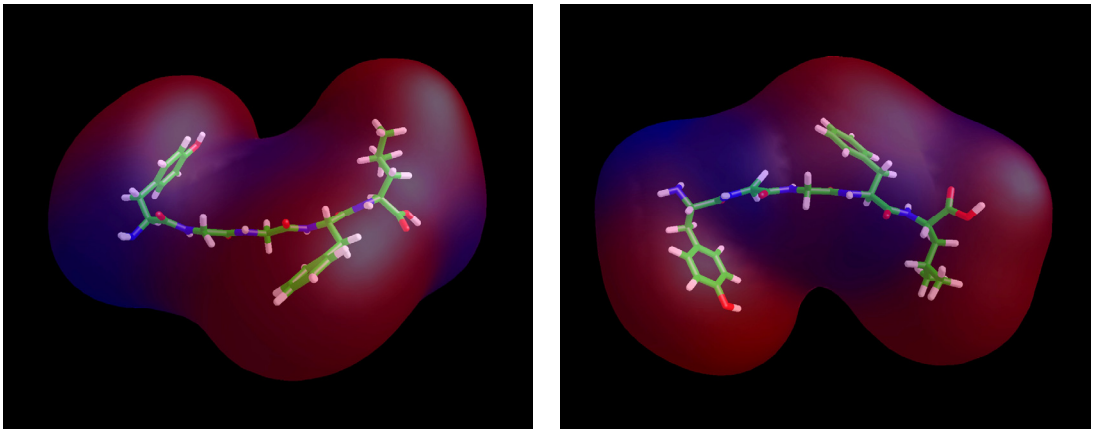

Fig. 6.14 *The structure of [Leu^5]-enkephalin, mapped with a molecular lipophilic potential (MLP). The lipophilic areas (red) dominate the solvent accessibility surface, whereas hydrophilicity (blue) can be assigned to the peptide backbone and the free amino group.*

Figure 6.14 shows one of the 4 X-ray structures of [Leu^5]-Enkephalin observed so far,[147] mapped with a calculated molecular lipophilic potential (MLP) using the pro-

gram.[228] The red color represents areas of high lipophilicity, while the blue color shows hydrophilic behaviour. Even though solvent influences and charge aspects have been left aside, the calculation gives at least an idea of the ratio of hydrophilic and hydrophobic residues in the peptide. As expected, the N-terminal amino group and the peptide back-bone can be identified as locations of elevated hydrophilicity, whereas the non-ionizable side-chains show high lipophilicity. This observation supports the finding that the lowest log*P* values of -1.20 and -0.72 belong to those Enk derivatives which possess free N-terminal amino groups. These are not only functional groups of very high polarity but their basic nature, even at physiological pH of 7.4, leads to the formation of positively charged ammonium cations and by that to a drastic decrease in lipophilicity. The free amino group is needed for the typical zwitterionic structure of amino acids, which explains the isolated positions of H-Enk-OH and H-Enk[Phe^4(NH-CO-Cc)]-OH with being the only derivatives of negative log*P* values. With the formation of a peptide bond, the basic character of the amino group is lost and as a consequence the lipophilicity is increased. The addition of a ferrocene group results in a strong increase in lipophilicity. Cobaltocenium has lower lipophilic properties, which is self-explanatory from the presence of the positive charge. *Table 6.8* provides a brief overview of log*P* change correlated to functional group introduction.

Tab 6.8 *Differences in logP, derived from correlation of the most important Enk-derivatives*

Δ log*P*	H-Enk-OH	Ac-Enk-OH	Fc-CO-Enk-OH	Cc-CO-Enk-OH	Ac-Enk[Phe^4(I)]-OH	Cc-CO-Enk[Phe^4(I)]-OH	Fc-CO-Enk[Phe^4(NH$_2$)]-OH	Fc-CO-Enk[Phe^4(NH-CO-Fc)]-OH
H-Enk-OH	--	6.10	6.99	3.38	7.63	5.64	6.25	7.69
Ac-Enk-OH	-6.10	--	0.89	-2.72	1.53	-0.46	0.15	1.59
Fc-CO-Enk-OH	-6.99	-0.89	--	-3.61	0.64	-1.35	-0.74	0.70
Cc-CO-Enk-OH	-3.38	2.72	3.61	--	4.25	2.26	2.87	4.31
Ac-Enk[Phe^4(I)]-OH	-7.63	-1.53	-0.64	-4.25	--	1.99	-1.38	0.06
Cc-CO-Enk[Phe^4(I)]-OH	-5.64	0.46	1.35	-2.26	-1.99	--	0.61	2.05
Fc-CO-Enk[Phe^4(NH$_2$)]-OH	-6.25	-0.15	0.74	-2.87	1.38	-0.61	--	1.44
Fc-CO-Enk[Phe^4(NH-CO-Fc)]-OH	-7.69	-1.59	-0.70	-4.31	-0.06	-2.05	-1.44	--

Log*P* values have been compared among the most important enkephalin derivatives, enabling a rough estimation of the expected log*P* change by introduction of a certain functional group. As stated above, cobaltocenium compounds are remarkably more hy-

drophilic than their ferrocene congeners, expressed by a log*P* difference of over 3. The introduction of an iodine atom, on the other hand, adds more than 1.5 to the log*P*. This could already be observed during the synthesis of *p*-iodo-phenylalanine, which turned out to be nearly insoluble in water after the iodine atom had been introduced. The comparison between Fc-CO-Enk-OH **6** and Fc-CO-Enk[Phe^4(NH_2)]-OH **15** indicates that hydrogen bonding is an important parameter to lipophilicity, lowering it by 0.76 units. Another interesting observation is the log*P* increase of 0.89 for the exchange of the acetyl group in Ac-Enk-OH with ferrocene, since a similar increase can be found for the introduction of the second ferrocene in Fc-CO-Enk[Phe^4(NH-CO-Fc)]-OH (1.44).
It can be concluded that the determined water/octanol partition coefficients have to be regarded as no absolute values but a fairly precise description of the lipophilic nature of [Leu^5]-Enkephalin. The results seem to be consistent and can be of predictive use as will be shown in *chapter 6.4.3*. The determination of lipophilicity by RP-HPLC methods has shown to be a time-saving approach without the loss of exactness, as confirmed by the compliance to literature values. The system's weakness lies in the description of ionic compounds, which often do not correlate due to their more complicated partitioning behaviour. Computational approaches have recently been made to overcome this problem.[179, 229]

6.4.2 Blood-brain-barrier permeation by apparent permeation coefficient P_{app}

The BBB permeation experiments resulted in P_{app} values between $3.3 \cdot 10^{-6}$ and $5.9 \cdot 10^{-6}$ $cm \cdot s^{-1}$ for H-Enk-OH **3** and Fc-CO-Enk-OH **6**, respectively. These results seem to be of correct dimension, when compared to other values presented in literature. However, it might be difficult to correlate permeation coefficients obtained from experiments which have been conducted under different conditions. Reproducibility is affected by choice of cell type (bovine, porcine, caco-2, etc.), filter inserts (polycarbonate, polyethylene), media, buffers and cultivation procedures. The reported value for [Met^5]-Enkephalin, for example, seems to be very high, compared to other compounds like morphine and nicotine, which are taken up fairly well. It should be noted that apart from cell type also the calculation of P_{app} has been carried out differently. But despite of various possible setups, apparent permeation coefficients P_{app} can still give valuable information on the blood-brain-barrier permeation behaviour of corresponding test substances. In case of

the above presented [Leu^5]-Enkephalin derivatives, the results clearly show that N-terminal modification, be it by acetylation or binding of a metallocene group, improves the BBB permeation. One explanation for this effect is the increase in lipophilicity, caused by blockage of the amino group as a potential proton acceptor. Since the transport experiments have been carried out only from apical to basolateral sides (blood→brain) no conclusion can be drawn on the permeation mechanism or the involvement of carriers. Comparison of both transport directions or the addition of carrier inhibitors would yield such information. Nonetheless, the relatively low P_{app} values of the 4 Enk compounds are most probably due to carrier promoted efflux and enzymatic degradation. It has been shown, for instance, that [Leu^5]-Enkephalin is a substrate to P-gp[219] and therefore shows reduced permeation, like many other small lipophilic compounds. Membrane bound peptidases like dipeptidyl dipeptidase,[230] enkephalinase[231] and aminopeptidase M[232] have been reported to hydrolyse small peptides like enkephalin. Such degradation effects could be observed during this work, when samples taken from the donor vials were subjected to HPLC. Multiple signals, originating from degradation, could be recorded for H-Enk-OH and Fc-CO-Enk-OH but not for Ac-Enk-OH and Cc-CO-Enk-OH.

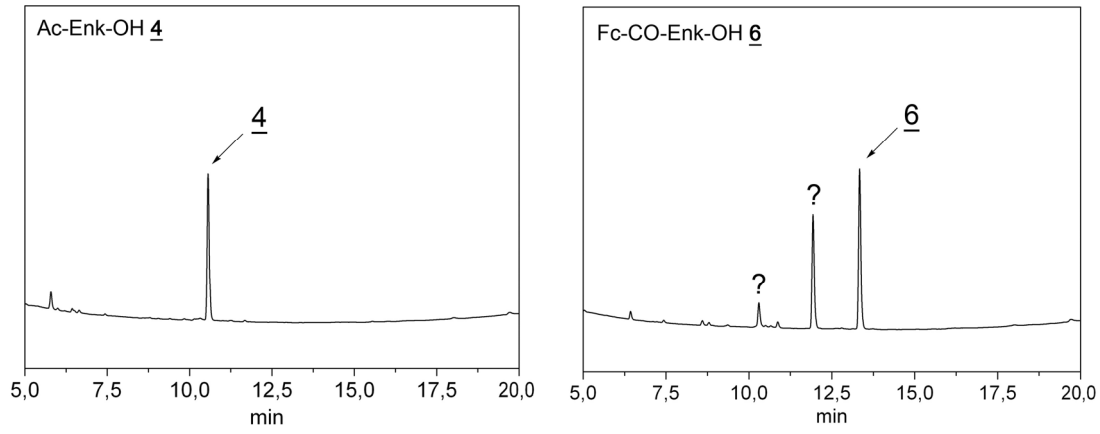

Fig. 6.15 *HPLCs of residual sample solutions, taken from donor vials after 90 minutes. Ac-Enk-OH **4** (left) appears to be in the same pure condition as applied but Fc-Enk-OH **6** shows reasonable concentrations of breakdown products (right).*

The decomposition products could also be observed in samples taken from the acceptor vials, but only in small concentrations. The degradation process seems to occur on the

apical side and inside of the epithelium, rather than basolaterally. Why only two Enk derivatives show these effects is still unclear and has to be eluded in future experiments.

6.4.3 Correlation of lipophilicity and permeation behaviour

It is known that relatively lipophilic drugs can cross the BBB by passive diffusion, whereas polar molecules normally do not enter the brain easily, although sometimes a process of active transport facilitates their penetration. The use of a lipophilicity descriptor like log*P* for predicting BBB permeation has been successfully demonstrated before (see also 'rule of 5', *chapter 6.2.2*). In many cases lipophilicity, expressed by log*P*, was shown to correlate with permeation coefficients, which had been measured using BBB *in vitro* models.[233-235] Only some lipophilic compounds, however, showed an unexpectedly low apparent transfer rate. These cases have been interpreted in terms of high binding to plasma proteins[207] or active efflux by P-glycoprotein.[236]

Lipophilicity and permeation behaviour have been measured for various compounds presented in this thesis and *Table 6.9* shows log*P* and apparent permeation coefficients P_{app} values of 4 selected Enk compounds.

Tab 6.9 *Selection of 4 [Leu^5]-Enkephalin derivatives with their corresponding logP and P_{app} values.*

substance	Nr.	log*P*	P_{app} [10^{-5} cm/s]
H-Enk-OH	**3**	-1.20	0.38 ± 0.04
Ac-Enk-OH	**4**	4.90	0.57 ± 0.15
Fc-CO-Enk-OH	**6**	5.79	0.68 ± 0.13
Cc-CO-Enk-OH	**9**	2.18	0.52 ± 0.12

It is obvious that H-Enk-OH, the most hydrophilic compound, also shows the worst permeation. Fc-CO-Enk-OH, on the other hand, as the most lipophilic substance in the test field, also shows the highest P_{app} value. Log*P* values have been plotted against the apparent permeation coefficients P_{app}. The result can be viewed in *Fig. 6.16*. It should be noted that the errors appear to be large, which is caused by the significant deviations between samples A, B and C from triplicate meaurements. Mean values have been used for all calculations, but a higher number of experiments would improve the significance, which is suggested for future experiments.

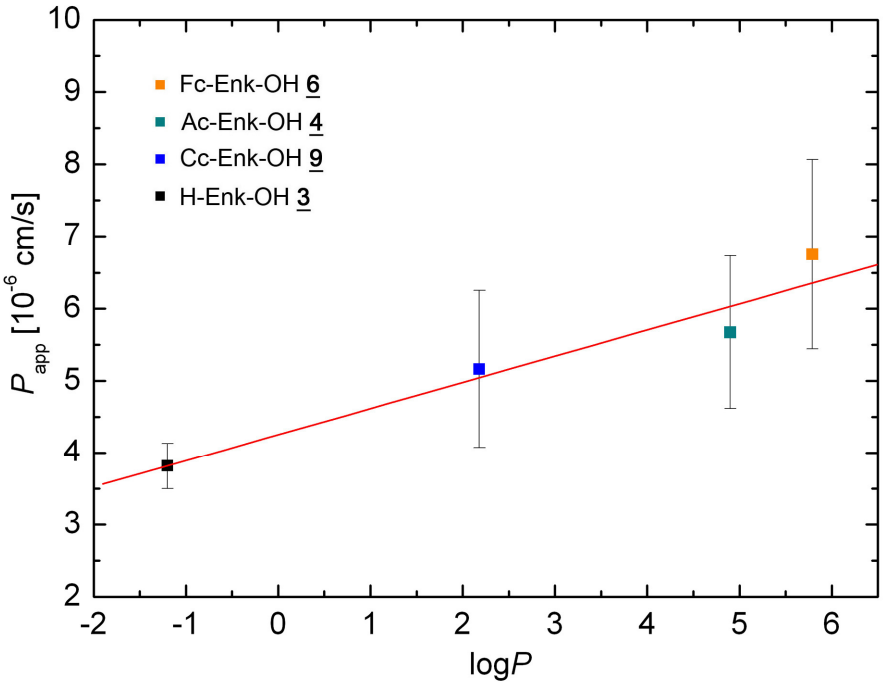

Fig. 6.16 *Correlation of logP versus apparent permeation coefficient P_{app}. LogP values have been determined using a RP-HPLC method, P_{app} values have been determined using an in vitro BBB model.*

Figure 6.16 shows a relatively good correlation between the lipophilicity descriptor log*P* and the apparent permeation coefficient P_{app}. This linear behaviour is in good consistency with reported data from literature. If exclusively passive diffusion is suggested for the observed transport mode, both lipophilicity and blood-brain-barrier permeation measurements seem to be of some significance, as they show the expected linear behaviour. Thus, it can be concluded that the presented experimental procedures can be of value for the biological characterization of peptides like [Leu^5]-Enkephalin and organometallic derivatives thereof.

7 Conclusion

7.1 Summary

The tethering of organometallic markers to biomolecules can provide unique spectroscopic properties, thus enabling the sensitive detection of the target molecule even inside biological systems.[60, 70] As a consequence, versatile synthetic methods for the selective labelling of biomolecules are needed.

The aim of this thesis was the development of techniques for the facile introduction of metal markers into peptides. The pentapeptide [Leu]-Enkephalin with the sequence of H-Tyr-Gly-Gly-Phe-Leu-OH was used as a model peptide, while ferrocene and cobaltocenium derivatives have been chosen as organometallic labels. The first class of compounds, presented in *chapter 4*, comprised N-terminal and side-chain bound metallocene derivatives of enkephalin. These compounds were completely prepared on solid phase by the coupling of the metallocene carboxylic acids **1** and **2** to free amino functions in the peptide.

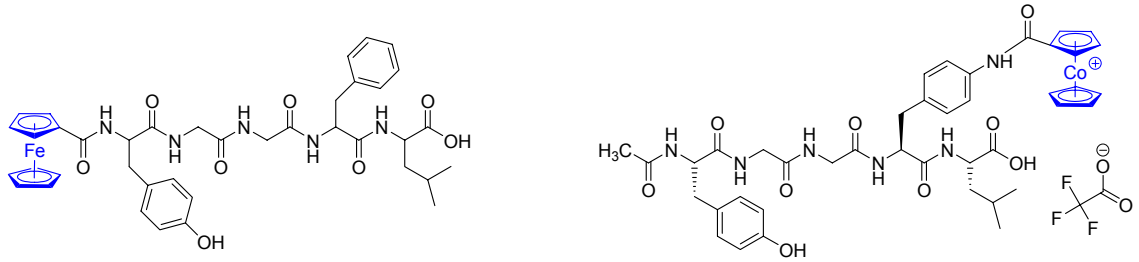

7 **14**

Fig. 7.1 *[Leu]-enkephalin N-terminally labelled by ferrocene (7) and cobaltocenium bound through the side-chain of a modified amino acid (phenylalanine)*

In addition to a full characterization by mass spectrometry, ^{1}H and ^{13}C NMR spectroscopy and UV-Vis techniques, the unique electrochemical attributes of ferrocene and cobaltocenium were elucidated. It was found that the bioconjugates still own the electrochemical behaviour of the introduced metal probes. Homo- and heterobimetallic species could be synthesized, showing that the techniques for terminal and side-chain introduction can be combined.

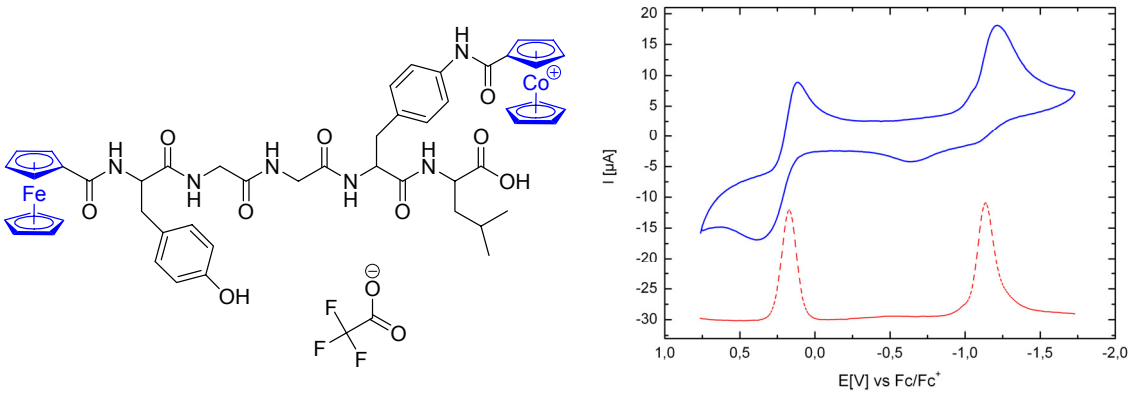

Fig. 7.2 *Structure of a bimetallic enkephalin derivative. The cyclovoltammogram (blue curve) shows both redox peaks, confirming the presence of Fc and Cc in the bioconjugate.*

It can be necessary to have another synthetic method available, especially if the target molecule does not tolerate the reaction conditions of the direct coupling route, presented above. The Pd catalyzed Sonogashira coupling[161] turned out to be a versatile system for the introduction of metal labels into peptides, as explained in *chapter 5*. An alkyne is cross coupled to a iodo-arene function by the help of a Pd catalyst. To evaluate the usability of the Sonogashira method, dipeptides were prepared, containing a *p*-iodophenylalanine residue. Alkynylated ferrocene derivatives were bound to these non-natural amino acid side-chains by the use of the above described Sonogashira reaction. These products were easily accessible and found to produce high quality electrochemical spectra.

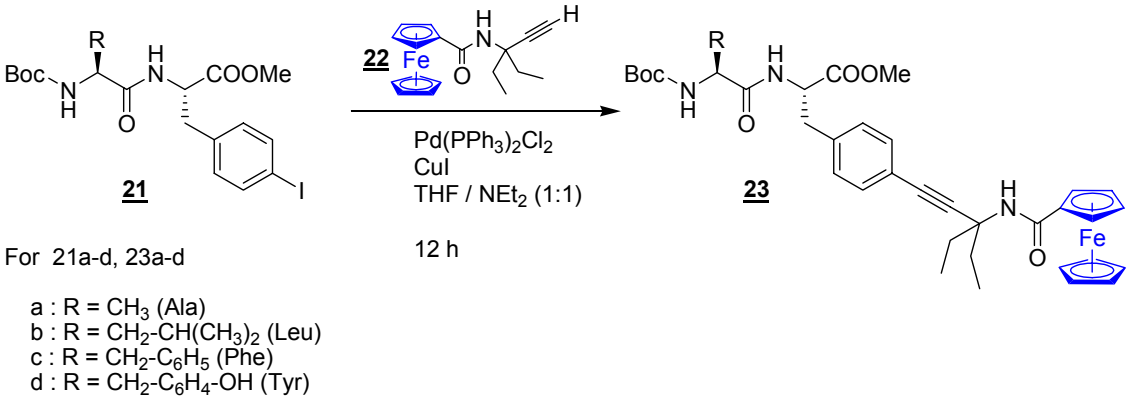

Fig. 7.3 *Reaction scheme for the synthesis of labelled dipeptides through Sonogashira coupling*

The dipeptide experiments had successfully shown that alkynyl metal markers can be attached to iodo-arene functions in biomolecules by application of the Pd catalyzed Sonogashira cross-coupling. To transfer these results onto enkephalin, an N^{α}-Fmoc protected *p*-iodo-phenylalanine building block was synthesized, which could be integrated into the standard solid phase peptide synthesis of [Leu^5]-Enkephalin, yielding a 4-iodo-phenylalanine modified peptide. To the newly inserted function, DEPA-Fc was bound according to the dipeptide technique (*Fig. 7.4*).

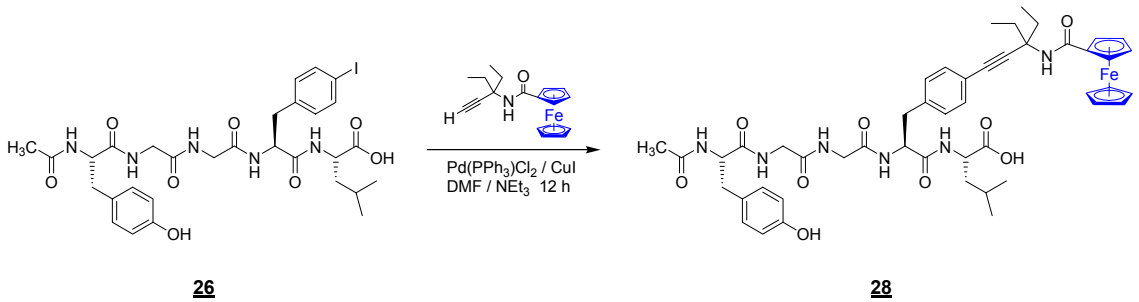

26 **28**

Fig. 7.4 *The alkynyl derivatized ferrocene is bound to the p-iodo-phenylalanine side-chain of modified enkephalin **26** to yield the labelled biomolecule **28***

Biological properties like receptor affinity, membrane permeation and recognition can be severely affected by the introduction of a metal marker group into a relatively small biomolecule like [Leu^5]-Enkephalin. Lipophilicity, as a physicochemical parameter, is connected to such biological properties like those mentioned above.[188] Therefore lipophilicity, expressed by the water/octanol partition coefficient log*P*, was determined for a selection of Enk derivatives by the use of a modern RP-HPLC method.[192] The results show the huge influence of the organometallic label on the bioconjugate's lipophilicity. The introduction of such lipid-soluble groups like ferrocene can obviously affect the target molecule's solubility in water, as well as cell uptake and permeation behaviour.

For a deeper insight into this change of biological attributes due to organometallic labelling, some compounds were tested for blood-brain-barrier permeation. These transport experiments were carried out using a BBB *in vitro* model, based on porcine brain capillary endothelial cells.[208] The test compounds H-Enk-OH **3**, Ac-Enk-OH **4**, Fc-CO-Enk-OH **6** and Cc-CO-Enk-OH **9** showed to have better permeation with higher lipophilicity,

as expected for a passive diffusion transport mechanism.[234] The correlation of both determined values, apparent permeation coefficient P_{app} and octanol/water partition coefficient log*P*, show a linear behaviour with a correlation of $R^2 = 0.95$ as can be seen in *Fig. 7.5*.

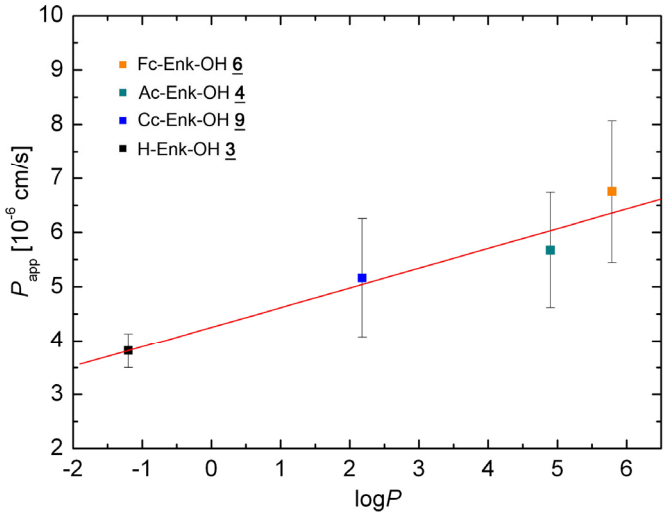

Fig. 7.5 *Plot of apparent permeation coefficients vs. logP values showed a linear behaviour, as expected for a passive diffusion transport mechanism.*

7.2 Outlook

The techniques for a regio-selective introduction of organometallic compounds into peptides, which were presented in this thesis, are subject to no restrictions in principle. It was shown that these methods are applicable to a number of functional groups and different organometallic fragments. The binding of the marker molecule is performed under mild conditions so that neither biomolecule nor labelling group denature or decompose, respectively. This process should therefore be suitable for the labelling of more complicated and larger biomolecules. The ‘expansion of the genetic code’ presented by Schultz and co-workers[237] may be an interface for that, since it provides the possibility to introduce unnatural amino acids like 4-iodo or 4-azido-phenylalanine into a large number of proteins by recombinant methods. Such labelled proteins could be purified by HPLC using electrochemical detection. In addition, future biological studies might reveal more about the altered physiological properties which the biomolecule receives together with the metal marker.

8 Experimental section

8.1 Methods and Materials

Elemental analysis

Elemental Analysis were performed on a Foss Heraeus Vario EL Elementar Analysator in C,H,N mode.

Infrared spectroscopy

Infrared spectra were recorded on a Brucker Equinox 55 FT-IR spectrometer between NaCl windows in distilled $CHCl_3$, or as KBr discs, with a spectral resolution of 2.0 cm^{-1}. Wavenumbers, *v*, are given in cm^{-1}.

UV-Vis spectroscopy

UV-Vis spectra were measured in distilled CH_3CN or MeOH on a Varian CARY 100 instrument in 1 cm quarz Suprasil cells thermostated at 25 °C. Absorption maxima, λ_{max}, and molar absorption coefficients, ε, are given in nm and l/mol·cm, respectively.

Mass spectrometry

EI (70eV) and FAB (glycerol or NBA matrix) mass spectra were measured on a Mat 8200 instrument. Characteristic mass fragments with probable composition are given in brackets. For fragments containing metals only the isotopomer with highest intensity was described. All ESI (neg./pos.) were recorded on a Finnigan TSQ 700 at 4.5 kV.

NMR Spectroscopy

NMR spectra were determined either on a Brucker AM 360 spectrometer, ^1H operating at 360.14 MHz and ^{13}C operating at 90.56 MHz or on a Bruker AM 300 with frequencies of 300.16 MHz (^1H) and 75.47 MHz (^{13}C). Peak positions in both ^1H and ^{13}C are reported in ppm relative to TMS, the internal standard. Spectra of peptides are referenced to the residual DMSO-d_6 signal (2.50 ppm in ^1H, 39.52 ppm in ^{13}C). All other compounds are referenced to the residual $CHCl_3$ signal (7.26 ppm in ^1H,

77.16 ppm in ^{13}C). Coupling constants, *J*, are given in Hz. Individual peaks are marked as: singlet (s), dublet (d), triplet (t) or multiplet (m)

Electrochemistry

Cyclic Voltammograms and square wave voltammograms in CH_3CN or CH_3CN/H_2O (1:1) solutions were recorded on a Perkin Elmer BES Potentiostat/Galvanostat. 0.1 M NBu_4PF_6 or $NaClO_4$ was added as supporting electrolytes A three-electrodes cell was employed with a glassy carbon or platinum working electrode, a platinum-wire as auxiliary electrode and a $Ag/AgNO_3$ reference electrode (0.01 M $AgNO_3$ in CH_3CN). For determination of the redox potentials, ferrocene was added as an internal standard. All analyte concentrations were 1.0 mM.

HPLC analysis and purification

High Performance Liquid Chromatography (HPLC) was performed by using Varian Dynastar C-18 reverse phase columns for analytical (250 x 8 mm) and preparative (250 x 21 mm) runs. Water and CH_3CN (Baker, HPLC-grade) were used as eluents, each containing 0.1% trifluoroacetic acid. All analytical samples were measured at a flowrate of 1 ml/min using the gradient, given in the the following table:

H_2O [%]	CH_3CN [%]	time [min]
90	10	0
0	100	18
90	10	20
90	10	25

For peptides also H_2O/MeOH gradients were used. No TFA was added to the methanol phase. The logP studies were carried out on the same system using specials buffers with the following composition:

Solvent A	Solvent B
H_2O (saturated with n-octanol)	MeOH
0.1% n-decylamine	0.25 % n-octanol
0.1 M MOPS	
pH adjusted to 7.4	

Chemicals / Material

All chemicals were used as obtained from commercial sources. THF and NEt_3 for the Sonogashira reactions were dried over CaH_2, thorougly degassed and stored under argon atmosphere. Isobutyl chloroformiate and oxalylchloride were destilled before use. Deuterated NMR solvents were stored in a glove box under inert gas. All standard peptide synthesis chemicals and solvents were analytical reagent grade or better and purchased from Novabiochem (Bad Soden, Germany) or from Iris Biotech (Marktredwitz, Germany). Resins were exclusively used in 200 mesh-size, with loadings between 0.59 and 0.63 mmol/g for Wang resins and 0.19 to 0.23 mmol/g for Tentagel HMBA resins. Peptide grade DMF, purchased from Roth (Karlsruhe, Germany), was used for all peptide syntheses. Preparations of buffers and solutions were conducted as follows:

Krebs-Ringer-buffer consisted of:

NaCl	8.30 g	142 mM
KCl	0.23 g	3 mM
$K_2HPO_4 \cdot 3\ H_2O$	0.34 g	1.5 mM
HEPES	2.40 g	10 mM
D-glucose	0.72 g	4 mM
$MgCl_2 \cdot 6\ H_2O$	0.24 g	1.2 mM
$CaCl_2 \cdot 2\ H_2O$	0.21 g	1.4 mM
H_2O	ad 1000 ml	

Culture medium, with serum (C+) consisted of:

Medium 199	500 ml	
L-glutamine	2 ml	0.8 mM*
PenStrep	5 ml	100 IE/ml or 100 µg/ml
HEPES	5 ml	10 mM
Equine serum	50 ml	9 %
* Medium 199 already contains 0.7 mM of L-glutamine, final concentration is therefore 1.5 mM		

Culture medium, without serum (C-) consisted of:

DMEM/Ham's F12 (1:1)	500 ml	
L-glutamine	5 ml	2 mM*
PenStrep	5 ml	100 IE/ml or 100 µg/ml
HEPES	5 ml	10 mM
* DMEM/Ham's F12 already contains 2.5 mM of L-glutamine, final concentration is therefore 4.5 mM		

Solid Phase Peptide Synthesis - general remarks

If not stated differently, all solid phase syntheses have been carried out according to standard procedures, which are described in the following.

Swelling: At the beginning of each synthesis the resin was swollen in DMF twice for 20 min. When the peptide sythesis had to be interrupted, the peptidyl resin was shrunk using MeOH and stored in the refridgerator overnight. Before the synthesis was continued the resin was again swollen in DMF.

Deprotection: The N-terminal Fmoc protection group was removed by a solution of 20% piperidine in DMF, which was freshly prepared prior each synthesis. Deprotection was carried out 10 plus 5 minutes.

Washing: After each deprotection and coupling step, the resin was excessively washed (3 times for 5 minutes) with DMF to remove any residual activation or deprotection reagents.

Coupling: Amino acids (3 or 5-fold excess) were mixed with equimolar amounts of TBTU and HOBt. Then, 10 equivalents of DIPEA were added and the whole mixture was dissolved in 4 ml of DMF. This was shaken until a clear and yellow solution was obtained, which took 3 to 5 minutes. Ferrocene and Cobaltocenium activation took sometimes longer and afforded an extra addition of DIPEA. The coupling was performed for 45 minutes for all amino acids and 1-2 hours for metallocene compounds.

Acetylation: N-terminal acetylation was carried out by treatment with a mixture of Ac_2O, NMI, Lutidine and THF (1:1:1:7) for 15 minutes. Before acetylation the N-terminally deprotected peptidyl resin was thoroughly washed with DMF and DCM

Cleavage: After the synthesis was finished, the peptidyl resin transferred into a round flask and treated with a mixture of 95% TFA, 2.5% H_2O and 2.5% TIS (6 ml/g resin) for 3 hours. If ferrocene was bound, the cleavage mixture consisted of 92.5% TFA, 5% phenol adn 2.5% TIS. After removal of all volatile compounds *in vacuo*, the crude product could be precipitated by addition of cold ether.

Calculation of apparent permeation coefficients P_{app}

The calculation of the apparent permeation coefficient P_{app} was based on the permeation rate of the respective test substance. At first, all samples taken from the acceptor compartment were measured quantitatively by HPLC, using a calibration curve. Because the removed volume of 200 µl for each sample was replaced by the same amount of fresh Krebs-Ringer buffer (KRB), the dilution had to be corrected mathematically, following equation (a).

$$c_{n,corr} = \frac{c_n \times V_{acceptor} + \sum_{i=1}^{n-1}(c_i \times V_{sample})}{V_{acceptor}} \qquad \text{(for n > 1)} \qquad \text{(a)}$$

$c_{n, corr}$ → corrected concentration at sample removal n [µmol/ml]
c_n → concentration at sample removal n [µmol/ml]
$V_{acceptor}$ → acceptor volume [ml]
V_{sample} → sample volume [ml]

From the corrected concentration $c_{n, corr}$ the permeated amount of substance M for the particular sample could be calculated by multiplication with the acceptor volume $V_{acceptor}$ (b). The initial amount M_0 was determined accordingly (c).

$$M_n = c_{n,corr} \times V_{acceptor} \qquad \text{(for n > 1)} \qquad \text{(b)}$$

$$M_0 = c_0 \times V_{donor} \qquad \text{(for n > 1)} \qquad \text{(c)}$$

M_n → permeated amount at sample removal n [µmol]
$c_{n, corr}$ → corrected concentration at sample removal n [µmol/ml]
M_0 → initial amount of substance in donor [µmol]
$V_{acceptor}$ → acceptor volume [ml]
c_0 → initial concentration in donor [µmol/ml]

The total amount of test substance, which had permeated from the beginning until the particular sample was removed, was determined from equation (d).

$$A_n = \frac{M_n}{M_0} \times 100 \qquad \text{(for n > 1)} \qquad \text{(d)}$$

A_n → percentage of substance at sample removal n [%]
M_n → permeated amount at sample removal n [µmol]
M_0 → initial amount of substance in donor [µmol]

Permeationcoefficients *P* are calculated according to Fick's law as shown in the following equation (e).

$$P = \frac{c_{acceptor} \times V_{acceptor}}{t} \times \frac{1}{A} \times \frac{1}{c_{donor}} \qquad \text{(e)}$$

P → permeation coefficient [cm/s]
$c_{acceptor}$ → concentration in the acceptor chamber [mg/ml]
$V_{acceptor}$ → acceptor volume [ml]
t → time [s]
A → diffusion area [cm^2]
c_{donor} → initial concentration in donor [mg/ml]

The permeated percentage A_n was plotted against time and the slope of the linear function was determined as the permeation rate dA/dt [%/s]. To calculate the apparent permeation coefficient P_{app} equation (e) was converted to euation (f)

$$\boxed{P_{app} = \frac{dA}{dt} \times \frac{V_{acceptor}}{A} \times \frac{1}{c_0} \times \frac{1}{x}} \qquad \text{(f)}$$

P_{app} → permeation coefficient [cm/s] dA/dt → permeation rate [%/s]
$V_{acceptor}$ → acceptor volume [ml]
A → diffusion area [cm^2]
c_0 → initial concentration in donor [mg/ml]
x → volume correction factor (ratio of $V_{acceptor}$: V_{donor})

8.2 Syntheses and Characterization

Synthesis of ferrocene carboxylic acid 2 (Fc-COOH)

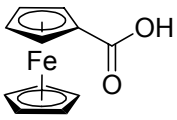

$C_{11}H_{10}FeO_2$ (M = 230.00 g/mol)

Ferrocene carboxylic acid was synthesized as reported by Reeves[238]. Some minor changes have been applied to the preparation.

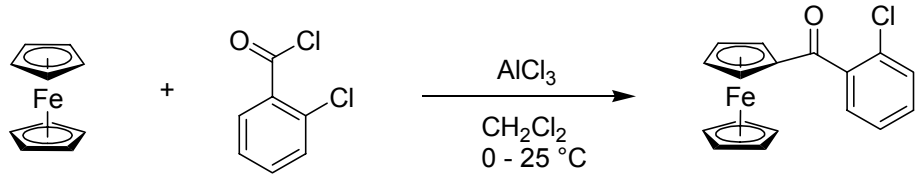

a.) (2-Chlorobenzoyl)ferrocene A thoroughly dried 1-l three-necked round-bottom flask was equipped with a mechanical stirrer, a funnel for adding solids and an adapter holding a thermometer and a gas-inlet tube. The system has been maintained under positive pressure of argon throughout the synthesis. The flask was charged with 18.6 g (100 mmol) of ferrocene, 17.5 g (100 mmol) of 2-chlorobenzoyl chloride and 250 ml of dried DCM. The flask was immersed in an ice bath and while stirring 14.0 g (105 mmol) of anhydrous aluminum chloride was added through the funnel at such a rate that the reaction mixture remained below 5 °C. The appearance of a deep blue color indicated that the reaction was occurring. After the addition was complete, stirring was continued for another 30 min with ice cooling and for 2 hours at room temperature.

The reaction mixture was cooled again in ice, 200 ml of water was added cautiously, and the resulting two-phase mixture was stirred vigorously for 30 minutes. After separating the layers in a separatory funnel, the aqueous layer was extracted with three 100

ml portions of DCM and the combined DCM solutions were washed twice with 100 of 10% aqueous sodium hydroxide, dried over Na_2SO_4, filtered and evaporated to dryness a reduced pressure yielding 28.1 g (87% from ferrocene) of a red viscous oil.

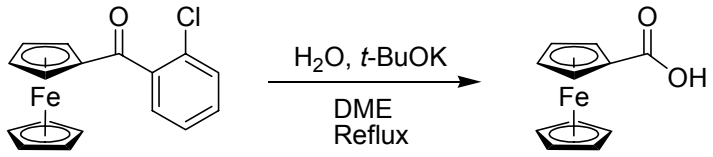

b.) Ferrocenecarboxylic acid **2** A dry, 1-l 3-necked round-bottom flask, equipped with a mechanical stirrer, a reflux condenser and a gas-inlet was charged with a solution of 46 g of potassium *tert*-butoxide (411 mmol) in 300 ml of DME. 2.2 ml of water was added with stirring, producing a slurry, to which the crude (2-chlorobenzoyl)ferrocene in 80 m of DME was added. The red solution was stirred and refluxed under argon until the color faded to tan, indicating completion of the reaction (1 hour). After the reaction mixture was allowed to cool it was poured into 1000 ml of water, washed three times with 200 ml of Et_2O and the combined organic solutions were back-extracted with three 100 ml portions of 10% aqueous sodium hydroxide. The aqueous phases were then combined and acidified with conc. hydrochloric acid. The light brown precipitate was collected by filtration and air dried, yielding 14.6 g (64% from ferrocene) of ferrocene-carboxylic acid as an air-stable orange powder.

1: Anal. calc. for $C_{11}H_{10}FeO_2$ (230.00 g/mol): C, 57.43; H, 4.38. Found: C, 55.94; H, 4.60. IR (cm^{-1}) in KBr: 2972, 2877 (w) υ_{CH}, 1654 (vs) υ_{COO}, 1283 (s) δ_{CO}. MS (EI): m/z 230 (100, $[M]^+$), 213 (18, $[Fc\text{-}CO]^+$). ^1H NMR (CD_3OD, 360.14 MHz): 4.77 (m, 2H, Cp$H_{2,5}$), 4.45 (m, 2H, Cp$H_{3,4}$), 4.21 (s, 5H, CpH). ^{13}C NMR (CD_3OD, 90.56 MHz): 175.9 (*C*OO), 72.6 ($C_{Cp,\,2,5}$), 72.3 ($C_{Cp,\,1}$), 71.4 ($C_{Cp'}$), 70.9 ($C_{Cp,\,3,4}$).

Synthesis of Cobaltoceniumcarboxylic acid 2 (Cc-COOH)

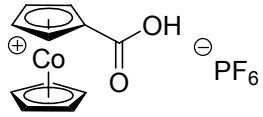

$C_{11}H_{10}FeO_2$ (M = 377.97 g/mol)

Cobaltoceniumcarboxylic acid **2** was synthesized as reported by Sheats and Rausch.[118] Some minor changes have been applied to the preparation.

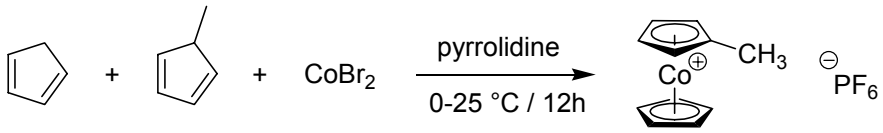

a.) Methylcobaltocenium 16.5 g (0.25 mol) of cyclopentadiene and 20 g of methylcyclopentadiene (0.25 mol) which had been freshly cracked from their dimers prior to the reaction, were dissolved in 200 ml of dried pyrrolidine in a 500 ml 3-necked round-bottom flask. The mixture was cooled to 0 °C and under positive argon pressure was added in little portions 20.75 g (0.1 mol) of anhydrous cobalt(II)bromide. The solution was allowed to warm to room temperature and the stirring was continued for another 12 h. The solvent was evaporated under reduced pressure and the purple residue was dissolved in 500 ml of hot water. A green residue containing cobalt(II)oxide remained. After the solution was extracted with three 50 ml portions of Et_2O to remove unreacted cyclopentadiene it was clarified with 10g of Norit. The crude product was precipitated as hexafluorophosphate salts by dropwise addition of a solution of 15 g of sodium hexafluorophosphate in 75 ml of water.

Yield: 7.7 g

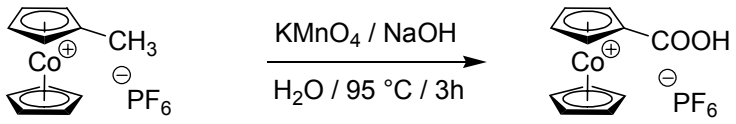

b.) Cobaltoceniumcarboxylic acid **2** 6 g (17 mmol) of the mixture obtained in a.) was dissolved in a solution of 8.05 g (51 mmol) of potassium permanganate and 1.36 g (34 mmol) of sodium hydroxide in 120 ml of water. The mixture was heated to 95 °C for 3 hours and the occurring manganese(II)oxide was removed by filtration through celite. Sodium hexafluorophosphate was added and the solution chilled. The yellow precipitate, identified as cobaltocenium hexafluorophosphate, was removed by filtration and dropwise addition of 6 *M* HCl yielded a mixture of cobaltoceniumcarboxylic acid and 1,n'-cobaltoceniumdicarboxylic acid. The precipitate washed repeatedly with hot acetone in a soxhlet apparatus. Cobaltoceniumcarboxylic acid dissolved readily, whereas the 1,n'di-acid was virtually insoluble. The acetone solution was evaporated to dryness on a rotary evaporator yielding 3.82 g (60%) of the product as yellow flakes.

2: Anal. calc. for $C_{11}H_{10}CoF_6O_2P$ (377.97 g/mol): C, 34.94; H, 2.67. Found: C, 32.20; H, 3.69. IR (cm^{-1}) in KBr: 3125 (s) υ_{CH}, 2914, 2645 (w) υ_{OH}, 1709 (vs) υ_{COO}, 1418 (s) $\delta_{CH,\ Cp'}$, 1302 (s) δ_{CO}. MS (EI): m/z 233 (12, $[M\text{-}PF_6]^+$), 188 (35, $[CoCp_2]^+$). ^1H NMR (D_2SO_4, 360.14 MHz): 5.93 (m, 2H, Cp$H_{2,5}$), 5.59 (m, 2H, Cp$H_{3,4}$), 5.50 (s, 5H, Cp*H*). ^{13}C NMR (D_2SO_4, 90.56 MHz): 168.9 (*C*OO), 86.9 ($C_{Cp,\ 2,5}$), 85.9 ($C_{Cp'}$), 85.5 ($C_{Cp,\ 1}$), 85.3 ($C_{Cp,\ 3,4}$).

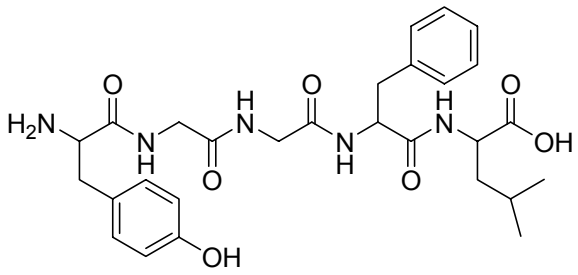

3

Resin	Loading (mmol/g)	AA excess	Cleavage mixture	Cleavage time	mg resin	yield
Wang	0.61	5	95% TFA 2.5% H_2O 2.5% TIS	3 h	500	146 mg (86.1 %)

3: $C_{28}H_{37}N_5O_7$ (555.27 g/mol): MS (ESI, neg): m/z 1109.18 $[2M - H^+]^-$, 554.27 $[M - H^+]^-$. ^{1}H NMR (DMSO-d_6, 300.14 MHz): 12.61 (s, br, 1H, COO*H*), 9.35 (s, br, 1H, O*H*-$_{Tyr}$), 8.74 (t, 1H, J=5.0Hz, NH_{Gly}), 8.35 (d, 1H, J=7.8Hz, NH_{Leu}), 8.11 (t, 1H, J=5.4Hz, NH_{Gly}), 8.04 (d, 1H, J=7.3Hz, NH_{Phe}), 7.26 (m, 5H, $H_{Ar,\ Phe}$), 7.06 (d, 2H, J=8.2Hz, $H_{Ar,\ Tyr}$), 6.71 (d, 2H, J=8.2Hz, $H_{Ar,\ Tyr}$), 4.58 (dt, 1H, J=3.6Hz, J=9.2Hz, C$_\alpha H_{Phe}$), 4.22 (m, 1H, C$_\alpha H_{Tyr}$), 3.98 (m, 1H, C$_\alpha H_{Leu}$), 3.74 (m, 4H, C$_\alpha H_{Gly}$), 2.90 (m, 4H, C$_\beta H_{Phe,\ Tyr}$), 1.64 (m, 1H, C*H*$(CH_3)_2$), 1.55 (m, 2H, C$_\beta H_{Leu}$), 0.88 (dd, 6H, J=6.2Hz, J=17.4Hz, CH(C*H*$_3)_2$). ^{13}C NMR (DMSO-d_6, 75.47 MHz): 173.7 (*C*OO), 171.0, 168.4, 168.0 (*C*ON), 155.6 ($C_{Ar}OH_{Tyr}$), 137.6 ($C_{Ar,\ q,\ Phe}$), 130.3 ($C_{Ar,\ q,\ Tyr}$), 129.1, 127.9, 126.1 (C_{Ar}), 124.7, 115.2 (C_{Ar}), 53.6 ($C_{\alpha,\ Phe}$), 53.4 ($C_{\alpha,\ Tyr}$), 50.2 ($C_{\alpha,\ Leu}$), 41.8, 41.5 ($C_{\alpha,\ Gly}$), 37.6 ($C_{\beta,\ Phe}$), 36.1 ($C_{\beta,\ Tyr}$), 24.2 ($C_{\beta,\ Leu}$), 22.7 ($CH_{3,\ Leu}$), 21.2 (*C*H$(CH_3)_2$).

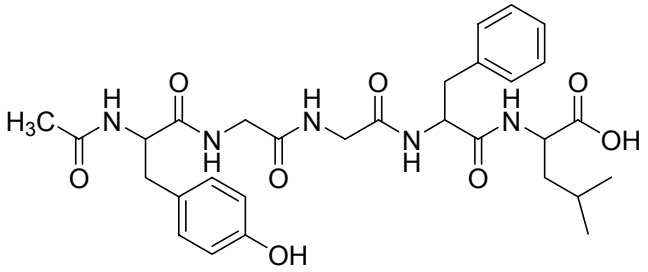

4

Resin	Loading (mmol/g)	AA excess	Cleavage mixture	Cleavage time	mg resin	yield
Wang	0.59	3	95% TFA 2.5% H_2O 2.5% TIS	2 h	510	140 mg (77.9 %)

4: $C_{30}H_{39}N_5O_8$ (597.28 g/mol): MS (ESI, neg): m/z 1193.73 $[2M - H^+]^-$, 596.30 $[M - H^+]^-$. ^{1}H NMR (DMSO-d_6, 400.13 MHz): 12.55 (s, br, 1H, COO*H*), 9.12 (s, br, 1H, O*H*-$_{Tyr}$), 8.22 (d, 1H, J=8.0Hz, NH_{Leu}), 8.19 (t, 1H, J=5.2Hz, NH_{Gly}), 8.03 (d, 1H, J=8.1Hz, NH_{Tyr}), 7.97 (d, 1H, J=8.0Hz, NH_{Phe}), 7.89 (t, 1H, J=5.3Hz, NH_{Gly}), 7.23 (m, 5H, $H_{Ar,\ Phe}$), 7.00 (d, 2H, J=8.2Hz, $H_{Ar,\ Tyr}$), 6.61 (d, 2H, J=8.2Hz, $H_{Ar,\ Tyr}$), 4.54 (dt, 1H, J=3.4Hz, J=8.6Hz, C$_\alpha H_{Phe}$), 4.38 (m, 1H, C$_\alpha H_{Tyr}$), 4.21 (m, 1H, C$_\alpha H_{Leu}$), 3.63 (m, 4H, C$_\alpha H_{Gly}$), 2.89 (m, 4H, C$_\beta H_{Phe,\ Tyr}$), 1.75 (s, 3H, C$H_{3,\ acteyl}$), 1.62 (m, 1H, C*H*(CH$_3$)$_2$), 1.53 (m, 2H, C$_\beta H_{Leu}$), 0.86 (dd, 6H, J=6.4Hz, J=16.4Hz, CH(CH_3)$_2$). ^{13}C NMR (DMSO-d_6, 100.61 MHz): 173.8 (*C*OO), 171.9, 171.0, 169.3, 168.9, 168.2 (*C*ON), 155.7 (C_{Ar}OH-$_{Tyr}$), 137.7 ($C_{Ar,\ q,\ Phe}$), 139.9 ($C_{Ar,\ q,\ Tyr}$), 129.2, 128.0, 127.9, 126.2, 114.6 (C_{Ar}), 54.4 ($C_{\alpha,\ Phe}$), 53.5 ($C_{\alpha,\ Tyr}$), 50.3 ($C_{\alpha,\ Leu}$), 42.0, 41.7 ($C_{\alpha,\ Gly}$), 37.6 ($C_{\beta,\ Phe}$), 36.6 ($C_{\beta,\ Tyr}$), 24.2 ($C_{\beta,\ Leu}$), 22.7 (*C*H$_{3,\ Leu}$), 22.4 (*C*H$_{3,\ acetyl}$), 21.3 (*C*H(CH$_3$)$_2$).

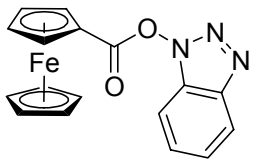

5

Ferrocenecarboxylic acid **1** (550 mg, 2.4 mmol) was dissolved in 12 ml of dried DCM. To the stirred suspension was added 500 mg (2.4 mmol) dicyclohexylcarbodiimide (DCC) and 340 mg (2.4 mmol) of hydroxybenzotriazole (HOBt). After 3 h of continuous stirring the solid was removed and the remaining solvent was purified by column chromatography using 100% DCM as an eluent (R_f = 0.35). The remaining reddish brown solid had a very characteristic smell of petroleum.

5: Anal. calc. for $C_{17}H_{13}FeN_3O_2$ (347.04 g/mol): C, 58.82; H, 3.77; N, 12.10. Found: C, 60.13; H, 4.37; N, 10.70. IR (cm^{-1}) in KBr: 2930 (w) υ_{CH}, 1775 (vs) υ_{COO}, 1261 (s) δ_{CO}. MS (EI): m/z 347 (40, $[M]^+$), 213 (100, $[Fc\text{-}CO]^+$). ^1H NMR ($CDCl_3$, 360.14 MHz): 8.08/7.47 (m, 4H, $H_{OBt,\ Ar}$), 5.07 (pseudo-t, 2H, Cp$H_{2,5}$), 4.67 (pseudo-t, 2H, Cp$H_{3,4}$), 4.43 (s, 5H, CpH). ^{13}C NMR ($CDCl_3$, 90.56 MHz): 168.2 (COO), 143.5 ($C_{OBt,\ 4}$), 128.5 ($C_{OBt,\ 9}$), 124.6 ($C_{OBt,\ 6,7}$), 120.4 ($C_{OBt,\ 5,8}$), 77.2 ($C_{Cp,\ 1}$), 73.4 ($C_{Cp,\ 3,4}$), 79.9 ($C_{Cp,\ 2,5}$), 70.7 ($C_{Cp'}$).

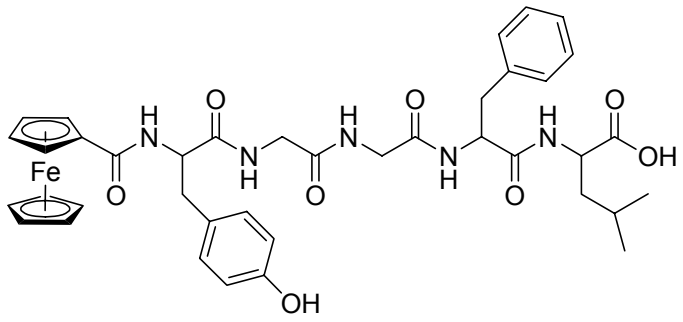

6

Resin	Loading (mmol/g)	AA excess	Cleavage mixture	Cleavage time	mg resin	yield
Wang	0.63	5	92.5% TFA 5.0% Phenol 2.5% TIS	3 h	200	84 mg (86.9 %)

6: $C_{39}H_{45}FeN_5O_8$ (767.26 g/mol): MS (ESI, pos): m/z 768.4 $[M + H^+]^+$, 790.5 $[M + Na^+]^+$, 806.4 $[M + K^+]^+$, MS (ESI, neg): m/z 766.4 $[M - H^+]^-$. ^{1}H NMR (DMSO-d_6, 300.14 MHz): 12.62 (s, br, 1H, COO*H*), 9.12 (s, br, 1H, OH_{Tyr}), 8.28 (d, 1H, J=7.8Hz, NH_{Leu}), 8.19 (t, 1H, J=5.2Hz, NH_{Gly}), 8.07 (d, 1H, J=8.4Hz, NH_{Phe}), 7.79 (d, 1H, J=8.2Hz, NH_{Tyr}), 7.25 (m, 5H, $H_{Ar,\ Phe}$), 7.17 (d, 2H, J=8.1Hz, $H_{Ar,\ Tyr}$), 6.67 (d, 2H, J=8.3Hz, $H_{Ar,\ Tyr}$), 4.83/4.72 (s, 1H, Cp$H_{2,5}$), 4.59 (m, 2H, C$_\alpha H_{Phe,\ Tyr}$), 4.30 (m, 2H, Cp$H_{3,4}$), 4.22 (m, 1H, C$_\alpha H_{Leu}$), 3.95 (s, 5H, Cp*H*), 3.67 (m, 4H, C$_\alpha H_{Gly}$), 2.92 (m, 4H, C$_\beta H_{Phe,\ Tyr}$), 1.62 (m, 1H, C*H*(CH$_3$)$_2$), 1.54 (m, 2H, C$_\beta H_{Leu}$), 0.87 (dd, 6H, J=6.3Hz, J=16.4Hz, CH(CH_3)$_2$). ^{13}C NMR (DMSO-d_6, 75.47 MHz): 173.5 (*C*OO), 171.8, 170.7, 168.8, 168.5, 167.8 (*C*ON), 155.4 ($C_{Ar}OH_{Tyr}$), 137.4 ($C_{Ar,\ q,\ Phe}$), 129.6, 128.8 (C_{Ar}), 128.2 ($C_{Ar,\ q,\ Tyr}$), 127.6, 125.8, 114.5 (C_{Ar}), 75.5 ($C_{Cp,1}$), 69.5 ($C_{Cp,\ 3,4}$), 68.9 ($C_{Cp'}$), 68.2/67.4 ($C_{Cp,\ 2,5}$), 54.3 ($C_{\alpha,\ Phe}$), 53.1 ($C_{\alpha,\ Tyr}$), 49.9 ($C_{\alpha,\ Leu}$), 41.7, 41.3 ($C_{\alpha,\ Gly}$), 37.2 ($C_{\beta,\ Phe}$), 35.7 ($C_{\beta,\ Tyr}$), 23.9 ($C_{\beta,\ Leu}$), 22.4 ($CH_{3,\ Leu}$), 21.0 (*C*H(CH$_3$)$_2$).

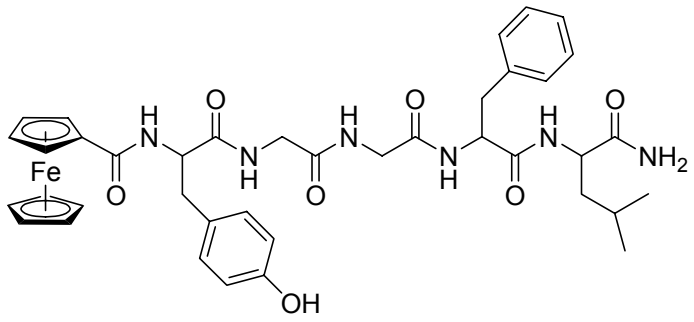

7

Resin	Loading (mmol/g)	AA excess	Cleavage mixture	Cleavage time	mg resin	yield
HMBA	0.23	5	NH_3 (sat.) in MeOH, 0 °C	24 h	800	76 mg (53.9 %)

7: $C_{39}H_{46}FeN_6O_7$ (766.28 g/mol): MS (ESI, neg): m/z 765.3 $[M - H^+]^-$. ^1H NMR (DMSO-d_6, 400.13 MHz): 9.07 (s, br, 1H, OH_{Tyr}), 8.12 (t, 1H, J=5.5Hz, NH_{Gly}), 8.07 (d, 1H, J=8.0Hz, NH_{Leu}), 8.01 (t, 1H, J=5.5Hz, NH_{Gly}), 7.94 (s, 2H, NH_2), 7.75 (d, 1H, J=8.2Hz, NH_{Phe}), 7.69 (d, 1H, J=7.8 Hz, NH_{Tyr}), 7.29 (m, 5H, $H_{Ar,\ Phe}$), 7.02 (d, 2H, J=8.6Hz, $H_{Ar,\ Tyr}$), 6.57 (d, 2H, J=8.6Hz, $H_{Ar,\ Tyr}$), 4.85/4.68 (s, 1H, Cp$H_{2,5}$), 4.59 (m, 1H, C$_\alpha H_{Tyr}$), 4.49 (dt, 1H, J=4.7Hz, J=8.8Hz, C$_\alpha H_{Phe}$), 4.31 (pseudo-t, 2H, Cp$H_{3,4}$), 4.19 (m, 1H, C$_\alpha H_{Leu}$), 3.94 (s, 5H, CpH), 3.67 (m, 4H, C$_\alpha H_{Gly}$), 2.89 (m, 4H, C$_\beta H_{Phe,\ Tyr}$), 1.55 (m, 1H, CH(CH$_3$)$_2$), 1.45 (m, 2H, C$_\beta H_{Leu}$), 0.83 (dd, 6H, J=6.4Hz, J=17.8Hz, CH(CH_3)$_2$). ^{13}C NMR (DMSO-d_6, 100.62 MHz): 173.8 (CONH$_2$), 170.6, 168.8, 168.5, 168.1, 167.8 (CON), 155.5 (C_{Ar}OH$_{Tyr}$), 137.7 ($C_{Ar,\ q,\ Phe}$), 129.9, 129.1 (C_{Ar}), 128.0 ($C_{Ar,\ q,\ Tyr}$), 127.0, 126.2, 114.6 (C_{Ar}), 75.0 ($C_{Cp,1}$), 69.7 ($C_{Cp,\ 3,4}$), 69.2 ($C_{Cp'}$), 67.2, 66.8 ($C_{Cp,\ 2,5}$), 54.0 ($C_{\alpha,\ Phe}$), 53.0 ($C_{\alpha,\ Tyr}$), 50.9 ($C_{\alpha,\ Leu}$), 41.3, 40.9 ($C_{\alpha,\ Gly}$), 37.8 ($C_{\beta,\ Phe}$), 35.8 ($C_{\beta,\ Tyr}$), 24.1 ($C_{\beta,\ Leu}$), 23.0 (CH$_{3,\ Leu}$), 21.6 (CH(CH$_3$)$_2$).

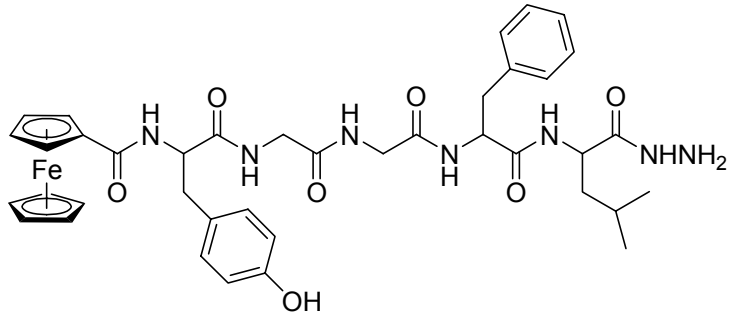

8

Resin	Loading (mmol/g)	AA excess	Cleavage mixture	Cleavage time	mg resin	yield
HMBA	0.24	5	5% NH_2NH_2 in DMF, 0 °C	3 h	795	73.5 mg (49.3 %)

8: $C_{39}H_{47}FeN_7O_7$ (781.29 g/mol): MS (ESI, pos): m/z 782.3 $[M + H^+]^+$, 804.4 $[M + Na^+]^+$, 820.3 $[M + K^+]^+$. ^{1}H NMR (DMSO-d_6, 300.14 MHz): 9.10 (s, br, 1H, OH_{Tyr}), 8.25 (m, 1H, NH_{Leu}), 8.16 (m, 1H, NH_{Gly}), 8.07 (d, 1H, J=8.4Hz, NH_{Phe}), 8.00 (m, 1H, NH_{Gly}), 7.78 (d, 1H, J=8.2Hz, NH_{Tyr}), 7.21 (m, 5H, $H_{Ar, Phe}$), 7.15 (d, 2H, J=8.1Hz, $H_{Ar, Tyr}$), 6.65 (d, 2H, J=8.2Hz, $H_{Ar, Tyr}$), 4.81/4.71 (s, 1H, Cp$H_{2,5}$), 4.59 (m, 2H, C$_\alpha H_{Phe, Tyr}$), 4.29 (m, 2H, Cp$H_{3,4}$), 4.22 (m, 1H, C$_\alpha H_{Leu}$), 3.94 (s, 5H, CpH), 3.67 (m, 4H, C$_\alpha H_{Gly}$), 2.83 (m, 4H, C$_\beta H_{Phe, Tyr}$), 1.60 (m, 1H, CH(CH$_3$)$_2$), 1.54 (m, 2H, C$_\beta H_{Leu}$), 0.86 (m, 6H, CH(CH_3)$_2$). ^{13}C NMR (DMSO-d_6, 75.47 MHz): 172.3, 171.0, 169.3, 169.0, 168.5 (CON), 155.8 ($C_{Ar}OH_{Tyr}$), 137.7 ($C_{Ar, q, Phe}$), 130.0, 129.1 (C_{Ar}), 128.5 ($C_{Ar, q, Tyr}$), 128.0, 126.3, 115.0 (C_{Ar}), 75.8 ($C_{Cp,1}$), 69.9 ($C_{Cp, 3,4}$), 69.3 ($C_{Cp'}$), 68.7, 67.9 ($C_{Cp, 2,5}$), 54.7 ($C_{\alpha, Phe}$), 53.8 ($C_{\alpha, Tyr}$), 49.9 ($C_{\alpha, Leu}$), 42.2, 41.9 ($C_{\alpha, Gly}$), 37.5 ($C_{\beta, Phe}$), 36.1 ($C_{\beta, Tyr}$), 24.3 ($C_{\beta, Leu}$), 22.9 (CH$_{3, Leu}$), 21.8 (CH(CH$_3$)$_2$).

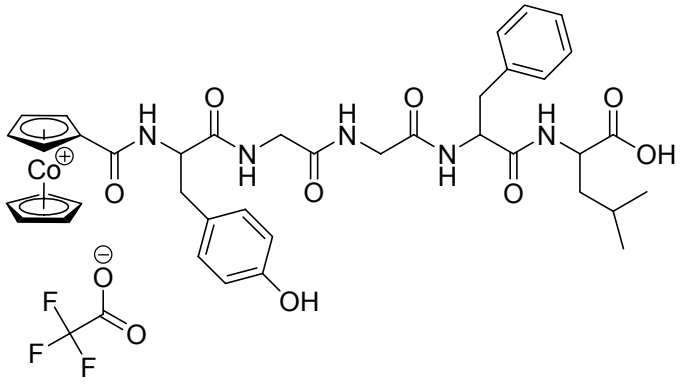

9

Resin	Loading (mmol/g)	AA excess	Cleavage mixture	Cleavage time	mg resin	yield
Wang	0.63	3	95% TFA 2.5% H_2O 2.5% TIS	3 h	500	189 mg (68.0 %)

9: $C_{41}H_{44}CoF_3N_5O_{10}$ (883.5g/mol): MS (ESI, pos): m/z 770.5 $[M + TFA^-]^+$, 404.9 $[M - TFA^- + K^+]^{2+}$. ^{1}H NMR (DMSO-d_6, 500.13 MHz): 12.50 (s, br, 1H, COO*H*), 9.24 (s, br, 1H, OH_{Tyr}), 8.87 (d, 1H, J=7.8Hz, NH_{Leu}), 8.19 (t, 1H, J=5.2Hz, NH_{Gly}), 8.07 (d, 1H, J=8.4Hz, NH_{Phe}), 7.79 (d, 1H, J=8.2Hz, NH_{Tyr}), 7.25 (m, 5H, $H_{Ar,\ Phe}$), 7.17 (d, 2H, J=8.1Hz, $H_{Ar,\ Tyr}$), 6.67 (d, 2H, J=8.3Hz, $H_{Ar,\ Tyr}$), 4.83, 4.72 (s, 1H, Cp$H_{2,5}$), 4.59 (m, 2H, C$_\alpha H_{Phe,\ Tyr}$), 4.30 (m, 2H, Cp$H_{3,4}$), 4.22 (dd, 1H, J=8.4Hz, J=13.9Hz, C$_\alpha H_{Leu}$), 3.95 (s, 5H, Cp*H*), 3.67 (m, 4H, C$_\alpha H_{Gly}$), 2.92 (m, 4H, C$_\beta H_{Phe,\ Tyr}$), 1.62 (m, 1H, C*H*$(CH_3)_2$), 1.54 (m, 2H, C$_\beta H_{Leu}$), 0.87 (dd, 6H, J=6.3Hz, J=16.4Hz, CH(CH_3)$_2$). ^{13}C NMR (DMSO-d_6, 75.47 MHz): 173.5 (*C*OO), 171.8, 170.7, 168.8, 168.5, 167.8 (*C*ON), 155.4 (C_{Ar}OH-$_{Tyr}$), 137.4 ($C_{Ar,\ q,\ Phe}$), 129.6, 128.8 (C_{Ar}), 128.2 ($C_{Ar,\ q,\ Tyr}$), 127.6, 125.8, 114.5 (C_{Ar}), 75.5 ($C_{Cp,1}$), 69.5 ($C_{Cp,\ 3,4}$), 68.9 ($C_{Cp'}$), 68.2, 67.4 ($C_{Cp,\ 2,5}$), 54.3 ($C_{\alpha,\ Phe}$), 53.1 ($C_{\alpha,\ Tyr}$), 49.9 ($C_{\alpha,\ Leu}$), 41.7, 41.3 ($C_{\alpha,\ Gly}$), 37.2 ($C_{\beta,\ Phe}$), 35.7 ($C_{\beta,\ Tyr}$), 23.9 ($C_{\beta,\ Leu}$), 22.4 ($CH_{3,\ Leu}$), 21.0 (*C*H$(CH_3)_2$).

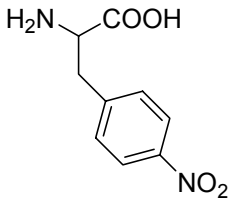

10

At 0°C, conc. H_2SO_4 (120ml) was slowly added under stirring to 120ml of conc. HNO_3. H-Phe-OH (100g, 605mmol) was added in portions over a period of 20min., giving a yellow, sticky solution. Stirring was continued overnight, the resulting slurry was poured over crushed ice and brought to pH = 7 with NaOH. The white precipitate was separated by filtration and dried *in vacuo*.
Yield: 92.6g (441mmol, 72.8%)

10: Anal. calc. for $C_9H_{10}N_2O_4$ (210.06 g/mol): C, 51.43; H, 4.80; N, 13.33. Found: C, 52.61; H, 5.34; N, 13.50. IR (cm^{-1}) in KBr: 3020 (m, br) υ_{CH}, 1677 (vs) υ_{COO}, 1200 (m) $\upsilon_{C\text{-}O}$. MS (EI): m/z 210 $[M]^+$, 165 $[M - NO_2]^+$, 137 $[CH_2\text{-}Ph\text{-}NO_2]^+$. ^1H NMR (D_2O, 360.14 MHz): 8.16 (d, 2H, J=8.4Hz, $H_{Ar,\ Phe}$), 7.45 (d, 2H, J=8.6Hz, $H_{Ar,\ Phe}$), 3.98 (m, 1H, $C_\alpha H_{Phe}$), 3.27 (m, 2H, $C_\beta H_{Phe}$). ^{13}C NMR (D_2O, 90.56 MHz): 173.9 (*C*OO), 144.4, 144.2 ($C_{Ar,\ q,\ Phe}$), 131.4, 125.0 (C_{Ar}), 56.2 ($C_{\alpha,\ Phe}$), 37.2 (C_β)

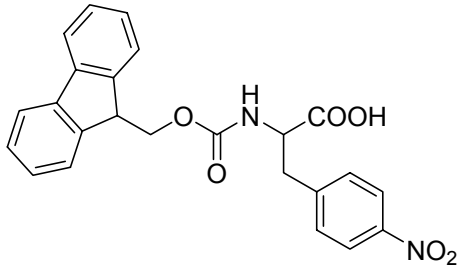

11

5.45 g (25 mmol) of *p*-nitro-phenylalanine was dissolved in a mixture of each 50 ml of H_2O and CH_3CN and treated with 1 equivalent of NEt_3 (2.5 g, 25 mmol). After 10 min. of stirring 8.0 g (23.75 mmol, 95%) of Fmoc-ONSu in 50 ml of CH_3CN was added dropwise over a period of 20 min, while pH was adjusted to 8.5 - 9.0. After 2 h of continuous stirring and subsequent filtration the solvents were removed *in vacuo* and a red oil remained. The oily residue was again dissolved in water and afterwards neutralized using 1 N HCl until the crude product precipitated. Recrystallization from EtOAc yielded 5.9 g (53%) of pure product in form of a white solid.

11: Anal. calc. for $C_{24}H_{20}N_2O_6$ (432.12 g/mol): C, 66.66; H, 4.66; N, 6.48. Found: C, 66.40; H, 4.71; N, 6.41. IR (cm^{-1}) in KBr: 3433 (m) υ_{NH}, 3222, 3055 (m, br) υ_{CH}, 1694 (vs) υ_{COO}, 1516 (s) δ_{NH}, 1227 (m) $\upsilon_{C\text{-}O}$. MS (FAB): m/z 433 $[M + H]^+$, 255 [M – Fluorenyl + H]$^+$, 165 [Fluorenyl]$^+$. ^{1}H NMR (DMSO-d_6, 360.14 MHz): 8.11 (d, 2H, J=8.6Hz, $H_{Ar,\ Phe}$), 7.84 (d, 2H, J=7.5Hz, $H_{Ar,\ Fluorenyl}$), 7.78 (d, 1H, J=8.6Hz, N*H*), 7.60 (m, 2H, $H_{Ar,\ Fluorenyl}$), 7.53 (d, 2H, J=8.6Hz, $H_{Ar,\ Phe}$), 7.38 (pseudo-t, 2H, $H_{Ar,\ Fluorenyl}$), 7.27 (dd, 2H, J=6.8Hz, J=13.1Hz, $H_{Ar,\ Fluorenyl}$), 4.30 (m, 1H, $C_\alpha H_{Phe}$), 4.23 (m, 2H, $CH_{2,\ Fluorenyl}$), 4.15 (m, 1H, $R_3CH_{Fluorenyl}$), 3.25, 3.02 (m, 2H, $C_\beta H_{Phe}$). ^{13}C NMR (DMSO-d_6, 90.56 MHz): 172.9 (*C*OO) 155.9 (*C*ON), 146.4, 146.2 ($C_{Ar,\ q,\ Phe}$), 143.7, 140.7 ($C_{Ar,\ q,\ Fluorenyl}$), 130.4, 127.6, 127.0, 125.1, 123.2, 120.1 (C_{Ar}), 65.6 ($CH_{2,\ Fluorenyl}$), 54.8 ($C_{\alpha,\ Phe}$), 46.6 ($R_3CH_{Fluorenyl}$), 36.1 (C_β)

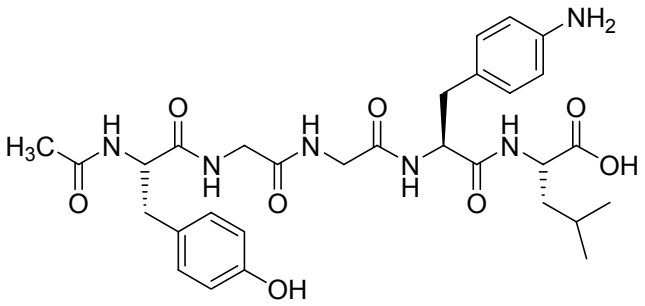

12

Resin	Loading (mmol/g)	AA excess	Cleavage mixture	Cleavage time	mg resin	yield
Wang	0.63	5	95% TFA 2.5% H_2O 2.5% TIS	3 h	200	70 mg (90.8 %)

12: $C_{30}H_{40}N_6O_8$ (612.29 g/mol): MS (ESI, pos): m/z 1263.8 $[2M + K^+]^+$, 1247.6 $[2M + Na^+]^+$, 1225.7 $[2M + H^+]^+$, 651.4 $[M + K^+]^+$, 635.5 $[M + Na^+]^+$, 613.4 $[M + H^+]^+$. ^{1}H NMR (DMSO-d6, 300.14 MHz): 9.23 (s, br, 1H, OH_{Tyr}), 8.26 (d, 1H, J=8.2Hz, NH_{Leu}), 8.25 (t, 1H, J=5.7Hz, NH_{Gly}), 8.08 (d, 1H, J=7.9Hz, NH_{Tyr}), 7.98 (d, 1H, J=8.6Hz, NH_{Phe}), 7.93 (t, 1H, J=5.7Hz, NH_{Gly}), 7.27 (d, 2H, J=8.3Hz, $H_{Ar,\ Phe}$), 7.07 (d, 2H, J=8.2Hz, $H_{Ar,\ Phe}$), 7.01 (d, 2H, J=8.4Hz, $H_{Ar,\ Tyr}$), 6.63 (d, 2H, J=8.4Hz, $H_{Ar,\ Tyr}$), 4.54 (dt, 1H, J=3.8Hz, J=9.4Hz, C$_\alpha H_{Phe}$), 4.39 (dt, 1H, J=4.8Hz, J=9.2Hz, C$_\alpha H_{Phe}$), 4.22 (m, 1H, C$_\alpha H_{Leu}$), 3.67 (m, 4H, C$_\alpha H_{Gly}$), 2.82 (m, 4H, C$_\beta H_{Phe,\ Tyr}$), 1.77 (s, 3H, CH_{Acetyl}), 1.64 (m, 1H, CH(CH$_3$)$_2$), 1.55 (m, 2H, C$_\beta H_{Leu}$), 0.87 (dd, 6H, J=6.3Hz, J=17.0Hz, CH(CH_3)$_2$). ^{13}C NMR (DMSO-d6, 75.47 MHz): 173.8 (*C*OO), 171.9, 170.9 (*C*ON), 169.3, 168.9, 168.2 (*C*ON), 155.6 (C_{Ar}OH$_{Tyr}$), 130.3, 129.9 (C_{Ar}), 127.9 ($C_{Ar,\ q,\ Tyr}$), 120.7, 114.8 (C_{Ar}), 54.5 ($C_{\alpha,\ Phe}$), 53.4 ($C_{\alpha,\ Tyr}$), 50.3 ($C_{\alpha,\ Leu}$), 42.0, 41.7 ($C_{\alpha,\ Gly}$), 36.9 ($C_{\beta,\ Phe}$), 36.5 ($C_{\beta,\ Tyr}$), 24.2 ($C_{\beta,\ Leu}$), 22.7 (CH$_{3,\ Leu}$), 22.4 (CH$_{3,\ Acetyl}$), 21.3 (CH(CH$_3$)$_2$).

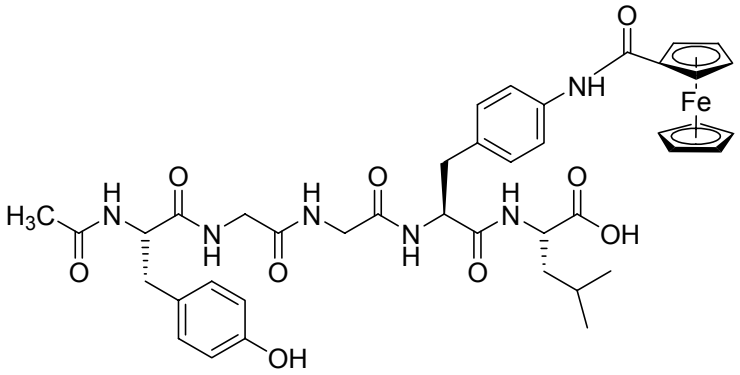

13

Resin	Loading (mmol/g)	AA excess	Cleavage mixture	Cleavage time	mg resin	yield
Wang	0.61	5	92.5% TFA 5% phenol 2.5% TIS	3 h	724 mg	281 mg (74.7 %)

13: $C_{41}H_{48}FeN_6O_9$ (824.28 g/mol): MS (ESI, pos): m/z 825.5 $[M + H^+]^+$, 847.4 $[M + Na^+]^+$, 863.4 $[M + K^+]^+$. (ESI, neg): m/z 823.5 $[M - H^+]^-$. ^{1}H NMR (DMSO-d6, 300.14 MHz): 9.36 (s, 1H, NH_{Fc}), 9.08 (s, br, 1H, OH_{Tyr}), 8.26 (d, 1H, J=7.9Hz, NH_{Leu}), 8.22 (t, 1H, J=5.8Hz, NH_{Gly}), 8.05 (d, 1H, J=7.9Hz, NH_{Tyr}), 7.97 (d, 1H, J=8.4Hz, NH_{Phe}), 7.94 (t, 1H, J=5.7Hz, NH_{Gly}), 7.58 (d, 2H, J=8.3Hz, $H_{Ar,\ Phe}$), 7.20 (d, 2H, J=8.3Hz, $H_{Ar,\ Phe}$), 7.00 (d, 2H, J=8.2Hz, $H_{Ar,\ Tyr}$), 6.62 (d, 2H, J=8.2Hz, $H_{Ar,\ Tyr}$), 4.89 (pseudo-t, 2H, Cp$H_{2,5}$), 4.55 (dt, 1H, J=3.8Hz, J=9.0Hz, C$_\alpha H_{Phe}$), 4.42 (pseudo-t, 2H, Cp$H_{3,4}$), 4.38 (m, 1H C$_\alpha H_{Phe}$), 4.23 (m, 1H, C$_\alpha H_{Leu}$), 4.20 (s, 5H, CpH), 3.68 (m, 4H, C$_\alpha H_{Gly}$), 2.78 (m, 4H, C$_\beta H_{Phe,\ Tyr}$), 1.75 (s, 3H, CH_{Acetyl}), 1.65 (m, 1H, CH(CH$_3$)$_2$), 1.53 (m, 2H, C$_\beta H_{Leu}$), 0.87 (dd, 6H, J=6.2Hz, J=16.4Hz, CH(CH_3)$_2$). ^{13}C NMR (DMSO-d6, 75.47 MHz): 173.8 (*C*OO), 172.0, 171.1, 169.4, 169.0, 168.3 (*C*ON), 168.0 (*C*ON$_{Fc}$), 155.7 (C_{Ar}OH-$_{Tyr}$), 137.5, 132.5 ($C_{Ar,\ q,\ Phe}$), 130.1, 129.4, 128.1, 120.1, 114.9 (C_{Ar}), 76.6 ($C_{Cp,1}$), 70.4 ($C_{Cp,\ 3,4}$), 69.5 ($C_{Cp'}$), 68.6 ($C_{Cp,\ 2,5}$), 54.6 ($C_{\alpha,\ Phe}$), 53.7 ($C_{\alpha,\ Tyr}$), 50.4 ($C_{\alpha,\ Leu}$), 42.2, 41.8 ($C_{\alpha,\ Gly}$), 37.2 ($C_{\beta,\ Phe}$), 36.7 ($C_{\beta,\ Tyr}$), 24.3 ($C_{\beta,\ Leu}$), 22.9 (CH$_{3,\ Leu}$), 22.5 (CH$_{3,\ Acetyl}$), 21.4 (CH(CH$_3$)$_2$).

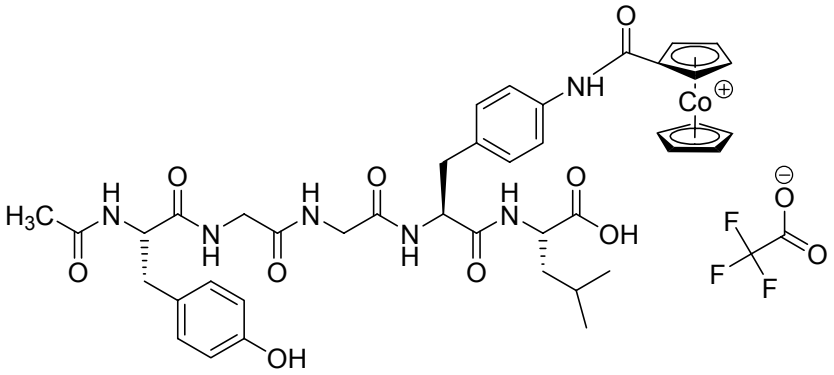

14

Resin	Loading (mmol/g)	AA excess	Cleavage mixture	Cleavage time	mg resin	yield
Wang	0.61	5	95% TFA 2.5% H_2O 2.5% TIS	3 h	500	189 mg (65.8 %)

14: $C_{43}H_{48}CoF_3N_6O_{11}$ (940.27 g/mol): MS (ESI, pos): m/z 827.3 $[M - TFA^-]^+$, 433.3 $[M - TFA^- + K^+]^{2+}$, 425.3 $[M - TFA^- + Na^+]^{2+}$. ^{1}H NMR (DMSO-d6, 300.14 MHz): 12.57 (s, br, 1H, COO*H*), 10.35 (s, 1H, NH_{CoCp2}), 9.16 (s, br, 1H, OH_{Tyr}), 8.29 (d, 1H, J=8.5Hz, NH_{Tyr}), 8.24 (t, 1H, J=5.5Hz, NH_{Gly}), 8.07 (d, 1H, J=7.9Hz, NH_{Leu}), 7.99 (d, 1H, J=8.2Hz, NH_{Phe}), 7.95 (t, 1H, J=5.7Hz, NH_{Gly}), 7.61 (d, 2H, J=8.2Hz, $H_{Ar, Phe}$), 7.28 (d, 2H, J=8.3Hz, $H_{Ar, Phe}$), 7.01 (d, 2H, J=8.0Hz, $H_{Ar, Tyr}$), 6.62 (d, 2H, J=8.1Hz, $H_{Ar, Tyr}$), 6.41 (s, 2H, Cp$H_{2,5}$), 5.98 (s, 2H, Cp$H_{3,4}$), 5.90 (s, 5H, Cp*H*), 4.56 (m, 1H, C$_\alpha H_{Phe}$), 4.38 (m, 1H, C$_\alpha H_{Tyr}$), 4.23 (m, 1H, C$_\alpha H_{Leu}$), 3.68 (m, 4H, C$_\alpha H_{Gly}$), 2.85 (m, 4H, C$_\beta H_{Phe, Tyr}$), 1.76 (s, 3H, $CH_{3, Acetyl}$), 1.64 (m, 1H, C*H*$(CH_3)_2$), 1.55 (m, 2H, C$_\beta H_{Leu}$), 0.88 (dd, 6H, J=6.1Hz, J=17.2Hz, CH(CH_3)$_2$). ^{13}C NMR (DMSO-d6, 75.47 MHz): 173.8 (*C*OO), 171.9, 170.9, 169.3, 168.9, 168.2 (*C*ON), 159.7 (*C*ON$_{CoCp2}$), 155.6 (C_{Ar}OH$_{Tyr}$), 136.2 ($C_{Ar, q, Phe}$), 134.1 ($C_{Ar, q, Tyr}$), 129.9, 129.4, 127.9, 120.3, 114.5 (C_{Ar}), 94.7 ($C_{Cp,1}$), 85.9 ($C_{Cp'}$), 85.4 ($C_{Cp, 2,5}$), 84.1 ($C_{Cp, 3,4}$), 56.0 ($C_{\alpha, Phe}$), 54.4 ($C_{\alpha, Tyr}$), 50.2 ($C_{\alpha, Leu}$), 42.0, 41.7 ($C_{\alpha, Gly}$), 37.0 ($C_{\beta, Phe}$), 36.4 ($C_{\beta, Tyr}$), 24.2 ($C_{\beta, Leu}$), 22.8 (*C*H$_{3, Leu}$), 22.3 (*C*H$_{3, Acetyl}$), 21.2 (*C*H$(CH_3)_2$).

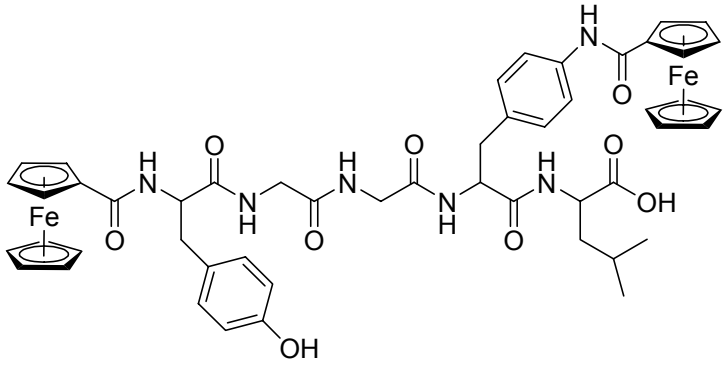

15

Resin	Loading (mmol/g)	AA excess	Cleavage mixture	Cleavage time	mg resin	yield
Wang	0.68	5	92.5% TFA 5% phenol 2.5% TIS	3 h	370	215 mg (86.0 %)

15: $C_{50}H_{54}Fe_2N_6O_9$ (994.27 g/mol): MS (ESI, neg): m/z 993.5 $[M - H^+]^-$. ^{1}H NMR (DMSO-d6, 300.14 MHz): 12.53 (s, br, 1H, COO*H*), 9.37 (s, 1H, NH_{Fc}), 9.04 (s, br, 1H, OH_{Tyr}), 8.26 (d, 1H, J=7.7Hz, NH_{Leu}), 8.17 (t, 1H, J=5.6 Hz, NH_{Gly}), 8.02 (t, 1H, J=4.6Hz), 7.98 (m, 1H, NH_{Phe}), 7.77 (d, 1H, J=8.1Hz, NH_{Tyr}), 7.58 (d, 2H, J=8.0Hz, $H_{Ar,\ Phe}$), 7.20 (d, 2H, J=8.8Hz, $H_{Ar,\ Phe}$), 7.16 (d, 2H, J=8.1Hz, $H_{Ar,\ Tyr}$), 6.66 (d, 2H, J=8.0Hz, $H_{Ar,\ Tyr}$), 4.99 (pseudo-t, 2H, $Cp_2H_{2,5}$), 4.81, 4.72 (s, 1H, $Cp_1H_{2,5}$), 4.59 (m, 2H, $C_\alpha H_{Phe,\ Tyr}$), 4.43 (pseudo-t, 2H, $Cp_2H_{3,4}$), 4.28 (pseudo-t, 2H, $Cp_1H_{3,4}$), 4.22 (m, 1H, $C_\alpha H_{Leu}$), 4.18 (s, 5H, Cp_2H), 3.94 (s, 5H, Cp_1H), 3.68 (m, 4H, $C_\alpha H_{Gly}$), 2.87 (m, 4H, $C_\beta H_{Phe,\ Tyr}$), 1.62 (m, 1H, C*H*$(CH_3)_2$), 1.55 (dd, 2H, J=6.5Hz, J=11.2Hz, $C_\beta H_{Leu}$), 0.87 (dd, 6H, J=6.1Hz, J=16.2Hz, CH(CH_3)$_2$). ^{13}C NMR (DMSO-d6, 75.47 MHz): 173.8 (*C*OO), 172.2, 171.0, 169.2, 168.9, 168.2, 167.9 (*C*ON), 155.7 ($C_{Ar}OH_{Tyr}$), 137.5 ($C_{Ar,\ q,\ Phe}$), 132.4 ($C_{Ar,\ q,\ Phe}$), 129.9, 129.3 (C_{Ar}), 128.5 ($C_{Ar,\ q,\ Tyr}$), 120.0, 114.9 (C_{Ar}), 76.5 ($C_{Cp2\text{-}1}$), 75.5 ($C_{Cp1\text{-}1}$), 70.4 ($C_{Cp2\text{-}3,4}$), 69.8 ($C_{Cp1\text{-}3,4}$), 69.4 ($C_{Cp'2}$), 69.2 ($C_{Cp'1}$), 68.4 ($C_{Cp2,\ 2,5}$), 68.2, 67.8 ($C_{Cp1,\ 2,5}$), ($C_{Cp,1}$), 54.6 ($C_{\alpha,\ Phe}$), 53.6 ($C_{\alpha,\ Tyr}$), 50.3 ($C_{\alpha,\ Leu}$), 42.1, 41.8 ($C_{\alpha,\ Gly}$), 37.1 ($C_{\beta,\ Phe}$), 36.0 ($C_{\beta,\ Tyr}$), 24.3 ($C_{\beta,\ Leu}$), 22.8 ($CH_{3,\ Leu}$), 21.3 (*C*H$(CH_3)_2$).

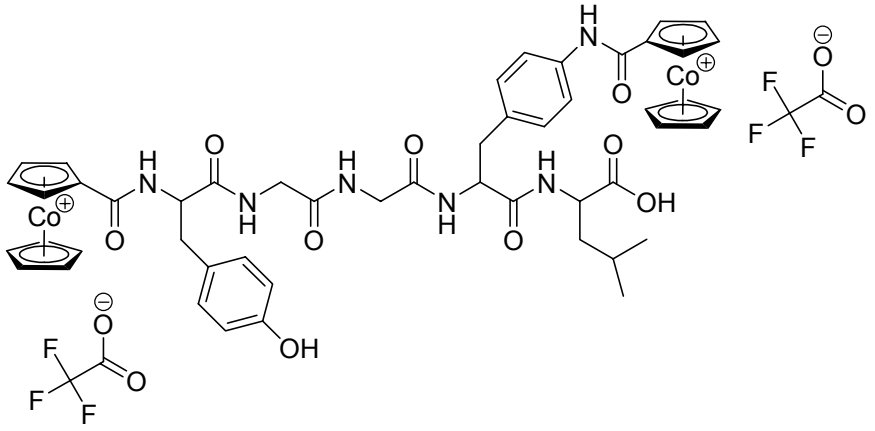

16

Resin	Loading (mmol/g)	AA excess	Cleavage mixture	Cleavage time	mg resin	yield
Wang	0.68	5	92.5% TFA 5% phenol 2.5% TIS	3 h	370	215 mg (86.0 %)

16: $C_{54}H_{54}Co_2F_6N_6O_{13}$ (1226.23 g/mol): MS (ESI, pos): m/z 999.3 [M - 2 TFA^- - H^+]$^+$, 500.3 [M - 2 TFA^-]$^{2+}$. ^{1}H NMR (DMSO-d6, 300.14 MHz): ca. 12.00 (1H, COO*H*, not obs.), 10.43 (s, br, 1H, NH_{CoCp2}), 8.88 (d, 1H, J=8.7Hz, NH_{Tyr}), 8.52 (t, 1H, J=5.0Hz, NH_{Gly}), 8.33 (d, 1H, J=8.2Hz, NH_{Leu}), 8.10 (d, 1H, J=9.18Hz, NH_{Phe}), 8.06 (t, 1H, J=5.0Hz, NH_{Gly}), 7.60 (d, 2H, J=8.3Hz, $H_{Ar, Phe}$), 7.26 (d, 2H, J=8.5Hz, $H_{Ar, Phe}$), 7.17 (d, 2H, J=8.5Hz, $H_{Ar, Tyr}$), 6.69 (d, 2H, J=8.5Hz, $H_{Ar, Tyr}$), 6.41 (m, 2H, Cp1$H_{2,5}$), 6.30, 6.24 (s, 1H, Cp2$H_{2,5}$), 5.98 (m, 2H, Cp$H_{3,4}$), 5.89 (s, 5H, Cp1*H*), 5.89 (m, 2H, Cp2$H_{3,4}$), 5.55 (s, 5H, Cp2*H*), 4.76 (m, 1H, C$_\alpha H_{Phe}$), 4.55 (m, 1H, C$_\alpha H_{Tyr}$), 4.19 (m, 1H, C$_\alpha H_{Leu}$), 3.69 (m, 4H, C$_\alpha H_{Gly}$), 2.95 (m, 4H, C$_\beta H_{Phe, Tyr}$), 1.61 (m, 1H, C*H*(CH$_3$)$_2$), 1.54 (m, 2H, C$_\beta H_{Leu}$), 0.87 (dd, 6H, J=6.2Hz, J=18.0Hz, CH(CH_3)$_2$). ^{13}C NMR (DMSO-d6, 75.47 MHz): 173.8 (*C*OO), 171.2, 171.0, 168.8, 168.3 (*C*ON), 161.3, 159.8 (*C*ON$_{CoCp}$), 155.9 (C_{Ar}OH$_{Tyr}$), 136.5 ($C_{Ar, q, Phe}$), 134.2 ($C_{Ar, q, Tyr}$), 130.0, 129.5, 128.1 (C_{Ar}), 120.2, 115.0 (C_{Ar}), 94.7 ($C_{Cp2,1}$), 92.7 ($C_{Cp1,1}$), 86.0 ($C_{Cp1'}$), 85.9 ($C_{Cp1, 2,5}$), 85.8 ($C_{Cp2'}$), 85.6 ($C_{Cp2, 2,5}$), 84.2 ($C_{Cp2, 3,4}$), 83.6 ($C_{Cp1, 3,4}$), 56.6 ($C_{\alpha, Phe}$), 54.6 ($C_{\alpha, Tyr}$), 50.3 ($C_{\alpha, Leu}$), 41.9, 41.5 ($C_{\alpha, Gly}$), 37.2 ($C_{\beta, Phe}$), 36.2 ($C_{\beta, Tyr}$), 24.3 ($C_{\beta, Leu}$), 22.8 (CH$_{3, Leu}$), 21.3 (CH(CH$_3$)$_2$).

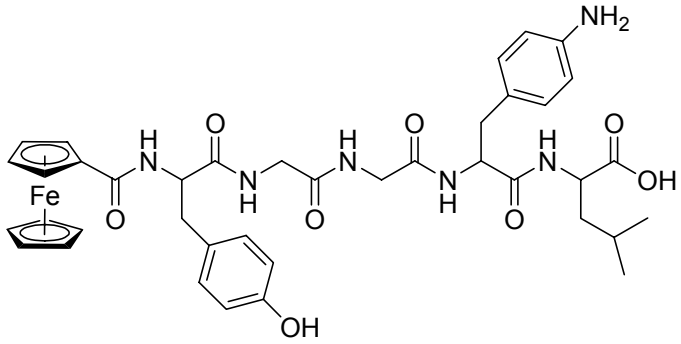

17

Resin	Loading (mmol/g)	AA excess	Cleavage mixture	Cleavage time	mg resin	yield
Wang	0.63	5	92.5% TFA 5% phenol 2.5% TIS	3 h	500	212 mg (86.3 %)

17: $C_{39}H_{46}FeN_6O_8$ (782.27 g/mol): MS (ESI, pos): m/z 783.3 $[M + H^+]^+$, 805.4 $[M + Na^+]^+$, 821.3 $[M + K^+]^+$, 411.4 $[M + H^+ + K^+]^{2+}$. ^{1}H NMR (DMSO-d6, 300.14 MHz): 9.14 (s, br, 1H, OH_{Tyr}), 8.27 (d, 1H, J=7.7Hz, NH_{Leu}), 8.20 (t, 1H, J=4.3Hz, NH_{Gly}), 8.04 (d, 1H, J=8.3Hz, NH_{Phe}), 8.01 (t, 1H, J=5.0Hz, NH_{Gly}), 7.79 (d, 1H, J=8.1Hz, NH_{Tyr}), 7.24 (d, 2H, J=8.0Hz, $H_{Ar,\ Phe}$), 7.17 (d, 2H, J=7.9Hz, $H_{Ar,\ Phe}$), 7.03 (d, 2H, J=8.0Hz, $H_{Ar,\ Tyr}$), 6.67 (d, 2H, J=7.9Hz, $H_{Ar,\ Tyr}$), 4.83, 4.72 (s, 1H, Cp$H_{2,5}$), 4.58 (m, 2H, C$_\alpha H_{Phe,\ Tyr}$), 4.30 (s, 2H, Cp$H_{3,4}$), 4.21 (m, 1H, C$_\alpha H_{Leu}$), 3.95 (s, 5H, CpH), 3.69 (m, 4H, C$_\alpha H_{Gly}$), 2.86 (m, 4H, C$_\beta H_{Phe,\ Tyr}$), 1.62 (m, 1H, CH(CH$_3$)$_2$), 1.55 (m, 2H, C$_\beta H_{Leu}$), 0.87 (dd, 6H, J=6.1Hz, J=16.9Hz, CH(CH_3)$_2$). ^{13}C NMR (DMSO-d6, 75.47 MHz): 173.8 (*C*OO), 172.2, 170.9, 169.2, 168.9, 168.2 (*C*ON), 155.7 (C_{Ar}OH$_{Tyr}$), 130.3, 129.9 (C_{Ar}), 128.4 ($C_{Ar,\ q,\ Tyr}$), 120.8, 114.9 (C_{Ar}), 75.7 ($C_{Cp,1}$), 69.9 ($C_{Cp,\ 3,4}$), 69.2 ($C_{Cp'}$), 68.6, 67.7 ($C_{Cp,\ 2,5}$), 54.6 ($C_{\alpha,\ Phe}$), 53.4 ($C_{\alpha,\ Tyr}$), 50.2 ($C_{\alpha,\ Leu}$), 42.0, 41.6 ($C_{\alpha,\ Gly}$), 36.9 ($C_{\beta,\ Phe}$), 36.0 ($C_{\beta,\ Tyr}$), 24.2 ($C_{\beta,\ Leu}$), 22.7 (CH$_{3,\ Leu}$), 21.3 (CH(CH$_3$)$_2$).

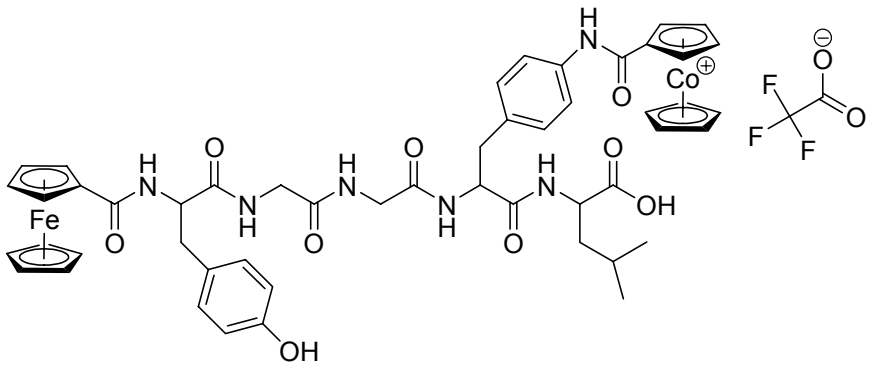

18

Resin	Loading (mmol/g)	AA excess	Cleavage mixture	Cleavage time	mg resin	yield
Wang	0.63	5	92.5% TFA 5% phenol 2.5% TIS	3 h	500	212 mg (86.3 %)

18: $C_{52}H_{54}CoF_3FeN_6O_{11}$ (1110.25 g/mol): MS (ESI, pos): m/z 997.3 $[M - TFA^-]^+$, 518.2 $[M - TFA^- + K^+]^{2+}$, 510.2 $[M - TFA^- + Na^+]^{2+}$. ^{1}H NMR (DMSO-d6, 300.14 MHz): 12.58 (s, br, 1H, COO*H*), 10.42 (s, 1H, NH_{CoCp2}), 9.13 (s, br, 1H, OH_{Tyr}), 8.28 (m, 1H, NH_{Leu}), 8.20 (m, 1H, NH_{Gly}), 8.02 (m, 2H, N$H_{Gly,\ Tyr}$), 7.78 (m, 1H, NH_{Phe}), 7.60 (m, 2H, $H_{Ar,\ Phe}$), 7.26 (m, 2H, $H_{Ar,\ Phe}$), 7.16 (m, 2H, $H_{Ar,\ Tyr}$), 6.66 (m, 2H, $H_{Ar,\ Tyr}$), 6.41 (s, 2H, Cp$H_{Co,\ 2,5}$), 5.97 (s, 2H, Cp$H_{Co,\ 3,4}$), 5.88 (s, 5H, CpH_{Co}), 4.81, 4.71 (s, 1H, Cp$H_{Fe,\ 2,5}$), 4.58 (m, 2H, C$_\alpha H_{Phe,\ Tyr}$), 4.28 (m, 2H, Cp$H_{Fe,\ 3,4}$), 4.22 (m, 1H, C$_\alpha H_{Leu}$), 3.94 (s, 5H, CpH_{Fe}), 3.70 (m, 4H, C$_\alpha H_{Gly}$), 2.86 (m, 4H, C$_\beta H_{Phe,\ Tyr}$), 1.61 (m, 1H, C*H*$(CH_3)_2$), 1.54 (m, 2H, C$_\beta H_{Leu}$), 0.86 (m, 6H, CH(CH_3)$_2$). ^{13}C NMR (DMSO-d6, 75.47 MHz): 173.7 (*C*OO), 172.1, 170.8, 169.1, 168.8, 168.2 (*C*ON), 159.7 (*C*ON$_{CoCp2}$), 155.6 (C_{Ar}OH$_{Tyr}$), 136.2 ($C_{Ar,\ q,\ Phe}$), 134.1 ($C_{Ar,\ q,\ Tyr}$), 129.8, 129.4 (C_{Ar}), 126.4, 120.3, 114.8 (C_{Ar}), 94.7 ($C_{CoCp,1}$), 85.9 ($C_{CoCp'}$), 85.5 ($C_{CoCp,\ 2,5}$), 84.1 ($C_{CoCp,\ 3,4}$), 75.7 ($C_{FeCp,1}$), 69.7 ($C_{FeCp,\ 3,4}$), 69.1 ($C_{FeCp'}$), 68.5, 67.7 ($C_{FeCp,\ 2,5}$), 54.5 ($C_{\alpha,\ Phe}$), 53.5 ($C_{\alpha,\ Tyr}$), 50.2 ($C_{\alpha,\ Leu}$), 42.0, 41.7 ($C_{\alpha,\ Gly}$), 37.0 ($C_{\beta,\ Phe}$), 35.9 ($C_{\beta,\ Tyr}$), 24.2 ($C_{\beta,\ Leu}$), 22.7 ($CH_{3,\ Leu}$), 21.2 (*C*H$(CH_3)_2$).

Synthesis of 4-Iodo-L-phenylalanin 19

$C_9H_{10}INO_2$ (M = 290.98 g/mol)

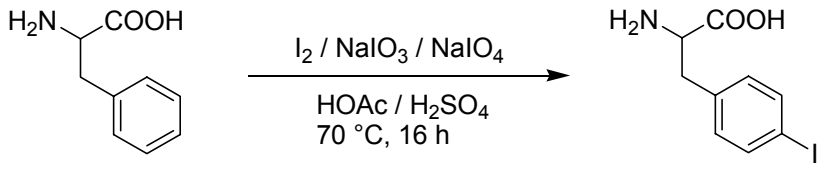

4-Iodo-L-phenylalanin was synthesized as reported by Alan W. Schwabacher et al.[166] Some minor changes have been applied to the preparation.

L-Phenylalanine (40.15 g, 243.2 mmol) was dissolved in 220 ml of HOAc and 29.0 ml of concentrated H_2SO_4. The clear and viscous solution was stirred while powdered Iodine (24.65 g, 97.1 mmol) and $NaIO_3$ (10.18 g, 51.4 mmol) were added. The mixture was heated to 70 °C. Completion was indicated by the I_2 color fading from dark red to light orange, which took 16 h and the addition of 2 g of $NaIO_4$. HOAc was removed in vacuo at 30 °C, and the residual viscous oil was diluted with 400 ml of water and washed twice each with 100 ml portions of Et_2O and CH_2Cl_2. The yellow aqueous solution was decolorized through treatment with 5 g of Norit and after filtration neutralized with NaOH to precipitate the crude product, which, after chilling, was filtered and rinsed with 800 ml of water and 300 ml of EtOH. The damp precipitate was dried in a cabinet desiccator to yield 42.5 g (60.0%).

Synthesis of 4-Iodo-L-phenylalaninmethylester <u>20</u>

$C_{10}H_{12}INO_2$ (M = 304.99 g/mol)

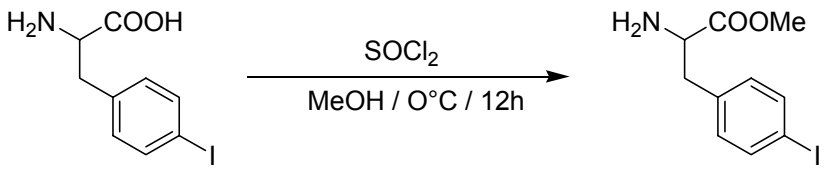

In an ice-bath thionylchloride (100 mmol, 11.90 g) was added dropwise to 100 ml of Methanol followed by the addition of 40 mmol 4-Iodo-L-Phenylalanin (11.64 g). After stirring for 12 hours the solvent was removed at 40°C under reduced pressure to obtain the crude product. The slightly green solid was dissolved in as little MeOH as possible and the solution was poured into 350 ml of diethylether to precipitate a white solid. After filtration and washing with an additional aliquot of 200 ml of diethylether the pure product was dried in vacuo.

Yield: 8.25 g (24.25 mmol, 60.5%)

<u>20</u>: Anal. calc. for $C_{10}H_{13}ClINO_2$ (340.96 g/mol): C, 35.16; H, 3.48; N, 4.10. Found: C, 34.52; H, 3.89; N, 4.00. IR (cm^{-1}) in KBr: 2838 (vs, br) υ_{CH}, 1738 (vs) υ_{COO}, 1245 (s) $\upsilon_{C\text{-}O}$, 835 (m) δ_{CH}. MS (FAB): m/z 306 $[M + Cl]^+$, 289 $[M - Cl - CH_3]^+$. ^1H NMR (D_2O, 360.14 MHz): 7.80 (d, 2H, J=8.0Hz, H_{Ar}), 7.08 (d, 2H, J=8.0Hz, H_{Ar}), 4.43 (t, 1H, J=6.7Hz, $C_\alpha H$), 3.38 (s, 3H, CH_3), 3.26 (m, 2H, $C_\beta H_{Phe}$). ^{13}C NMR (D_2O, 90.56 MHz): 170.8 (*C*OO), 139.2, 132.3 (C_{Ar}), 134.5 ($C_{Ar,\,q}$), 94.0 ($C_{Ar\text{-}I}$), 54.8 (C_α), 54.5 (CH_3), 36.2 (C_β)

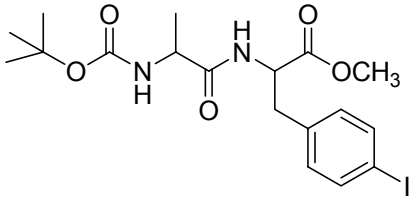

21a

To a stirred solution of 1.89 g of Boc-L-alanine (10 mmol) in THF was added N-methylmorpholine (1.12 ml, 1.02 g, 10 mmol) followed by the addition of isobutyl chloroformiate (1.32 ml, 1.36 g, 10 mmol), resulting in a precipitation of a white solid. In a second flask 4-iodo-L-phenylalaninemethylester hydrochloride (3.41 g, 10 mmol) was suspended in 50 ml of THF containing triethylamine (1.38 ml, 1.02 g, 10 mmol). Both suspensions were mixed and stirred for 60 min. at room temperature. After removal of the white precipitates by filtration the solvent was removed under reduced pressure and the residual oil dissolved in 100 ml of $CHCl_3$. The solution was washed with H_2O (50 ml) and the aqueous solution was back-extracted with three 50ml aliquots of $CHCl_3$. The combined $CHCl_3$ solutions were dried over Na_2SO_4. Evaporation of the solvent under reduced pressure yielded 3.68 g of Boc-Ala-Phe(I)-OMe as a white solid. The product could be recrystallised from THF/Heptane.

Yield: 3.68 g (77 %)

21a: Anal. calc. for $C_{18}H_{25}IN_2O_5$ (476.08 g/mol): C, 45.39; H, 5.29; N, 5.88. Found: C, 44.89; H, 5.26; N, 5.81. IR (cm^{-1}) in KBr: 3336 (s) υ_{NH}, 2981 (m) υ_{CH}, 1743 (s) υ_{COO}, 1664 (vs) υ_{CON}, 1522 (s) δ_{NH}. MS (FAB): m/z 477 $[M + 1]^+$, 463 $[M - CH_3]^+$, 421 $[M - C_4H_9]^+$, 377 $[M - Boc]^+$. ^{1}H NMR (DMSO-d_6, 360.14 MHz): 8.13 (d, 1H, J=7.5Hz, NH_{Phe}), 7.61 (d, 2H, J=7.9Hz, H_{Ar}), 7.03 (d, 2H, J=7.5Hz, H_{Ar}), 6.85 (d, 1H, J=7.2Hz, NH_{Boc}), 4.47 (m, 1H, C$_\alpha H_{Phe}$), 3.95 (m, 1H, C$_\alpha H_{Ala}$), 3.60 (s, 3H, CH_3), 2.92 (m, 2H, C$_\beta H$), 1.37 (s, 9H, C$H_{3,\ Boc}$), 1.11 (d, 3H, J=6.4Hz, C$H_{3,\ Ala}$). ^{13}C NMR (DMSO-d_6, 90.56 MHz): 172.7, 171.4 (*C*OO, *C*ON), 154.7 (CO_{Boc}), 136.8 ($C_{Ar,\ q}$), 136.8, 131.5 (C_{Ar}), 92.3 ($C_{Ar\text{-}I}$), 77.9 ($C_{Boc,\ q}$), 52.8 ($C_{\alpha,\ Ala}$), 51.7 (CH_3), 49.4 ($C_{\alpha,\ Phe}$), 35.9 (C_β), 28.0 ($CH_{3,\ Boc}$), 17.9 ($CH_{3,\ Ala}$). UV-Vis (λ in nm, [ε in $M^{-1}cm^{-1}$]): 232, [15440]

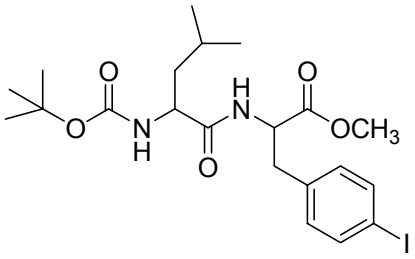

21b

The synthesis was carried out in analogy to **21a**. 2.31 g (10 mmol) of Boc-L-leucine was used.

Yield: 4.26 g (82 %)

21b: Anal. calc. for $C_{21}H_{31}IN_2O_5$ (518.13 g/mol): C, 48.66; H, 6.03; N, 5.40. Found: C, 48.33; H, 6.01; N, 5.37. IR (cm^{-1}) in KBr: 3338 (s) υ_{NH}, 2955 (m) υ_{CH}, 1747 (m) υ_{COO}, 1658 (vs) υ_{CON}, 1521 (s) δ_{NH}. MS (FAB): m/z 519 $[M + 1]^+$, 463 $[M - C_4H_9]^+$, 417 $[M - Boc]^+$. ^1H NMR (DMSO-d_6, 360.14 MHz): 8.12 (d, 1H, J=7.8Hz, NH_{Phe}), 7.61 (d, 2H, J=8.1Hz, H_{Ar}), 7.04 (d, 2H, J=8.1Hz, H_{Ar}), 6.80 (d, 1H, J=8.4Hz, NH_{Boc}), 4.50 (dd, 1H, C$_\alpha H_{Phe}$), 3.94 (dd, 1H, C$_\alpha H_{Ala}$), 3.61 (s, 3H, CH_3), 2.95 (m, 2H, C$_\beta H_{Phe}$), 1.51 (sep, 1H, J=6.6Hz, CH(CH_3)), 1.38 (s, 9H, C$H_{3,\ Boc}$), 1.30 (m, 2H, C$_\beta H_{Leu}$), 0.84 (pseudo-t, 6H, C$H_{3,\ Leu}$). ^{13}C NMR (DMSO-d_6, 90.56 MHz): 172.5, 171.6 (COO, CON), 155.1 (CO_{Boc}), 136.9 ($C_{Ar,\ q}$), 136.9, 131.6 (C_{Ar}), 92.3 ($C_{Ar\text{-}I}$), 78.1 ($C_{Boc,\ q}$), 52.8 ($C_{\alpha,\ Ala,\ Phe}$), 51.9 (CH_3), 40.0 ($C_{\beta,\ Leu}$), 36.1 ($C_{\beta,\ Phe}$), 28.2 ($CH_{3,\ Boc}$), 24.1, 22.8 ($CH_{3,\ Leu}$), 21.7 ($C(CH_3)_2$). UV-Vis (λ in nm, [ε in $M^{-1}cm^{-1}$]): 231, [15151]

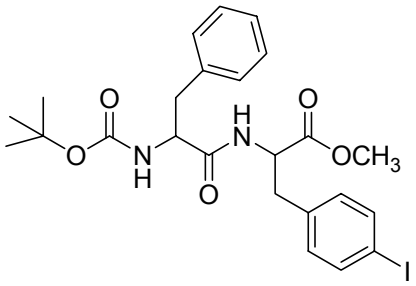

21c

The synthesis was carried out in analogy to **21a**. 2.65 g (10 mmol) of Boc-L-phenylalanine was used.

Yield: 5.03 g (91 %)

21c: Anal. calc. for $C_{24}H_{29}IN_2O_5$ (552.11 g/mol): C, 52.18; H, 5.29; N, 5.07. Found: C, 51.59; H, 5.36; N, 5.07. IR (cm^{-1}) in KBr: 3337 (s) υ_{NH}, 2980 (m) υ_{CH}, 1739 (s) υ_{COO}, 1662 (vs) υ_{CON}, 1521 (s) δ_{NH}. MS (FAB): m/z 553 $[M + 1]^+$, 497 $[M - C_4H_9]^+$, 453 $[M - Boc]^+$. ^1H NMR (DMSO-d_6, 360.14 MHz): 8.33 (d, 1H, J=7.6Hz, NH_{Phe}), 7.62 (d, 2H, J=7.5Hz, H_{Ar}), 7.22 (m, 5H, H_{Ar}), 7.05 (d, 2H, J=7.5Hz, H_{Ar}), 6.87 (d, 1H, J=8.6Hz, NH_{Boc}), 4.50 (dd, 1H, J=7.1Hz, J=13.2Hz, C$_\alpha H_{Phe-I}$), 4.17 (dd, 1H, J=7.2 Hz, J=13.4Hz, C$_\alpha H_{Phe}$), 3.60 (s, 3H, CH_3), 2.97 (m, 2H, C$_\beta H_{Phe-I}$), 2.74 (m, 2H, C$_\beta H_{Phe}$), 1.29 (s, 9H, C$H_{3,\ Boc}$). ^{13}C NMR (DMSO-d_6, 90.56 MHz): 171.7, 171.5 (*C*OO, *C*ON), 155.0 (*C*O$_{Boc}$), 137.9, 136.8 ($C_{Ar,\ q}$), 136.9, 131.5, 129.0, 127.9, 126.1 (C_{Ar}), 92.4 ($C_{Ar\text{-}I}$), 78.0 ($C_{Boc,\ q}$), 55.5 ($C_{\alpha,\ Phe}$), 53.1 ($C_{\alpha,\ Phe\text{-}I}$), 51.8 (*C*H$_3$), 37.3 ($C_{\beta,\ Phe}$), 36.1 ($C_{\beta,\ Phe\text{-}I}$), 28.0 (*C*H$_{3,\ Boc}$). UV-Vis (λ in nm, [ε in $M^{-1}cm^{-1}$]): 231, [14153]

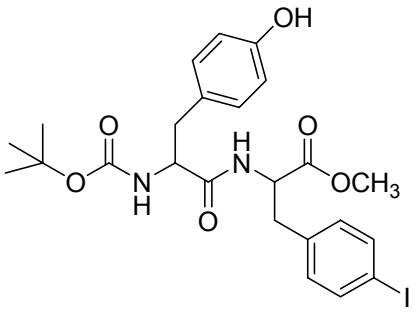

21d

The synthesis was carried out in analogy to **21a**. 2.81 g (10 mmol) of Boc-L-tyrosine was used.

Yield: 5.24 g (92 %)

21d: Anal. calc. for $C_{24}H_{29}IN_2O_6$ (568.11 g/mol): C, 50.71; H, 5.14; N, 4.93. Found: C, 50.43; H, 5.17; N, 4.88. IR (cm^{-1}) in KBr: 3306 (s) υ_{NH}, 2978 (m) υ_{CH}, 1709 (s) υ_{COO}, 1661 (vs) υ_{CON}, 1522 (s) δ_{NH}. MS (FAB): m/z 569 $[M + 1]^+$, 513 $[M - C_4H_9]^+$, 469 $[M - Boc]^+$. ^1H NMR (DMSO-d_6, 360.14 MHz): 9.14 (s, OH_{Tyr}), 8.25 (d, 1H, J=7.7Hz, NH_{Phe}), 7.60 (d, 2H, J=8.0Hz, $H_{Ar,\ Phe}$), 7.03 (d, 2H, J=8.0Hz, $H_{Ar,\ Phe}$), 6.98 (d, 2H, J=8.2Hz, $H_{Ar,\ Tyr}$), 6.76 (d, 1H, J=8.6Hz, NH_{Boc}), 6.62 (d, 2H, J=8.1Hz, $H_{Ar,\ Tyr}$), 4.48 (dd, 1H, J=7.9Hz, J=13.6Hz, C$_\alpha H_{Phe\text{-}I}$), 4.06 (dd, 1H, J=7.6 Hz, J=13.2Hz, C$_\alpha H_{Phe}$), 3.58 (s, 3H, CH_3), 2.94 (m, 2H, C$_\beta H_{Phe\text{-}I}$), 2.62 (m, 2H, C$_\beta H_{Phe}$), 1.29 (s, 9H, C$H_{3,\ Boc}$). ^{13}C NMR (DMSO-d_6, 90.56 MHz): 172.0, 171.6 (*C*OO, *C*ON), 155.6 ($C_{Ar}OH_{Tyr}$), 154.9 (CO_{Boc}), 136.7, 127.8 ($C_{Ar,\ q}$), 136.8, 131.5, 129.9, 114.7 (C_{Ar}), 92.4 ($C_{Ar\text{-}I}$), 77.9 ($C_{Boc,\ q}$), 55.7 ($C_{\alpha,\ Tyr}$), 52.9 ($C_{\alpha,\ Phe\text{-}I}$), 51.8 ($CH_3$), 36.5 ($C_{\beta,\ Tyr}$), 36.0 ($C_{\beta,\ Phe\text{-}I}$), 28.1 ($CH_{3,\ Boc}$). UV-Vis (λ in nm, [ε in $M^{-1}cm^{-1}$]): 229, [19492]; 276, [1172]

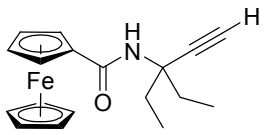

22

To a suspension of 2.3 g of ferrocene carboxylic acid (10 mmol) in 50 ml of dried and degassed DCM was added under argon 1.78 g of thionyl chloride (15 mmol). The mixture was heated at reflux for 1 hour. The clear and orange solution was allowed to cool down and the solvent was removed under reduced pressure, leaving a dark orange solid. The latter was dissolved in 50 ml of dried DCM and treated with 1.1 g of 1,1-diethylpropargylamine (10 mmol) and 1.01 g of NEt_3 (10 mmol). After 6 h of stirring at ambient temperature and removal of triethylamine hydrochloride by filtration through celite, the solvent was removed by rotary evaporation. The remaining orange solid was dissolved in 50 ml of chloroform and washed three times with water. After drying over Na_2SO_4 and filtration the solution was rotary evaporated to dryness. The crude product could be recrystallised from methanol.

Yield: 2.89 g (89 %) of DEPA-Fc as an orange solid.

22: Anal. calc. for $C_{18}H_{21}FeNO$ (323.10 g/mol): C, 66.89; H, 6.55; N, 4.33. Found: C, 66.65; H, 6.60; N, 4.30. IR (cm^{-1}) in KBr: 3300 (s) $\upsilon_{CC,\ alkyne}$, 3276 (s) υ_{NH}, 2972, 2877 (m) υ_{CH}, 1630 (vs) υ_{CON}, 1526 (s) δ_{NH}. MS (EI): m/z 323 (100, $[M]^+$), 295 (12, $[M - Ethyl]^+$), 267 (10, $[M - 2\ Ethyl]^+$), 213 (40, $[Fc\text{-}CO]^+$), 185 (22, $[Fc]^+$) . ^1H NMR (DMSO-d_6, 360.14 MHz): 7.08 (s, N*H*), 4.89 (m, 2H, Cp$H_{1,2}$), 4.33 (m, 2H, Cp$H_{3,4}$), 4.18 (s, 5H, Cp*H*), 3.19 (s, 1H, CH_{alkyne}), 2.01 (qd, 2H, J=7.3Hz, J=14.5 Hz, C$H_{2,\ DEPA}$), 1.83 (qd, 2H, J=7.3Hz, J=14.6 Hz, C$H_{2,\ DEPA}$), 0.95 (t, 6H, J=7.3Hz, C$H_{3,DEPA}$). ^{13}C NMR (DMSO-d_6, 90.56 MHz): 168.0 (*C*ON), 85.9, 72.8 (C_{alkyne}), 76.6 ($C_{Cp,\ 1}$), 69.6 ($C_{Cp,\ 2,5}$), 69.0 ($C_{Cp'}$), 68.2 ($C_{Cp,\ 3,4}$), 55.1 ($C_{DEPA,\ q}$), 29.7 ($CH_{2,\ DEPA}$), 8.2 ($CH_{3,\ DEPA}$). UV-Vis (λ in nm, [ε in $M^{-1}cm^{-1}$]): 259, [3649]; 304, [760]; 444, [232]

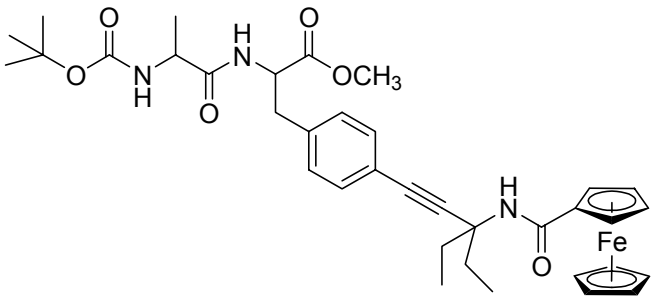

23a

12 ml of a mixture of dried THF and NEt_3 (1:1) was thoroughly degassed in a Schlenck-tube. To this solution was added 476 mg of Boc-Ala-Phe(I)-OMe (1 mmol) and 356 mg (1.1 mmol) of DEPA-Fc. Then was added a mixture of 14 mg of $Pd(PPh_3)_2Cl_2$ (0.02 mmol, 2 mol%) and CuI (6 mg, 0.03 mmol, 3 mol%) as a catalyst. The mixture was stirred under argon until no more triethylamine hydroiodide precipitated (6h). After removal of the salts by filtration the solvents were removed under reduced pressure and the product was purified by column chromatography on silica using ethyl acetate / hexane (2:1, $R_f = 0.42$). Yield: 504.0 mg (74 %)

23a: Anal. calc. for $C_{36}H_{45}FeN_3O_6$ (671.27 g/mol): C, 64.38; H, 6.75; N, 6.26. Found: C, 64.26; H, 6.64; N, 5.68. IR (cm^{-1}) in KBr: 3321 (s) υ_{NH}, 2974 (m) υ_{CH}, 1743 (s) υ_{COO}, 1653 (vs) υ_{CON}, 1508 (s) δ_{NH}, 821 (m) δ_{CH}. MS (FAB): m/z 671 $[M]^+$, 572 $[M - Boc]^+$, 213 $[Fc\text{-}CO]^+$, 185 $[Fc]^+$. ^1H NMR ($CDCl_3$, 360.14 MHz): 7.36 (d, 2H, J=8.0Hz, H_{Ar}), 7.04 (d, 2H, J=8.0Hz, H_{Ar}), 6.67 (d, 1H, J=7.5Hz, NH_{Phe}), 5.74 (s, 1H, NH_{Fc}), 5.03 (d, 1H, J=5.6Hz, NH_{Boc}), 4.81 (m, 1H, $C_\alpha H_{Phe}$), 4.64 (m, 2H, $CpH_{1,2}$), 4.31 (m, 2H, $CpH_{3,4}$), 4.21 (s, 5H, Cp*H*), 4.14 (m, 1H, $C_\alpha H_{Ala}$), 3.69 (s, 3H, CH_3), 3.09 (m, 2H, $C_\beta H_{,Phe}$), 2.38 (qd, 2H, J=7.2Hz, J=14.4Hz, $CH_{2,\ DEPA}$), 1.91 (qd, 2H, J=7.3Hz, J=14.5Hz, $CH_{2,\ DEPA}$), 1.41 (s, 9H, $CH_{3,\ Boc}$), 1.30 (d, 3H, J=7.1Hz, $CH_{3,\ Ala}$), 1.09 (t, 6H, J=7.3Hz, $CH_{3,\ DEPA}$). ^{13}C NMR ($CDCl_3$, 90.56 MHz): 172.3, 171.4 (*C*OO, *C*ON), 169.0 (CO_{Fc}), 155.3 (CO_{Boc}), 136.2 ($C_{Ar,\ q}$), 131.9, 129.2 (C_{Ar}), 121.5 ($C_{Ar,\ alkyne}$), 91.1, 83.3 (C_{alkyne}), 80.0 ($C_{Boc,\ q}$), 76.8 ($C_{Cp,\ 1}$), 70.2 ($C_{Cp,\ 2,5}$), 69.6 ($C_{Cp'}$), 68.0 ($C_{Cp,\ 3,4}$), 58.4 ($C_{DEPA,\ q}$), 53.0 ($C_{\alpha,\ Phe}$), 52.3 (CH_3), 50.0 ($C_{\alpha,\ Ala}$), 36.6 ($C_{\beta,\ Phe}$), 30.9 ($CH_{2,\ DEPA}$), 28.2 ($CH_{3,\ Boc}$), 18.1 ($CH_{3,\ Ala}$), 9.0 ($CH_{3,\ DEPA}$). UV-Vis (λ in nm, [ε in $M^{-1}cm^{-1}$]): 246, [24825]; 256, [22152]; 442, [236]

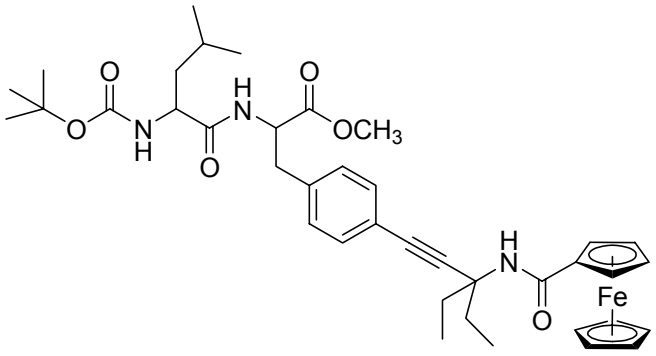

23b

The synthesis was carried out in analogy to **23a**. 581 mg (1 mmol) of Boc-Leu-Phe(I)-OMe was used. The product was purified by column chromatography on silica using ethyl acetate / hexane (1:2, $R_f = 0.33$).

Yield: 650.0 mg (91 %)

23b: Anal. calc. for $C_{39}H_{51}FeN_3O_6$ (713.31 g/mol): C, 65.63; H, 7.20; N, 5.89. Found: C, 65.53; H, 7.41; N, 5.50. IR (cm^{-1}) in KBr: 3318 (s) υ_{NH}, 2964 (m) υ_{CH}, 1748 (s) υ_{COO}, 1662 (vs) υ_{CON}, 1507 (s) δ_{NH}, 822 (m) δ_{CH}. MS (FAB): m/z 713 $[M]^+$, 614 $[M - Boc]^+$, 213 $[Fc\text{-}CO]^+$, 185 $[Fc]^+$. ^1H NMR ($CDCl_3$, 360.14 MHz): 7.37 (d, 2H, J=8.0Hz, H_{Ar}), 7.06 (d, 2H, J=8.0Hz, H_{Ar}), 6.57 (d, 1H, J=7.7Hz, NH_{Phe}), 5.73 (s, 1H, NH_{Fc}), ca. 5.00 (NH_{Boc}, not obs.), 4.83 (m, 1H, C$_\alpha H_{Phe}$), 4.65 (m, 2H, Cp$H_{1,2}$), 4.32 (m, 2H, Cp$H_{3,4}$), 4.23 (s, 5H, CpH), 4.18 (m, 1H, C$_\alpha H_{Ala}$), 3.71 (s, 3H, CH_3), 3.11 (m, 2H, C$_\beta H_{,Phe}$), 2.40 (qd, 2H, J=7.3Hz, J=14.5Hz, C$H_{2,\ DEPA}$), 1.92 (qd, 2H, J=7.2Hz, J=14.3Hz, C$H_{2,\ DEPA}$), 1.43 (s, 9H, C$H_{3,\ Boc}$), 1.43 (m, 2H, C$_\beta H_{,Leu}$), 1.10 (t, 6H, J=7.3Hz, C$H_{3,\ DEPA}$), 0.91 (t, 6H, J=6.0Hz, C$H_{3,\ Leu}$). ^{13}C NMR ($CDCl_3$, 90.56 MHz): 172.1, 171.4 (COO, CON), 169.0 (CO$_{Fc}$), 155.5 (CO$_{Boc}$), 136.2 ($C_{Ar,\ q}$), 131.9, 129.3 (C_{Ar}), 121.6 ($C_{Ar,\ alkyne}$), 91.2, 83.4 (C_{alkyne}), 80.1 ($C_{Boc,\ q}$), 76.9 ($C_{Cp,\ 1}$), 70.2 ($C_{Cp,\ 2,5}$), 69.7 ($C_{Cp'}$), 68.1 ($C_{Cp,\ 3,4}$), 58.6 ($C_{DEPA,\ q}$), 53.2 ($C_{\alpha,\ Leu}$), 53.1 ($C_{\alpha,\ Phe}$), 52.3 (CH$_3$), 41.1 ($C_{\beta,\ Leu}$), 37.7 ($C_{\beta,\ Phe}$), 31.0 (CH$_{2,\ DEPA}$), 28.2 (CH$_{3,\ Boc}$), 24.7 (CH$_{3,\ Leu}$), 22.8 (CH(CH$_3$)$_2$), 9.1 (CH$_{3,\ DEPA}$). UV-Vis (λ in nm, [ε in $M^{-1}cm^{-1}$]): 246, [28332]; 255, [24239]; 444, [249]

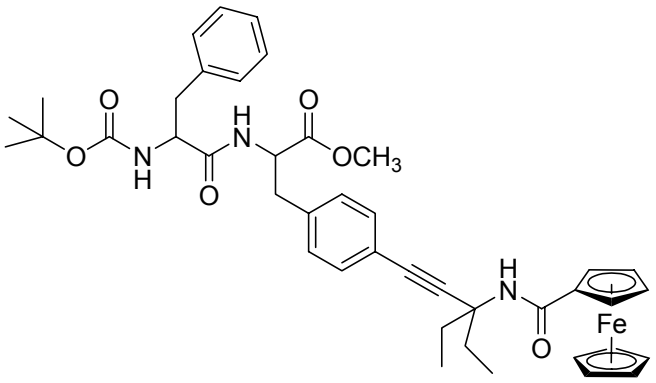

23c

The synthesis was carried out in analogy to **23a**. 552 mg (1 mmol) of Boc-Phe-Phe(I)-OMe was used. The product was purified by column chromatography on silica using ethyl acetate / hexane (1:1, R_f = 0.38).

Yield: 539.0 mg (72 %)

23c: Anal. calc. for $C_{42}H_{49}FeN_3O_6$ (747.30 g/mol): C, 67.47; H, 6.61; N, 5.62. Found: C, 66.92; H, 6.42; N, 5.44. IR (cm^{-1}) in KBr: 3316 (s) υ_{NH}, 2973 (m) υ_{CH}, 1744 (s) υ_{COO}, 1663 (vs) υ_{CON}, 1507 (s) δ_{NH}, 821 (m) δ_{CH}. MS (FAB): m/z 747 $[M]^+$, 648 $[M - Boc]^+$, 582 $[M - Boc - Cp]^+$, 213 $[Fc\text{-}CO]^+$, 185 $[Fc]^+$. ^1H NMR ($CDCl_3$, 360.14 MHz): 7.33 (d, 2H, J=8.1Hz, $H_{Ar,\ Phe}$), 7.23 (m, 5H, H_{Ar}), 6.94 (d, 2H, J=7.9Hz, H_{Ar}), 6.35 (d, 1H, J=7.4Hz, NH_{Phe}), 5.73 (s, 1H, NH_{Fc}), 4.97 (m, 1H, NH_{Boc}), 4.77 (m, 1H, $C_\alpha H_{Phe2}$), 4.65 (m, 2H, $CpH_{1,2}$), 4.33 (m, 2H, $CpH_{3,4}$), 4.24 (s, 5H, CpH), 4.18 (m, 1H, $C_\alpha H_{Phe1}$), 3.66 (s, 3H, CH_3), 3.04 (m, 4H, $C_\beta H$), 2.41 (qd, 2H, J=7.2Hz, J=14.4Hz, $CH_{2,\ DEPA}$), 1.93 (qd, 2H, J=7.3Hz, J=14.6Hz, $CH_{2,\ DEPA}$), 1.40 (s, 9H, $CH_{3,\ Boc}$), 1.11 (t, 6H, J=7.4Hz, $CH_{3,\ DEPA}$). ^{13}C NMR ($CDCl_3$, 90.56 MHz): 171.0, 170.7 (*C*OO, *C*ON), 169.0 (CO_{Fc}), 155.2 (CO_{Boc}), 136.4, 136.0 ($C_{Ar,\ q}$), 131.9, 129.3, 129.1, 128.6, 126.9 (C_{Ar}), 121.6 ($C_{Ar,\ alkyne}$), 91.2, 83.3 (C_{alkyne}), 80.2 ($C_{Boc,\ q}$), 76.9 ($C_{Cp,\ 1}$), 70.3 ($C_{Cp,\ 2,5}$), 69.6 ($C_{Cp'}$), 68.0 ($C_{Cp,\ 3,4}$), 58.5 ($C_{DEPA,\ q}$), 55.7 ($C_{\alpha,\ Phe1}$), 53.1 ($C_{\alpha,\ Phe}$), 52.3 (CH_3), 38.1 ($C_{\beta,\ Phe1}$), 37.7 ($C_{\beta,\ Phe2}$), 31.0 ($CH_{2,\ DEPA}$), 28.2 ($CH_{3,\ Boc}$), 9.1 ($CH_{3,\ DEPA}$). UV-Vis (λ in nm, [ε in $M^{-1}cm^{-1}$]): 246, [27984]; 256, [24511]; 442, [276]

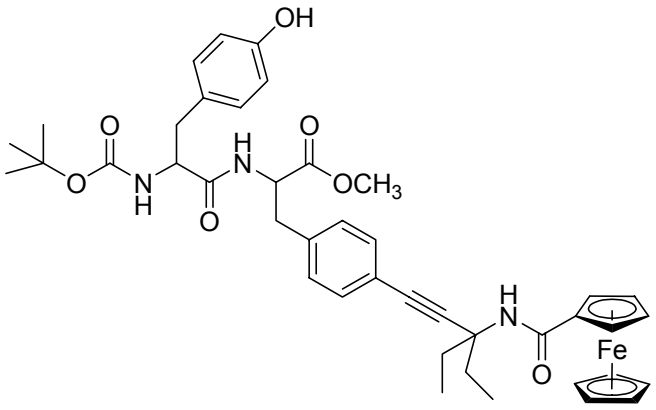

23d

The synthesis was carried out in analogy to **23a**. 568 mg (1 mmol) of Boc-Tyr-Phe(I)-OMe was used. The product was purified by column chromatography on silica using ethyl acetate / hexane (1:1, $R_f = 0.33$).

Yield: 581.0 mg (76 %)

23d: Anal. calc. for $C_{42}H_{49}FeN_3O_7$ (763.29 g/mol): C, 66.05; H, 6.47; N, 5.50. Found: C, 65.52; H, 6.79; N, 5.02. IR (cm^{-1}) in KBr: 3337 (s) υ_{NH}, 2972 (m) υ_{CH}, 1740 (s) υ_{COO}, 1663 (vs) υ_{CON}, 1516 (s) δ_{NH}, 821 (m) δ_{CH}. MS (FAB): m/z 764 $[M+1]^+$, 664 [M - Boc]$^+$, 598 [M - Boc - Cp]$^+$, 213 [Fc-CO]$^+$, 185 [Fc]$^+$. ^{1}H NMR ($CDCl_3$, 360.14 MHz): 8.63 (s, 1H, OH_{Tyr}), 7.32 (d, 2H, J=7.9Hz, $H_{Ar,\ Phe}$), 6.92 (d, 2H, J=7.9Hz, $H_{Ar,\ Phe}$), 6.81 (m, br, 4H, $H_{Ar,\ Tyr}$), 6.26 (d, 1H, J=8.1Hz, NH_{Phe}), 5.82 (s, 1H, NH_{Fc}), 4.97 (s, br, 1H, NH_{Boc}), 4.84 (dd, 1H, J=7,5Hz, J=13.0Hz, C$_\alpha H_{Phe}$), 4.70 (m, 2H, Cp$H_{1,2}$), 4.35 (m, 2H, Cp$H_{3,4}$), 4.31 (m, 1H, C$_\alpha H_{Tyr}$), 4.24 (s, 5H, CpH), 3.70 (s, 3H, CH_3), 3.13 (m, 2H, C$_\beta H_{Phe}$), 2.80 (m, 2H, C$_\beta H_{Tyr}$), 2.14 (m, 2H, C$H_{2,\ DEPA}$), 2.04 (m, 2H, C$H_{2,\ DEPA}$), 1.45 (s, 9H, C$H_{3,\ Boc}$), 1.11 (t, 6H, J=7.4Hz, C$H_{3,\ DEPA}$). ^{13}C NMR ($CDCl_3$, 90.56 MHz): 171.3, 171.2 (*C*OO, *C*ON), 170.2 (*C*O$_{Fc}$), 156.3 (C_{Ar}OH$_{Tyr}$), 155.2 (*C*O$_{Boc}$), 135.6, 126.4 ($C_{Ar,\ q}$), 131.8, 139.2, 128.9, 115.7 (C_{Ar}), 121.6 ($C_{Ar,\ alkyne}$), 90.7, 83.5 (C_{alkyne}), 80.2 ($C_{Boc,\ q}$), 76.7 ($C_{Cp,\ 1}$), 70.7 ($C_{Cp,\ 2,5}$), 69.7 ($C_{Cp'}$), 68.1 ($C_{Cp,\ 3,4}$), 56.8 ($C_{DEPA,\ q}$), 55.3 ($C_{\alpha,\ Tyr}$), 52.7 ($C_{\alpha,\ Phe}$), 52.3 (*C*H$_3$), 37.6 ($C_{\beta,\ Phe}$), 36.7 ($C_{\beta,\ Tyr}$), 31.0 (*C*H$_{2,\ DEPA}$), 28.2 (*C*H$_{3,\ Boc}$), 8.7 (*C*H$_{3,\ DEPA}$). UV-Vis (λ in nm, [ε in $M^{-1}cm^{-1}$]): 246, [26010]; 256, [22840]; 442, [231]

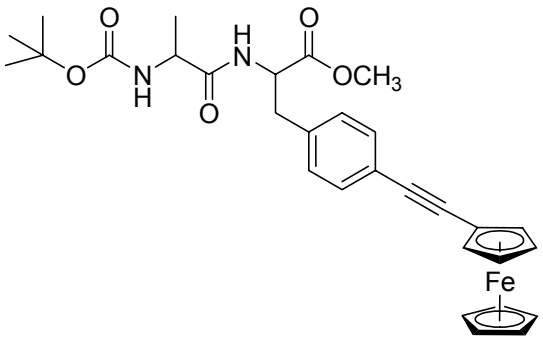

24a

12 ml of a mixture of dried THF and NEt_3 (1:1) was thoroughly degassed in a Schlenck-tube. To this solution was added 476 mg of Boc-Ala-Phe(I)-OMe (1 mmol) and 231 mg (1.1 mmol) of ethynylferrocene. Then was added a mixture of 14 mg of $Pd(PPh_3)_2Cl_2$ (0.02 mmol, 2 mol%) and CuI (6 mg, 0.03 mmol, 3 mol%) as a catalyst. The mixture was stirred under argon until no more triethylamine hydroiodide precipitated (6h). After removal of the salts by filtration the solvents were removed under reduced pressure and the product was purified by column chromatography on silica using ethyl acetate / hexane (4:5, $R_f = 0.41$). Yield: 385.5 mg (69 %)

24a: Anal. calc. for $C_{30}H_{34}FeN_2O_5$ (558.18 g/mol): C, 64.52; H, 6.14; N, 5.02. Found: C, 62.53; H, 6.24; N, 4.52. IR (cm^{-1}) in KBr: 3315 (s) υ_{NH}, 2976 (m) υ_{CH}, 1710 (s) υ_{COO}, 1662 (vs) υ_{CON}, 1515 (s) δ_{NH}, 820 (m) δ_{CH}. MS (EI): m/z 558 (100, $[M + 1]^+$), 502 (21, $[M - C_4H_9]^+$) , 484 (20, $[M - OC_4H_9]^+$), 458 (18, $[M - Boc]^+$) , 299 (80, [Fc-alkinyl-Ph-$CH_2]^+$). ^1H NMR ($CDCl_3$, 360.14 MHz): 7.32 (d, 2H, J=8.0Hz, H_{Ar}), 6.99 (d, 2H, J=8.0Hz, H_{Ar}), 6.55 (d, 1H, J=7.4Hz, NH_{Phe}), 4.90 (m, 1H, NH_{Boc}), 4.77 (dd, 1H, J=5.9Hz, J=13.3Hz, C$_\alpha H_{Phe}$), 4.41 (m, 2H, Cp$H_{1,2}$), 4.16 (s, 2H, Cp$H_{3,4}$), 4.16 (s, 5H, CpH), 4.09 (m, 1H, C$_\alpha H_{Ala}$), 3.64 (s, 3H, CH_3), 3.05 (m, 2H, C$_\beta H$), 1.38 (s, 9H, C$H_{3,\ Boc}$), 1.25 (d, 3H, J=7.0Hz, C$H_{3,\ Ala}$). ^{13}C NMR ($CDCl_3$, 90.56 MHz): 172.3, 171.5 (COO, CON), 155.3 (CO$_{Boc}$), 135.4 ($C_{Ar,\ q}$), 131.5, 129.2 (C_{Ar}), 122.7 ($C_{Ar,\ alkyne}$), 88.5, 85.3 (C_{alkyne}), 80.21 ($C_{Boc,\ q}$), 71.3 ($C_{Cp,\ 2,5}$), 69.9 ($C_{Cp'}$), 68.7 ($C_{Cp,\ 3,4}$), 65.1 ($C_{Cp,\ 1}$), 53.0 ($C_{\alpha,\ Phe}$), 52.3 (CH$_3$), 50.1 ($C_{\alpha,\ Ala}$), 37.7 (C_β), 28.2 (CH$_{3,\ Boc}$), 18.1 (CH$_{3,\ Ala}$). UV-Vis (λ in nm, [ε in $M^{-1}cm^{-1}$]): 256, [18335]; 300, [16305]; 445, [563]

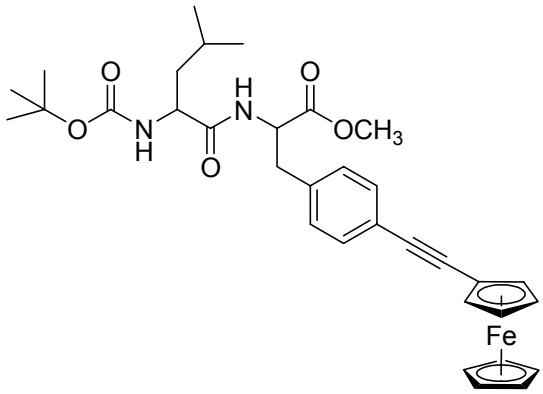

24b

The synthesis was carried out in analogy to **24a**. 518 mg (1 mmol) of Boc-Leu-Phe(I)-OMe was used. The product was purified by column chromatography on silica using ethyl acetate / hexane (2:5, $R_f = 0.29$).

Yield: 430.0 mg (72 %)

24b: Anal. calc. for $C_{33}H_{40}FeN_2O_5$ (600.23 g/mol): C, 66.00; H, 6.71; N, 4.66. Found: C, 65.06; H, 6.63; N, 4.40. IR (cm^{-1}) in KBr: 3303 (s) υ_{NH}, 2956 (m) υ_{CH}, 1709 (s) υ_{COO}, 1659 (vs) υ_{CON}, 1515 (s) δ_{NH}, 820 (m) δ_{CH}. MS (FAB): m/z 600 $[M]^+$, 545 $[M - C_4H_9]^+$, 501 $[M - Boc]^+$), 299 $[Fc\text{-alkinyl-Ph-}CH_2]^+$. ^{1}H NMR ($CDCl_3$, 360.14 MHz): 7.32 (d, 2H, J=8.1Hz, H_{Ar}), 7.00 (d, 2H, J=8.0Hz, H_{Ar}), 6.59 (d, 1H, J=7.5Hz, NH_{Phe}), 4.86 (d, 1H, J=7.8Hz, NH_{Boc}), 4.77 (m, 1H, C$_\alpha H_{Phe}$), 4.41 (m, 2H, Cp$H_{1,2}$), 4.16 (s, 2H, Cp$H_{3,4}$), 4.16 (s, 5H, CpH), 4.16 (m, 1H, C$_\alpha H_{Ala}$), 3.63 (s, 3H, CH_3), 3.04 (m, 2H, C$_\beta H$), 1.56 (m, 1H, CH(CH_3)), 1.38 (s, 9H, C$H_{3,\,Boc}$), 0.85 (pseudo-t, 6H, J=6.2Hz, C$H_{3,\,Leu}$). ^{13}C NMR ($CDCl_3$, 90.56 MHz): 172.2, 171.5 (*C*OO, *C*ON), 155.5 (*C*O$_{Boc}$), 135.4 ($C_{Ar,\,q}$), 131.4, 129.2 (C_{Ar}), 122.7 ($C_{Ar,\,alkyne}$), 88.4, 85.4 (C_{alkyne}), 79.9 ($C_{Boc,\,q}$), 71.3 ($C_{Cp,\,2,5}$), 69.9 ($C_{Cp'}$), 68.7 ($C_{Cp,\,3,4}$), 65.2 ($C_{Cp,\,1}$), 53.0 ($C_{\alpha,\,Phe}$), 52.9 ($C_{\alpha,\,Leu}$), 52.2 (*C*H$_3$), 41.1 ($C_{\beta,\,Leu}$), 37.7 ($C_{\beta,\,Phe}$), 28.2 (*C*H$_{3,\,Boc}$), 24.6 (*C*H$_{3,\,Leu}$), 22.8 (*C*H(CH$_3$)$_2$). UV-Vis (λ in nm, [ε in $M^{-1}cm^{-1}$]): 256, [17927]; 301, [16026]; 445, [582]

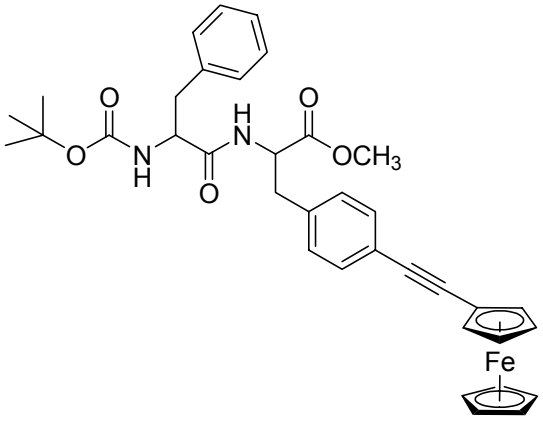

24c

The synthesis was carried out in analogy to **24a**. 552 mg (1 mmol) of Boc-Phe-Phe(I)-OMe was used. The product was purified by column chromatography on silica using ethyl acetate / hexane (1:2, $R_f = 0.33$).

Yield: 489.0 mg (77 %)

24c: Anal. calc. for $C_{36}H_{38}FeN_2O_5$ (634.21 g/mol): C, 68.14; H, 6.04; N, 4.41. Found: C, 67.70; H, 6.12; N, 4.29. IR (cm^{-1}) in KBr: 3308 (s) υ_{NH}, 2976 (m) υ_{CH}, 1696 (s) υ_{COO}, 1662 (vs) υ_{CON}, 1516 (s) δ_{NH}, 820 (m) δ_{CH}. MS (FAB): m/z 634 $[M]^+$, 579 $[M - C_4H_9]^+$, 535 $[M - Boc]^+$), 299 $[Fc\text{-alkinyl-Ph-}CH_2]^+$. ^1H NMR ($CDCl_3$, 360.14 MHz): 7.35 (d, 2H, J=8.1Hz, H_{Ar}), 7.25 (m, 5H, $H_{Ar,\ Ph}$), 6.93 (d, 2H, J=8.1Hz, H_{Ar}), 6.35 (d, 1H, J=7.3Hz, NH_{Phe}), 4.97 (m, 1H, NH_{Boc}), 4.79 (m, 1H, $C_\alpha H_{Phe2}$), 4.48 (m, 2H, $CpH_{1,2}$), 4.36 (m, 1H, $C_\alpha H_{Phe1}$), 4.23 (s, 2H, $CpH_{3,4}$), 4.23 (s, 5H, CpH), 3.67 (s, 3H, CH_3), 3.05 (m, 4H, $C_\beta H$), 1.41 (s, 9H, $CH_{3,\ Boc}$). ^{13}C NMR ($CDCl_3$, 90.56 MHz): 171.1, 170.8 (*C*OO, *C*ON), 155.2 (CO_{Boc}), 136.4, 135.2 ($C_{Ar,\ q}$), 131.4, 129.3, 129.1, 128.7, 126.9 (C_{Ar}), 122.7 ($C_{Ar,\ alkyne}$), 88.5, 85.4 (C_{alkyne}), 80.2 ($C_{Boc,\ q}$), 71.3 ($C_{Cp,\ 2,5}$), 69.9 ($C_{Cp'}$), 68.7 ($C_{Cp,\ 3,4}$), 65.2 ($C_{Cp,\ 1}$), 55.0 ($C_{\alpha,\ Phe1}$), 53.1 ($C_{\alpha,\ Phe2}$), 52.2 (CH_3), 38.1 ($C_{\beta,\ Phe1}$), 37.8 ($C_{\beta,\ Phe}$), 28.2 ($CH_{3,\ Boc}$). UV-Vis (λ in nm, [ε in $M^{-1}cm^{-1}$]): 256, [18338]; 301, [16234]; 446, [586]

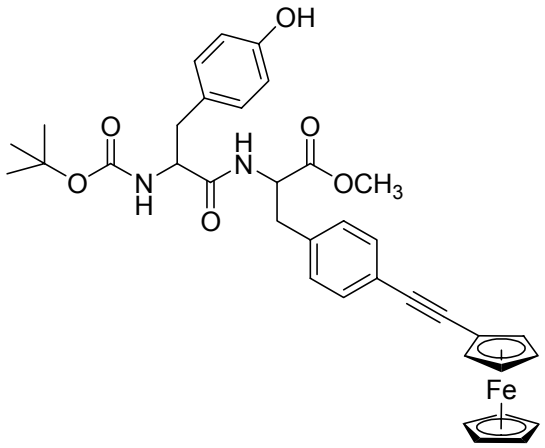

24d

The synthesis was carried out in analogy to **24a**. 568 mg (1 mmol) of Boc-Tyr-Phe(I)-OMe was used. The product was purified by column chromatography on silica using ethyl acetate / hexane (1:1, $R_f = 0.29$).

Yield: 525.0 mg (81 %)

24d: Anal. calc. for $C_{36}H_{38}FeN_2O_6$ (650.21 g/mol): C, 66.47; H, 5.89; N, 4.31. Found: C, 64.93; H, 5.92; N, 4.04. IR (cm^{-1}) in KBr: 3334 (s) υ_{NH}, 2977 (m) υ_{CH}, 1739 (s) υ_{COO}, 1662 (vs) υ_{CON}, 1516 (s) δ_{NH}, 822 (m) δ_{CH}. MS (FAB): m/z 650 $[M]^+$, 595 $[M - C_4H_9 + H]^+$, 551 $[M - Boc]^+$), 299 $[Fc\text{-alkinyl-Ph-}CH_2]^+$. ^1H NMR (DMSO-d_6, 360.14 MHz): 9.16 (s, 1H, OH_{Tyr}), 8.24 (d, 1H, J=7.7Hz, NH_{Phe}), 7.35 (d, 2H, J=7.9Hz, $H_{Ar,\ Phe}$), 7.20 (d, 2H, J=7.9Hz, $H_{Ar,\ Phe}$), 6.97 (d, 2H, J=8.1Hz, $H_{Ar,\ Tyr}$), 6.71 (d, 1H, J=8.6Hz, NH_{Boc}), 6.62 (d, 2H, J=8.1Hz, $H_{Ar,\ Tyr}$), 4.52 (m, 2H, Cp$H_{1,2}$), 4.49 (m, 1H, $C_\alpha H_{Tyr}$), 4.29 (m, 2H, Cp$H_{3,4}$), 4.23 (s, 5H, CpH), 4.07 (m, 1H, $C_\alpha H_{Phe}$), 3.58 (s, 3H, CH_3), 2.97 (m, 2H, $C_\beta H_{,Phe}$), 2.65 (m, 2H, $C_\beta H_{,Tyr}$), 1.29 (s, 9H, C$H_{3,\ Boc}$). ^{13}C NMR (DMSO-d_6, 90.56 MHz): 171.9, 171.6 (*C*OO, *C*ON), 155.7 ($C_{Ar}OH_{Tyr}$), 155.0 (CO_{Boc}), 137.1, 127.9 ($C_{Ar,\ q}$), 130.9, 130.0, 129.5, 114.7 (C_{Ar}), 121.2 ($C_{Ar,\ alkyne}$), 88.3, 85.3 (C_{alkyne}), 78.0 ($C_{Boc,\ q}$), 71.0 ($C_{Cp,\ 2,5}$), 69.7 ($C_{Cp'}$), 68.9 ($C_{Cp,\ 3,4}$), 64.4 ($C_{Cp,\ 1}$), 55.8 ($C_{\alpha,\ Tyr}$), 53.0 ($C_{\alpha,\ Phe}$), 51.8 (CH_3), 36.6 ($C_{\beta,\ Phe}$), 36.5 ($C_{\beta,\ Tyr}$), 28.1 ($CH_{3,\ Boc}$). UV-Vis (λ in nm, [ε in $M^{-1}cm^{-1}$]): 256, [18338]; 301, [16234]; 446, [586]

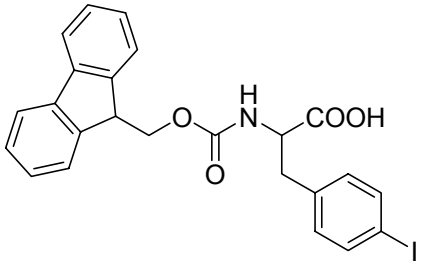

25

11.63 g (40 mmol) of p-iodo-phenylalanine was dissolved in a mixture of 100 ml of H_2O and 150 ml of 1,4-dioxane, followed by the addition of 2 equivalents of sodium carbonate (8.48 g, 80 mmol) as a base. The mixture was cooled to 5 °C and a solution of 13.5 g (40 mmol) of Fmoc-ONSu in 50 ml dioxane was added under continuous stirring. After 1 h the reaction mixture was filtered and the solvents were removed by rotary evaporation. The viscous residue was re-dissolved in 250 ml of water and precipitated by the addition of 6 N HCl. Recrystallization from chloroform yielded 17.8 g (86.7%) of Fmoc-*p*-iodo-phenylalanine in high purity.

25: Anal. calc. for $C_{24}H_{20}INO_4$ (513.04 g/mol): C, 56.15; H, 3.93; N, 2.73. Found: C, 55.17; H, 4.09; N, 2.62. IR (cm^{-1}) in KBr: 3314 (s) υ_{NH}, 3063, 2947 (m) υ_{CH}, 1693 (vs) υ_{COO}, 1539 (s) δ_{NH}, 1255 (s) $\upsilon_{C\text{-}O}$. MS (FAB): m/z 514 $[M + H]^+$, 388 $[M - I + H]^+$, 203 $[M - C_6H_5I]^+$, 165 $[Fluorenyl]^+$. ^1H NMR (DMSO-d_6, 360.14 MHz): 7.88 (d, 2H, J=7.5Hz, $H_{Ar,\ Fl}$), 7.73 (d, 1H, J=8.5Hz, N*H*), 7.63 (m, 4H, $H_{Ar,\ Fl,\ Phe}$), 7.41 (pseudo-t, 2H, $H_{Ar,\ Fl}$), 7.30 (dd, 2H, J=7.9Hz, J=16.8Hz, $H_{Ar,\ Fl}$), 7.09 (d, 2H, J=8.1Hz, $H_{Ar,\ Phe}$), 4.17 (m, 4H, $C_\alpha H_{Phe}$, R_3CH_{Fl}, $CH_{2,\ Fl}$), 3.04, 2.82 (m, 2H, $C_\beta H_{Phe}$). ^{13}C NMR (DMSO-d_6, 90.56 MHz): 173.0 (*C*OO) 155.8 (*C*ON), 143.7, 140.6, 137.7 ($C_{Ar,\ q}$), 136.8, 131.5, 127.5, 126.9, 125.1, 120.0 (C_{Ar}), 92.2 ($C_{Ar\text{-}I}$), 65.5 ($CH_{2,\ Fl}$), 55.1 ($C_{\alpha,\ Phe}$), 46.5 (R_3CH_{Fl}), 35.8 (C_β)

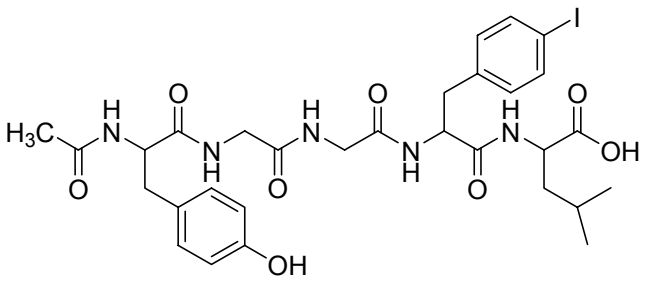

26

Resin	Loading (mmol/g)	AA excess	Cleavage mixture	Cleavage time	mg resin	yield
Wang	0.63	5	95% TFA 2.5% H_2O 2.5% TIS	3 h	800	288 mg (79.0 %)

26: $C_{30}H_{38}IN_5O_8$ (723.18 g/mol): MS (FAB): m/z 746 $[M + Na]^+$, 724 $[M + H]^+$, 593 [M – H-Leu-OH]$^+$, 320 [M – H-Phe(I)-Leu-OH]$^+$, 263 [M – H-Gly-Phe(I)-Leu-OH]$^+$. ^{1}H NMR (DMSO-d6, 360.14 MHz): 12.58 (s, br, 1H, COO*H*), 9.15 (s, br, 1H, OH_{Tyr}), 8.27 (d, 1H, J=8.1Hz, NH_{Leu}), 8.22 (t, 1H, J=5.4Hz, NH_{Gly}), 8.06 (d, 1H, J=8.0Hz, NH_{Tyr}), 7.99 (d, 1H, J=8.5Hz, N$H_{I\text{-}Phe}$, 7.93 (t, 1H, J=5.5Hz, NH_{Gly}), 7.60 (d, 2H, J=8.1Hz, $H_{Ar,\ I\text{-}Phe}$), 7.07 (d, 2H, J=8.2Hz, $H_{Ar,\ I\text{-}Phe}$), 7.02 (d, 2H, J=8.3Hz, $H_{Ar,\ Tyr}$), 6.63 (d, 2H, J=8.3Hz, $H_{Ar,\ Tyr}$), 4.54 (dt, 1H, J=3.7Hz, J=9.0Hz, C$_\alpha H_{I\text{-}Phe}$), 4.39 (dt, 1H, J=4.8Hz, J=9.1Hz, C$_\alpha H_{Tyr}$), 4.21 (pseudo-dd, 1H,), 3.66 (m, 4H, C$_\alpha H_{Gly}$), 2.81 (m, 4H, C$_\beta H_{Phe,\ Tyr}$), 1.61 (m, 1H, C*H*(CH$_3$)$_2$), 1.54 (m, 2H, C$_\beta H_{Leu}$), 0.87 (dd, 6H, J=6.2Hz, J=17.0Hz, CH(C*H*$_3$)$_2$). ^{13}C NMR (DMSO-d6, 90.56 MHz): 173.7 (*C*OO), 171.8, 170.7, 169.3 (*C*ON), 168.9 (*C*ON$_{Ac}$), 168.3 (*C*ON), 155.6 (C_{Ar}OH$_{Tyr}$), 137.5 ($C_{Ar,\ q,\ I\text{-}Phe}$), 136.7 ($C_{Ar,\ I\text{-}Phe}$), 131.7 ($C_{Ar,\ q,\ Tyr}$), 129.8, 128.0, 114.8 ($C_{Ar}$), 92.1 ($C_{Ar,\ q,\ I\text{-}Phe}$), 54.4 ($C_{\alpha,\ I\text{-}Phe}$), 53.2 ($C_{\alpha,\ Tyr}$), 50.2 ($C_{\alpha,\ Leu}$), 42.0, 41.7 ($C_{\alpha,\ Gly}$), 37.0 ($C_{\beta,\ Phe}$), 36.5 ($C_{\beta,\ Tyr}$), 24.2 ($C_{\beta,\ Leu}$), 22.7 (*C*H$_{3,\ Leu}$), 22.4 (*C*H$_{3,\ Ac}$), 21.2 (*C*H(CH$_3$)$_2$).

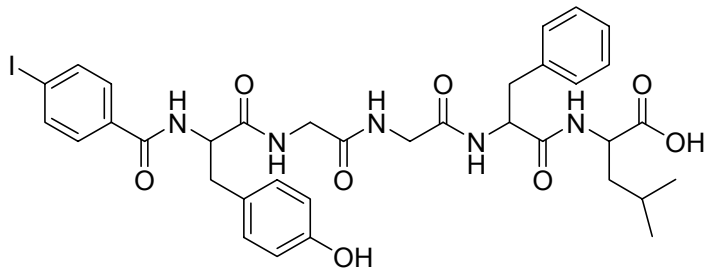

27

Resin	Loading (mmol/g)	AA excess	Cleavage mixture	Cleavage time	mg resin	yield
Wang	0.63	5	95% TFA 2.5% H_2O 2.5% TIS	3 h	800	367 mg (92.7 %)

27: $C_{35}H_{40}IN_5O_8$ (785.19 g/mol): MS (FAB): m/z 808 $[M + Na]^+$, 786 $[M + H]^+$, 655 $[M – H\text{-Leu-OH}]^+$, 508 $[M – H\text{-Phe-Leu-OH}]^+$, 451 $[M – H\text{-Gly-Phe-Leu-OH}]^+$. ^{1}H NMR (DMSO-d6, 360.14 MHz): 12.54 (s, br, 1H, COO*H*), 9.12 (s, br, 1H, OH_{Tyr}), 8.61 (d, 1H, J=8.2Hz, NH_{Tyr}), 8.31 (t, 1H, J=5.5Hz, NH_{Gly}), 8.26 (d, 1H, J=7.9Hz, NH_{Leu}), 8.04 (d, 1H, J=8.4Hz, NH_{Phe}), 7.96 (t, 1H, J=5.5Hz, NH_{Gly}), 7.82 (d, 2H, J=8.4Hz, $H_{Ar, I\text{-}Ph}$), 7.57 (d, 2H, J=8.4Hz, $H_{Ar, I\text{-}Ph}$), 7.25 (m, 5H, $H_{Ar, Phe}$), 7.09 (d, 2H, J=8.3Hz, $H_{Ar, Tyr}$), 6.61 (d, 2H, J=8.4Hz, $H_{Ar, Tyr}$), 4.59 (m, 2H, C$_\alpha H_{Phe, Tyr}$), 4.22 (dd, 1H, J=8.4HZ, J=14.0Hz, C$_\alpha H_{Leu}$), 3.63 (m, 4H, C$_\alpha H_{Gly}$), 2.85 (m, 4H, C$_\beta H_{Phe, Tyr}$), 1.64 (m, 1H, C*H*(CH$_3$)$_2$), 1.54 (m, 2H, C$_\beta H_{Leu}$), 0.87 (dd, 6H, J=6.3Hz, J=16.8Hz, CH(C*H*$_3$)$_2$). ^{13}C NMR (DMSO-d6, 90.56 MHz): 173.7 (*C*OO), 171.6, 170.9, 168.8, 168.1 (*C*ON), 165.6 (*C*ON$_{I\text{-}Ph}$), 155.6 (C_{Ar}OH$_{Tyr}$), 137.6 ($C_{Ar, q, Phe}$), 136.9 ($C_{Ar, I\text{-}Ph}$), 133.4 ($C_{Ar, q, I\text{-}Ph}$), 129.9, 129.3, 129.1 (C_{Ar}), 128.3 ($C_{Ar, q, Tyr}$), 127.9, 126.1, 114.8 (C_{Ar}), 98.7 ($C_{Ar, q, I\text{-}Ph}$), 55.2 ($C_{\alpha, Phe}$), 52.7 ($C_{\alpha, Phe}$), 53.4 ($C_{\alpha, Tyr}$), 50.2 ($C_{\alpha, Leu}$), 42.0, 41.6 ($C_{\alpha, Gly}$), 37.5 ($C_{\beta, Phe}$), 36.1 ($C_{\beta, Tyr}$), 24.2 ($C_{\beta, Leu}$), 22.7 (CH$_{3, Leu}$), 21.2 (*C*H(CH$_3$)$_2$).

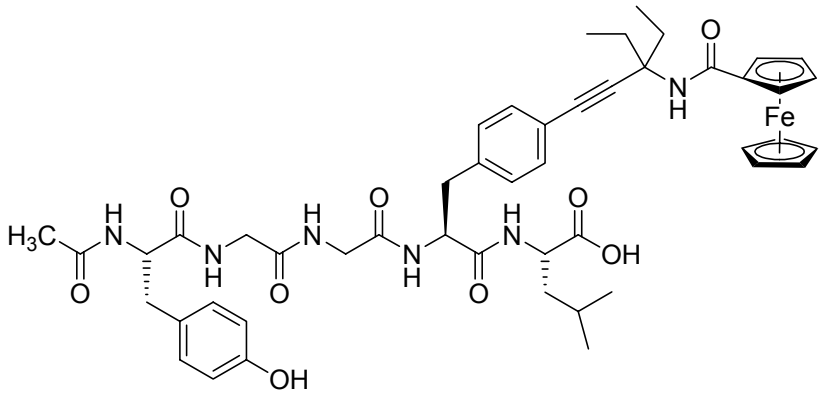

28

100 mg (0.134 mmol) of Ac-Enk[Phe^4(I)]-OH **26** were dissolved in 8 ml of a well degassed mixture of DMF/NEt_3 (1:1) in a Schlenck-tube. After complete dissolution 1.1 equivalents (47.6 mg, 0.147 mmol) of DEPA-Fc **22** were added, followed by another 15 min. of degassing. 14 mg of CuI and 28 mg of $Pd(PPh_3)_2Cl_2$ are added and the mixture is stirred for 12 hours. The solution was filtered through a syringe filter (22 µm pore size), the solvent was evaporated *in vacuo* and the residual oil was re-dissolved in acetonitrile. The compound was purified by preparative HPLC.

Yield: 58.6 mg (47.6%)

28: $C_{48}H_{58}IN_6O_9$ (918.36 g/mol): MS (ESI, -Q1MS): m/z 917.4 $[M - H]^-$, (+Q1MS): m/z 919.4 $[M + H]^+$, 941.4 $[M + Na]^+$, 957.5 $[M + K]^+$. ^{1}H NMR (DMSO-d6, 399.90 MHz): 12.59 (s, br, 1H, COO*H*), 9.17 (s, 1H, OH_{Tyr}), 8.30 (d, 1H, J=7.9Hz, NH_{Leu}), 8.25 (t, 1H, J=5.6Hz, NH_{Gly}), 8.07 (d, 1H, J=8.1Hz, NH_{Tyr}), 8.02 (d, 1H, J=8.7Hz, NH_{Phe}, 7.94 (t, 1H, J=5.5Hz, NH_{Gly}), 7.58 (m, 2H, $H_{Ar,\ Phe}$), 7.25 (d, 2H, 5.8Hz, $H_{Ar,\ Phe}$), 7.01 (d, 2H, J=8.4Hz, $H_{Ar,\ Tyr}$), 6.63 (d, 2H, J=8.4Hz, $H_{Ar,\ Tyr}$), 4.92 (pseudo-t, 2H, Cp$H_{1,4}$), 4.56 (dt, 1H, J=3.8Hz, J=9.5Hz, C$_\alpha H_{Phe}$), 4.38 (dt, 1H, J=4.6Hz, J=9.4Hz, C$_\alpha H_{Tyr}$), 4.33 (pseudo-t, 2H, Cp$H_{2,3}$), 4.19 (s, 5H, Cp*H*), 4.16 (m, 1H, C$_\alpha H_{Leu}$), 3.63 (m, 4H, C$_\alpha H_{Gly}$), 2.82 (m, 4H, C$_\beta H_{Phe,\ Tyr}$), 2.10 (m, 2H, C$H_{2,\ DEPA}$), 1.90 (m, 2H, C$H_{2,\ DEPA}$), 1.76 (s, 3H, C$H_{3,\ Acetyl}$), 1.62 (m, 1H, C$H(CH_3)_2$), 1.54 (m, 2H, C$_\beta H_{Leu}$), 1.01 (t, 6H, J=7.3Hz, C$H_{3,\ DEPA}$), 0.87 (dd, 6H, J=6.4Hz, J=2.80Hz, CH(CH_3)$_2$). ^{13}C NMR (DMSO-d6, 100.56 MHz): 173.6 (*C*OO), 171.7, 170.7 (*C*ON), 169.1 (*C*ON$_{Ac}$), 168.6, 168.0, 167.9 (*C*ON), 155.4 ($C_{Ar}OH_{Tyr}$), 137.7 ($C_{Ar,\ q,\ Phe}$), 130.6 ($C_{Ar,\ q,\ Tyr}$), 129.7, 129.1, 127.8, 120.6, 114.5 (C_{Ar}),

91.6, 82.0 (C_{alkyne}), 76.5 ($C_{Cp,1}$), 69.6 ($C_{Cp,\ 2,5}$), 68.9 ($C_{Cp'}$), 68.1 ($C_{Cp,\ 3,4}$), 55.6 ($C_{DEPA,\ q}$), 54.2 ($C_{\alpha,\ Phe}$), 53.0 ($C_{\alpha,\ Tyr}$), 50.0 ($C_{\alpha,\ Leu}$), 41.7, 41.3 ($C_{\alpha,\ Gly}$), 37.2 ($C_{\beta,\ Phe}$), 36.3 ($C_{\beta,\ Tyr}$), 29.9 ($CH_{2,\ DEPA}$), 24.0 ($C_{\beta,\ Leu}$), 22.5 ($CH_{3,\ Leu}$), 22.1 ($CH_{3,\ Ac}$), 21.0 ($CH(CH_3)_2$), 8.4 ($CH_{3,\ DEPA}$). UV-Vis (λ in nm, [ε in $M^{-1}cm^{-1}$]): 246, [25165]; 257, [22570]; 444, [272]

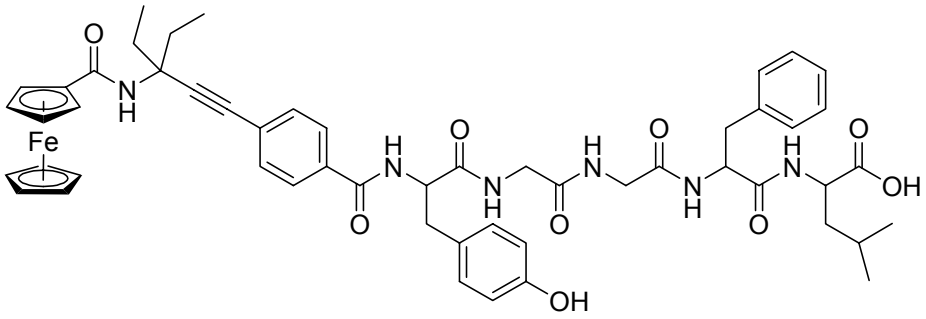

29

The synthesis was carried out in analogy to **28**. 100 mg (0.127 mmol) of I-Ph-Enk-OH **27** was used. The product was purified by preparative HPLC.

Yield: 28.0 mg (22.5 %)

29: $C_{53}H_{60}FeN_6O_9$ (980.38 g/mol): MS (ESI, -Q1MS): m/z 979.5 $[M - H]^-$. ^1H NMR (DMSO-d6, 399.90 MHz): 12.58 (s, br, 1H, COO*H*), 9.16 (s, br, 1H, OH_{Tyr}), 8.64 (d, 1H, J=8.1Hz, NH_{Tyr}), 8.35 (t, 1H, J=5.7Hz, NH_{Gly}), 8.29 (d, 1H, J=7.9Hz, NH_{Leu}), 8.08 (d, 1H, J=8.4Hz, NH_{Phe}), 7.99 (t, 1H, J=5.6Hz, NH_{Gly}), 7.81 (d, 2H, J=8.3Hz, $H_{Ar,\ Ph}$), 7.48 (d, 2H, J=8.3Hz, $H_{Ar,\ Ph}$), 7.27 (m, 5H, $H_{Ar,\ Phe}$), 7.11 (d, 2H, J=7.6Hz, $H_{Ar,\ Tyr}$), 6.63 (d, 2H, J=8.4Hz, $H_{Ar,\ Tyr}$), 5.73 (s, 1H, NH_{Fc}), 4.95 (m, 2H, Cp$H_{1,2}$), 4.62 (m, 2H, C$_\alpha H$-$_{Phe,\ Tyr}$), 4.37 (m, 2H, Cp$H_{3,4}$), 4.21 (s, 5H, Cp*H*), 4.19 (m, 1H, C$_\alpha H_{Leu}$), 3.69 (m, 4H, C$_\alpha H_{Gly}$), 2.91 (m, 4H, C$_\beta H_{Phe,\ Tyr}$), 2.13 (m, 2H, $CH_{2,\ Ethyl}$), 1.97 (m, 2H, $CH_{2,\ Ethyl}$), 1.66 (m, 1H, C*H*$(CH_3)_2$), 1.55 (m, 2H, C$_\beta H_{Leu}$), 1.05 (t, 6H, $CH_{3,\ Ethyl}$), 0.88 (dd, 6H, J=6.4Hz, J=22.6Hz, CH(C$H_3)_2$). UV-Vis (λ in nm, [ε in $M^{-1}cm^{-1}$]): 269, [27210]; 442, [329]

9 Literature

1. Tsuji, J., *Transition Metal Reagents and Catalysts: Innovations in Organic Synthesis*. **2000**; p 477 pp.

2. Shinokubo, H.; Oshima, K., *Eur. J. Org. Chem.* **2004**, 2081-2091.

3. Soderberg, B. C. G., *Coord. Chem. Rev.* **2004,** *248*, 1085-1158.

4. Merrifield, R. B., *J. Am. Chem. Soc.* **1963,** *85*, 2149-54.

5. Grant, G. A., *Synthetic Peptides: A User's Guide*. **2002**; p 390 pp.

6. Fields, G. B.; Lauer-Fields, J. L.; Liu, R.-q.; Barany, G., *Synth. Pept.* **2002**, 93-219.

7. Bodanszky, M., *Principles of Peptide Synthesis*. **1984**; p 307 pp.

8. Volbeda, A.; Charon, M. H.; Piras, C.; Hatchikian, E. C.; Frey, M.; Fontecilla-Camps, J. C., *Nature* **1995,** *373*, 580-7.

9. Schilling, O.; Wenzel, N.; Naylor, M.; Vogel, A.; Crowder, M.; Makaroff, C.; Meyer-Klaucke, W., *Biochemistry* **2003,** *42*, 11777-11786.

10. Williams, R. J. P., *Chem. Comm.* **2003**, 1109-1113.

11. Gitschier, J.; Moffat, B.; Reilly, D.; Wood, W. I.; Fairbrother, W. J., *Nat. Struct. Buiol.* **1998,** *5*, 47-54.

12. Finney Lydia, A.; O'Halloran Thomas, V., *Science* **2003,** *300*, 931-6.

13. Stryer, L.; Editor, *Biochemistry, 4th Revised Edition*. **1996**; p 1100 pp.

14. Alberts, B.; Bray, D.; Lewis, J.; Raff, M.; Roberts, K.; Watson, J. D., *Molecular Biology of the Cell. 3rd Ed*. **1995**; p 1512 pp.

15. MacKinnon, R., *Angew. Chem., Int. Ed.* **2004,** *43*, 4265-4277.

16. Bertini, I.; Gray, H. B.; Lippard, S. J.; Valentine, J. S., *Bioinorganic Chemistry*. **1994**; p 611 pp.

17. Crabtree, R. H., *Principles of bioinorganic chemistry. Stephen J. Lippard and Jeremy M. Berg*. **1994**; 'Vol.' 266, p 1591-2.

18. Abu-Soud, H. M.; Hazen, S. L., *Biochemistry* **2001,** *40*, 10747-10755.

19. Mazmanian, S. K.; Skaar, E. P.; Gaspar, A. H.; Humayun, M.; Gornicki, P.; Jelenska, J.; Joachmiak, A.; Missiakas, D. M.; Schneewind, O., *Science* **2003,** *299*, 906-909.

20. Schlichting, I.; Berendzen, J.; Chu, K.; Stock, A. M.; Maves, S. A.; Benson, D. E.; Sweet, R. M.; Ringe, D.; Petsko, G. A.; Sligar, S. G., *Science* **2000,** *287*, 1615-1622.

21. Ogliaro, F.; Cohen, S.; Filatov, M.; Harris, N.; Shaik, S., *Angew. Chem., Int. Ed.* **2000,** *39*, 3851-3855.

22. Groves, J. T., *Proc. Natl. Acad. Sci. U. S. A.* **2003,** *100*, 3569-3574.

23. Prasad, S.; Mitra, S., *Biochemistry* **2002,** *41*, 14499-14508.

24. Lange, S. J.; Que, L., *Curr. Opin. Chem. Biol.* **1998,** *2*, 159-172.

25. Solomon Edward, I.; Decker, A.; Lehnert, N., *Proc. Natl. Acad. Sci. U. S. A.* **2003,** *100*, 3589-94.

26. Kim, J.; Rees, D. C., *Nature* **1992,** *360*, 553-60.

27. Kim, J.; Rees, D. C., *Science* **1992,** *257*, 1677-82.

28. Einsle, O.; Tezcan, F. A.; Andrade, S. L. A.; Schmid, B.; Yoshida, M.; Howard, J. B.; Rees, D. C., *Science* **2002,** *297*, 1696-1700.

29. Buenning, P., *Clin. Exp. Hypert.* **1983,** *A5*, 1263-75.

30. Natesh, R.; Schwager, S. L. U.; Sturrock, E. D.; Acharya, K. R., *Nature* **2003,** *421*, 551-554.

31. Hodgkin, D. C.; Kamper, J.; Mackay, M.; Pickworth, J.; Trueblood, K. N.; White, J. G., *Nature* **1956,** *178*, 64-6.

32. Auterhoff, H.; Knabe, J.; Höltje, H.-D., *Lehrbuch der pharmazeutischen Chemie*. 13 ed.; Wissenschaftliche Verlagsgesellschaft Stuttgart: **1994**.

33. Mutschler, E., *Arzneimittelwirkungen*. 8 ed.; Wissenschaftliche Verlagsgesellschaft Stuttgart: Stuttgart, **2001**.

34. Carepo, M.; Tierney, D. L.; Brondino, C. D.; Yang, T. C.; Pamplona, A.; Telser, J.; Moura, I.; Moura, J. J. G.; Hoffman, B. M., *J. Am. Chem. Soc.* **2002,** *124*, 281-286.

35. Teixeira, M.; Moura, I.; Xavier, A. V.; Moura, J. J. G.; LeGall, J.; DerVartanian, D. V.; Peck, H. D., Jr.; Huynh Boi, H., *J. Biol. Chem.* **1989,** *264*, 16435-50.

36. Dole, F.; Fournel, A.; Magro, V.; Hatchikian, E. C.; Bertrand, P.; Guigliarelli, B., *Biochemistry* **1997,** *36*, 7847-7854.

37. Happe, R. P.; Roseboom, W.; Pierik, A. J.; Albracht, S. P.; Bagley, K. A., *Nature* **1997,** *385*, 126.

38. de Lacey, A. L.; Hatchikian, E. C.; Volbeda, A.; Frey, M.; Fontecilla-Camps, J. C.; Fernandez, V. M., *J. Am. Chem. Soc.* **1997,** *119*, 7181-7189.

39. Togni, A.; Hayashi, T.; Editors, *Ferrocenes: homogeneous catalysis, organic synthesis, materials science*. **1995**; p 540 pp.

40. Togni, A.; Halterman, R. L., *Metallocenes*. **1998**; p 500 pp.

41. Long, N. J., *Metallocenes*. Blackwell Science: **1998**; p 285.

42. Parker, C. W., *Methods Enzymol.* **1990,** *182*, 700-18.

43. Otto, M., *Analytische Chemie*. 2 ed.; Wiley-VCH: **2000**; p 673.

44. Edwards, R.; Editor, *Immunodiagnostics*. **1999**; p 281 pp.

45. Spiehler, V.; Isenschmid, D. S.; Matthews, P.; Kemp, P.; Kupiec, T., *J. Anal. Tox.* **2003,** *27*, 587-591.

46. Landi, A. P. G.; Wilson, A. B.; Davies, A.; Lachmann, P. J.; Ferriani, V. P. L.; Seilly, D. J.; Assis-Pandochi, A. I., *Immunol. Lett.* **2003,** *90*, 209-213.

47. Nistor, C.; Oubina, A.; Marco, M. P.; Barcelo, D.; Emneus, J., *Anal. Chim. Acta* **2001,** *426*, 185-195.

48. Czajka, J.; Batt, C. A., *J. Appl. Bacteriol.* **1996,** *81*, 601-607.

49. Becker, M. J., *Methods Immunol. Anal.* **1993,** *1*, 459-65.

50. Maeda, M., *J. Pharm. Biomed. Anal.* **2003,** *30*, 1725-1734.

51. Frank, L. A.; Petunin, A. I.; Vysotski, E. S., *Anal. Biochem.* **2004,** *325*, 240-246.

52. Brewster, J. D.; Mazenko, R. S., *J. Immunol. Methods* **1998,** *211*, 1-8.

53. Weetall, H. H.; Hotaling, T., *Biosensors* **1987,** *3*, 57-63.

54. Salmain, M.; Vessieres, A.; Brossier, P.; Butler, I. S.; Jaouen, G., *J. Immunol. Methods* **1992,** *148*, 65-75.

55. Hesse, M.; Meier, H.; Zeeh, B., *Spektroskopische Methoden in der organischen Chemie*. 5 ed.; Gerog Thieme Verlag Stuttgart - New York: **1995**.

56. Salmain, M.; Fischer-Durand, N.; Cavalier, L.; Rudolf, B.; Zakrzewski, J.; Jaouen, G., *Bioconj. Chem.* **2002,** *13*, 693-8.

57. Varenne, A.; Salmain, M.; Brisson, C.; Jaouen, G., *Bioconj. Chem.* **1992,** *3*, 471-6.

58. Philomin, V.; Vessieres, A.; Jaouen, G., *J. Immunol. Methods* **1994,** *171*, 201-10.

59. Varenne, A.; Vessieres, A.; Salmain, M.; Brossier, P.; Jaouen, G., *J. Immunol. Methods* **1995,** *186*, 195-204.

60. Vessieres, A.; Salmain, M.; Brossier, P.; Jaouen, G., *J. Pharm. Biomed. Anal.* **1999,** *21*, 625-33.

61. Fischer-Durand, N.; Salmain, M.; Rudolf, B.; Vessieres, A.; Zakrzewski, J.; Jaouen, G., *ChemBioChem* **2004,** *5*, 519-525.

62. Metzler-Nolte, N., *Angew. Chem., Int. Ed.* **2001,** *40*, 1040-1043.

63. Clarke, M. J.; Sadler, M. J., *Metallopharmaceuticals: Diagnosis and Therapy*. 1 ed.; Springer: **1999**; 'Vol.' 2, p 215.

64. Sorensen, J. A.; Phelps, M. E., *Physics in Nuclear Medicine*. 2 ed.; Grune & Stratton, Orlando: **1987**.

65. Abrams, M. J.; Davison, A.; Jones, A. G.; Costello, C. E.; Pang, H., *Inorg. Chem.* **1983,** *22*, 2798-800.

66. Tulip, T. H.; Calabrese, J.; Kronauge, J. F.; Davidson, A.; Jones, A. G., *Technetium and Rhenium in chemistry and nuclear medicine*. Raven press, New York: **1986**; 'Vol.' 2.

67. Alberto, R.; Schibli, R.; Egli, A.; Schubiger, A. P.; Abram, U.; Kaden, T. A., *J. Am. Chem. Soc.* **1998,** *120*, 7987-7988.

68. Alberto, R.; Ortner, K.; Wheatley, N.; Schibli, R.; Schubiger, A. P., *J. Am. Chem. Soc.* **2001,** *123*, 3135-3136.

69. Schibli, R.; Schubiger, P. A., *Eur. J. Nucl. Med. Mol. Imag.* **2002,** *29*, 1529-1542.

70. van Staveren, D. R.; Mundwiler, S.; Hoffmanns, U.; Pak, J. K.; Spingler, B.; Metzler-Nolte, N.; Alberto, R., *Org. Biomol. Chem.* **2004,** *2*, 2593-2603.

71. Waibel, R.; Alberto, R.; Willuda, J.; Finnern, R.; Schibli, R.; Stichelberger, A.; Egli, A.; Abram, U.; Mach, J.-P.; Pluckthun, A.; Schubiger, P. A., *Nat. Biotech.* **1999,** *17*, 897-901.

72. Kopf, H.; Kopf-Maier, P., *Angew. Chem., Int. Ed.* **1979,** *18*, 477-8.

73. Moebus, V. J.; Stein, R.; Kieback, D. G.; Runnebaum, I. B.; Sass, G.; Kreienberg, R., *Anticancer Res.* **1997,** *17*, 815-21.

74. Koepf-Maier, P.; Hesse, B.; Koepf, H., *J. Canc. Res. Clin. Onc.* **1980,** *96*, 43-51.

75. Keppler, B. K., *Metal Complexes in Cancer Chemotherapy*. VCH Winheim: **1993**.

76. Fricker, S. P., *Metal Compounds in Cancer Therapy*. Chapman & Hall, New York: **1994**.

77. Waern, J. B.; Dillon, C. T.; Harding, M. M., *J. Med. Chem.*, ACS ASAP.

78. Harding, M. M.; Mokdsi, G., *Curr. Med. Chem.* **2000,** *7*, 1289-1303.

79. Lippert, B., *Cisplatin*. Wiley-VCH: **1999**; p 560.

80. Clarke, M. J.; Sadler, P. J., *Metallopharmaceuticals: DNA Interactions*. Springer, Stuttgart: **1999**; 'Vol.' 1, p 199.

81. Motohashi, N.; Meyer, R.; Gollapudi, S. R.; Bhattiprolu, K. R., *J. Organomet. Chem.* **1990,** *398*, 205-17.

82. Johnson, M. T.; Kreft, E.; N'Da, D. D.; Neuse, E. W.; van Rensburg, C. E. J., *J. Inorg Organomet. Pol.* **2003,** *13*, 255-267.

83. Hocek, M.; Stepnicka, P.; Ludvik, J.; Cisarova, I.; Votruba, I.; Reha, D.; Hobza, P., *Chem. Eur. J.* **2004,** *10*, 2058-2066.

84. Weber, B.; Serafin, A.; Michie, J.; Van Rensburg, C.; Swarts, J. C.; Bohm, L., *Anticancer Res.* **2004,** *24*, 763-770.

85. Caldwell, G.; Meirim, M. G.; Neuse, E. W.; Van Rensburg, C. E. J., *App. Organomet. Chem.* **1998,** *12*, 793-799.

86. Hublau, P.; Sergheraert, C.; Ballester, L.; Dautrevaux, M., *Eur. J. Med. Chem.* **1983,** *18*, 131-3.

87. Harmsen, D.; Erker, G.; Frohlich, R.; Kehr, G., *Eur. J. Inorg. Chem.* **2002**, 3156-3171.

88. Giese, R. W.; Vallee, B. L., *J. Am. Chem. Soc.* **1972,** *94*, 6199-200.

89. Kunugi, S.; Murakami, Y.; Ikeda, K.; Itoh, N., *Int. J. Biol. Macromol.* **1992,** *14*, 210-14.

90. Walton, C. D. *Metallocene-modified proteins*. **1989**.

91. Misterkiewicz, B.; Salmain, M.; Jaouen, G., *Tetrahedron Lett.* **2004,** *45*, 7511-7513.

92. Schlogel, K., *Monatsh. Chem.* **1957,** *88*, 601-21.

93. Cuingnet, E.; Dautrevaux, M.; Sergheraert, C.; Tartar, A.; Attali, B.; Cros, J., *Eur. J. Med. Chem.* **1982,** *17*, 203-6.

94. Brunet, J. C.; Cuingnet, E.; Gras, H.; Marcincal, P.; Mocz, A.; Sergheraert, C.; Tartar, A., *J. Organomet. Chem.* **1981,** *216*, 73-7.

95. Brunner, H.; Koenig, W.; Nuber, B., *Tetrahedron: Asymmetry* **1993,** *4*, 699-707.

96. Cuingnet, E.; Sergheraert, C.; Tartar, A.; Dautrevaux, M., *J. Organomet. Chem.* **1980,** *195*, 325-9.

97. Brunet, J. C.; Cuingnet, E.; Dautrevaux, M.; Demarly, A.; Gras, H.; Marcincal, P.; Sergheraert, C.; Tartar, A.; Vanvoorde, J. C.; Vanpoucke, M., *Pept., Proc. Eur. Pept. Symp., 16th* **1981**, 603-7.

98. Tartar, A.; Demarly, A.; Sergheraert, C.; Escher, E., *Pept.: Struct. Funct., Proc. Am. Pept. Symp., 8th* **1983**, 377-80.

99. Maes, P.; Ricouart, A.; Escher, E.; Tartar, A.; Sergheraert, C., *Collect. Czech. Chem. Commun.* **1988,** *53*, 2914-19.

100. van Staveren, D. R.; Metzler-Nolte, N., *Chem. Rev.* **2004,** *104*, 5931-5985.

101. Kealy, T. J.; Pauson, P. L., *Nature* **1951**, 1039-1040.

102. Miller, S. A.; Tebboth, J. A.; Tremaine, J. F., *J. Chem. Soc.* **1952**, 632-635.

103. Wilkinson, G.; Rosenblum, M.; Whiting, M. C.; Woodward, R. B., *J. Am. Chem. Soc.* **1952,** *74*, 2125-6.

104. Pfab, W.; Fischer, E. O., *Z. anorg. u. allgem. Chem.* **1953,** *274*, 316-22.

105. Shea, T. M. *Coupled multielectron/group transfer in ruthenocene and osmocene systems*. **1999**.

106. Riesen, H.; Krausz, E.; Luginbuehl, W.; Biner, M.; Guedel, H. U.; Ludi, A., *J. Chem. Phys.* **1992,** *96*, 4131-5.

107. Elschenbroich, C.; Salzer, A., *Organometallchemie*. Teubner Studienbücher: **1993**.

108. Gubin, S. P.; Smirnova, S. A.; Denisovich, L. I.; Lubovich, A. A., *J. Organomet. Chem.* **1971,** *30*, 243-55.

109. Kuwana, T.; Bublitz, D. E.; Hoh, G., *J. Am. Chem. Soc.* **1960,** *82*, 5811-17.

110. Abbate, F. W. *Mechanism of electrophilic substitution of ferrocene*. **1967**.

111. Koehler, F. H., *J. Organomet. Chem.* **1978,** *160*, 299-306.

112. Brett, C. M.; Bursten, B. E., *Polyhedron* **2004,** *23*, 2993-3002.

113. Borrell, P.; Henderson, E., *Inorg. Chim. Acta* **1975,** *12*, 215-18.

114. Cotton, F. A.; Whipple, R. O.; Wilkinson, G., *J. Am. Chem. Soc.* **1953,** *75*, 3586-7.

115. Zagorevskii, D. V.; Holmes, J. L., *Organometallics* **1992,** *11*, 3224-7.

116. Buender, W.; Weiss, E., *J. Organomet. Chem.* **1975,** *92*, 65-8.

117. Sheats, J. E., *Journal of Organometallic Chemistry Library* **1979,** *7*, 461-521.

118. Sheats, J. E.; Rausch, M. D., *J. Org. Chem.* **1970,** *35*, 3245-9.

119. Remy, I.; Brossier, P., *Analyst* **1993,** *118*, 1021-5.

120. Ertas, O. S.; Tezel, H., *J. Pharm. Biomed. Anal.* **2004,** *36*, 893-897.

121. Pas, M.; Milacic, R.; Draslar, K.; Pollak, N.; Raspor, P., *BioMetals* **2004,** *17*, 25-33.

122. Bihoreau, N.; Pin, S.; de Kersabiec, A. M.; Vidot, F.; Fontaine-Aupart, M. P., *Eur. J. Biochem.* **1994,** *222*, 41-8.

123. Cais, M., *Methods Enzymol.* **1983,** *92*, 445-58.

124. Padeste, C.; Steiger, B.; Grubelnik, A.; Tiefenauer, L., *Biosensors & Bioelectronics* **2004,** *20*, 545-552.

125. Chowdhury, S.; Schatte, G.; Kraatz, H.-B., *J. Chem. Soc., Dalton Trans.* **2004**, 1726-1730.

126. Snegur, L. V.; Simenel, A. A.; Nekrasov, Y. S.; Morozova, E. A.; Starikova, Z. A.; Peregudova, S. M.; Kuzmenko, Y. V.; Babin, V. N.; Ostrovskaya, L. A.; Bluchterova, N. V.; Fomina, M. M., *J. Organomet. Chem.* **2004,** *689*, 2473-2479.

127. Eckert, H.; Koller, M., *Z. Naturforsch., B: Chem. Sci.* **1990,** *45*, 1709-14.

128. Eckert, H.; Koller, M., *J. Liq. Chromatogr.* **1990,** *13*, 3399-414.

129. Sewald, N.; Jakubke, H. D., *Peptides: Chemistry and Biology*. 1 ed.; Wiley-VCH: **2002**; p 562.

130. Adams, R. L. P.; Knowler, J. P.; Leader, D. P., *The Biochemistry of the Nucleic Acids*. Chapman & Hall, London: **1992**.

131. Novabiochem, *Novabiochem catalogue*. **2004**.

132. Zadina, J. E.; Banks, W. A.; Kastin, A. J., *Peptides* **1986,** *7*, 497-537.

133. Ahmed, B.; Kastin, A. J.; Banks, W. A.; Zadina, J. E., *Peptides* **1994,** *15*, 1105-55.

134. Pan, W.; Kastin, A. J.; Banks, W. A.; Zadina, J. E., *Peptides* **1999,** *20*, 1127-1138.

135. Vaccarino, A. L.; Olson, G. A.; Olson, R. D.; Kastin, A. J., *Peptides* **1999,** *20*, 1527-1574.

136. Humblet, C.; Mirzadegan, T., *Annu. Rep. Med. Chem.* **1992,** *27*, 291-300.

137. Gainer, H.; Russell, J. T.; Loh, Y. P., *Neuroendocrinology* **1985,** *40*, 171-84.

138. Mains, R. E.; Eipper, B. A., *J. Biol. Chem.* **1979,** *254*, 7885-94.

139. Spector, S.; Donnerer, J., *Handbook of Experimental Pharmacology*. Springer, Berlin: **1993**.

140. Terenius, L., *Acta pharmacologica et toxicologica* **1973,** *33*, 377-84.

141. Simon, E. J.; Hiller, J. M.; Edelman, I., *Proc. Natl. Acad. Sci. U. S. A.* **1973,** *70*, 1947-9.

142. Pert, C. B.; Snyder, S. H., *Proc. Natl. Acad. Sci. U. S. A.* **1973,** *70*, 2243-7.

143. Hughes, J.; Smith, T. W.; Kosterlitz, H. W.; Fothergill, L. A.; Morgan, B. A.; Morris, H. R., *Nature* **1975,** *258*, 577-80.

144. Pasternak, G. W.; Editor, *The Opiate Receptors*. **1988**; p 499 pp.

145. Goodchild, C. S.; Nadeson, R.; Cohen, E., *Eur. J. Anaesth.* **2004,** *21*, 179-185.

146. Fontaine, J.; Reuse, J., *Br. J. Pharmacol.* **1985,** *85*, 861-7.

147. Camerman, A.; Mastropaolo, D.; Karle, I.; Karle, J.; Camerman, N., *Nature* **1983,** *306*, 447-50.

148. Schiller, P. W.; Yam, C. F.; Lis, M., *Biochemistry* **1977,** *16*, 1831-8.

149. Teschmacher, H., *Handbook of Experimental Pharmacology*. Springer, Berlin: **1993**.

150. Sehnert, J.; Hess, A.; Metzler-Nolte, N., *J. Organomet. Chem.* **2001,** *637-639*, 349-355.

151. Hess, A.; Brosch, O.; Weyhermuller, T.; Metzler-Nolte, N., *J. Organomet. Chem.* **1999,** *589*, 75-84.

152. Bublitz, D. E.; Rinehart, K. L., Jr., *Org. React. (N.Y.)* **1969,** *17*, 1-154.

153. Biehl, E. R.; Reeves, P. C., *Synthesis* **1973**, 360-1.

154. Kraatz, H.-B.; Lusztyk, J.; Enright, G. D., *Inorg. Chem.* **1997,** *36*, 2400-2405.

155. Kraatz, H. B.; Galka, M., *Metal ions in biological systems* **2001,** *38*, 385-409.

156. Herz, A.; Gramsch, C.; Hoellt, V.; Meo, T.; Riethmueller, G., *Life Sci.* **1982,** *31*, 1721-4.

157. Song, A.; Zhang, J.; Lebrilla, C. B.; Lam, K. S., *J. Comb. Chem.* **2004,** *6*, 604-610.

158. Lee, J.; Murray, W. V.; Rivero, R. A., *J. Org. Chem.* **1997,** *62*, 3874-3879.

159. Morales, G. A.; Corbett, J. W.; DeGrado, W. F., *J. Org. Chem.* **1998,** *63*, 1172-1177.

160. Bergel, F.; Stock, J. A., *J. Chem. Soc., Abstr.* **1954**, 2409-17.

161. Sonogashira, K.; Tohda, Y.; Hagihara, N., *Tetrahedron Lett.* **1975**, 4467-70.

162. Hudson, R. H. E.; Li, G.; Tse, J., *Tetrahedron Lett.* **2002,** *43*, 1381-1386.

163. Coutouli-Argyropoulou, E.; Tsitabani, M.; Petrantonakis, G.; Terzis, A.; Raptopoulou, C., *Org. Biomol. Chem.* **2003,** *1*, 1382-1388.

164. Xie, J.; Wang, L.; Wu, N.; Brock, A.; Spraggon, G.; Schultz, P. G., *Nat. Biotech.* **2004,** *22*, 1297-1301.

165. Chin, J. W.; Santoro, S. W.; Martin, A. B.; King, D. S.; Wang, L.; Schultz, P. G., *J. Am. Chem. Soc.* **2002,** *124*, 9026-9027.

166. Schwabacher, A. W.; Lei, H.; Stoakes, M. S.; Herath, K. P. B.; Lee, J., *J. Org. Chem.* **1994,** *59*, 4206-4210.

167. Sheehan, J. C.; Hess, G. P., *J. Am. Chem. Soc.* **1955,** *77*, 1067-8.

168. Brosch, O. *Selektive Markierung von Aminosäuren und Peptiden mit kovalent gebundenen Organometallfragmenten*. Mülheim, **1999**.

169. Brosch, O.; Weyhermulle, T.; Metzler-Nolte, N., *Eur. J. Inorg. Chem.* **2000**, 323-330.

170. Randles, J. E. B., *Trans. Farad. Soc.* **1948,** *44*, 327-38.

171. Richter, J., *European pharmacopoeia 4, edition 3 addition: Official German edition*. **2004**; 'Vol.' 59, p 80.

172. Mirrlees, M. S.; Moulton, S. J.; Murphy, C. T.; Taylor, P. J., *J. Med. Chem.* **1976,** *19*, 615-9.

173. McCall, J. M., *J. Med. Chem.* **1975,** *18*, 549-52.

174. Oldendorf, W. H., *Proc. Soc. Exp. Biol. Med.* **1974,** *147*, 813-16.

175. Robinson, P. J.; Rapoport, S. I., *Handb. Exp. Pharmacol.* **1992,** *103*, 279-300.

176. Buchwald, P.; Bodor, N., *Curr. Med. Chem.* **1998,** *5*, 353-80.

177. Hansch, C.; Fujita, T., *J. Am. Chem. Soc.* **1964,** *86*, 1616-26.

178. Fujita, T.; Iwasa, J.; Hansch, C., *J. Am. Chem. Soc.* **1964,** *86*, 5175-80.

179. Valko, K., *J. Chromatogr.* **2004,** *1037*, 299-310.

180. Horvath, C.; Lin, H.-J., *J. Chromatogr.* **1976,** *126*, 401-20.

181. Colin, H.; Ward, N.; Guiochon, G., *J. Chromatogr.* **1978,** *149*, 169-97.

182. Roumeliotis, P.; Unger, K. K., *J. Chromatogr.* **1978,** *149*, 211-24.

183. Scott, R. P. W.; Kucera, P., *J. Chromatogr.* **1979,** *175*, 51-63.

184. Snyder, L. R.; Dolan, J. W.; Gant, J. R., *J. Chromatogr.* **1979,** *165*, 3-30.

185. Hammers, W. E.; Meurs, G. J.; De Ligny, C. L., *J. Chromatogr.* **1982,** *247*, 1-13.

186. El Tayar, N.; Van de Waterbeemd, H.; Testa, B., *QSAR Strategies Des. Bioact. Compd., Proc. Eur. Symp. Quant. Struct.-Act. Relat., 5th* **1985**, 268-71.

187. Testa, B.; Carrupt, P.-A.; Gaillard, P.; Billois, F.; Weber, P., *Pharm. Res.* **1996,** *13*, 335-43.

188. Lipinski, C. A.; Lombardo, F.; Dominy, B. W.; Feeney, P. J., *Adv. Drug Deliv. Rev.* **2001,** *46*, 3-26.

189. Lipinski, C. A., Computational alerts for potential absorption problems. Part. 2. Predicting human absorption. In *Biotec, PDD symposium*, AAPS, Miami, 1995.

190. *Chemoffice Ultra 2004*, version 8.0; **2004**.

191. *ACD PhysChem batch logP*, version 8.0; **2004**.

192. Minick, D. J.; Frenz, J. H.; Patrick, M. A.; Brent, D. A., *J. Med. Chem.* **1988,** *31*, 1923-33.

193. Fauchere, J. L.; Pliska, V., *Eur. J. Med. Chem.* **1983,** *18*, 369-75.

194. Akamatsu, M.; Katayama, T.; Kishimoto, D.; Kurokawa, Y.; Shibata, H.; Ueno, T.; Fujita, T., *J. Pharm. Sci.* **1994,** *83*, 1026-33.

195. Lang, V. B.; Langguth, P.; Ottiger, C.; Wunderli-Allenspach, H.; Rognan, D.; Rothen-Rutishauser, B.; Perriard, J. C.; Lang, S.; Biber, J.; Merkle, H. P., *J. Pharm. Sci.* **1997,** *86*, 846-53.

196. Bauer, B. *in vitro Zellkulturmodelle der Blut-Hirn-Schranke zur Untersuchung der Permeation und P-Glycoprotein Interaktion von Arzneistoffen*. Ruprecht-Karls-University, Heidelberg, **2002**.

197. Golovanov, I. B.; Tsygankova, I. G., *Russ. J. Gen. Chem* **2002,** *72*, 137-143.

198. Pliska, V.; Testa, B.; van de Waterbeemd, H.; Editors, *Lipophilicity in Drug Action and Toxicology. [In: Methods Princ. Med. Chem. 1996, 4]*. **1996**; p 438 pp.

199. Pomper, M. G.; VanBrocklin, H.; Thieme, A. M.; Thomas, R. D.; Kiesewetter, D. O.; Carlson, K. E.; Mathias, C. J.; Welch, M. J.; Katzenellenbogen, J. A., *J. Med. Chem.* **1990,** *33*, 3143-55.

200. Braumann, T., *J. Chromatogr.* **1986,** *373*, 191-225.

201. Ehrlich, P., *Das Sauerstoffbedürfnis des Organismus. Eine farbenanalytische Studie*. Verlag August Hirschwald: **1885**; p 167.

202. Goldmann, E. E., *Die äussere und innere Sekretion des gesunden und kranken Organismus im Lichte der "vitalen Färbung"*. Beiträge zur klinischen Chirurgie: **1909**; 'Vol.' 64, p 192-265.

203. Reese, T. S.; Karnovsky, M. J., *J. Cell Biol.* **1967,** *34*, 207-17.

204. Thiebaut, F.; Tsuruo, T.; Hamada, H.; Gottesman, M. M.; Pastan, I.; Willingham, M. C., *J. Histochem. Cytochem.* **1989,** *37*, 159-64.

205. Cordon-Cardo, C.; O'Brien, J. P.; Casals, D.; Rittman-Grauer, L.; Biedler, J. L.; Melamed, M. R.; Bertino, J. R., *Proc. Natl. Acad. Sci. U. S. A.* **1989,** *86*, 695-8.

206. Rubin, L. L.; Staddon, J. M., *Annu. Rev. Neurosc.* **1999,** *22*, 11-28.

207. Pardridge, W. M.; Triguero, D.; Yang, J.; Cancilla, P. A., *J. Pharmacol. Exp. Ther.* **1990,** *253*, 884-91.

208. Eddy, E. P.; Maleef, B. E.; Hart, T. K.; Smith, P. L., *Adv. Drug Deliv. Rev.* **1997,** *23*, 185-198.

209. Gumbleton, M.; Audus, K. L., *J. Pharm. Sci.* **2001,** *90*, 1681-1698.

210. Spatz, M.; Bembry, J.; Dodson, R. F.; Hervonen, H.; Murray, M. R., *Brain research* **1980,** *191*, 577-82.

211. Franke, H.; Galla, H.-J.; Beuckmann, C. T., *Brain Research* **1999,** *818*, 65-71.

212. Franke, H.; Galla, H. J.; Beuckmann, C. T., *Brain Res. Prot.* **2000,** *5*, 248-256.

213. Audus, K. L.; Bartel, R. L.; Hidalgo, I. J.; Borchardt, R. T., *Pharm. Res.* **1990,** *7*, 435-51.

214. Takakura, Y.; Audus, K. L.; Borchardt, R. T., *Adv. Pharmacol.* **1991,** *22*, 137-65.

215. Cornford, E. M.; Braun, L. D.; Crane, P. D.; Oldendorf, W. H., *Endocrinology* **1978,** *103*, 1297-303.

216. Zlokovic, B. V.; Begley, D. J.; Chain-Eliash, D. G., *Brain Research* **1985,** *336*, 125-32.

217. Thompson, S. E.; Cavitt, J.; Audus, K. L., *J. Cardiovasc. Pharmacol.* **1994,** *24*, 818-25.

218. Kastin, A. J.; Pearson, M. A.; Banks, W. A., *Pharmacol., Biochem. Behav.* **1991,** *40*, 771-4.

219. Oude Elferink, R. P. J.; Zadina, J., *Peptides* **2001,** *22*, 2015-2020.

220. Brownlees, J.; Williams, C. H., *J. Neurochem.* **1993,** *60*, 793-803.

221. Weber, S. J.; Abbruscato, T. J.; Brownson, E. A.; Lipkowski, A. W.; Polt, R.; Misicka, A.; Haaseth, R. C.; Bartosz, H.; Hruby, V. J.; Davis, T. P., *J. Pharmacol. Exp. Ther.* **1993,** *266*, 1649-55.

222. Anda, T.; Yamashita, H.; Khalid, H.; Tsutsumi, K.; Fujita, H.; Tokunaga, Y.; Shibata, S., *Neurol. Res.* **1997,** *19*, 369-376.

223. Huwyler, J.; Drewe, J.; Klusemann, C.; Fricker, G., *Br. J. Pharmacol.* **1996,** *118*, 1879-1885.

224. Lundquist, S.; Renftel, M.; Brillault, J.; Fenart, L.; Cecchelli, R.; Dehouck, M.-P., *Pharm. Res.* **2002,** *19*, 976-81.

225. Akamatsu, M.; Fujita, T., *J. Pharm. Sci.* **1992,** *81*, 164-74.

226. Engelman, D. M.; Steitz, T. A.; Goldman, A., *Annu. Rev. Biophysics and Biophysical Chem.* **1986,** *15*, 321-53.

227. Urry, D. W.; Gowda, D. C.; Parker, T. M.; Luan, C. H.; Reid, M. C.; Harris, C. M.; Pattanaik, A.; Harris, R. D., *Biopolymers* **1992,** *32*, 1243-50.

228. Pedretti, A.; Villa, L.; Vistoli, G., *J. Comput. Aided Mol. Des.* **2004,** *18*, 167-173.

229. Szegezdi, J.; Csizmadia, F., *Abstr. Pap. 227th National Meeting, Anaheim, CA* **2004**, COMP-232.

230. Marks, N.; Benuck, M.; Sachs, L., *Chem. Brain, Proc. Symp.* **1981**, 136-46.

231. Vijayaraghavan, J.; Scicli, A. G.; Carretero, O. A.; Slaughter, C.; Moomaw, C.; Hersh, L. B., *J. Biol. Chem.* **1990,** *265*, 14150-5.

232. Brownson, E. A.; Abbruscato, T. J.; Gillespie, T. J.; Hruby, V. J.; Davis, T. P., *J. Pharmacol. Exp. Ther.* **1994,** *270*, 675-80.

233. Levin, V. A., *J. Med. Chem.* **1980,** *23*, 682-4.

234. Rim, S.; Audus, K. L.; Borchardt, R. T., *Int. J. Pharm.* **1986,** *32*, 79-84.

235. Banks, W. A.; Kastin, A. J., *Brain Res. Bull.* **1985,** *15*, 287-92.

236. Tsuji, A., *Proc. Int. Contr. Rel. Bio. Mat.* **1997,** *24th*, 219-220.

237. Wang, L.; Schultz, P. G., *Angew. Chem., Int. Ed.* **2004,** *44*, 34-66.

238. Reeves, P. C., *Org. Synth.* **1977,** *56*, 28-31.